

Global ecological drivers of transpiration regulation in trees

DOCTORADO EN ECOLOGIA TERRESTRE

Centre de Recerca Ecològica i Aplicacions Forestals

Autonomous University of Barcelona

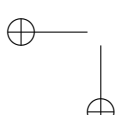
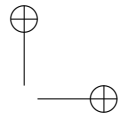
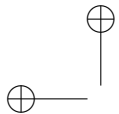
Author:

Víctor Flo Sierra

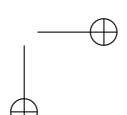
Advisors:

Rafael Poyatos López
Jordi Martínez Vilalta

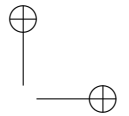
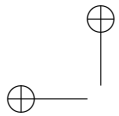
Dec 2020



|

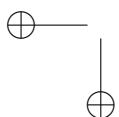


“thesis” — 2020/12/29 — 11:18 — page 2 — #2

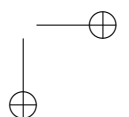


—

—



|



Acknowledgements

Mucha gente es co-responsable de este trabajo, de haberme empujado y acompañado hasta aquí. Me gustaría empezar agradeciendo a mis directores de tesis, Rafa y Jordi, sin los que esta tesis no hubiera sido posible, gracias por la oportunidad de trabajar con vosotros. He sido muy afortunado de haber contado con dos mentores excelentes en lo profesional y en lo personal. Rafa, tu dedicación es envidiable, gracias por todas las buenas ideas, los comentarios y críticas, las correcciones perfectas, por los viajes a congresos y por sufrir de mi insomnio y jet-lag. Jordi, ha sido un privilegio tenerte como tutor, por tu conocimiento transversal y profundo, por tu capacidad inata e inmediata de entenderlo todo, por mejorar siempre todas las ideas y textos, y por tu calidad humana.

Esta tesis tampoco hubiera sido igual sin haber compartido estos cuatro años con tantos buenos compañeros. Gracias a los compañeros de despacho, a Anna, Javi, Judit, Carlos, Manu, Aina, Marta, Pere y Pol. Creo que habéis sido los mejores compañeros posibles y que tuve mucha suerte de acabar en el -150. Sé que me llevo grandes amistades para toda la vida. No quiero olvidarme tampoco de muchos otros compañeros como Jordi, Sara, Kevin, Xavi, Vicenç, Joan, Marina, con los que hemos compartido café, discusiones y charlas. Gracias también a Luciana por acompañarnos en ese genial viaje relámpago por el desierto americano.

Gracias también en especial a los compañeros que estan o han pasado por el grupo. Maurizio, Tere, Miquel, Lucia, Víctor, Raul, Rosella, Pipo, Mireia, Lies, David, Jacob, Aude, Antonine, Pablo, Luca y Brenda, sin duda un grupo envidiable. Gracias por tantos buenos momentos, por la vertiente

académica, pero especialmente por las salidas de grupo, por las barbacoas, cenas y cervezas. Me gustaría agradecer especialmente a Víctor Granda, por su excelente trabajo, sin el que hubiera sido imposible enfrentarnos a la difícil tarea de llevar adelante SAPFLUXNET. Gracias por enseñarme a querer R, pero sobre todo por las risas y los enfados jugando a basquet. A Jordi Bosch, Anselm Rodrigo, Joan Oca e Ingrid Masaló por permitirme iniciarme en el mundo de la investigación.

Durante estos años he tenido la suerte de vivir y conocer a mucha gente lejos de casa. Muchas personas que me han enseñado otras maneras de ver el mundo. Me gustaría mencionar especialmente a Martin y a Elena, gracias por acogerme y hacerme sentir como en casa en Salt Lake City. Gracias por darnos cobijo cuando nos quedamos en la calle por unos días, dejarme vuestro coche, y gracias por un viaje inolmidable a Glacier. No os lo podré agradecer suficiente. Gracias a Bill Anderegg por acogerme en su laboratorio donde he tenido la suerte de conocer a gente genial como Kelly, Nicole, Jaycee. Me gustaría agradecer también a Kathy Steppe por darme la oportunidad de visitar su laboratorio en Ghent y por sus buenos consejos. A Roberto por enseñarme a intalar mi primera sonda de flujo de sabia.

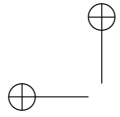
Gracias también a los que llevan tiempo compartiendo su camino conmigo o han caminado alguna etapa, me han marcado y ayudado, a los amigos de toda la vida y a mis compañeros de andanzas musicales. Gracias Trufa, Pablo, Marc, Laura, Oscar, Carles, Jordi, Larry, Cristian, Pol, Kuni, Julio, Lorenzo, Barbara, Edgar, Jan, Arnau. También a Marta, Rosa, Florian, Daniel, Lola, Magdalena y Esther, por haber creído tanto en mi y haber sido parte de mi vida durante muchos años. A Tuti, Tona y Flor porque os hecho de menos.

Quiero agradecer también a mi familia. A mis abuelos, a mis tíos y primos, por haber sido una referencia.

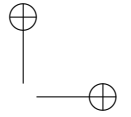
Gracias sobre todo a quien desde hace cuatro años es mi compañera de viaje. Gracias Mari Angeles por tu sonrisa, tu apoyo incondicional y tu amor. Esta tesis no hubiera sido sin ti. Gracias por ser brillante, por que es un placer

escucharte y por intentar “salvar al mundo”. Gracias por dejarme formar parte de tu familia murciana.

Gracias finalmente a mis padres, por dejarme decidir mi camino, por apoyarme en cada decisión que he tomado. Me habeis hecho libre y feliz. Mil gracias Ana por haber creido en mi, por ser un ejemplo desde que eramos pequeños, por ser tan buena y trabajadora. Si alguien es responsable directo de que me lanzara ha recorrer este camino esa eres tu. Gracias Clara por ser la alegría de nuestra casa y ser una hermana maravillosa. Gracias Marc y Jose por formar parte de nuestra vida y por esas charlas sobre tecnologia y negocios. Para acabar, gracias Arnau, el último fichaje de la familia. ¡Os quiero!

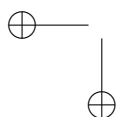


“thesis” — 2020/12/29 — 11:18 — page iv — #6



—

—



|

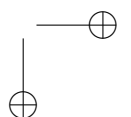
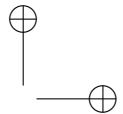
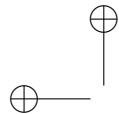


Table of Contents

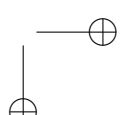
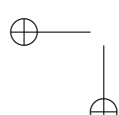
1: Introduction	1
1.1 Transpiration and earth system functioning	2
1.2 Transpiration across scales	5
1.2.1 Water transport in plants	5
1.2.2 Upscaling to the stand and ecosystem levels	7
1.3 Transpiration quantification	8
1.4 Transpiration in a changing world	10
1.5 Research aims and outline	12
—	
2: Bias and uncertainty in sap flow methods	15
2.1 Introduction	17
2.2 Material and methods	21
2.2.1 Sap flow calibration datasets	21
2.2.2 Calibration assessment	23
2.2.3 Statistical analyses	26
2.3 Results	28
2.3.1 Calibration performance compared among methods and families of methods	29
2.3.2 Influence of wood traits	32
2.4 Discussion	34
2.4.1 Sap flow measurement errors across methods and methodological families	34
2.4.2 The performance of sap flow calibrations is largely unrelated to species wood traits	39

2.4.3	Implications and recommendations	42
2.5	Conclusions	44
3:	The SAPFLUXNET database	45
3.1	Introduction	47
3.2	The SAPFLUXNET data workflow	50
3.2.1	An overview of sap flow measurements	50
3.2.2	Data compilation	52
3.2.3	Data harmonisation and quality control: QC1	53
3.2.4	Data harmonisation and quality control: QC2	55
3.2.5	Data structure	56
3.3	The SAPFLUXNET database	56
3.3.1	Data coverage	56
3.3.2	Methodological aspects	60
3.3.3	Plant characteristics	61
3.3.4	Stand characteristics	65
3.3.5	Temporal characteristics	66
3.3.6	Availability of environmental data	68
3.4	Potential applications	68
3.4.1	Applications in plant ecophysiology and functional ecology	68
3.4.2	Applications in ecosystem ecology and ecohydrology . .	73
3.5	Limitations and future developments	77
3.5.1	Limitations	77
3.5.2	Outlook	79
3.6	Data availability, access and feedback	80
3.7	Conclusion	81
4:	Analysis of hydrometeorological drivers.	83
4.1	Introduction	85
4.2	Material and methods	87
4.2.1	Sapflow and environmental data	87
4.2.2	Data filtering	88
4.2.3	Whole-tree canopy conductance calculation	88

4.2.4	Hydrometeorological coupling quantification	88
4.2.5	Biome classification and site-level bioclimatic data . . .	90
4.2.6	Statistical analyses	91
4.3	Results	92
4.4	Discussion	95
5:	Climate and functional traits jointly mediate tree water use strategies	101
5.1	Introduction	103
5.2	Material and methods	106
5.2.1	Sap flow data	107
5.2.2	Evaporative demand and soil water availability data .	108
5.2.3	Data filtering	109
5.2.4	Whole-tree canopy conductance calculation	110
5.2.5	Traits and climatic data	111
5.2.6	G_{Asw} sensitivity to soil water availability and water demand	112
5.2.7	Statistical analyses	112
5.3	Results	115
5.3.1	Water use parameters and differences between angiosperms and gymnosperms	115
5.3.2	Coordination with hydraulic and allocation traits . . .	116
5.4	Discussion	122
5.4.1	Climate influence on water use strategies across species	123
5.4.2	Water use parameters	123
5.4.3	Coordination between water use parameters and water relations traits	124
5.4.4	Conclusions	126
6:	General discussion and conclusions	129
6.1	Improving sap flow techniques to obtain reliable estimates of tree level transpiration	130
6.2	The SAPLUXNET database. What next?	132
6.3	The hydroclimatic drivers of transpiration and their complexity	133



6.4 On the use of plant traits to characterize water use strategies at the global level	135
6.5 Towards a global characterization of plant water use strategies.	136
6.6 Conclusions	138
Appendix A: Appendix Chapter 2	141
A.1 Figures A	142
A.2 Tables A	145
Appendix B: Appendix Chapter 3	151
B.1 Figures B	153
B.2 Tables B	158
Appendix C: Appendix Chapter 4	175
C.1 Figures C	176
C.2 Tables C	180
Appendix D: Appendix Chapter 5	191
D.1 Notes D	192
D.2 Figures D	193
D.3 Tables D	214
References	221



List of Tables

2.1	Analysis summary for the different methods and families.	28
2.2	Error analysis of different sap flow methods.	32
2.3	Least-squares means and 95% CI calculated from the LMM models testing the effect of different wood porosity types	34
2.4	Synthesis of the potential sources of error and use adequacy for each method.	36
3.1	Number of sap flow times series in SAPFLUXNET depend- ing on whether they were calibrated for the different sap flow methods.	62
3.2	Number of plants in the SAPFLUXNET database using differ- ent radial and azimuthal integration.	63
3.3	Number of datasets, plants and species by stand-level treat- ment in the SAPFLUXNET database.	72
4.1	Analysis of variance testing differences among biomes in the coupling of tree-level water conductance to each of the main hydrometeorological drivers.	93
4.2	Parameters of the models explaining GAsw coupling to VPD, SWC, PPFD and to all three hydrometeorological drivers.	95
5.1	Description of variables and units in this study.	107
5.2	Results of the bi-variate linear models relating water use pa- rameters and water relations traits	117
5.3	Results of the bi-variate linear models relating water use pa- rameters, water relations traits, climate and tree height.	120

A.1	Summary table of the studies used in the analyses.	145
A.2	Anova summary of the LMM models.	148
A.3	Summary of the LMM models of Ln-Ratio (accuracy), Slope (proportional bias), Slope (ln-ln) (linearity) and Z-Cor (precision) as a function of Methods and Calibration material.	149
B.1	Data checks implemented in the first level of data quality control (QC1).	158
B.2	Description of site metadata variables.	159
B.3	Description of species metadata variables.	160
B.4	Description of environmental metadata variables.	161
B.5	Description of plant metadata variables.	161
B.6	Description of environmental metadata variables.	162
B.7	Data checks implemented in the second level of data quality control (QC2).	163
B.8	Datasets in the SAPFLUXNET database identified by numeric code, dataset code and site name.	164
B.9	Number of plants and number of datasets for each species present in the SAPFLUXNET database.	170
B.10	Number of plants per genus present in the SAPFLUXNET database.	173
C.1	SAPFLUXNET sites included in the study. Biome was calculated using Whittaker diagram.	180
C.2	SAPFLUXNET stand treatments included in the this study (Poyatos <i>et al.</i> 2020).	183
C.3	Summary table of plot level.	184
C.4	Table of equivalence between Whittaker biomes and the groups of biomes used in the study.	189
D.1	SAPFLUXNET plot treatments included in this study (Poyatos <i>et al.</i> 2020).	214
D.2	Species resume table.	215

D.3	Results of the linear models relating water use parameters calculated using G'_{Asw} to water relations traits.	218
D.4	Results of the linear models relating water use parameters to water relations traits using REW instead of SWC.	219
D.5	Results of the linear models relating water use parameters calculated using G'_{Asw} , water relations traits, climate and tree height.	220

“thesis” — 2020/12/29 — | 11:18 — page xii — #14

List of Figures

2.1	Graphical representation of the calibration performance metrics.	26
2.2	Distribution of the calibration performance metrics for each method.	29
2.3	Predictions of the LMM models of the four calibration metrics.	31
2.4	Relationship between the four calibration performance and wood density, for different sap flow methods.	33
2.5	Relationship between measured and reference sap-flux density (SFD) for different sap flow methods, studies and calibrations.	38
2.6	Relationship between measured and reference sap flow (SF) for different sap flow methods, studies and calibrations.	40
3.1	Overview of the SAPFLUXNET data workflow.	54
3.2	Geographic, bioclimatic and vegetation type distribution of SAPFLUXNET datasets.	58
3.3	Taxonomic distribution of genera and species in SAPFLUXNET.	59
3.4	Distribution of plants according to major taxonomic group and sap flow method.	61
3.5	Characteristics of trees and stands in the SAPFLUXNET database.	64
3.6	Duration and number of plants measured in each dataset.	67
3.7	Fingerprint plots showing hourly sap flow per unit sapwood area.	69
3.8	Summary of the availability of different environmental variables in SAPFLUXNET datasets.	70
3.9	Potential for upscaling species-specific plant sap flow to stand-level.	75

4.1	Bi-variate and uni-variate distributions of the coupling of G _{Asw} to the hydrometeorological drivers.	94
4.2	Global projection of G_{Asw} coupling to VPD, SWC and PPFD.	96
4.3	Relative importance (partial R ²) of the three hydrometeorological drivers of transpiration regulation.	97
5.1	Distribution of the plots from the SAPFLUXNET database included in this study.	108
5.2	Boxplots of water use parameters for both Angiosperms and Gymnosperms.	114
5.3	Bi-variate relationships between G_{REF} water relations traits.	116
5.4	Bi-variate relationships between β_{VPD} water relations traits.	118
5.5	Bi-variate relationships between β_{SWC} water relations traits.	119
5.6	Path analyses of species-specific water use parameters.	121
A.1	Representation of the cumulative number of studies using different sap flow methods between 1957 and 2017	142
A.2	Relationship between root mean square error (RMSE) and sap flux density.	143
A.3	Predictions of the LMM models calculated from least-squares means of the intercept (β_0) of the linear model.	144
B.1	Overview of the data QC process.	153
B.2	Structure of sfn_data objects.	154
B.3	Example screenshot of the app used for handling outliers and out of range values in time series.	155
B.4	Detailed geographic distribution of SAPFLUXNET datasets . .	156
C.1	SAPFLUXNET global scaling relationship between basal area and sapwood area. Shaded areas are 95% model confidence interval.	176
C.2	Bioclimatic distribution of the SAPFLUXNET datasets used in the study.	177
C.3	Global projection of climatic, soil and stand structure variables.	178

C.4 Log relationships of the three environmental variables estimated with the TOTAL model (VPD + SWC + PPFD) and grouped by biome.	179
D.1 PCA plot of water relations traits using imputations.	193
D.2 Water use parameters at the species level.	195
D.3 Species G_{Asw} responses to VPD. Each species have different curves representing distinct levels of SWC (from dark to light, 0.1, 0.2, 0.3 [$m^3 m^{-3}$]).	202
D.4 Species G_{Asw} responses to SWC. Curves are fitted using a VPD reference level of 1 kPa.	209
D.5 Scatterplot between G_{REF} and β_{VPD} parameters.	210
D.6 Species’ climatic variables and water relations traits relationships.	211
D.7 Species’ climatic variables and water use parameters relationships.	212
D.8 Boxplots of water relations traits for angiosperms and gymnosperms.	213

“thesis” — 2020/12/29 — | 11:18 — page xvi — #18

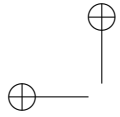
Abstract

Understanding how climate affects species' distribution and performance is a central issue in ecology since its origins. In last decades, however, the interest in this question has been reactivated by the current context of climate change. Species Niche Modelling has been widely used to assess shifts in species distribution and to test the relationship between species' climatic niche and species physiological and demographic performance, implicitly assuming that species occurrence portrays the environmental and biotic species' suitable conditions. Nevertheless it is still largely undetermined whether these models can portray population and community responses, particularly in relation to extreme climatic episodes.

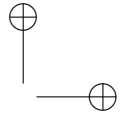
In this thesis I aim at exploring the capacity of niche modelling to predict species decay under extreme climatic conditions, particularly droughts, addressing some constraints of this approach and proposing possible solutions. To achieve this goal, I counted with 3 vegetation decay datasets measured in the Spanish SE after the extreme drought year 2013-2014. Two of these datasets were based on defoliation sampling of individual plants belonging to more than 40 semiarid shrubland species (chapters 2, 4 and 5), while the other one was based on regional compiled data of *Pinus halepensis* L. affection in plots of 1km^2 (chapter 3). In second chapter I used different Species Distribution Model (SDMs) algorithms to estimate species' climatic suitability before (1950-2000) and during the extreme drought, in order to test the possible correlation between suitability and decay, and whether the existence of this relationship depended on the applied SDM algorithm. I consistently found a

positive correlation between remaining green canopy and species' climatic suitability before the event, suggesting that populations historically living closer to their species' tolerance limits are more vulnerable to drought. Contrastingly, decreased climatic suitability during the drought period did not correlate with remaining green canopy, likely because of extremely low climatic suitability values achieved during the exceptional climatic episode. In order to test whether this extremely low suitability values could derive as a consequence of only considering climatic averages when calibrating SDMs, in the third chapter I developed a method to include inter-annual climatic variability into niche characterization. I then compared the respective capacities of climatic suitabilities obtained from averaged-based and from inter-annual variability-based niches to explain demographic responses to extreme climatic events. I found that climatic suitability obtained from both niches quantifications significantly explained species demographic responses. However, climatic suitability from inter-annual variability-based niches showed higher explanatory capacity, especially for populations that tend to be more geographically marginal. In the fourth chapter I tried to overcome the inability of the SDMs to predict populations decay during extreme conditions, as observed in the second chapter, by using Euclidean distances to species' niche in the environmental space. I compared the capacities of both population distances in the climatic environmental space and population climatic suitability derived from SDMs to explain population observed physiological and demographic responses to an extreme event. Additionally, I tested such relationship in populations located in three different bedrock sites, corresponding to a gradient of water availability. I found that SDMs-derived suitability failed to explain population decay while distances to the niche centroid and limit significantly explained population die-off, highlighting that population displaced farther from species' niche during the extreme episode showed higher vulnerability to drought. The results also suggested a relevant role of some bedrocks buffering species decay responses to extreme drought events mainly according to soil water holding capacity. Finally, in the fifth chapter, I used species niche characterizations in the environmental space and demographic data to address the impact of extreme events

at community level. Particularly, I estimated the community climatic disequilibrium before and after a drought episode along a gradient of water availability in three bedrock types. Disequilibrium was computed as the difference between observed climate and community-inferred climate, which was calculated as the mean of species' climatic optimum weighted by species abundance collected in field surveys. I found that extreme drought nested within a decadal trend of increasingly aridity led to a reduction in community climatic disequilibrium, particularly when combined with low water-retention bedrocks. In addition, community climatic disequilibrium also varied before the extreme event across bedrock types, according to soils water-retention capacity. In conclusion, by developing different techniques, derived from species distribution, that characterize climatic accuracy at population and community level, this work reveals the capacity of species climatic niche to explain demographic responses under climate change-induced episodes of extreme drought.

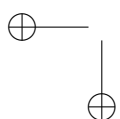


“thesis” — 2020/12/29 —| 11:18 — page xx — #22

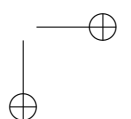


—

—



|



— “*No one will protect what they don’t care about;
and no one will care about what they have never experienced*” —

David Attenborough

“thesis” — 2020/12/29 — |11:18 — page xxii — #24

1

Introduction

1.1 Transpiration and earth system functioning

Transpiration is a dynamic process in which water from plants evaporates and diffuses into the atmosphere. Transpiration occurs as a result of the need to incorporate carbon dioxide for assimilation in photosynthesis. This is because the carbon dioxide molecule is larger than the water molecule, and when it enters the plant tissues, water escapes through the same pathway. Given that plants require proper hydration to maintain physiological processes, water loss by transpiration determines the need to absorb and transport large quantities of water from the soil (Prasad et al. 2008??). Yet, transpiration also contributes to regulate leaf temperature, keeping it within an tolerable range for leaf functioning. Thus, carbon uptake and transpiration water loss are inexorably linked and have to be dynamically controlled to avoid desiccation and maintain plant function. This control occurs on the long-term by changes in plant structure and anatomy, and in the short-term through the regulation of stomatal aperture in the leaves (Jones 1998). Stomata are small epidermal valves with a pore aperture that is usually regulated by plant water status and hydraulic characteristics (Buckley 2005, Buckley 2019). Stomata close to protect plants from excessive water loss when atmospheric humidity or water availability drops, but this closure increases physiological stress due to reduced carbon gain (Bréda et al. 2006, McDowell 2008). Transpiration, which is therefore determined in just a few micrometres in the leaves, but is the outcome of the plant integrated hydraulics and chemical signalling upstream, has crucial implications for biological processes at the whole-plant level such as growth, competition and survival. These influences scale up to the population and species level and determine the water, carbon and energy cycles from the local to the global level (Bonan et al. 2003), which are essential cycles for the maintenance of life on Earth. Therefore, due to the relevance of transpiration patterns on climate and Earth system function it is crucial to correctly understand and model stomatal regulation and vegetation water use.

Within the global hydrological cycle, vegetation transpiration accounts for about $45,000 \text{ km}^3 \text{ yr}^{-1}$ of water flowing from the soil to the atmosphere

1.1. Transpiration and earth system functioning

3

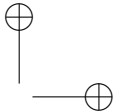
(Schlesinger and Jasencko 2014), which represents around a 40% of global terrestrial precipitation (Oki and Kanae, 2006). Vegetation is thus the major user of the precipitation and directly affects surface runoff and subsurface recharge. Transpiration accounts for about 61% of total terrestrial surface evapotranspiration (which is the sum of transpiration and the abiotic evaporation from canopy and soil surfaces). However, this proportion is highly variable within and among regions (Schlesinger and Jasechko 2014), which is largely explained by the different vegetation structures (e.g., leaf area index, Wei et al. 2017) and water use strategies. Total land surface evapotranspiration and its partition between transpiration and evaporation drives other biosphere processes, such as vegetation dynamics or energy balance, that in turn produce feedbacks on evapotranspiration. For instance, transpiration is determinant of energy balance impacting in land surface temperature through changes in latent heat, and mediates land-atmosphere feedbacks via soil moisture depletion (Miralles et al. 2018). It also promotes clouding formation (Aemisegger et al. 2014) which alters regional albedo and influences large scale precipitation regimes (Spracklen et al. 2012).

At the same time, climate affects vegetation physiology and how it regulates transpiration. Different tree species have a specific control of their stomata in response to environmental changes (Klein et al., 2014), which means that the distribution of these species and their physiological traits will have consequences for ecosystem functioning and, ultimately, for global cycles. Environments with high regional water availability and resources generally support highly diverse and productive vegetation, whereas unfavourable environments support slow-growing vegetation and restrict species richness. Fast-growing plants tend to have higher transpiration rates (Smith and Sperry 2014), and therefore accelerate the hydrological cycle. There is a large global heterogeneity both in space and time in water availability distribution, which drives heterogeneity in vegetation distribution and feedbacks on the spatio-temporal variability in transpiration patterns.

In addition to the water and energy cycles, transpiration is intimately linked to the carbon cycle through stomatal gas exchange. The carbon assimilated by plants in photosynthesis depends mainly on the internal leaves

$[CO_2]$, which enters the leaves by diffusion at a rate controlled by stomatal conductance (Ball et al. 1987 ??). At the plant level, carbon is used for growth and metabolism but drought-driven reductions in stomatal conductance limit the amount of carbon fixed by vegetation (Bréda et al. 2006). Drought stress constrains ecosystem transpiration and photosynthesis, reducing the potential CO_2 uptake by terrestrial ecosystems (van der Molen et al. 2011). Transpiration could also be affected by atmospheric $[CO_2]$, because as atmospheric $[CO_2]$ increases, the ratio between carbon intake and water loss increases so that plants would theoretically maintain similar photosynthetic rates using less water, leading to more efficient water use (Keenan et al. 2013 ??). However, CO_2 effects on transpiration seem to be complex and ‘water savings’ not as clear (Walker et al. 2020). In addition, current $[CO_2]$ are approaching saturation levels of the Rubisco enzyme, at least for the C_3 plants, which implies that future increases in atmospheric $[CO_2]$ will have progressively less impact on water use efficiency, and therefore on CO₂ transpiration constrain (Flexas et al. 2015 ??, Sage 2002 ??).

Stomatal conductance (g_s) is therefore a central component of models characterizing land surface processes, since it is the main regulator of water, energy, carbon and nutrient fluxes between the terrestrial biosphere and atmosphere (Knauer et al. 2015, Mencuccini et al 2019). Thus, g_s is used in many ecosystem and terrestrial biosphere models at multiple spatial and temporal scales. For example, it is included in Land Surface Models to resolve the effects of vegetation (Matheny et al. 2017) on global climate models (Wang and Dickinson 2012, Fisher and Koven 2020), or in Dynamic Global Vegetation Models to predict plant dynamics and vegetation distribution and changes under future climates (Smith et al. 1992). Most ecosystem and terrestrial biosphere models are parametrized to separately estimate transpiration –calculated using diverse formulations of stomatal or canopy conductance (G) (Knauer et al. 2015)–, soil evaporation and evaporation of water intercepted by the canopy or the litter layer. The mechanisms that regulate stomatal behaviour are still not completely understood, which is reflected in the different ways these processes are implemented in models. There are several approaches for modelling g_s or G , from semi-empirical (Damour et al.

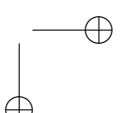
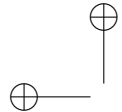


2010??), mechanistical (Chuang et al. 2006) or models employing optimality criteria (Wang et al. 2020). Early models, represented vegetation g_s and G responses with a static set of parameters across plant functional classes or climates (Manzoni et al. 2011). This oversimplification of diverse species into functional classes leads these models to great uncertainties (Poulter et al. 2011). Therefore, new modelling approaches are moving towards a more versatile characterization of vegetation which could represent the stomatal responses to environment emerging from an integration of hydraulic traits (which are increasingly available at the species level, Mencuccini et al. 2019, Sanchez-Martinez et al. 2020) at the whole-plant level. There is an increasing recognition that water transport from roots to leaves play a key role defining plant water use strategy and stomatal conductance regulation.

1.2 Transpiration across scales

1.2.1 Water transport in plants

The water in soil and plants moves under high tensions following the framework of the cohesion-tension theory (Tyree 1997). Water flow (J [$cm^3 s^{-1}$]) between any two points of the soil-plant-atmosphere continuum is given by its difference in Ψ ($\Delta\Psi$) and the resistance –or its inverse, the hydraulic conductance (K_H [$cm^3 s^{-1} MPa^{-1}$])– that the system exerts to the flow between these two points. This relationship can be expressed as $J = K_H \cdot \Delta\Psi$ which is an expression of Darcy’s law (Scheidegger 1974). Within the plant, water moves along a gradient of water potential (Ψ ; normally negative in plant tissues) from high Ψ in the soil (i.e. less negative) to lower Ψ (i.e. more negative) in the leaves. Similarly, water diffuses out of the leaf and into the atmosphere following a gradient of water vapour concentration ($\Delta\Psi$, the difference in water mole fraction in the air, which could also be expressed as water potential, see e.g. Tyree & Ewers 1991). Water potential –measured as water pressure in Pascals (Pa)– is the energy of water per unit volume compared to pure water and, along the soil-plant-atmosphere system, is the sum of hydrostatic potential, osmotic potential and gravitational potential. Hydrostatic potential is



the physical pressure that the system exerts to the water and is positive inside turgid living cells but negative inside xylem conduits, a tissue conformed by dead cells and where water is under tension. The osmotic potential is related to a difference in solute concentration across a semi-permeable membrane, where the solution with more solutes has a lower Ψ . The gravitational potential arises because water ascent from soils to leaves must overcome gravity, but it is only important for tall trees (Franks 2004).

Transport of water in unsaturated soil also follows mass conservation and Darcy’s law. Water enters the roots mainly due to a gradient in hydrostatic pressure maintained largely by the transpiration stream (Passioura 1988). As soils dry out, the Ψ of soils decreases because the matrix potential, i.e. the negative hydrostatic potential produced by the force by which water molecules are held on surfaces, becomes more negative as the water layer covering soil particles becomes thinner. This decrease in soil Ψ produces a parallel decrease in plant Ψ in order to maintain water movement into the plant. Water absorbed by roots reaches xylem vessels, which by the hydrostatic pressure gradient generated by water evaporation in the leaves transported downstream. Water transport in plant tissues is therefore controlled by the combination of water potentials and plant-specific hydraulic conductivity (k), which is a measure of conductance per unit path length. Xylem k is in turn dependent on water potential $k(\Psi)$, since cavitation and subsequent embolism formation occur at low Ψ , when the plant is under drought stress. Xylem k declines non-linearly with Ψ typically following a sigmoidal shape (vulnerability curve), which is characteristic of each species due to specific anatomical traits of the xylem (Venturas et al. 2017). Once in the leaves, water from the mesophyll, epidermis and guard cells evaporate into the stomatal cavity. The difference in Ψ between the nearly water saturated stomatal cavity and the atmosphere represents the steepest potential gradient in all the soil-plant-atmosphere continuum. It is in the plant-atmosphere interface, therefore, where the control of water loss is critical to avoid dangerous tensions in the plant tissues. Stomatal control and its link with plant hydraulics—but also anatomy, size, density and location of stomata—determine plant water status (McCulloh et al. 2019). The mechanistic control of stomata

1.2. Transpiration across scales

7

in response to environmental drivers is still not fully understood, although it appears quite evident that there are feedback processes (and probably feedforward processes) between stomatal conductance and leaf water status (Jones 1998, Franks 2004), and hormonal or chemical signalling from the roots to the leaves (Tardieu et al. 1993 ??).

Quantification of transpiration and stomatal control by leaves and canopies also require a careful consideration of aerodynamic processes involved in the vapour transfer between the leaves and the atmosphere. Leaf boundary layer conductance also controls the vapour transport between the leaf and the surrounding air, as this conductance occurs in series with g_s . Leaf boundary layer conductance depends on atmospheric turbulent flux inside the canopy and it is generally much higher than g_s , especially for trees and forests under well-ventilated conditions. Under these conditions, canopies are considered well-coupled to the atmosphere and transpiration is largely controlled by stomata. However, for large-leaved species under poor ventilation boundary layer conductance can be similar to stomatal conductance and this can affect estimations of the degree of stomatal control based on transpiration measurements. When dealing with whole plants and canopies, not with individual leaves, the sum of all the plant stomatal conductances and the boundary layer conductance can be considered as the whole-plant canopy conductance (Jarvis & McNaughton 1986, Raupach & Finnigan 1988).

1.2.2 Upscaling to the stand and ecosystem levels

The quantification of water transport in the soil-plant-atmosphere continuum from a micro-scale perspective (i.e. at the stomata-level) is a complex challenge due to the heterogeneity of the transporting medium and the different temporal scales of the water flux drivers (Katul et al 2007). Therefore, most studies on plant water transport have been undertaken at the organ (leaves) and the plant levels, observing emergent macroscopic responses of transpiration to environmental changes. Upscaling from the leaf to the ecosystem level requires consideration of processes that occur at the level of individual

plants such as hydraulics. In addition, by using a whole-plant level perspective, the micro-environmental and physiological gradients within the canopy are integrated, so we can focus on compositional, size-related patterns that influence the upscaling to the ecosystem. However, there is further challenge when trying to upscale both in space and time, due to the heterogeneity of the distribution of processes and the non-linearities of whole-plant responses shaped by the link between physiology and ecosystem functioning (Jarvis 1995). Thus, to scale up to ecosystem, regional or global level, we should make simplifications to allow a proper estimation of those processes distributions, either by a representation of the vegetation by functional types, or a description by hydraulic or functional traits. Both vegetation classes and traits are suitable for scaling up, but the latter is a more flexible approach since they are continuous variables, which overcome the rigidness of vegetation classes (i.e. functional type or species), and also allows to include intra-species environmental gradients and variability, and diversity within the ecosystem (Anderegg et al. 2018).

1.3 Transpiration quantification

There are several methods to quantify evaporative fluxes from the leaf to the ecosystem level (Shuttleworth 2008), which differ in their spatial and temporal domain and in their ability to separately measure transpiration and evapotranspiration. At the ecosystem level, continuous sub-daily estimations of evapotranspiration are usually performed using micrometeorological methods such as Bowen ration energy balance (Bowen 1926) and, mainly, Eddy covariance methods (Brutsaert 1982), which are based on the measure of turbulence fluxes of latent heat and moisture (see Wang and Dickinson 2012, Kool et al. 2014, Stoy et al. 2019, for further details). These methods have been standardized, and currently there is a global network of measuring stations (FLUXNET) that includes more than 900 sites worldwide (Pastorello et al. 2020). The FLUXNET network initiative provides a valuable tool to study global land hydrological fluxes. However, micrometeorological methods do not allow to easily and directly separate transpiration from evaporation

1.3. Transpiration quantification

9

fluxes, thus requiring partitioning isotopic methods (Kool et al. 2014) or complex algorithms to isolate the contribution of transpiration (Nelson et al. 2020). Since some seminal works such as Sellers (1985), several attempts have been made to estimate regional transpiration and evapotranspiration patterns using remote sensing (Miralles et al. 2011, Miralles et al. 2016). Although remote sensing is the best method for containing continuous estimates of transpiration at large spatial scales, these estimations (e.g., GLEAM, Miralles et al. 2011) are indirect and based on the combination of remotely-sensed variables and models of vegetation responses and surface energy balance.

Since the 1970s, several methods have been developed to independently measure plant level transpiration, however most of them are impractical in the field, either because of their low temporal resolution and low ecological representativeness such as leaf gas exchange methods (Evans & Santiago 2014), or because of their limited use on a broad scale due to their elevated cost such as whole-tree gas exchange chambers (Corelli & Magnanini 1993) or lysimeters (Howell 2005). Yet one method that can be applied continuously, unsupervised, for extended periods and at relatively low cost, is the measurement of sap flow rate (from now on Sap Flow Methods, see **Chapter 2 and 3** for details). Sap flow methods are thermal-based techniques that were first developed by Huber (1932), which have diversified into different methodologies since then (e.g. Cermak 1973, Swanson and Whitfied 1981, Granier 1985). Sap flow methods basically apply to woody plants and estimate transpiration by measuring the water flowing through stems (Schulze et al. 1985). To do that, semi-invasive probes are installed in the trunk and heat is applied as a tracer of the sap flux. The quantification of the flux can be largely characterized using 4 major variants: heat balance, heat dissipation, heat pulse or heat field deformation methods, which follow different operation principles, probe configuration, and method specific flux quantification (see **Chapter 2**, Vandegehuchte and Steppe 2013). Despite their advantages, all sap flow methods suffer from potential methodological issues, they assume that the sensors installation does not alter the sap flow, and they rely on a correct determination of sapwood cross-sectional area to scale punctual measurements to the whole-tree level (Vandegehuchte and Steppe 2013, see **Chapter 2**). However,

most of these issues can be addressed using specific calibration and applying suitable corrections (e.g. Clearwater et al. 1999, Richards et al. 2020). Also, sap flow methods error have been associated with wood properties but not consistent patterns have been found (Wullschleger et al. 2011).

Despite the potential of sap flow measures, the lack of a global compilation of sap flow measurements has precluded their use to scale up plant water use strategies and generalize actual transpiration responses to environmental drivers, at the regional or global scale. Similarly, a global sap flow database would allow a much better characterization of species’ water use strategies and the underlying functional traits. Seminal works of sap flow data synthesis have only been able to focus on answering partial questions, such as the characterization of transpiration responses along climatic gradients within a species (Poyatos et al. 2007), or across a few species, typically addressing responses to single hydroclimatic factors (Oren et al. 1999), or the various studies focused on maximum water use (Manzoni et al. 2013). However, increased data availability and the growing trend of data sharing for reuse, has paved the way to the creation of a global collaborative database of sap flow measurements (Poyatos et al. 2016). A preliminary survey conducted in December 2015 showed that potential contributors could provide data sets for >160 species and >120 globally distributed sites (Poyatos et al. 2016). Thus, in 2016 the design of the first global database of sap flow measurements (SAPFLUXNET) was initiated, with the intention of gathering, harmonizing and homogenizing the largest possible number of sap flow data sets at the whole-plant level together with hydrometeorological variables at the stand-level, and making them freely available to the scientific community.

1.4 Transpiration in a changing world

Forests are changing rapidly in response to climate change and all models predict that these changes will accelerate in the future (Anderegg et al. 2020, McDowell et al. 2020). Importantly an improved understanding of the regulation of tree water use is key to assess both species vulnerability and the functional changes expected under new climate regimes (Choat et al. 2018,

1.4. Transpiration in a changing world

11

Brodribb et al. 2020). The SAPFLUXNET database will allow us to study, for the first time, the regulation of whole-plant transpiration to environmental changing conditions from a global perspective. It will enable the observation of broad patterns of the water use strategies of woody plants and generate the knowledge to improve predictions of vegetation responses to future climate scenarios. A first approach to understand global dynamics of regulation of transpiration at the whole-plant level can be achieved by using semi-empirical models of sap flow or canopy conductance (G) responses to key environmental drivers, including atmospheric vapour pressure deficit, soil moisture and solar radiation. This approach would allow us to parameterize the plant’s transpiration response, obtaining species-specific maximum values and sensitivities to hydroclimatic variables, and thus characterizing the corresponding water use strategies, their spatial distribution and their physiological and ecological determinants. In addition, this approach may help to study which hydrometeorological variables are the main drivers of the regulation of transpiration globally, as well as its bio-geographical patterns. In this way, modelling efforts, such as LSMs, could be optimized and focused on the responses to the environmental variables with greater predictive power.

It is expected that water transport through the soil-plant-atmosphere and its regulation require of a coordination between stomatal behaviour and hydraulic traits (Meinzer 2002). This coordination is expected because vegetation has evolved to be adapted to the conditions of its typical climate (Sanchez-Martinez et al. 2020), achieving a balance in its traits in such a way that they optimize the transport of water and nutrients while maximizing CO_2 uptake and fitness (Manzoni et al. 2013). This coordination of traits at the organ level would be a good basis to study the water use strategy that entire plant use to cope with drought, and would pave the way to trait-based models of vegetation water use at large spatial scales (Eller et al. 2020, Sperry et al. 2019). Thus, if there was a clear correlation between hydraulic traits (some of which are relatively easily to measure) and water use strategies, they could be used for parameterization of G on a continuous basis.

Therefore, a better understanding of transpiration and its regulation is key under the Earth’s system uncertainty added by global change and the

expected increase in drought conditions (Dai 2013). It is expected that evaporation and precipitation will be globally intensified but unevenly distributed, which could trigger large forest mortality events, even in cold or wet places (Allen et al. 2015). This motivates further work to improve the predictability of global transpiration estimates and vegetation drought responses, in order to obtain better predictions of vegetation dynamics and climate, so as to assist in decision-making for water resource management, climate change mitigation and forest management.

1.5 Research aims and outline

In this thesis I address the question of whether we can find global patterns in daily transpiration regulation at the plant level in response to hydrometeorological drivers using a global database of sap flow measurements. The ultimate goal is to characterize the global variation in plant water use strategies and to relate this variation to ecosystem eco-hydrological conditions and to species traits, emphasizing plant water relations and hydraulics (**Chapter 4 and 5**). Prior to this synthesis work, I first assessed the suitability of sap flow methods as reliable estimators of the variation in plant water use (**Chapter 2**). And, last, but not least, together with the rest of the members of the sapfluxnet core team, I worked on the compilation and harmonization of the datasets in SAPFLUXNET database, which is also presented as part of this thesis (**Chapter 3**). The specific objectives for each research chapter are listed bellow:

Chapter 2: To test whether there is systematic variability in sap flow measurements associated with the sap flow method employed. Here, (i) I compile all sap flow methodological calibrations obtained under laboratory or field conditions and perform a meta-analysis to obtain the mean systematic bias, the proportional bias, the linearity, and the precision of each method. In addition, I test whether (ii) the performance of each method is associated to wood anatomy or wood density.

Chapter 3: To introduce SAPFLUXNET and explain how the database was built from individual data sets contributed by the scientific

community. I (i) explain the data structure design, the data harmonization and quality control process and the overall workflow, (ii) summarise the main hydrometeorological drivers and metadata documented in each dataset, and (iii) discuss the potential applications of the database, its limitations, and future perspectives.

Chapter 4: To test the absolute and relative importance of vapour pressure deficit, soil moisture and solar radiation as drivers of tree transpiration at the global scale. I quantify the predictive capacity of each hydrometeorological driver of plant-level canopy conductance (G) using empirical models. I explain the differences in hydrometeorological coupling of G (i) across biomes and (ii) their biogeographical patterns as a function of climate, soil properties and vegetation structure.

Chapter 5: To explore water use strategies across tree species using a trait-based approach, by parameterizing the response of G to vapour pressure deficit and soil water content at the species level and for major taxonomic groups (Angiosperms vs. Gymnosperms). I aim to understand how water use strategies emerge from the covariation between traits, accounting for the influence of tree size and climate. I also characterize the relationships between transpiration regulation parameters and key hydraulic and allocation traits among species, controlling also for the effect produced by differences in precipitation.

* A reproducible copy of the thesis can be found online at <https://github.com/vflo/PhD>

“thesis” — 2020/12/29 —| 11:18 — page 14 — #38

2

A synthesis of bias and uncertainty in sap flow methods

Victor Flo, Jordi Martinez-Vilalta, Kathy Steppe, Bernhard Schuldt, Rafael Poyatos

Abstract

Sap flow measurements with thermometric methods are widely used to measure transpiration in plants. Different method families exist depending on how they apply heat and track sapwood temperature (heat pulse, heat dissipation, heat field deformation or heat balance). These methods have been calibrated for many species, but a global assessment of their uncertainty and reliability has not yet been conducted. Here we perform a meta-analysis of 290 individual calibration experiments assembled from the literature to assess calibration performance and how this varies across methods, experimental conditions and wood properties (density and porosity types). We used different metrics to characterize mean accuracy (closeness of the measurements to the true, reference value), proportional bias (resulting from an effect of measured flow on the magnitude of the error), linearity in the relationship between measurements and reference values, and precision (reproducibility and repeatability). We found a large intra- and inter-method variability in calibration performance, with a low proportion of this variability explained by species. Calibration performance was best when using stem segments. We did not find evidence of strong effects of wood density or porosity type in calibration performance. Dissipation methods showed lower accuracy and higher proportional bias than the other methods but they showed relatively high linearity and precision. Pulse methods also showed significant proportional bias, driven by their overestimation of low flows. These results suggest that Dissipation methods may be more appropriate to assess relative sap flow (e.g., treatment effects within a study) and Pulse methods may be more suitable to quantify absolute flows. Nevertheless, all sap flow methods showed high precision, allowing potential correction of the measurements when a study-specific calibration is performed. Our understanding of how sap flow methods perform across species would be greatly improved if experimental conditions and wood properties, including changes in wood moisture, were better reported.

2.1 Introduction

Quantifying transpiration of vegetation is of major importance for hydrological, ecological, and agricultural sciences, since it represents 60-80% of the water that returns from the land surface to the atmosphere (Jasechko et al. (2013); Schlesinger & Jasechko (2014); Wei et al. (2017)). The study of transpiration and its environmental sensitivity is essential to understand vegetation water cycling (D. C. Frank et al. (2015); Konings, Williams, & Gentile (2017); Novick et al. (2016)) and to forecast changes in vegetation functioning and composition under climate change (C. D. Allen, Breshears, & McDowell (2015)). Addressing these questions requires non-destructive measurements of whole-plant transpiration at multiple timescales (S. D. Wullschleger, Meinzer, & Vertessy (1998)). Thermal methods of sap flow measurement show a number of advantages over other methods such as those based on isotopes tracing or leaf gas exchange (D. M. Smith (1995)), and have become the most widely used approach to estimate tree-level transpiration (Poyatos et al. (2016)) (Fig. A1). When compared against independent estimates of evapotranspiration components, sap flow methods have provided reasonable qualitative and quantitative results (Diawara, Loustau, & Berbigier (1991), Hogg et al. (1997), Kool et al. (2014), Schlesinger & Jasechko (2014), Zhang, Manzoni, Katul, Porporato, & Yang (2014), but see K. B. Wilson, Hanson, Mulholland, Baldocchi, & Wullschleger (2001), A. C. Oishi, Oren, & Stoy (2008), T. Shimizu et al. (2015)). However, sap flow measurements may be subject to various potential sources of error. Some of these errors are related to scaling sap flow variability both within trees and from tree to stand level (T. J. Hatton, Moore, & Reece (1995); Hernandez-Santana, Hernandez-Hernandez, Vadeboncoeur, & Asbjornsen (2015); Mitchell, Irwin, Flanagan, & Karron (2009)), while others are related to intrinsic limitations of the methods or to how these methods are applied (see Vandegehuchte & Steppe (2013)). Although these biases have been studied, they have not yet been quantified globally and there is no conclusive assessment of how they differ across methods or species characteristics, including wood properties (Poyatos et al. (2016)).

Sap flow methods (Vandegehuchte & Steppe (2013)) can measure sap

flow rate (SF, g h⁻¹ or equivalent units) or sap flux density (i.e., sap flow rate per unit sapwood area, SFD, cm³ cm⁻² h⁻¹ or equivalent units) in a plant’s conductive tissue and can be classified in four families depending on how they heat the sapwood and how they measure sapwood temperatures: (1) the Dissipation family, including thermal dissipation (TD; Granier & Une (1985)) and transient thermal dissipation (Do & Rocheteau (2002), TTD (????)) methods, which measure the dissipation of heat from a heated probe inserted in the sapwood with reference to a reference, non-heated probe; (2) the Pulse family, including the compensation heat pulse (CHP; Swanson & Whitfield (1981)), heat ratio (HR; S. S. Burgess et al. (2001)), T-max (Y. Cohen, Fuchs, & Green (1981)), calibrated average gradient (CAG; Testi & Villalobos (2009)), sapflow+ (SF+; Vandegehuchte & Steppe (2012b), Vandegehuchte, Steppe, & Phillips (2012)), single probe heat pulse (SPHP; (????)) and dual heat pulse methods (Dual; Pearsall, Williams, Castorani, Bleby, & McElrone (2014)), which all apply heat in pulses and track sapwood temperature changes caused by thermal convection and conduction; (3) the Field family, including the heat field deformation (HFD; N. Nadezhina (2018); N. Nadezhina, Čermák, & Nadezhdin (1998)) and its derivatives, which measure the shape changes of a continuous heat field in the sapwood, using axial and tangential probes; and (4) the Balance family, represented by stem heat balance (SHB; (????); Sakuratani (1981); (????)) and trunk heat balance (THB; Čermák, Kučera, & Nadezhina (2004); Čermák 1973) methods, which measure the energy balance across a heated wood section. This latter family is the only one directly measuring sap flow rate, while all the others measure sap flux density.

Methodological errors in sap flux density measurements may be caused by wounding following probe insertion into the sapwood (except for the miniaturized non-invasive ones; see (Michael J. Clearwater, Luo, Mazzeo, & Dichio (2009); Hanssens, De Swaef, Nadezhina, & Steppe (2013); Schreel & Steppe (2018)), biological variation in wood parameters and diverse raw data processing approaches (A. C. Oishi, Hawthorne, & Oren (2016); Peters et al. (2018); Vergeynst, Vandegehuchte, McGuire, Teskey, & Steppe (2014)). Wounding affects heat and water transport and thus may disrupt sap flow measurements (Barrett, Hatton, Ash, & Ball (1995); S. S. Burgess et al. (2001); S. Green,

Clothier, & Perie (2009); Steve Green, Clothier, & Jardine (2003); S. R. Green & Clothier (1988); Steppe, Vandegehuchte, Tognetti, & Mencuccini (2015)), especially during long-term installations (S. Marañón-Jiménez et al. (2018); A Wiedemann, Jiménez, Rebman, Cuntz, & Herbst (2013)). While wound corrections have been available for a long time for some Pulse family methods (Steve Green et al. (2003); Swanson & Whitfield (1981)), they have only become recently available for other methods such as TD (Andreas Wiedemann et al. (2016)). Sap flux density methods are also affected by changes in radial patterns, which are not constant over time, so these methods have to measure the entire sapwood depth by sufficiently large probes, or by individual measurement points at different depths (T. Hatton (1990)). Although some methods have a more solid theoretical background based on the physics of thermal transport (Pulse and Balance methods), all of them rely on a certain degree of empiricism, which may introduce errors caused by biological variability and/or variation in signal processing approaches: species-specific empirical calibrations in Dissipation methods (S. Fuchs, Leuschner, Link, Coners, & Schuldert (2017)), zero-flow determination or baselining (Ping Lu, Urban, & Zhao (2004); Peters et al. (2018)), and different parameterization of thermal sapwood properties in Pulse and Field methods (Chen, Miller, Rubin, & Baldocchi (2012)). These thermal sapwood parameters could change over time, introducing further errors in the measurements (e.g. changes in stem water content; Vergeynst et al. (2014)). Within the Balance family, those using external heating do not suffer from potential errors due to wounding, but they all require zero-flow determination (D. Smith & Allen (1996)). Balance methods have often been considered to better integrate spatial variability in sap flow (Čermák et al. (2004)), but whether they perform generally better than sap flux density methods remains unknown.

Other errors in sap flow measurement may result from not accounting properly for method-specific assumptions. For many sap flow methods, natural temperature gradients (NTG) need to be minimized and/or accounted for to obtain unbiased estimates of sap flow (Reyes-Acosta, Vandegehuchte, Steppe, & Lubczynski (2012); Vandegehuchte, Burgess, Downey, & Steppe (2015)). Incorrect sensor geometry (misalignment) affects the accuracy of the

measurements (S. S. Burgess et al. (2001); Cabibel & F (1991); Ren et al. (2017); Swanson (1983); Swanson & Whitfield (1981)). Other application errors, such as those arising from the incomplete contact of TD probes with the sapwood (Michael J Clearwater, Meinzer, Andrade, Goldstein, & Holbrook (1999)) are difficult to prevent, though they can be reasonably corrected a posteriori (e.g. Clearwater correction, K. R. Hultine et al. (2010); Paudel, Kanety, & Cohen (2013)). Despite that these application errors have been well described in individual studies, a general quantification of these errors for the most employed sap flow methods is currently lacking.

Comparisons of sap flow measurements with respect to a reference method (hereafter, for simplicity, ‘sap flow calibrations’) are usually aimed at obtaining species-specific calibrations (Vandegehuchte & Steppe (2013)) to assess different parameterizations of wood thermal properties (Vandegehuchte & Steppe (2012a)) or to validate empirical corrections (e.g., wounding, NTG, changes in water content, misalignment; S. S. Burgess et al. (2001); Vergeynst et al. (2014)). Although few studies calibrate multiple sap flow methods for different species (S. Fuchs et al. (2017)), collectively these calibration studies have shown the inherent limitations of different sap flow methods to deal with low (Steve Green et al. (2003)) or high flows (S. Green et al. (2009)). Variability and quality in calibration performance may also be related to specific wood properties such as wood density (Suleiman, Larfeldt, Leckner, & Gustavsson (1999); Wullschleger, Childs, King, & Hanson (2011)), especially given the fact that wood density enters the calculation of sap flux density for some methods (Vandegehuchte & Steppe (2012a)) and co-varies with wood moisture content (Looker, Martin, Jencso, & Hu (2016)). Because thermal properties of wood are dependent on both, i.e. wood density and moisture content (MacLean (1941)), they might additionally be influenced by wood anatomical traits such as wood porosity type, i.e. coniferous, diffuse-porous or ring-porous wood. In conifers, however, no clear effects of wood density on calibration variability have been reported (Peters et al. (2018)). Therefore, a quantitative synthesis of sap flow calibrations, accounting for variation caused by different flow ranges and wood properties is needed to generalize and understand the patterns observed in individual calibration studies.

Here, we compile a global database of published sap flow calibrations to quantify the measurement errors associated with different sap flow methods and to assess the factors underlying variability across methods. In assessing calibrations, we distinguished between mean systematic bias (accuracy), a measure of the average degree of closeness of the measurements to the value obtained with a reference method; proportional bias, which occurs when the magnitude of the error is a function of the flow; linearity in the relationship between measurements and values obtained with a reference method; and precision, a measure of reproducibility and repeatability. Our main objective is to assess the differences in accuracy, proportional bias, linearity and precision among methodological families and individual sap flow methods; in addition, we will determine whether calibration performance across methods is associated with species wood traits (wood density and porosity type).

2.2 Material and methods

2.2.1 Sap flow calibration datasets

We retrieved sap flow calibration studies of the seven most common methods (CHP, T-max, HR, HFD, SHB, TD, TTD) applied on trees, palms or lianas, using standard database searching tools (i.e. Scopus, Web of Science and Google Scholar). The search was conducted in June 2017 applying the following keywords: sap fl*, sap flux density, calibration, potomet*, gravimet*, thermal dissipation, heat pulse, heat balance, heat field deformation, compensation heat pulse, T-max, and their combinations. Other sources of data were obtained from the references of previously collected studies. For each calibration experiment, we obtained paired observations of sap flow, measured with a thermal method and with an independent reference method (typically gravimetric or volumetric). Data was digitized from published figures (using GetData Graph Digitalizer version 2.26.0.20). We asked the authors to supply the raw data when these were unavailable from the original publication. We obtained data from 60 studies (see Table A1) reporting 374 individual calibration experiments performed on 81 different shrub and trees species (10,186

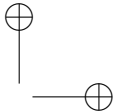
data points in total). In the analysis, we only used calibrations that were properly applied according to our definition below (i.e. 290 calibrations out of 374) to restrict the variability to the intrinsic characteristics of the methods.

We always considered sap flow observations obtained with the original parameters of the methods (e.g. Granier’s original calibration for TD), without applying the coefficients derived from the calibrations themselves. Some calibrations with TD gave measured K values (i.e. sap flow index, calculated from raw sapwood temperature differences) instead of measured SFD and, in these cases, K values were transformed to SFD using Granier’s original equation and calibration coefficients (Eq. 1, $a = 42.84 \text{ cm}^3\text{cm}^{-2}\text{h}^{-1}$, $b = 1.231$) (Granier & Une (1985)).

$$SFD = a \times K^b \quad (2.1)$$

For each calibration, we recorded the type of calibration material: whole plants, whole plants without roots or cut stem segments. We also assessed whether the sap flow method was properly applied using the best available protocol specified for each method. We considered a proper application of Dissipation methods when the probe was shorter than the sapwood depth and radial profile correction was applied, when the probe was approximately equal to the sapwood depth, or when the probe was longer than the sapwood depth and this effect was corrected for following Clearwater et al. (1999). To test whether our results could have been affected by this correction, we performed a preliminary analysis with the same structure as the main statistical model (cf. section 1.3.3) comparing TD calibrations with or without the Clearwater correction and we did not find significant effects on any of the metrics of calibration performance (cf. section 1.3.2) (data not shown). We considered a proper application of Pulse methods when wound correction was applied and either the probe had multiple measuring points along the sapwood or a radial sap flow profile correction was applied. We always considered Balance methods and Field methods as properly applied, because they always integrate (or account for) spatial variability of sap flow.

Finally, to analyze the influence of wood traits on calibration performance we used wood density, defined as fresh volume over oven-dry mass, and



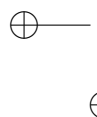
2.2. Material and methods

23

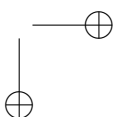
wood porosity type of the species employed in each study. Wood density was supplied in only a few studies (7 species ~ 80 calibration experiments ~ 4 studies). Assuming that for wood density between-species variability is typically larger than within-species variability (Siefert et al., 2015; Vilà-Cabrera et al., 2015), we retrieved wood density of each species from the TRY database (Kattge et al., 2011). Wood densities of *Carica papaya*, *Phoenix dactylifera* and *Vitis vinifera* were obtained from Kempe (2014), Fathi (2014) and Castelan-Estrada (2002), respectively, as they were not recorded in TRY. When wood density could not be found for a given species, we used the phylogenetically nearest species of the same genus if available in TRY (10 of 81 species; e.g. *Citrus sinensis* for *Citrus reticulata*). We could not estimate wood density for three taxa (*Humulus lupulus*, *Musa* sp. and *Siagrus romanzoffiana*). A correlation between calibration-specific and species-level wood density extracted from the TRY database ($r = 0.78$, $P < 0.01$, $n = 12$ calibrations, 6 species) indicates that species-level wood density values indeed are applicable for our purpose, but the results should be interpreted with caution. Finally, wood porosity was obtained from the InsideWood database (Wheeler (2011), (????)), using four categories: ring-porous, diffuse-porous (i.e. diffuse and semi-diffuse porous), conifer and monocots.

2.2.2 Calibration assessment

Although the reference methods always provide an estimate of sap flow through plants or stem segments, sap flow measurements can be reported as SF or SFD. It was not possible for us to interconvert between SF and SFD in all cases because sapwood areas were not always reported. This precluded a joint analysis of all the paired observations in the same linear model because units differ between SF and SFD. To overcome this problem and to maximize the amount of data considered in the analyses, we first evaluated calibration performance using four complementary dimensionless metrics at the calibration level, which allowed us to analyze globally all calibrations regardless of the magnitude they reported (SF or SFD). In a second stage, we quantified the variability in the absolute errors in sap flow measurements across methods and flow ranges separately for SF and SFD



|



methods. We did not expect differences between calibrations reported with SF or SFD because the inter-conversion between them only involves a scalar transformation. In addition, preliminary analyses confirmed that there was no significant difference between SF and SFD for any of the calibration performance metrics reported in this study (Table A2).

For the global analysis, the following metrics were calculated for each calibration (SF and SFD): the average ln ratio (Ln-Ratio) between measured and reference values as a measure of overall accuracy; the slope of the relationship between measured and reference sap flow to characterize proportional bias (Slope); the slope of the ln-ln relationship between measured and reference sap flow as a measure of linearity (Slope (ln-ln)); and Z Pearson’s Correlation to describe precision (Z-Cor) (Fig. 1.1). To calculate these metrics, we filtered out data points with measured or reference flows less or equal to 0. All calibration metrics and subsequent statistical models were performed in R 3.4.2 (R Core Team (2017)). For model-based metrics, we always checked residuals to ensure they satisfied normality and homoscedasticity assumptions. Accuracy was evaluated as the mean of the natural logarithm of the ratio between paired measurements (j) of each calibration (i):

$$\text{Ln - Ratio}_i = \frac{\sum_{j=1}^n \ln(\frac{\text{measured}_j}{\text{reference}_j})_i}{n_i} \quad (2.2)$$

where measured_j and reference_j are the paired measurements of sensor-estimated and reference flow, respectively, and n the number of paired measurements for each calibration i (see Fig. 1.1). The Ln-Ratio varies between $-\infty$ and $+\infty$, and equals 0 for a calibration with perfect mean accuracy (i.e. lack of systematic bias). We also expressed this metric as the exponential of Ln-ratio minus one multiplied by 100, as an indicator of accuracy deviation (in %).

The slope of the linear relationship (Eq. 3) describes how the magnitude of the error changes (linearly) as a function of the reference flow. The slope of the ln-ln relationship (Eq. 4) captures the linearity between the measured and the reference flow. Both slope estimates were calculated for each calibration

2.2. Material and methods

25

using a simple linear regression (lm - package stats):

$$measured_{ij} \sim \beta_{0i} + \beta_{1i} reference_{ij} + e_{ij} \quad (2.3)$$

$$\ln(measured_{ij}) \sim \beta'_{0i} + \beta'_{1i} \ln(reference_{ij}) + e_{ij} \quad (2.4)$$

where β_{0i} and β'_{0i} are the intercepts and β_{1i} and β'_{1i} are the slopes for each calibration (i), and j indicates individual calibration points. Hereafter, we will refer to β_{1i} as *Slope* and to β'_{1i} as *Slope(ln – ln)*; slope values equal to 1 characterize measurements without proportional bias (Eq. 3) and with high linearity (Eq. 4), respectively.

We used Pearson’s correlation coefficients r between measured and reference flow of each calibration experiment (i) as a metric to describe the precision of the methods. The distribution of the resulting variable was skewed due to the large amount of correlation coefficients close to 1, so we used Fisher’s Z transformation (Eq. 5) to achieve normality:

$$Z - Cor_i = \frac{1}{2} \ln\left(\frac{1+r_i}{1-r_i}\right) \quad (2.5)$$

Low values of $Z - Cor$ correspond to low r correlations, and high values of $Z - Cor$ correspond to high r correlations and thus high precision (data set range $r = [0.0491 - 0.9999]$; $r = 0.0491 \sim z = 0.0491$; $r = 0.9999 \sim z = 5.1594$).

In the analysis of the absolute errors of sap flow measurements, we calculated the Normalized Root Mean Square Error (NRMSE) for each calibration (i) (Eq. 6), separately for SFD and SF methods, in order to obtain the percentage of absolute error at the mean range of each calibration (i).

$$NRMSE_i = \frac{\left(\sqrt{\frac{\sum_{j=1}^n (measured_j - reference_j)^2}{n}} \right)_i \times 100}{range\ mean_i} \quad (2.6)$$

Subsequently, from the NRMSE and the mean range of each calibration, we fitted a linear model for each method allowing to quantify the absolute error (RMSE) at a given sap flow and also to obtain a RMSE at a reference flow (cf. section 2.3).

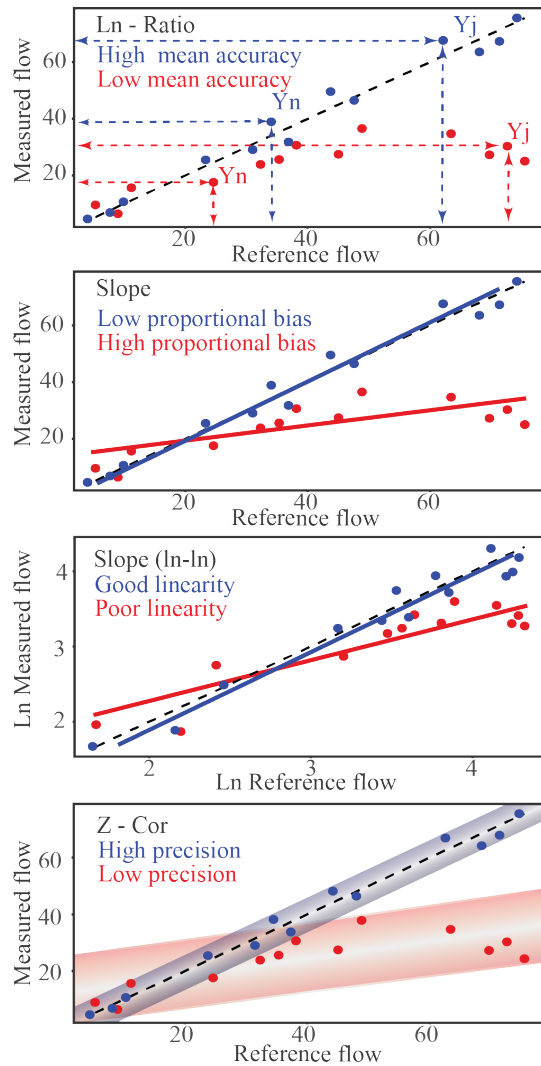


Figure 2.1: Graphical representation of the calibration performance metrics used in the analyses. Each panel presents the same simulated calibration points, representing plausible data. Blue dots represent an accurate, unbiased, linear and precise calibration, while red dots represent an inaccurate, biased, non-linear and imprecise calibration.

2.2.3 Statistical analyses

All the analyses were performed using linear mixed-effects models (LMM) with the package lmer (Bates, Mächler, Bolker, & Walker (2015)). Least-square means were estimated with package lsmeans (Lenth (2016)) and used

to summarise the effects of fixed factors and to test contrasts among predictions. In all models, we used the variables Study and Species as partially crossed random effects (Schielzeth & Nakagawa (2013)), as we are interested in taking into account the variability associated with study and species, and also to analyze within- and between-group variability. We used Study as we expect experimental variability between researchers or laboratories, and Species because calibration performance has been reported to vary across species (S. Fuchs et al. (2017); D. Smith & Allen (1996); Steppe et al. (2015)). For each model, R_m^2 and R_c^2 (marginal and conditional coefficients of determination, respectively) based on Nakagawa & Schielzeth (2013) were calculated using the function `r.squaredGLMM` of the package MuMIn (Barton (2017)) in R. Intraclass Correlation Coefficients (ICC) were also calculated for the random factors to quantify the proportion of variance within and among groups (low ICC implies high intra-group variability).

In a first analysis, we were interested in assessing the differences in calibration metrics (Ln-Ratio, Slope, Slope (ln-ln), Z-Cor) between different families of methods (Family: Pulse, Dissipation, Balance and Field methods), because methods within a family share similar physical principles. We also analyzed differences between individual methods with a sufficient sample size (Method: CHP, T-max, HR, HFD, SHB, TD, TTD). As the calibration material determines, to a large extent, the experimental conditions, we also included this variable in our models (Material: whole plants, whole plants without roots or cut stem segments). For the analysis of absolute errors of sap flow measurements, we modelled NRMSE as a function of Method and the Mean Range of SFD (or SF for Balance methods) in each calibration, as well as their interaction. We used the same random structure as in previous models.

Finally, we assessed how each calibration metric depended on Wood Density and Wood Porosity. A first model included all methods available, with Method interacting with Wood Density as predictors. In order to test Wood Porosity effects, we fitted separate models for CHP and TD calibrations, as these two methods were the only ones that had enough data (> 5 calibrations) for more than one type of porosity. Separate models were needed because not

Table 2.1: Analysis summary for the different methods and families of methods obtained from the LMM models (least-squares means). We provide the four dimensionless metrics: the Ln-ratio as a measure of accuracy, the accuracy deviation calculated as the exponential of the Ln-ratio minus one multiplied by 100, the Slope to characterize the proportional bias, the slope of the ln-ln-relationship, Slope (ln-ln), as a measure of linearity, and Z Pearson’s correlation (Z-Cor) to describe overall precision; n: number of calibrations; studies: number of studies of each method; species: number of different species; r is the correlation calculated as the tanh of Z-Cor.

Method	Family	n	studies	species	Ln-Ratio	Accuracy deviation %	Slope	Slope (ln-ln)	Z-Cor	r
CHP	Pulse	63	16	21	0.133	14.225	0.887	0.783	1.837	0.950
T-max	Pulse	11	5	6	-0.053	-5.162	0.614	0.697	1.755	0.942
HR	Pulse	23	6	7	-0.145	-13.498	0.845	0.841	2.000	0.964
HFD	Field	57	3	4	-0.073	-7.040	0.901	0.782	2.378	0.983
SHB	Balance	8	5	6	-0.242	-21.494	0.847	0.967	2.287	0.980
TD	Dissipation	115	18	35	-0.519	-40.488	0.683	1.066	1.711	0.937
TTD	Dissipation	14	2	6	-0.493	-38.921	0.669	0.985	1.464	0.899
all	Pulse	97	NA	30	0.012	1.167	0.844	0.787	1.874	0.954
all	Field	57	NA	4	-0.008	-0.820	0.896	0.762	2.322	0.981
all	Balance	8	NA	6	-0.244	-21.650	0.854	0.972	2.294	0.980
all	Dissipation	129	NA	37	-0.464	-37.153	0.681	1.052	1.666	0.931

— all wood porosity types were represented for all methods. In both models we also included Material as an explanatory cofactor, and the same random structure as in the first analysis explained above.

—

2.3 Results

Most of the published calibrations were performed with Pulse and Dissipation methods (Table 1.1). In particular, 61% of the total number of the properly applied calibrations were conducted using TD or CHP, followed by HFD and HR. SHB, T-max and TTD methods were less represented, with 8 – 14 calibrations each. The metrics extracted from the raw calibrations were highly variable within methods (Fig. 1.2). Calibration metrics often followed a quasi-normal distribution, but in most cases distributions were truncated or skewed, particularly for methods with fewer calibrations (Fig. 1.2).

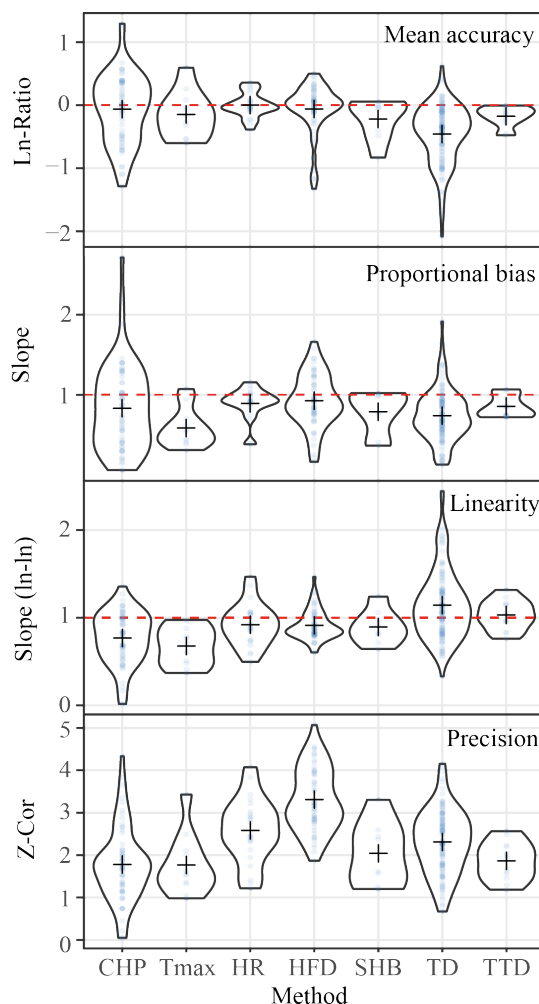


Figure 2.2: Distribution of the calibration performance metrics for each method. Dots represents the value of each individual calibration metric. Crosses represent the average of the metric for each method. Horizontal, dashed lines specify reference, perfect calibration values for a given metric.

2.3.1 Calibration performance compared among methods and families of methods

The average accuracy deviation across sap flow methods (properly applied) ranged between 14.2% for CHP and -40.5% for TD (Table 1.1). There were significant differences in accuracy (Ln-Ratio) among families of methods and for methods but not for calibration materials (Fig. 1.3). The Dissipation

family in general and the TD and TTD methods in particular were the only cases for which the Ln-Ratio was significantly different from 0 ($p<0.001$) (Fig. 1.3), indicating systematic bias (underestimation).

Proportional bias, estimated by Slope, varied among methods and families of methods ($p<0.01$). Among families, Dissipation methods showed a significantly smaller Slope than Pulse and Field methods (Fig. 1.3(a)), which was largely driven by the low value of TD (Fig. 1.3(b)). Also, both Pulse and Dissipation families had slopes significantly different from 1 ($p<0.01$ and $p<0.001$, respectively), but only the slope of the TD method was significantly lower than 1 ($p<0.001$) (Fig. 1.3). As for the effects of calibration material, calibrations made with whole plants had a significant proportional bias (Slope < 1 , $p<0.001$) (Fig. 1.3). Calibration linearity, as denoted by Slope (ln-ln), varied across methods and families of methods ($p<0.001$). We observed higher values of Slope (ln-ln) for the TD method compared to CHP, T-max, HR and HFD. Consistently, the Dissipation family in general also had a higher Slope (ln-ln) than the Pulse and Field families (Fig. 1.3). CHP, T-max and HFD (and Pulse and Field methods in general) had a Slope (ln-ln) significantly lower than 1 (Table 1.1 and Fig. 1.3(b)), indicating a convex relationship between reference and measured flow. Calibrations performed with whole plants suffered from lack of linearity, indicated by Slope (ln-ln) significantly lower than 1 (Fig. 1.3).

Precision (Z-Cor) was explained by both method and calibration material. The HFD method (and Field methods in general) provided significantly higher precision than either Pulse or Dissipation methods (particularly CHP, TD and TTD) (Table 1.1 and Fig. 1.3(b)). Calibrations performed on stem segments provided higher precision than those conducted on whole plants (with or without roots) (Fig. 1.3).

In all the previous models, little variability was explained by species (τ_{00} , species), relative to the higher variability associated to Study, particularly for the Ln-Ratio and Z-Cor models (τ_{00} , study, Table A3). This is consistent with the low ICC values observed for the species factor, indicating that there is more variability within than among species (Table A3).

2.3. Results

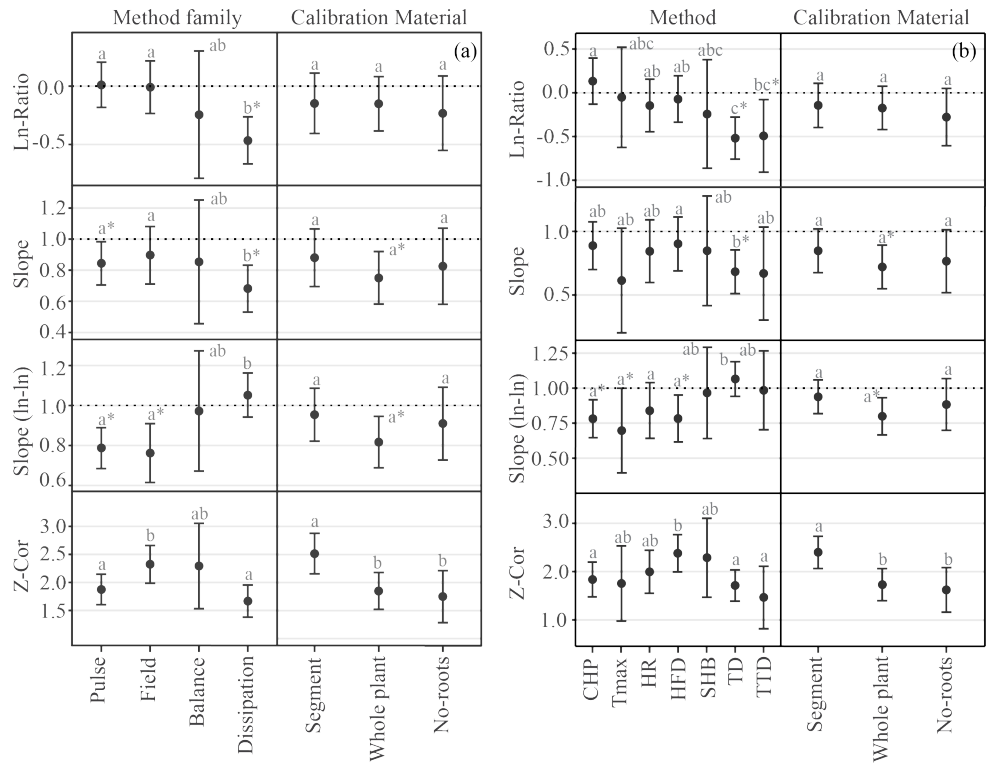


Figure 2.3: Predictions of the LMM models calculated from least-squares means of the four calibration metrics (Ln-Ratio as a proxy for mean accuracy, Slope for proportional bias, Slope (ln-ln) for linearity and Z-Cor for precision) for (a) different families of sap flow methods or for (b) different sap flow methods and for different calibration materials (Segment: stem segment; Whole plant: whole plant on a container or lysimeter; No-roots: whole plant without roots). 95% confidence intervals of the estimates are also shown. Different letters indicate significant differences between factors levels evaluated with Tukey’s test. Horizontal, dotted lines indicate reference, perfect calibration values for a given metric. Asterisks (*) indicate significant departure from those reference values.

In addition, the analysis of the normalized absolute error for the different methods showed that NRMSE decreased linearly with increasing measured sap flow in CHP, HFD and TTD methods and increased for T-max, SHB and TD (Table 1.2 and Fig. A2). For HR the increase in NRMSE with measured sap flow was not significant. For all the methods that measure SFD, the absolute error at a typical flow of $25 \text{ cm}^3 \text{ cm}^{-2} \text{ h}^{-1}$ ranged between $6.3 \text{ cm}^3 \text{ cm}^{-2} \text{ h}^{-1}$ for CHP and $10.7 \text{ cm}^3 \text{ cm}^{-2} \text{ h}^{-1}$ for the TTD method (Table 1.2).

Table 2.2: Error analysis of different sap flow methods. The normalized root mean square error (NRMSE) is modelled as a function of method and the mean flow range for each calibration (and their interaction) using a LMM model with the same random structure as the main models (cf. section 2.3). β_0 and β_1 are the corresponding intercepts and slopes, respectively (β_0 expressed as % NRMSE; β_1 expressed as % NRMSE per change in $\text{cm}^3 \text{ cm}^{-2} \text{ h}^{-1}$ for SFD or as % NRMSE per change in $\text{cm}^3 \text{ h}^{-1}$ for SF). This linear model, was also used to calculate a reference NRMSE at a sap flux equivalent to the percentile 50 of the range of the data in the calibrations (SFD: $25 \text{ cm}^3 \text{ cm}^{-2} \text{ h}^{-1}$; SF: $1300 \text{ cm}^3 \text{ h}^{-1}$). The expected NRMSE and RMSE (in brackets, in $\text{cm}^3 \text{ cm}^{-2} \text{ h}^{-1}$, except for SHB that is in $\text{cm}^3 \text{ h}^{-1}$) at a typical flow are also given.

Method	NRMSE			
	β_0	%	β_1	reference NRMSE (and RMSE)
CHP	27.03***	-0.08***		25.04% (6.26)
T-max	31.56.	0.25***		37.83% (9.46)
HR	9.38	0.81		29.59% (7.40)
HFD	30.33***	-0.12***		27.45% (6.86)
SHB	14.85	0.02***		42.95% (558.36)
TD	34.93***	0.10***		37.31% (9.33)
TTD	44.04***	-0.04***		42.94% (10.73)

Statistical significant levels: “.” p<0.1 ; “*” p<0.05; “**” p<0.01; “***” p<0.001.

2.3.2 Influence of wood traits

We did not find any significant influence of wood density on accuracy and linearity metrics (Fig. 1.4). Nonetheless, we observed a negative effect of wood density on proportional bias of HFD and TD calibrations (p<0.05 and

2.3. Results

33

$p < 0.1$, respectively). In addition, a significant positive effect of wood density on the precision of HFD measurements was observed ($p < 0.001$), indicating that the higher the wood density, the higher the precision (Fig. 1.4).

We did not find any significant difference among wood porosity types in calibration metrics for studies using the TD or CHP methods. Nevertheless, the non-linearity (Slope ($\ln\text{-}\ln$) < 1) observed in general for the CHP method (Fig. 1.3(b)) was only significant for species with diffuse-porous wood, not for conifer species (Table 1.3).

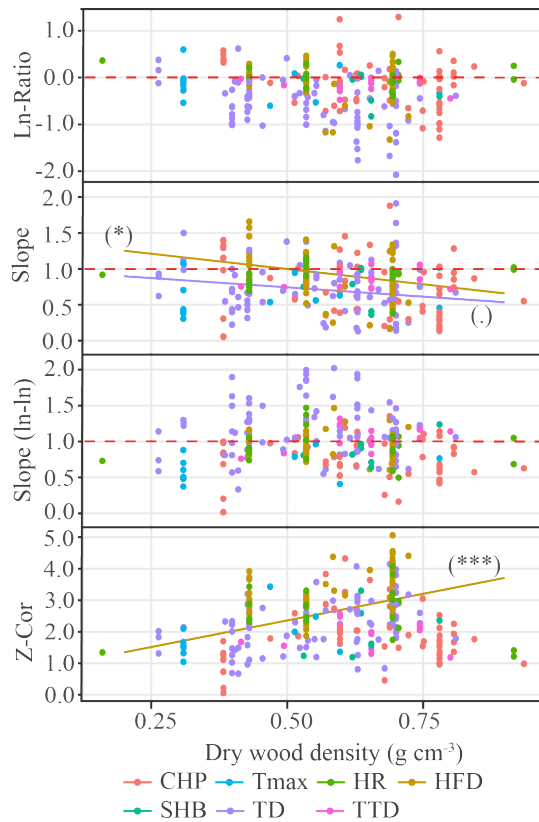


Figure 2.4: Relationship between the four calibration performance metrics (Ln-Ratio as a proxy for accuracy, Slope for proportional bias, Slope ($\ln\text{-}\ln$) for linearity, and Z-Cor for precision) and wood density, for different sap flow methods. Horizontal, dashed red lines indicate reference, perfect calibration values for a given metric. Regression lines are shown for significant effects only, and the corresponding level of significance (p -value: < 0.1 : (.), < 0.05 : (*), < 0.01 : (**), < 0.001 : (***)) is also reported

Table 2.3: Least-squares means and 95% CI calculated from the LMM models testing the effect of different wood porosity types (Wood porosity) on sap flow calibration performance metrics (Ln-Ratio as a proxy for accuracy, Slope for proportional bias, Slope (ln-ln) for linearity, and Z-Cor for precision) for CHP and TD methods. No differences were detected among wood anatomies. Significance levels indicate departure from an ideal calibration (Ln-Ratio = 0; Slope = 1; Slope (ln-ln) = 1)

Method	Wood porosity	n	Accuracy		Proportional bias		Linearity		Precision	
			Ln-Ratio	Slope	Slope	Slope (ln-ln)	Z-Cor			
CHP	diffuse	48	-0.055 [-0.370 , 0.259]	0.795 [0.557 , 1.033].	0.799 [0.671, 0.927]	1.980 [1.729 , 2.231]				
CHP	conifers	15	0.066 [-0.603 , 0.734]	1.043 [0.459 , 1.627]	0.777 [0.469 , 1.085]	1.381 [0.775 , 1.988]				
TD	diffuse	81	-0.273 [-0.658 , 0.111]	0.752 [0.491 , 1.014].	1.126 [0.917 , 1.336]	1.672 [1.085 , 2.260]				
TD	ring	16	-0.405 [-0.866 , 0.056].	0.743 [0.410 , 1.077].	0.984 [0.681 , 1.286]	2.260 [1.572 , 2.947]				
TD	conifers	15	-0.396 [-0.873 , 0.080].	0.808 [0.468 , 1.147]	1.142[0.842 , 1.441]	1.606 [0.892 , 2.321]				

Statistical significant levels: ** p<0.1 ; *** p<0.05; **** p<0.01; ***** p<0.001.

2.4 Discussion

Our results show a large variability in the quality of sap flow calibrations, even within the same sap flow method (Fig. 1.2), highlighting the large variability among and even within studies. This implies that, even if methods are properly applied (as defined in section 2.1), sap flow measurements can still produce biased estimates of water transport rates in plants, and these errors will need to be considered in quantitative analyses based on this type of measurements. On average, however, all sap flow methods assessed here produced results that may be acceptable for qualitative use in most applications, as shown by the typical high correlation between measured and reference values ($r > 0.89$ for all methods and method families, Table 1.1). For quantitative use, no method appears to be suitable for all experimental contexts, and researchers need to consider both the inherent limitations of the methods and the need to perform study-specific calibrations (see Implications and recommendations, Table 1.4).

2.4.1 Sap flow measurement errors across methods and methodological families

A relatively small part of the total variability in the quality of calibrations is related to methods and families of methods and, to a lesser extent, to the

calibration material (fixed effects explain 8 – 28% of the variability in calibration metrics; see R_m^2 values in Table A3). Despite the high variability within methods, we detected significant differences between methods. Dissipation methods were the only methods for which accuracy was significantly lower than expected for an ideal calibration. This is consistent with previous reports (Braun & Schmid (1999); S. E. Bush, Hultine, Sperry, Ehleringer, & Phillips (2010); Caterina, Will, Turton, Wilson, & Zou (2014); (????); de Oliveira Reis, Campostrini, Sousa, & Silva (2006); S. Fuchs et al. (2017); Ping Lu & Chacko (1998); McCulloh et al. (2007); Montague & Kjelgren (2006); Rubilar, Hubbard, Yañez, Medina, & Valenzuela (2017); Steppe, De Pauw, Doody, & Teskey (2010); Taneda & Sperry (2008); Uddling, Teclaw, Pregitzer, & Ellsworth (2009)) and our synthesis confirms that most of the individual TD and all TTD calibrations underestimate sap flow systematically (Fig. 1.5). Interestingly, however, other studies have found the opposite result (Cain (2009); K. R. Hultine et al. (2010); P Lu (2002); Sperling et al. (2012); Sun, Aubrey, & Teskey (2012)) and simulation models (Hölttä, Linkosalo, Riikinen, Sevanto, & Nikinmaa (2015); Wullschleger et al. (2011)) suggest that it is difficult to state a priori whether TD will over- or underestimate flow, as the measurements obtained are highly dependent on wood properties and on flux conditions. Our results show that, globally, the conditions leading to underestimation are more frequent and support the existence of a proportional bias underlying this systematic underestimation by TD (Fig. 1.3). It must be also noted, however, that Dissipation methods have been tested against a much wider range of flow conditions compared to the rest of the methods (Fig. 1.5, Fig.6).

Calibration parameters of the TD method were originally considered to be universal but subsequent studies have claimed that species-specific calibrations are necessary to obtain correct sap flow measurements (S. Fuchs et al. (2017); Ping Lu et al. (2004); Steppe et al. (2010)). For a set of diffuse-porous species, using a pooled calibration also substantially improved TD (but not HFD) performance compared to measurements obtained with the original calibration (S. Fuchs et al. (2017)). However, our results show that species in general and wood porosity type in particular explain a small

Table 2.4: Synthesis of the potential sources of error and use adequacy for each method. Crosses indicates that the method is sensitive to the respective source of error (updated from Vandegehuchte and Steppe, 2013). Methods are classified according to their use effectiveness under different flow conditions: dark grey, light grey and white indicate highly, partially and no recommended use, respectively. When assessing use adequacy for high/low flows, dark and light gray indicate a Normalized Root Mean Square Error (NRMSE) less than a 22% and a 44%, respectively, calculated with the NRMSE model (Table 1.2). In Absolute flows use recommendation, dark grey shows methods with both accuracy (Ln-Ratio) and proportional bias (Slope) not significantly different from a perfect calibration. In Relative flows use recommendation, dark grey shows methods with linearity (Slope (ln-ln)) not significantly different from a perfect calibration and with reasonable precision. Potentiality of measuring small stems diameters (< 125mm) is also reported.

Method	Potential source of measure error										Effectiveness in measuring				
	Wounding	Radial velocity profile	Wood properties	Natural thermal gradients	Sensor installation	Sensor design	Baseline	Power input	Pulse length	Reverse flows	Low flows*	High flows*	Absolute flows	Relative flows	Small stems
CHP	x	x	x	x	x				x						
T-max	x	x	x		x		x								
HR	x	x	x		x										
HFD	x	x		x	x	x	x	x							
SHB				x			x	x							
TD	x	x	x	x		x	x	x							
TTD	x	x	x	x		x	x	x							

* (Low/High: SFD methods: <5 / >80 $cm^3 cm^{-2} h^{-1}$; SF methods: <260 / >3900 $cm^3 h^{-1}$)

or even no proportion of the variability in the calibrations (Table 1.3 and A3). This implies that factors related to the experimental context and, possibly, to intraspecific variability in wood properties (cf. section 1.5.2) may have a large contribution to overall uncertainty. Therefore, our results suggest that

calibration parameters for TD or HFD, obtained under different experimental contexts, may not be generalizable to species level, as also suggested by Fuchs et al. (2017).

In addition to Dissipation methods, Pulse methods also suffer proportional bias, probably driven by overestimation at low flows, although this was significant for T-max only (i.e. positive intercepts in linear models fitted to calibration data; Fig. 1.5 and 1.6 and A3). It is well known that the equations of CHP and T-max cannot be solved at sap flows close to 0, and the calibration intercepts observed here (Fig. A3) are consistent with the detection thresholds reported for T-max ($\sim 10 \text{ cm}^3 \text{ cm}^{-2} \text{ h}^{-1}$; Steve Green et al. (2003)) and CHP ($2\text{-}4 \text{ cm}^3 \text{ cm}^{-2} \text{ h}^{-1}$; T. M. Bleby, Burgess, & Adams (2004); Steve Green et al. (2003)). Our results confirm and generalize a previously reported low-flow detectability problem for T-max (S. Green et al. (2009), Steve Green et al. (2003); Vandegehuchte & Steppe (2012b)), but we could not confirm it for CHP as described before (Barrett et al. (1995); Becker (1998); T. M. Bleby et al. (2004); Vandegehuchte & Steppe (2012b)). Despite overestimation at low flows, the average accuracy of CHP and T-max is good, which implies that low-flow overestimations may be compensated with underestimations at high flows. This is also shown by the lack of linearity observed in both methods (Slope (ln-ln) < 1 ; Fig. 1.3(b)).

Our analysis did not detect the saturation effect for the HR method at high flows that has been reported elsewhere (T. Bleby, McElrone, & Burgess (2008); S. Green et al. (2009); Steppe et al. (2015)). This is likely due to the fact that HR calibrations considered here include few observations in the region where this overestimation occurs ($> \sim 45 \text{ cm}^3 \text{ cm}^{-2} \text{ h}^{-1}$; Figs 5 and 6). Moreover, the high variability in the calibrations probably precluded detection of the saturation effect (Fig. 1.3 and 1.5) and of the apparent trend of increasing NRMSE with sap flow range for HR (Table 1.3 and Fig. A2). A lack of linearity can also be observed for HFD, consistent with the suggested tendency of this method to underestimate at high flows (Vandegehuchte & Steppe (2012c)).

Despite the large variability in precision within methods, our results show that calibrations performed with HFD give more precise results than

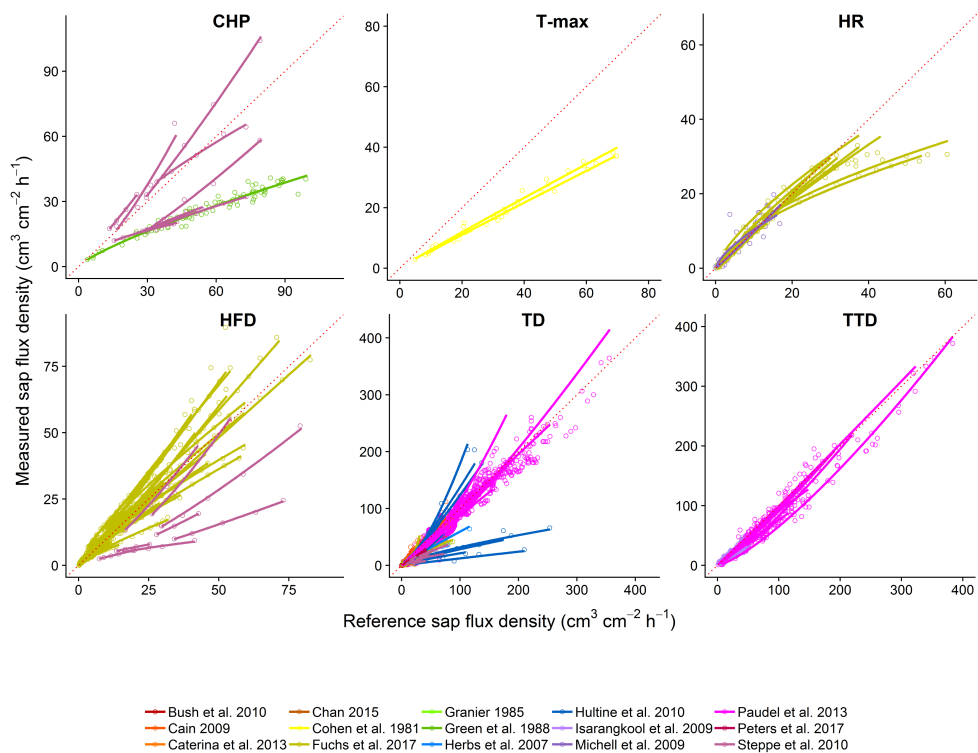


Figure 2.5: Relationship between measured and reference sap-flux density (SFD) for different sap flow methods, studies and calibrations. The fits of ln–ln regressions (Eq. 4) for each calibration are also depicted. Different colors represent different studies that report results in sap-flux density units. Scales vary across panels to facilitate intra method comparison. The red dotted line indicates the 1:1 relationship.

those conducted using the CHP, TD and TTD methods. Although this result should be interpreted with care as it is based on 57 calibrations but only from 3 studies, the higher precision observed with HFD could lie in the second dimension included in the method, which could better capture the effect of anisotropy of the wood structure. This would also be consistent with the fact that SHB, a method that is assumed to integrate sap flow variability within the stem, was the method with the second highest precision on average, albeit precision was very variable for this method (Fig. 1.3(b)).

We did not detect differences in accuracy, proportional bias or linearity of the calibrations across calibration materials. However, compared to an ideal calibration, we did find proportional bias and lack of linearity in calibrations performed on whole plants, probably because these calibrations use large scales whose sensitivity and resolution are usually low, potentially affecting low-flow measurements and leading to artefactual overestimation at low flows. Poor linearity may also be due to non-linear changes in belowground hydraulic resistance as the sap flow increases (J. Martínez-Vilalta, Korakaki, Vanderklein, & Mencuccini (2007)). In cut plants, we may have two opposite effects, as cutting could eliminate belowground resistance (favoring flow) but add resistance due to putative embolism formation after cutting. Similarly, the higher precision of calibrations conducted on cut stems relative to those conducted on whole plants (with and without roots), likely reflects that cut stem calibrations are normally conducted in laboratories with precision scales and under controlled conditions that minimize experimental random errors.

2.4.2 The performance of sap flow calibrations is largely unrelated to species wood traits

Species-specific wood density and wood porosity type explained little variability in overall calibration performance, although we detected some effects of wood density for HFD and TD calibrations. Wood density affected HFD measurements by increasing precision, which could be related to the response time of the sensors. If we assume that maximum sapwood water content is reduced as wood density increases (Simpson (1993)), associated changes

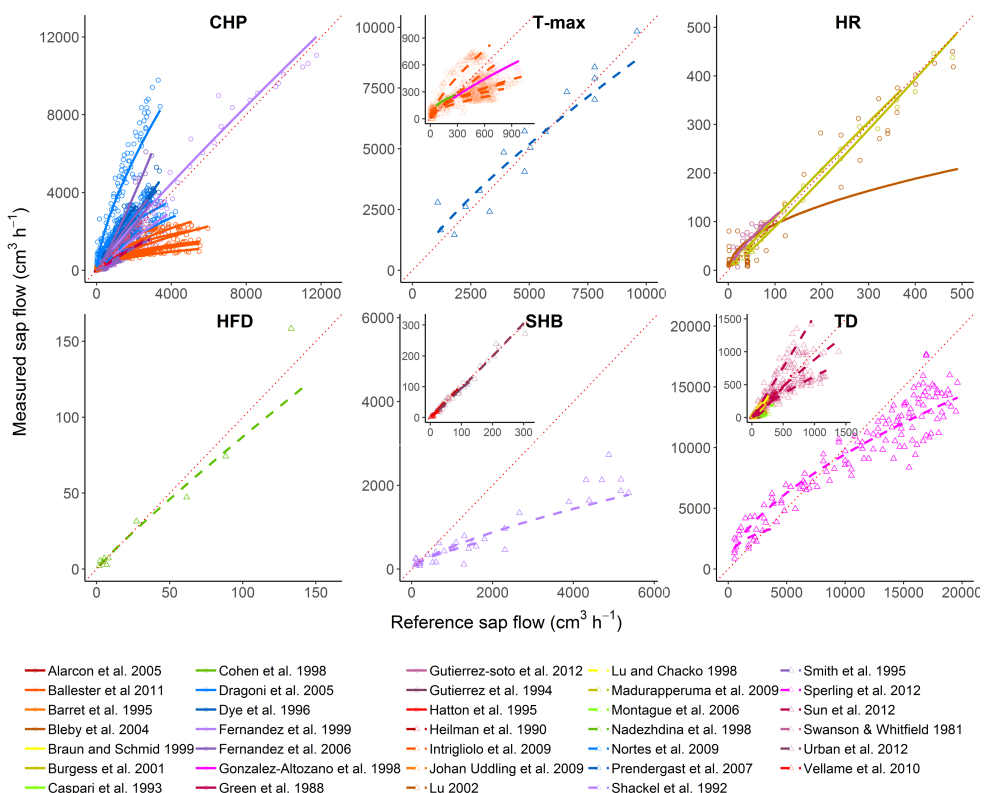


Figure 2.6: Relationship between measured and reference sap flow (SF) for different sap flow methods, studies and calibrations. The fits of ln–ln regressions (Eq. 4) for each calibration are also depicted. Different color symbols and line types represent different studies. Scales varies across panels to facilitate intra method comparison. Insets are shown in some panels (T-max, SHB, TD) to facilitate visualization when the flow ranges differed markedly among calibrations for the same method. The red dotted line indicates 1:1 relationship.

in thermal diffusivity could lead to a faster sensor response (Hölttä et al. (2015)), higher correlation between actual and measured flows. Wood density also showed a negative relationship with proportional bias for HFD and TD, a pattern that could be caused by the combined effects of wood density and water content on wood thermal diffusivity (Vandegehuchte & Steppe (2012c); Vergeynst et al. (2014)). The fact that we did not find clear effects of wood density on calibration accuracy and linearity, despite that wood density affects thermal diffusivity and hence heat transport (Wullschleger et al. (2011)), could be explained by two reasons. Firstly, we could not use the actual wood density for most of the calibrations, because it was not reported in the corresponding studies, and using species-level averages instead of the wood density of the plant material specifically used on the calibrations may mask the effect of wood density on calibration performance. Secondly, wood density in angiosperms appears to be only weakly correlated to some wood properties that could be important for sap flow calibrations, such as lumen fraction (Zanne et al. (2010)).

Our global analysis did not show clear and consistent differences in calibration quality between different wood porosity types (Table 1.2) as previously suggested by several studies for both CHP (S. R. Green & Clothier (1988)) and TD methods (S. E. Bush et al. (2010); Sun et al. (2012)). According to heat transport theory, we should expect declining performance from conifer to ring-porous species (i.e. from most homogenous to most heterogeneous wood). For CHP, we found that proportional bias (only marginally) and nonlinearity departed from an ideal calibration for diffuse-porous species, but these patterns did not differ significantly from those observed for conifers. Our results did not clearly support either an inferior performance of TD in ring-porous species compared to diffuse-porous or conifers, as could be expected from the reported underestimation driven by large sap flow gradients along sensor length or by the imperfect probe contact with hydroactive xylem in species with narrow sapwood (Michael J Clearwater et al. (1999); but see Wullschleger et al. (2011)). Wood porosity effects on sap flow calibrations have been inferred in individual studies from measurements in few species representative of each wood porosity type (S. E. Bush et al. (2010); Sun et

al. (2012); Xie & Wan (2018)) and our inability to detect these effects here may be caused by the high variability in experimental context within our dataset. Furthermore, the effect of the different anatomies may be masked by high structural variability within wood porosity types, as for example the variation in latewood to earlywood in conifers (Fan, Guyot, Ostergaard, & Lockington (2018)) and we cannot discard that calibration performance could be related to quantitative anatomical traits not assessed in this study (cf. Xie & Wan (2018)). Although the low variability we observed at the species level suggests that quantitative anatomical traits might not explain much of the variability in sap flow calibrations, we encourage that quantitative wood traits are measured in the same plant material used to calibrate sap flow sensors to better understand the influence of wood properties on the variability of sap flow calibrations.

2.4.3 Implications and recommendations

Our global analysis shows that even when the methods are applied following standard recommendations the quality of individual calibrations can be very low (Fig. 1.3). This result reflects, on one hand, systematic bias in TD and lack of linearity in CHP, two of the most widely used methods (Fig. A1) and, on the other hand, unknown sources of error related to experimental conditions and/or sample characteristics (Table 1.4). In our study, we could not account for all the experimental conditions to evaluate these sources of variability, except for the effect of the calibration material. Examples of factors that may affect calibrations when using the same type of calibration material include sensor design (S. Fuchs et al. (2017)), sensor installation (T. M. Bleby et al. (2004); Ping Lu & Chacko (1998); Ren et al. (2017)), variation in calculations of wood thermal properties (Looker et al. (2016)), zero flow determination (Looker et al. (2016); Peters et al. (2018)) or the mechanism of flow generation in cut stem calibrations (negative vs positive pressures) (S. Fuchs et al. (2017)) (Table 1.4). Previous reports, however, usually focus on only one of the sources of experimental error. Importantly, relevant methodological information that could be used to assess (and account for) these sources of error is frequently not reported (Peters et al. (2018);

Steppe et al. (2015)). Clearly, further research into the effects of experimental conditions on the quality of different sap flow methods should be a priority, as well as more complete, standardized reporting of experimental conditions, including information on the sources of potential methodological errors listed in Table 1.4.

Our results show that calibrations may be needed to obtain correct absolute values of sap flow, even when Pulse methods are used (see also S. Fuchs et al. (2017); Steppe et al. (2010)). However, sap flow calibrations provide a snapshot of the performance of a given sap flow method under relatively stable conditions, which may greatly differ from those experienced by plants in the field. Moreover, our analysis could not address the methodological variability related to more dynamic effects such as errors caused by changes in sapwood water content (Vergeynst et al. (2014)), long-term wounding or signal dampening (Maranon-jimenez2018; Peters et al. (2018); A Wiedemann et al. (2013)). In this sense, more studies should assess calibration applicability to mid- or long-term measurements (e.g., Oliveras & Llorens (2001)), possibly combined with independent estimates of sapwood water content (Vandegeuchte & Steppe (2012b)) and whether calibrations obtained from excised segments are valid for whole-plants.

Considering only their performance in calibration tests (i.e. no other logistic or technical issues, such as sensor, datalogging, or power constraints, which will be study-specific) we can provide some general recommendations on the use of sap flow methods (Table 1.4). The most widely used method, TD, appears to be consistently inaccurate, shows proportional bias and generally underestimates sap flow, by 40% on average (if used with its original calibration coefficients). However, it presents good linearity, which implies that this method can be used when sap flow responses to environmental variables and/or treatments are the primary focus of the study (i.e., good estimates of absolute sap flow values are not critical). In comparison, CHP, T-max and HFD all present a certain nonlinearity which may affect the estimation of these environmental responses. At least for CHP and T-max (specially for the latter) this pattern seems to be driven by overestimation at low flows and underestimation at high flows canceling out each other. This implies that

both Pulse methods could be suitable for studies interested in absolute values of transpiration. For the HFD method, the nonlinearity could be influencing the estimations of radial sap flow patterns, as these measurements would need to correctly measure both high and low flows simultaneously. We also confirm that the HR method may not be suitable to measure high flows but it is probably the best method for detailed physiological studies involving low flows.

2.5 Conclusions

In conclusion, our global assessment contributes towards a proper incorporation of measurement errors in the interpretation of individual case studies and in modelling studies aimed at upscaling sap flow data (T. J. Hatton et al. (1995); Hernandez-Santana et al. (2015)). Perhaps even more importantly, it paves the way towards improved intercomparison of sap flow datasets obtained with different methods to assess regional or global patterns in plant water use (e.g., the SAPFLUXNET initiative; Poyatos et al. (2016)). Although providing explicit correction factors for each method is beyond the scope of this paper, the typical accuracy deviations provided in Table 1.1 can be used as a first order correction when combining sap flow data from different methods (and no additional information on study-specific uncertainty sources is available).

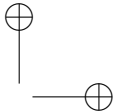
3

Global transpiration data from sap flow measurements: the SAPFLUXNET database

Rafael Poyatos, Víctor Granda, Víctor Flo, Jordi Martínez-Vilalta *et al.*

Abstract

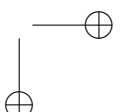
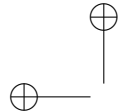
Plant transpiration links physiological responses of vegetation to water supply and demand with hydrological, energy and carbon budgets at the land-atmosphere interface. However, despite being the main land evaporative flux at the global scale, transpiration and its response to environmental drivers are currently not well constrained by observations. Here we introduce the first global compilation of whole-plant transpiration data from sap flow measurements (SAPFLUXNET, <https://sapfluxnet.creaf.cat/>). We harmonised and quality-controlled individual datasets supplied by contributors worldwide in a semi-automatic data workflow implemented in the R programming language. Datasets include sub-daily time series of sap flow and hydrometeorological drivers for one or more growing seasons, as well as metadata on the stand characteristics, plant attributes and technical details of the measurements. SAPFLUXNET contains 202 globally distributed datasets with sap flow time series for 2714 plants, mostly trees, of 174 species. SAPFLUXNET has a broad bioclimatic coverage, with woodland/shrubland and temperate forest biomes especially well-represented (80% of the datasets). The measurements cover a wide variety of stand structural characteristics and plant sizes. The datasets encompass the period between 1995 and 2018, with 50% of the datasets being at least 3 years long. Accompanying radiation and vapour pressure deficit data are available for most of the datasets, while on-site soil water content is available for 56% of the datasets. Many datasets contain data for species that make up 90% or more of the total stand basal area, allowing the estimation of stand transpiration in diverse ecological settings. SAPFLUXNET adds to existing plant trait datasets, ecosystem flux networks and remote sensing products to help increase our understanding of plant water use, plant responses to drought and ecohydrological processes. SAPFLUXNET version 0.1.5 is freely available from the Zenodo repository (<https://doi.org/10.5281/zenodo.3971689>, Poyatos et al. 2020a). The ‘sapfluxnetr’ R package, designed to access, visualise and process SAPFLUXNET data is available from CRAN.



3.1 Introduction

Terrestrial vegetation transpires ca. 45000 km³ of water per year (Schlesinger and Jasechko, 2014; Wang-Erlandsson et al., 2014; Wei et al., 2017), a flux that represents 40% of global land precipitation, 70% of total land evapotranspiration (Oki and Kanae, 2006), and is comparable in magnitude to global annual river discharge (Rodell et al., 2015). For most terrestrial plants, transpiration is an inevitable water loss to the atmosphere because they need to open stomata to allow CO₂ diffusion into the leaves for photosynthesis. Latent heat from transpiration represents 30–40% of surface net radiation globally (Schlesinger and Jasechko, 2014; Wild et al., 2015). Transpiration is therefore a key process coupling land-atmosphere exchange of water, carbon and energy, determining several vegetation-atmosphere feedbacks, such as land evaporative cooling or moisture recycling. Regulation of transpiration in response to fluctuating water availability and/or evaporative demand is a key component of plant functioning and one of the main determinants of a plant’s response to drought (Martin-StPaul et al., 2017; Whitehead, 1998). Despite its relevance for earth functioning, transpiration and its spatiotemporal dynamics are poorly constrained by available observations (Schlesinger and Jasechko, 2014) and not well represented in models (Faticchi et al., 2016; Mencuccini et al., 2019). An improved understanding on how plants regulate transpiration is thus needed to better predict future trajectories of land evaporative fluxes and vegetation functioning under increased drought conditions driven by global change.

Conceptually, transpiration can be quantified at different organisational scales: leaves, branches and whole plants, ecosystems and watersheds. In practice, transpiration is relatively easy to isolate from the bulk evaporative flux, evapotranspiration, only from the leaf to the plant levels. In terrestrial ecosystems, evapotranspiration includes evaporation from the soil and from water-covered surfaces, including plants. Transpiration measurements on individual leaves or branches with gas exchange systems are difficult to upscale to the plant level (Jarvis, 1995). Likewise, transpiration measurements using whole-plant chambers (e.g. Pérez-Priego et al., 2010) or gravimetric methods



(e.g. weighing lysimeters) in the field are still challenging. At the ecosystem scale and beyond, evapotranspiration is generally determined using micrometeorological methods, catchment water budgets or remote sensing approaches (Shuttleworth, 2007; Wang and Dickinson, 2012). In some cases, isotopic methods and different algorithms applied to measured ecosystem fluxes can provide an estimation of transpiration at the ecosystem scale (Kool et al., 2014; Stoy et al., 2019).

Transpiration drives water transport from roots to leaves in the form of sap flow through the plant’s xylem pathway (Tyree and Zimmermann, 2002), and this sap flow affects heat transport in the xylem. Taking advantage of this, thermometric sap flow methods were first developed in the 1930s (Huber, 1932) and further refined over the following decades (Čermák et al., 1973; Marshall, 1958) to provide operational measurements of plant water use. These methods have become widely used in plant ecophysiology, agronomy and hydrology (Poyatos et al., 2016), especially after the development of simple, easily replicable methods (e.g. Granier, 1985, 1987). Whole-plant measurements of water use using thermometric sap flow methods provide estimates of water flow through plants from sub-daily to interannual timescales, and have been mostly applied in woody plants (but see Baker and Van Bavel (1987) for measurements on herbaceous species). Xylem sap flow is measured semi-invasively (Brodersen et al., 2019) and can be upscaled to the whole plant, obtaining a near-continuous quantification of plant water use. Multiple sap flow sensors can be deployed, in almost any terrestrial ecosystem, to determine the magnitude and temporal dynamics of transpiration across species, environmental conditions or experimental treatments. All sap flow methods are subject to methodological and scaling issues, which may affect the quantification of absolute water use in some circumstances (Čermák et al., 2004; Köstner et al., 1998; Smith and Allen, 1996; Vandegehuchte and Steppe, 2013). Nevertheless, all methods are suitable for the assessment of the temporal dynamics of transpiration and of its responses to environmental changes or to experimental treatments (Flo et al., 2019).

The generalised application of sap flow methods in ecological and hydrological research in the last 30 years has thus generated a large volume of

3.1. Introduction

data, with an enormous potential to advance our understanding of the spatiotemporal patterns and the ecological drivers of plant transpiration and its regulation (Poyatos et al., 2016). However, this large volume of data needs to be compiled and harmonised to enable global syntheses and comparative studies across species and regions. Across-species data syntheses using sap flow data have mostly focused on maximum values extracted from publications (Kallarackal et al., 2013; Manzoni et al., 2013; Wullschleger et al., 1998). Multi-site syntheses have focused on the environmental sensitivity of sap flow, using site means of plant-level sap flow or sap flow-derived stand transpiration (Poyatos et al., 2007; Tor-ngern et al., 2017). Since data sharing is only incipient in plant ecophysiology, sap flow datasets have not been traditionally available in open data repositories. Open data practices are now being implemented in databases, which fosters collaboration across monitoring networks in research areas relevant to plant functional ecology (Falster et al., 2015; Gallagher et al., 2020; Kattge et al., 2020) and ecosystem ecology (Bond-Lamberty and Thomson, 2010). The success of the data sharing and data re-use policies within the FLUXNET global network of ecosystem level fluxes has shown how these practices can contribute to scientific progress (Bond-Lamberty, 2018).

Here we introduce SAPFLUXNET, the first global database of sap flow measurements built from individual community-contributed datasets. We implemented this compilation in a data structure designed to accommodate time series of sap flow and the main hydrometeorological drivers of transpiration, together with metadata documenting different aspects of each dataset. We harmonised all datasets and performed basic semi-automated quality assurance and quality control procedures. We also created a software package that provides access to the database, allows easy visualisation of the datasets and performs basic temporal aggregations. We present the ecological and geographic coverage of SAPFLUXNET version 0.1.5, (Poyatos et al., 2020a) followed by a discussion of potential applications of the database, its limitations and a perspective of future developments.

3.2 The SAPFLUXNET data workflow

3.2.1 An overview of sap flow measurements

The main characteristics of sap flow methods have been reviewed elsewhere (Čermák et al., 2004; Smith and Allen, 1996; Swanson, 1994; Vandegehuchte and Steppe, 2013). Given the already broad scope of the paper, here we only provide a brief methodological overview, without delving into the details of the individual methods. Sap flow sensors track the fate of heat applied to the plant’s conducting tissue, or sapwood, using temperature sensors (thermocouples or thermistors), usually deployed in the plant’s main stem. Both heating and temperature sensing can be done either internally, by inserting needle-like probes containing electrical resistors (or electrodes for some methods) and temperature sensors into the sapwood, or externally; these latter systems being especially designed for small stems. Depending on how the heat is applied and the principles underlying sap flow calculations, sap flow sensors can be classified into three major groups: heat dissipation methods, heat pulse methods and heat balance methods (Flo et al., 2019). Heat dissipation and heat pulse methods estimate sap flow per unit sapwood area and they have been called ‘sap flux density methods’ (Vandegehuchte and Steppe, 2013); heat balance methods directly yield sap flow for the entire stem or for a sapwood section. Heat dissipation methods include the constant heat dissipation (HD; Granier 1985, 1987), the transient (or cyclic) heat dissipation (CHD; Do and Rocheteau, 2002) and the heat deformation (HFD; Nadezhina 2018) methods. Heat pulse methods include the compensation heat pulse (CHP; Swanson and Whitfield, 1981), heat ratio (HR; Burgess et al. 2001), T-max (HPTM; Cohen et al. 1981) and Sapflow+ (Vandegehuchte and Steppe, 2012) methods. Heat balance methods include the trunk sector heat balance (TSHB; Čermák et al. 1973) and the stem heat balance (SHB; Sakuratani, 1981) methods. The suitability of a certain method in a given application largely depends on plant size and the flow range of interest (Flo et al., 2019), but HD and CHP are the most widely used (Flo et al., 2019; Peters et al., 2018; Poyatos et al., 2016). Apart from these different methodologies, within

3.2. The SAPFLUXNET data workflow

51

each sap flow method variants exist in sensor design and in data processing approaches, resulting in relatively high levels of methodological uncertainty comparable to those in other areas of plant ecophysiology.

The output from sap flow sensors is automatically recorded by dataloggers, at hourly or even higher temporal resolution. This output relates to heat transport in the stem and needs to be converted to meaningful quantities of water transport, such as sap flow per plant or per unit sapwood area. How this conversion is achieved varies greatly across methods, with some relying on empirical calibrations and others being more physically-based and requiring the estimation of wood thermal properties and other parameters (Čermák et al., 2004; Smith and Allen, 1996; Vandegehuchte and Steppe, 2013). Depending on the method and the specific sensor design, sap flow measurements can be representative of single points, linear segments along the sapwood, sapwood area sections or entire stems. Except for stem heat balance methods, these measurements need to be spatially integrated to account for radial (Berdanier et al., 2016; Cohen et al., 2008; Nadezhina et al., 2002; Phillips et al., 1996) and azimuthal (Cohen et al., 2008; Lu et al., 2000; Oren et al., 1999a) variation of sap flow within the stem to obtain an estimate of whole-plant water use (Čermák et al., 2004). At a minimum, an estimate of sapwood area is needed to upscale the measurements to whole-plant sap flow rates. Sap flow rates can thus be expressed per individual (i.e. plant or tree), per unit sapwood area (normalising by water-conducting area), and per unit leaf area (normalising by transpiring area).

Here we will use the term ‘sap flow’ when referring, in general, to the rate at which water moves through the sapwood of a plant and, more specifically, when we refer to sap flow per plant (i.e. water volume per unit time, Edwards et al., 1996). We acknowledge that the term ‘sap flux’ has also been proposed for this quantity (Lemeur et al., 2009), but more generally, ‘sap flux density’ (e.g. Vandegehuchte and Steppe, 2013) or just ‘sap flux’ are used to refer to ‘sap flow per unit sapwood area’. Since here we include methods natively measuring sap flow per plant or per sapwood area, throughout this paper we will use the more general term ‘sap flow’, and, when necessary, we

will indicate explicitly the reference area used: ‘sap flow per (unit) sapwood area’, ‘sap flow per (unit) leaf area’ or ‘sap flow per (unit) ground area’.

3.2.2 Data compilation

SAPFLUXNET was conceived as a compilation of published and unpublished sap flow datasets (Table B8) and thus the ultimate success of the initiative critically depended on the contribution of datasets by the sap flow community. An expression of interest showed that a critical mass of datasets with a wide geographic distribution could potentially be contributed and the results of this survey were used to raise the interest of the sap flow community (Poyatos et al., 2016). The data contribution stage was open between July 2016 and December 2017 although a few additional datasets were updated during the data quality control process and contain more recent data.

All contributed datasets had to meet some minimum criteria before they were accepted, both in terms of content and format. We required that all datasets contained sub-daily, processed sap flow data, representative of whole-plant water use under different hydrometeorological conditions. This meant that both the processing from raw temperature data to sap flow quantities and the scaling from single-point measurements to whole-plant data had been performed by the data contributor responsible for each dataset. Time-series of sap flow data and hydrometeorological drivers were required to be representative of one growing-season, setting, as broad reference, a minimum duration of 3 months. Sap flow could be either expressed as total flow rate per plant or per unit sapwood area. Contributors also needed to provide metadata on relevant ecological information of the site, stand, species and measured plants as well as on basic technical details of the sap flow and hydrometeorological time-series. Datasets had to be formatted using a documented spreadsheet template (cf. ‘sapfluxnet_metadata_template.xlsx’ in <https://github.com/vflo/PhD/tree/master/Chapter3/Supplementary>) and uploaded to a dedicated server at CREAF, Spain, using an online form.

3.2.3 Data harmonisation and quality control: QC1

Once datasets were received, they were stored and entered a process of data harmonisation and quality control (Fig. 1, Fig. B1). This process combined automatic data checks with human supervision, and the entire workflow was governed by functions and scripts in the R language (R Core Team, 2019), including other related tools, such as R markdown documents and Shiny applications. All R code involved in this QC process was implemented in the sapfluxnetQC1 package (Granda et al., 2016). To aid in the detection of potential data issues throughout the entire process (Fig. 1, Fig. B1), we implemented several elements of control: (1) automatic log files tracking the output of each QC function applied, (2) automatic creation and update of status files, tracking the QC level reached by each dataset, (3) automatic QC summary reports in the form of R markdown documents, (4) interactive Shiny applications for data visualisation, (5) documentation of manual changes applied to the datasets using manually-edited text files, (6) storage of manual data cleaning operations in text files, and (7) automatic data quality flagging associated with each dataset. All these items ensure a robust, transparent, reproducible and scalable data workflow. Example files for (2), (3) and (6) can be found in the Supplement.

The first stage of the data QC (QC1) performed several data checks (Table B1) on received spreadsheet files and produced an interactive report in an R markdown document, which signalled possible inconsistencies in the data and warned of potential errors. These data issues were addressed, with the help of data contributors, if needed. Once no errors remained, the dataset was converted into an object of the custom-designed ‘sfn_data’ class (Fig. B2, see also section 2.5), which contained all data and metadata for a given dataset (Tables B2–B6 list all variable names). Data and metadata belonging to all Level 1 datasets were further visually inspected using an interactive R Shiny application, and, if no major issues were detected, they were subjected to the second QC process, QC2.

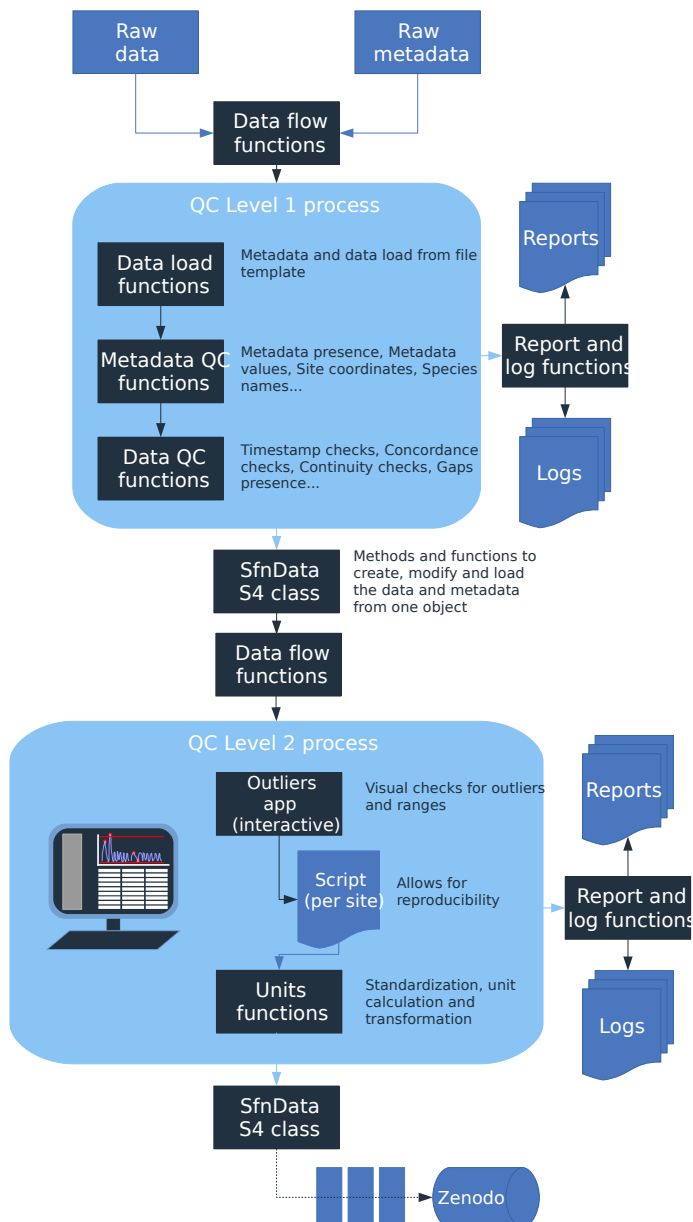


Figure 3.1: Overview of the SAPFLUXNET data workflow. Data files are received from data contributors, and undergo several quality-control processes (QC1 and QC2). Both, QC1 and QC2 produce an .RData object of the custom-designed sfn-data S4 class storing all data, metadata and data flags for each dataset. The progress and results of the QC processes are monitored through individual reports and log files. The final outcome, is stored in a folder structure with a either single .RData file for each dataset or a set of seven csv files for each dataset.

3.2. The SAPFLUXNET data workflow

3.2.4 Data harmonisation and quality control: QC2

Datasets entering QC2 underwent several data cleaning and data harmonisation processes (Table B7). We first ran outlier detection and out of range checks; these checks did not delete or modify the data, only warned about any suspicious observation ('outlier' and 'range' warnings). The outlier detection algorithm was based on a Hampel filter, which also estimates a replacement value for a candidate outlier (Hampel, 1974). For the range checks, we defined minimum and maximum allowed values for all the time series variables, based on published values of extreme weather records and maximum transpiration rates (Cerveny et al., 2007; Manzoni et al., 2013). The outcome of outlier and range checks were visually inspected on the actual time series being evaluated using an interactive R Shiny application (Fig. B3). Following expert knowledge, visually confirmed outliers were replaced by the values estimated by the Hampel filter. Similarly, we replaced out of range values by NA if the variable was out of its physically allowed range (Fig. B3). Outlier and out of range 'warnings' for each observation (e.g. for each variable and timestep) were documented in two data flags tables, with the same dimensions as the corresponding data tables (Fig. B2). Likewise, those observations with confirmed problematic values, which were removed or replaced, were also flagged; further information can be found in the 'data flags' vignettes in the 'sapfluxnetr' package Granda et al. (Granda et al., 2019)

Final data harmonisation processes in QC2 involved unit transformations and the calculation of derived variables (Table B7). When plant sapwood area was provided by data contributors, we interconverted between sap flow rate per plant and per unit sapwood area. If leaf area was supplied, we also calculated sap flow per unit leaf area, but note that this transformation does not take into account the seasonal variation in leaf area. In QC2 we estimated missing environmental variables which could be derived from related variables in the dataset (Table B7). We also estimated the apparent solar time and extraterrestrial global radiation from the provided timestamp and geographic coordinates using the R package 'solaR' (Perpiñán, 2012). All estimated or interconverted observations were flagged as 'CALCULATED' in the 'env_flags' or 'sap_flags' table (Fig. B2).

3.2.5 Data structure

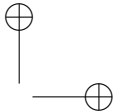
One of the major benefits of the SAPFLUXNET data workflow is the encapsulation of datasets in self-contained R objects of the S4 class with a predefined structure. These objects belong to the custom-designed ‘sfn_data’ class, which display different slots to store time series of sap flow and environmental data, their associated data flags, and all the metadata (Fig. B2). For further information please see the ‘sfn_data classes’ vignette in the ‘sapfluxnetr’ package (Granda et al., 2019). The code identifying each dataset was created by the combination of a ‘country’ code, a ‘site’ code and, if applicable, a ‘stand’ code and a ‘treatment’ code. This means that several ‘stands’ and/or ‘treatments’ can be present within one ‘site’ (Table B3).

At the end of the QC process, we generated a folder structure with a first-level storing datasets as either ‘sfn_data’ objects or as a set of comma-separated (csv) text files. Within each of these formats, a second-level folder groups datasets according to how sap flow is normalized (per plant, sapwood or leaf area); note that the same dataset, expressing different sap flow quantities, can be present in more than one folder (e.g. ‘plant’ and ‘sapwood’). Finally, the third level contains the data files for each dataset: either a single ‘sfn_data’ object storing all data and metadata, or all the individual csv files. More details on the data structure can be found in the ‘sapfluxnetr-quick-guide’ vignette in the ‘sapfluxnetr’ package (Granda et al., 2019).

3.3 The SAPFLUXNET database

3.3.1 Data coverage

The SAPFLUXNET version 0.1.5 database harbours 202 globally distributed datasets (Fig. 2a, Fig. B4 and Table B8), from 121 geographical locations, with Europe, Eastern USA and Australia especially well represented. These datasets were represented in the bioclimatic space using the terrestrial biomes delimited by Whittaker (Fig. 2b), but note that, as any bioclimatic classification, it has its limitations. Datasets have been compiled from all terrestrial biomes, except for temperate rainforests, although some tropical montane

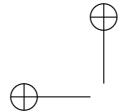


3.3. The SAPFLUXNET database

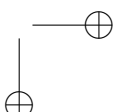
57

sites have been included. Woodland/shrubland and temperate forest biomes are the most represented in the database adding up to 80% of the datasets (Fig. 2b). However, large forested areas in the tropics and in boreal regions are still not well represented (Fig. 2a,b). Looking at the distribution by vegetation type (Fig. 2c), evergreen needleleaf forest is the most represented vegetation type (65 datasets), followed by deciduous broadleaf forest (47 datasets) and evergreen broadleaf forest (43 datasets).

SAPFLUXNET contains sap flow data for 2714 individual plants (1584 angiosperms and 1130 gymnosperms), belonging to 174 species (141 angiosperms and 33 gymnosperms), 95 different genera and 45 different families (Table B9-B10). All species but one, *Elaeis guineensis*, a palm, are tree species. *Pinus* and *Quercus* are the most represented genera (Fig. 3b). Amongst the gymnosperms, *Pinus sylvestris*, *Picea abies* and *Pinus taeda* are the three most represented species with data provided on 290, 178 and 107 trees, respectively (Fig. 3a). For the angiosperms, *Acer saccharum*, *Fagus sylvatica* and *Populus tremuloides* are the most represented species, with 162, 116 and 104 trees, respectively, although most *Acer saccharum* data come from a single study with a very large sample size (Fig. 3a). Some species are present in more than 10 datasets: *Pinus sylvestris*, *Picea abies*, *Fagus sylvatica*, *Acer rubrum*, *Liriodendron tulipifera* and *Liquidambar styraciflua* (Fig. 3a, Table B4).



|



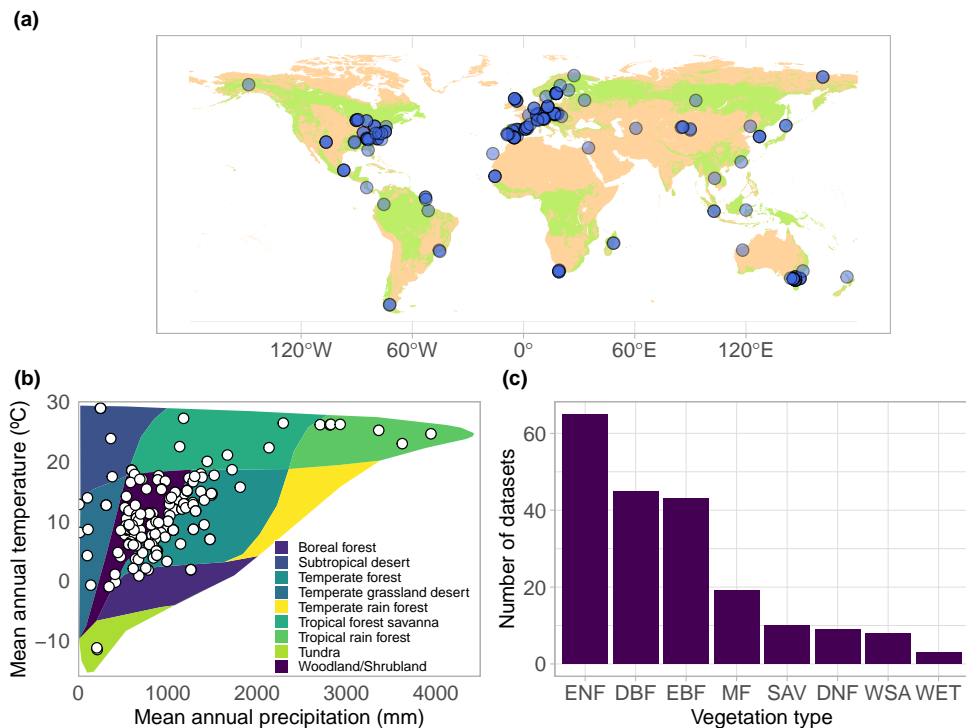


Figure 3.2: (a) Geographic, (b) bioclimatic and (c) vegetation type distribution of SAPFLUXNET datasets. In (a) woodland area from Crowther et al. (2015) is shown in green. In (b) we represent the different datasets according to their mean annual temperature and precipitation in a Whittaker diagram showing the classification of the main terrestrial biomes. In (c) vegetation types are defined according to the International Geosphere-Biosphere Programme (IGBP) classification (ENF: Evergreen Needleleaf Forest; DBF: Deciduous Broadleaf Forest; EBF: Evergreen Broadleaf Forest; MF: Mixed Forest; DNF: Deciduous Needleleaf forest; SAV: Savannas; WSA: Woody Savannas; WET: Permanent Wetlands).

3.3. The SAPFLUXNET database

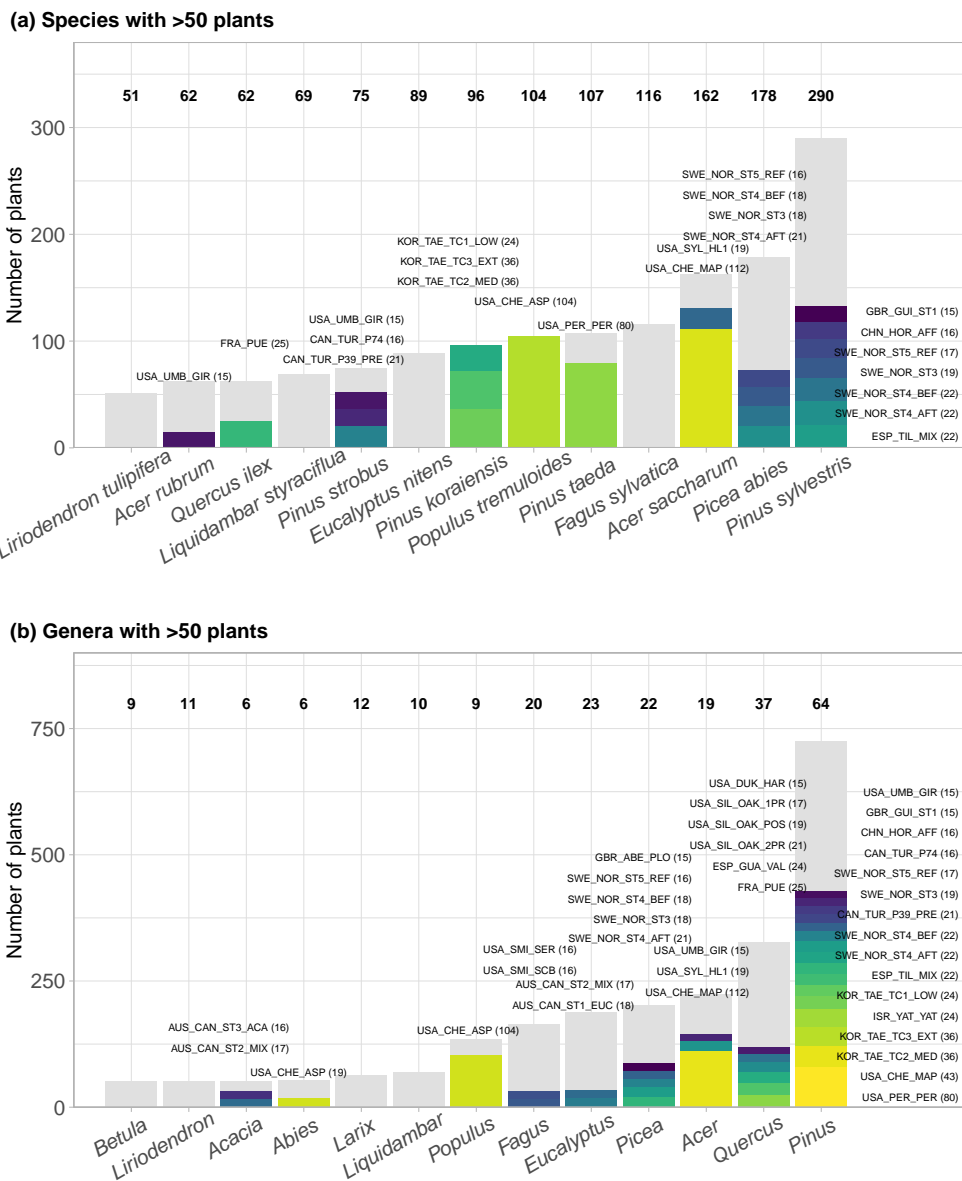


Figure 3.3: Taxonomic distribution of genera and species in SAPFLUXNET, showing (a) species and (b) genera with > 50 plants in the database. Total bar height depicts number of plants per species (a) or genera (b). Numbers on top of each bar show the number of datasets where each species (a) or genus (b) is present. Colours other than grey highlight datasets with 15 or more plants of a given species (a) or genus (b). Bar height for a given colour is proportional to the number of plants in the corresponding dataset, which is also shown in parentheses next to the dataset code.

3.3.2 Methodological aspects

For more than 90% of the plants, sap flow at the whole-plant level is available (either directly provided by contributors or calculated in the QC process); this is important for upscaling SAPFLUXNET data to the stand level (cf. section 4.2). Because the leaf area of the measured plants is often not available as metadata, sap flow per unit leaf area was estimated for only 18.6% of the individuals (Fig. 4). The heat dissipation method is the most frequent method in the database (HD, 66.4% of the plants), followed by the trunk sector heat balance (TSHB, 16.4%) and the compensation heat pulse method (CHP, 8.4%) (Fig. 4). This distribution is broadly similar to the use of each method documented in the literature, although the TSHB method is overrepresented here, compared to the current use of this method by the sap flow community (Flo et al., 2019; Poyatos et al., 2016). Some methods, especially those belonging to the heat pulse family and the cyclic (or transient) heat dissipation (CHD) method are mostly used in angiosperms, while the TSHB and the heat field deformation (HFD) methods are more frequently used in gymnosperms (Fig. 4).

Calibration of sap flow sensors and scaling from point measurements to the whole-plant can be critical steps towards accurate estimates of absolute sap flow rates. In SAPFLUXNET, most of the sap flow time series have not undergone a species-specific calibration, with the CHD method showing the highest percentage of calibrated time series (Table 1). This lack of calibrations may be relevant for the more empirical heat dissipation methods (HD and CHD), which have been shown to consistently underestimate sap flow rates (Flo et al., 2019; Peters et al., 2018; Steppe et al., 2010). Radial integration of single-point sap flow measurements is more frequent than azimuthal integration (Table 2), except for the CHD method. A large number of plants using the HD method, and all plants measured using the HPTM method, do not employ any radial integration procedure. In contrast, the CHP, HR, SHB, and TSHB methods are those which more frequently addressed radial variation in one way or another (Table 2). Azimuthal integration procedures are also more frequent when the TSHB method is used (Table 2).

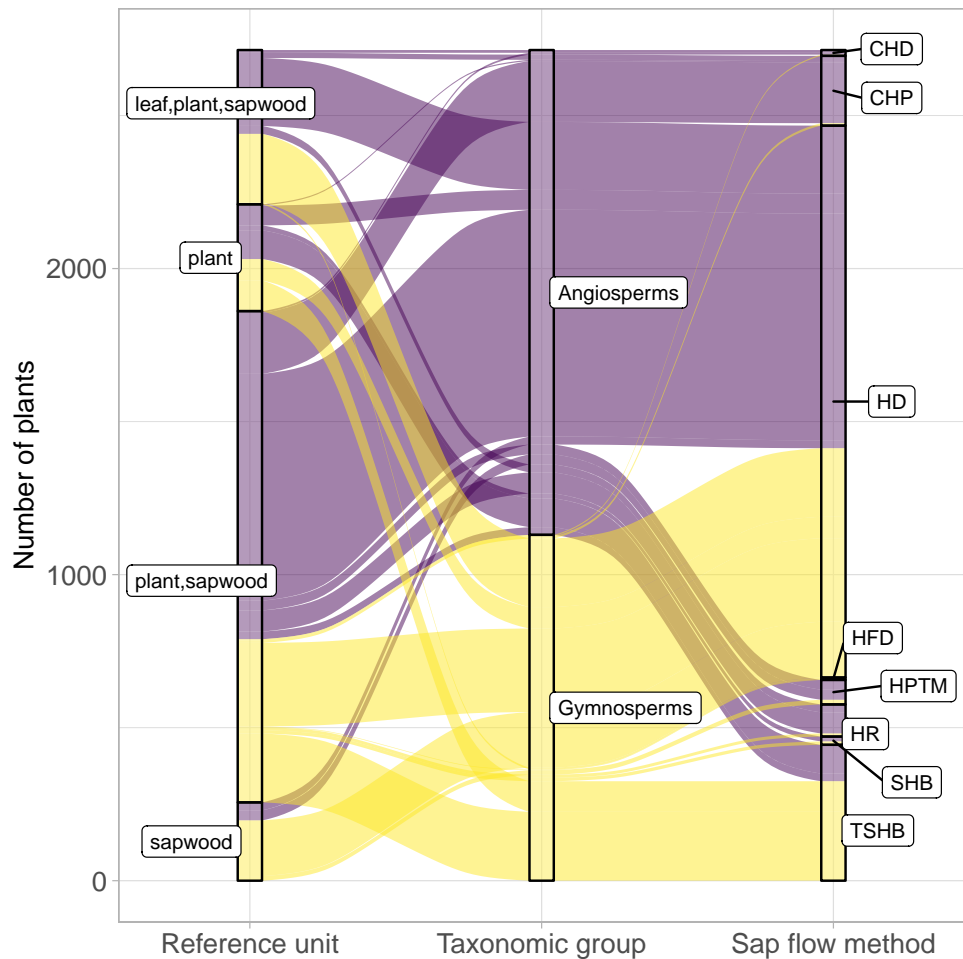


Figure 3.4: Distribution of plants in SAPFLUXNET according to major taxonomic group (angiosperms, gymnosperms), sap flow method (CHD:cycling heat dissipation; CHP: compensation heat pulse; HD: heat dissipation; HFD: heat field deformation; HPTM: heat pulse T-max (HPTM); HR: heat ratio (HR); SHB: stem heat balance; TSHB: trunk sector heat balance) and reference unit for the expression of sap flow (plant, sapwood area, leaf area). Combinations of reference units imply that data are present in multiple units.

3.3.3 Plant characteristics

Plant-level metadata is almost complete (99.5% of the individuals) for diameter at breast height (DBH), while sapwood area and sapwood depth, important variables for sap flow upscaling, are not available, or could not be estimated, for 23% and 47% of the plants, respectively. Plant height and

Table 3.1: Number of sap flow times series in SAPFLUXNET depending on whether they were calibrated (species-specific), non-calibrated or this information was not provided, for the different sap flow methods: cyclic (or transient) heat dissipation (CHD), compensation heat pulse (CHP), heat dissipation (HD), heat field deformation (HFD), heat pulse T-max (HPTM), heat ratio (HR), stem heat balance (SHB) and trunk sector heat balance (TSHB). The percentage of calibrated time series was expressed with respect to the total number of sap flow time series for each method.

Method	Calibrated	Non-calibrated	Not provided	% calibrated
CHD	6	13	0	31.6
CHP	29	42	157	12.7
HD	214	1491	98	11.9
HR	3	55	47	2.9
TSHB	7	433	4	1.6
HFD	0	8	0	0.0
HPTM	0	80	0	0.0
SHB	0	27	0	0.0

plant age are missing for 42% and 62% of the individuals, respectively. Sap flow data in SAPFLUXNET are representative of a broad range of plant sizes (Fig. 5a). The distribution of DBH showed a median of 25.0 cm and 20.4 cm for gymnosperms and angiosperms, respectively, with a long tail towards the largest plants, two *Mortoniadendron anisophyllum* trees from a tropical forest in Costa Rica that measured > 200 cm (Fig. 5a). The largest gymnosperm tree in SAPFLUXNET (176 cm in DBH) is a kauri tree (*Agathis australis*) from New Zealand. The distribution of plant heights is less skewed, with similar medians for angiosperms (17.6 m) and gymnosperms (17.5 m). The tallest plants are located in a tropical forest in Indonesia, where a *Pouteria firma* tree reached 44.7 m. Remarkably, of the 16 plants taller than 40 m, over 60% are Eucalyptus species. The tallest gymnosperm (36.2 m) is a *Pinus strobus* from NE USA.

Plant size metadata in SAPFLUXNET is complemented with plant-level data of sapwood and leaf area, that provide information on the functional areas for water transport and loss (Fig. 5a). Distributions of sapwood and leaf area show highly skewed distributions, with long tails towards the largest values and slightly higher median values for gymnosperms (262 cm² and 33.0

3.3. The SAPFLUXNET database

Table 3.2: Number of plants in the SAPFLUXNET database using different radial and azimuthal integration approaches for the different sap flow methods: cyclic (or transient) heat dissipation (CHD), compensation heat pulse (CHP), heat dissipation (HD), heat field deformation (HFD), heat pulse T-max (HPTM), heat ratio (HR), stem heat balance (SHB) and trunk sector heat balance (TSHB).

Azimuthal integration					
Method	Measured	Sensor-integrated	Corrected, measured azimuthal variation	No azimuthal correction	Not provided
CHD	15	0	0	0	4
CHP	61	0	0	167	0
HD	216	0	520	1021	46
HFD	0	0	0	8	0
HPTM	0	0	0	80	0
HR	7	0	2	88	8
SHB	0	0	0	27	0
TSHB	0	25	191	219	9

Radial integration					
Method	Measured	Sensor-integrated	Corrected, measured radial variation	No radial correction	Not provided
CHD	0	0	6	13	0
CHP	222	0	6	0	0
HD	77	3	645	703	142
HFD	2	0	0	6	0
HPTM	0	0	0	80	0
HR	57	1	42	3	2
SHB	0	27	0	0	0
TSHB	0	338	8	89	9

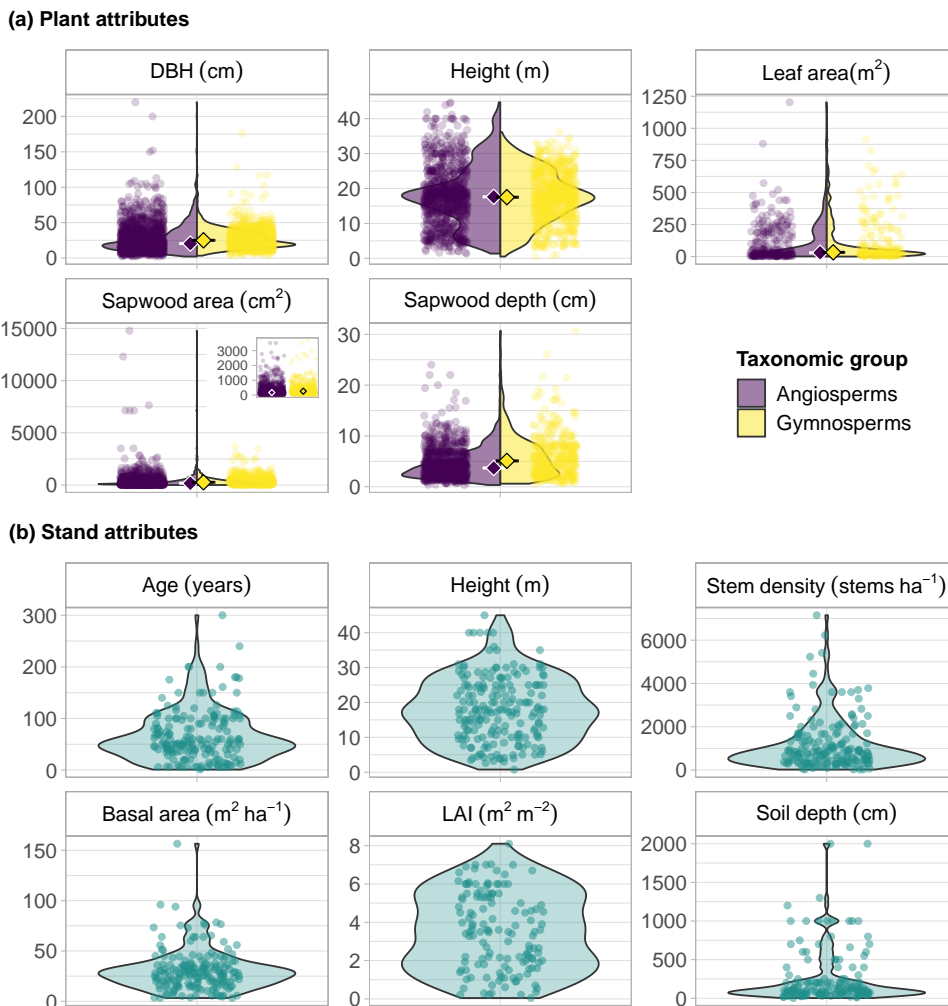
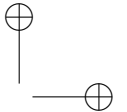
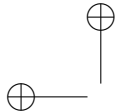


Figure 3.5: Characteristics of trees and stands in the SAPFLUXNET database. Panel (a) shows plant data and kernel density plots of the main plant attributes, coloured by taxonomic group (angiosperms and gymnosperms): diameter at breast height (DBH), plant height, sapwood area, sapwood depth and leaf area. The inset in the sapwood area panel zooms in values lower than 5000 cm^2 . Panel (b) shows stand data and kernel density plots of the main stand attributes: stand age, stand height, stem density, stand basal area, leaf area index (LAI) and soil depth.

m^2 for sapwood and leaf areas, respectively), compared to angiosperms (168 cm^2 and 29.9 m^2). Accordingly, median sapwood depth is also higher for gymnosperms (5.1 cm) compared to angiosperms (3.7 cm). The largest trees (Mortoniodendron, Pouteria, Agathis) with deep sapwood ($17\text{--}24 \text{ cm}$) are also



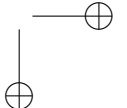
those with largest sapwood areas. Many large angiosperm trees from tropical (CRI_TAM_TOW, IDN_PON_STE, GUF_GUY_ST2; see Table B3 for dataset codes) and temperate forests (*Fagus grandifolia*, USA_SMIC_SCB) also show large sapwood areas (> 5000 cm²), but the plant with the deepest sapwood is a gymnosperm, an *Abies pinsapo* in Spain with 30.7 cm of sapwood depth.

3.3.4 Stand characteristics

Stand-level metadata include several variables associated with management, vegetation structure and soil properties. Half of the datasets originate from naturally regenerated, unmanaged stands, and 13.9% come from naturally regenerated but managed stands. Plantations add up to 32.2% and orchards only represent 4% of the datasets. Reporting of structural variables is mixed, with stand height, age, density and basal area showing relatively low missingness (6.4%, 11.4%, 12.9% and 13.4%, respectively); in contrast, soil depth and LAI are missing from 26.7% and 33.7% of the datasets.

SAPFLUXNET datasets originate from stands with diverse structural characteristics. Median stand age is 54 years and there are several datasets coming from >100 year-old forests (Fig. 5b). Stand height shows a similar range and distribution of values compared to individual plant height (Fig. 5a,b). The denser stands correspond to coppiced evergreen oak stands from Mediterranean forests (FRA_PUE, ESP_TIL_OAK), species-rich tropical forests (MDG_SEM_TAL) or relatively young temperate forests (e.g. FRA_HES_HE1_NON, USA_CHE_MAP). The sparsest stands (< 200 stems ha⁻¹) correspond to tree-grass savanna systems (Spain, Portugal, Australia, Senegal), dry woodlands (China), or oil palm plantations in Indonesia (IDN_JAM_OIL). Stands with the largest basal areas (> 70 m² ha⁻¹) are mostly dominated by broadleaf species, except for a *Picea abies* plantation in Sweden (SWE_SKO_MIN).

The distribution of leaf area index (LAI) shows a median of 3.5 m² m⁻², with the largest values observed in temperate (CZE_BIK, USA_DUK_HAR, HUN_SIK) and tropical (GUF_GUY_GUY, COL_MAC_SAF_RAD)



forests. The stands with the lowest LAI correspond to the sparse woodlands from Mediterranean and semi-arid locations and also those from forests near altitudinal or latitudinal tree-lines (FIN_PET, AUT_TSC). SAPFLUXNET datasets show a median soil depth of 100 cm, with only a dozen datasets originated from sites with soils deeper than 10 m (Fig. 5b).

The number of plants per dataset is highly variable, with most of the datasets (86%) containing data for at least 4 trees and 46% of the datasets having data for at least 10 trees (Fig. 6a, see also Fig. 9).

3.3.5 Temporal characteristics

The oldest datasets in SAPFLUXNET go back to 1995 (GBR_DEV_CON, GBR_DEV_DRO) while the most recent data reach up to 2018 (datasets from the ESP_MAJ cluster of sites). Several multi-year datasets are present in SAPFLUXNET (Fig. 6), with 50% of the datasets spanning a period of at least 3 years, and some datasets being extraordinarily long (16 years in FRA_PUE). Frequently, the datasets only cover the ‘growing season’ periods, or even shorter periods for some sites which were eventually included because they improved the ecological and geographic coverage of the database (e.g. ARG_MAZ, ARG_TRE as representative of deciduous Nothofagus forest in South Patagonia). In contrast, a few datasets show continuous records over multiple years (Fig. 6b). Amongst the longest datasets, most of them come from European or North American sites (Fig. 6), except some datasets from Israel (ISR_YAT_YAT, 7 years), Russia (RUS_FYO, 7 years), South Korea (KOR_TAE cluster of sites, 6 years) or New Zealand (NZL_HUA_HUA, 5 years).

SAPFLUXNET provides an unprecedented database to study the detailed temporal dynamics of plant transpiration across species and sites globally. Sub-daily records of sap flow (e.g. at least at hourly timesteps) are available for extended periods (Fig. 6b), allowing to address both seasonal and diel patterns in water use regulation by trees and how these temporal patterns change across species or years across terrestrial biomes, reflecting different phenologies and water-use strategies. For instance, in Mediterranean forests,

3.3. The SAPFLUXNET database

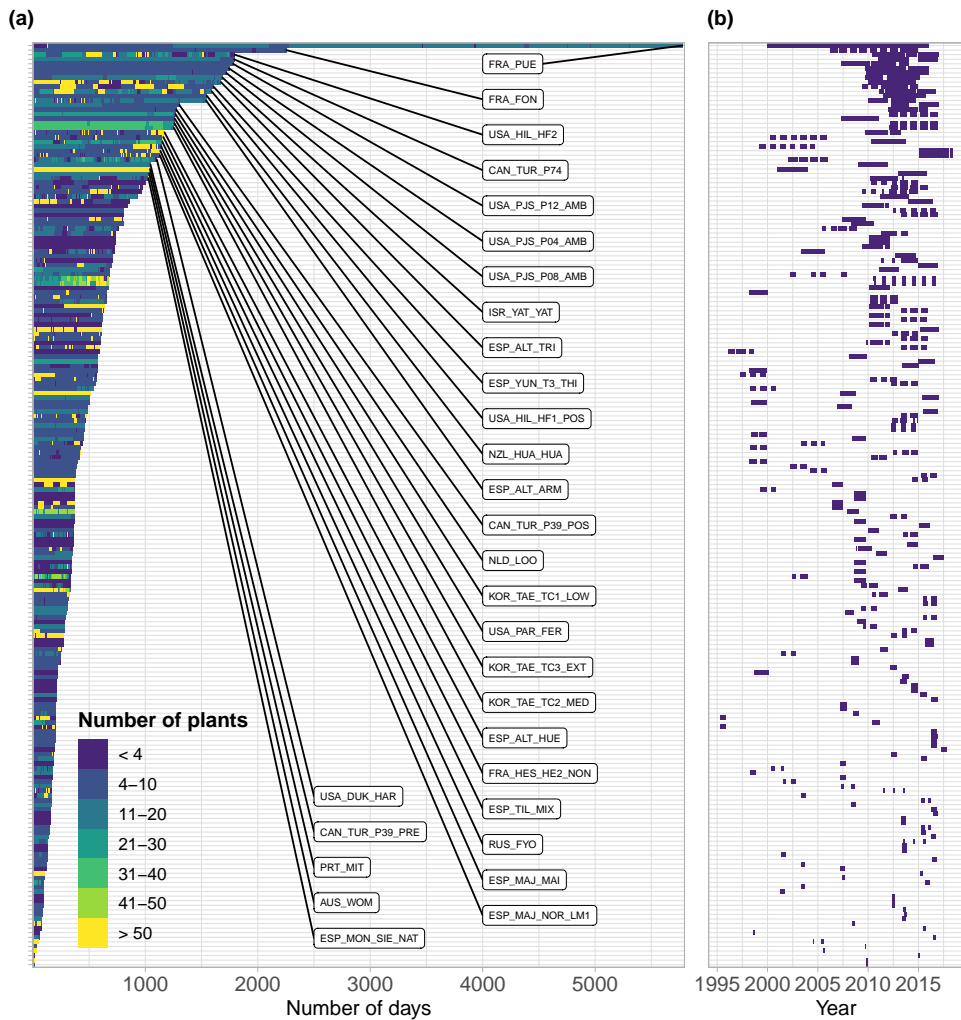


Figure 3.6: (a) Measurement duration of SAPFLUXNET datasets expressed in number of days with sap flow data and coloured by the number of plants measured on each day . The 30 longest datasets are labelled. For each dataset in panel (a), panel (b) shows its corresponding measurement period.

evergreen species such as *Quercus ilex*, *Arbutus unedo* and *Pinus halepensis* show moderate sap flow the whole year round, while the deciduous *Quercus pubescens* shows higher sap flow density during a shorter period and its water use is heavily reduced during a dry year (2012) (Fig. 7a). Temperate forests without water availability limitations show relatively high flows during the growing season and similar diel sap flow patterns among species (Fig. 7b).

In contrast, tropical forests show moderate to high sap flow rates during the entire year, with different dynamics in the intradaily water use regulation across species. For example, *Inga* sp. in a highly diverse wet tropical forest in Costa Rica, reduced sap flow during mid-day hours compared to co-existing species (Fig. 7c).

3.3.6 Availability of environmental data

All SAPFLUXNET datasets contain ancillary time series of the main hydrometeorological drivers of transpiration, accompanied by information on where these variables had been measured (Fig. 8a). Air temperature is available for all datasets. Although vapour pressure deficit (VPD) was originally absent in 38% of the datasets (Fig. 8a,b), we could estimate it for those sites providing air temperature and relative humidity data (QC Level 2, see section 2.3), and finally only 2 out of the 202 datasets have missing VPD information. For radiation variables, shortwave radiation was most often provided, compared to photosynthetically active and net radiation; only 8 out of 202 datasets do not have any accompanying radiation data. Most of these environmental variables were measured on-site, with precipitation being the variable most frequently retrieved from nearby meteorological stations (48% of the datasets) (Fig. 8a). Soil water content measured at shallow depth, typically between 0 and 30 cm below the soil surface, is provided for 56% of the datasets, while soil moisture from deep soil layers is available for only 27% of the datasets.

3.4 Potential applications

3.4.1 Applications in plant ecophysiology and functional ecology

There are multiple potential applications of the SAPFLUXNET database to assess whole-plant water use rates and their environmental sensitivity, both across species (e.g. Oren et al., 1999b) and at the intraspecific level (Poyatos et al., 2007). SAPFLUXNET will allow disentangling the roles of evaporative demand and soil water content in controlling transpiration at the plant level,

3.4. Potential applications

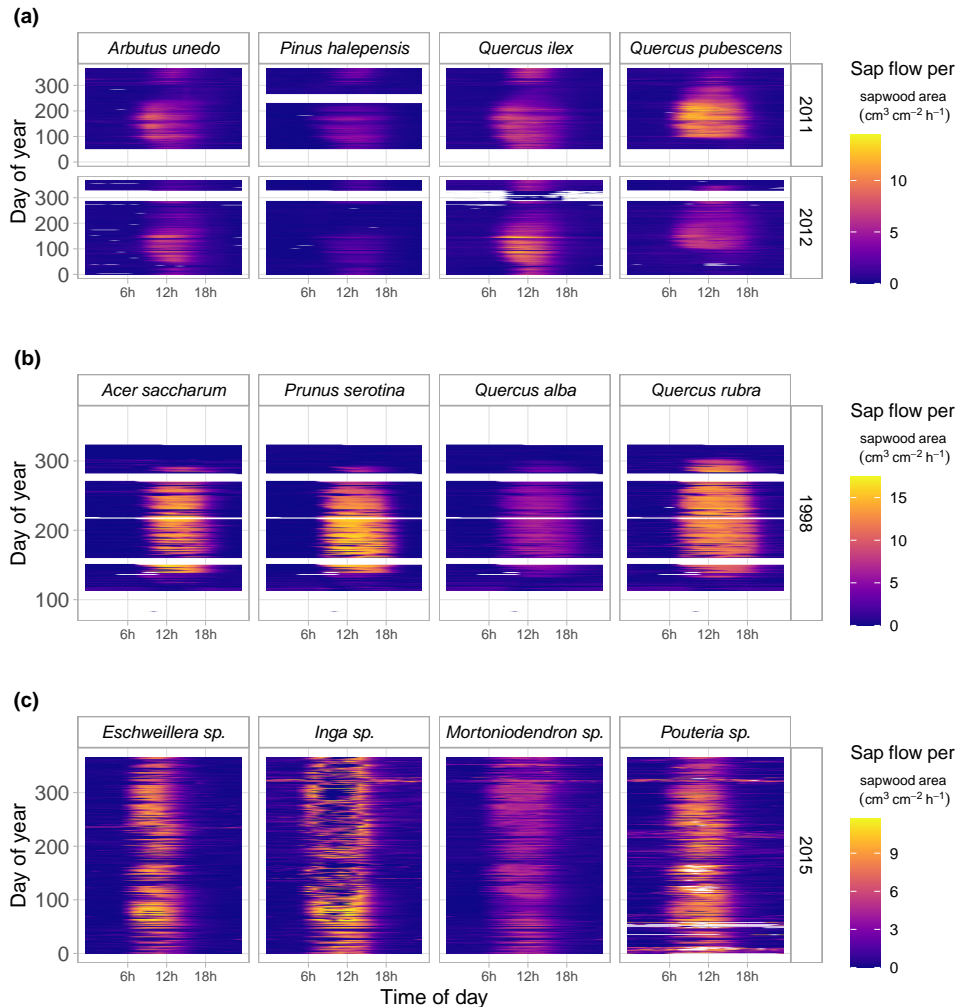


Figure 3.7: Fingerprint plots showing hourly sap flow per unit sapwood area ($\text{cm}^3 \text{cm}^{-2} \text{h}^{-1}$) as a function of hour of day (x-axis) and day of year (y-axis) for a selection of SAPFLUXNET sites with at least four co-occurring species. Panel (a) shows data from a Woodland/Shrubland forest in NE Spain (ESP_CAN), for an average (2011) and a dry (2012) year. Panel (b) shows data for a mesic Temperate forest (USA_WVF) and panel (c) shows data for a Tropical forest (CRI_TAM_TOW). For this latter site, only 4 of the 17 measured species are shown and some of them were only identified at the genus level.

complementing recent studies looking at how water supply and demand affect evapotranspiration at the ecosystem level (Anderegg et al., 2018; Novick et al., 2016). The availability of global sap flow data at sub-daily time resolution

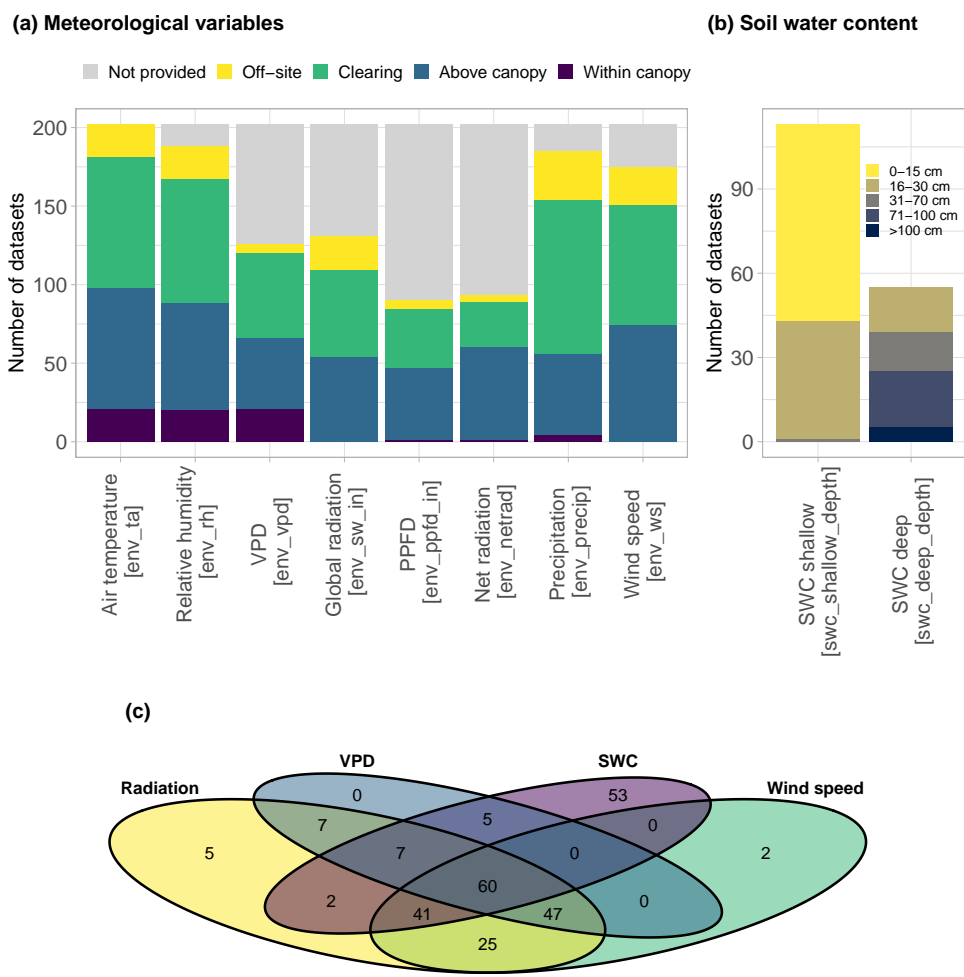


Figure 3.8: Summary of the availability of different environmental variables in SAPFLUXNET datasets. (a) Distribution of meteorological variables according to sensor location (in brackets, names of the variables in the database), (b) Distribution of soil moisture variables according to the measurement depth (in brackets, names of the variables in the database). (c) Venn diagram showing the number of datasets where each combination of different environmental variables are present, grouping shortwave, PPFD and net radiation under ‘Radiation’ variables.

and spanning entire growing seasons will allow focusing on how maximum water use and its environmental sensitivity varies with plant-level attributes such as stem diameter (Dierick and Hölscher, 2009; Meinzer et al., 2005), tree height (Novick et al., 2009; Schäfer et al., 2000), hydraulic (Manzoni et

al., 2013; Poyatos et al., 2007) and other plant traits (Grossiord et al., 2019; Kallarackal et al., 2013). SAPFLUXNET thus provides an unprecedented tool to understand how structural and physiological traits scale-up to whole-plant regulation of water fluxes (McCulloh et al., 2019), and how this integration determines drought responses (Choat et al., 2018) and post-drought recovery patterns (Yin and Bauerle, 2017). Analyses of the temporal dynamics of plant water use in response to specific drought events, as recently assessed for gross primary productivity (e.g. Schwalm et al., 2017), can also help to quantify drought legacy effects, including the reversibility of drought-induced losses of hydraulic conductivity at the plant level.

SAPFLUXNET will allow new insights into within-day patterns and controls in whole-plant water use, which can disclose the fine details of its physiological regulation. Circadian rhythms can modulate stomatal responses to the environment, potentially affecting sap flow dynamics (e.g. de Dios et al., 2015). Hysteresis in diel sap flow relationships with evaporative demand and time-lags between evaporative demand and sap flow, are two linked phenomena likely arising from plant capacitance and other mechanisms (O’Brien et al., 2004; Schulze et al., 1985), that also influence diel evapotranspiration dynamics (Matheny et al., 2014; Zhang et al., 2014). A major driver of time-lags is the use of stored water to meet the transpiration demand (Phillips et al., 2009), which can now be analysed across species, plant sizes or drought conditions using time series analyses, simplified electric analogies (Phillips et al., 1997, 2004; Ward et al., 2013) or detailed water transport models (Bohrer et al., 2005; Mirfenderesgi et al., 2016). Night-time water use can be substantial for some species (Forster, 2014; Resco de Dios et al., 2019). However, available syntheses rely on study-specific quantification of what constitutes nocturnal sap flow and do not address possible methodological influences (Zeppel et al., 2014). SAPFLUXNET will allow applying a consistent estimation of nocturnal sap flow and control for datasets that are less suitable for the quantification of night-time fluxes, as information on zero-flow determination is included in the metadata (‘pl_sens_cor_zero’, Table B5).

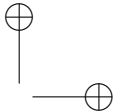
Sap flow data have been widely employed to assess changes in tree wa-

ter use after biotic (e.g. Hultine et al., 2010) or abiotic (Oren et al., 1999a) disturbances. Likewise, sap flow data have been used to report changes in species and stand water use following experimental treatments involving resource availability modifications (e.g. Ewers et al., 1999) or density changes (i.e. thinning, Simonin et al., 2007). The SAPFLUXNET database includes datasets with experimental manipulations, applied either at the stand or at the individual level (Table 3). The main treatments present are related to thinning, water availability changes (irrigation, throughfall exclusion) and wildfire impact (Table 3), potentially facilitating new data syntheses and meta-analyses using these datasets (e.g. Grossiord et al., 2017).

Table 3.3: Number of datasets, plants and species by stand-level treatment in the SAPFLUXNET database.

Treatment	N sites	N plants	N species
None/control	155	2198	170
Thinning	18	332	18
Irrigation	9	36	4
Post-fire	6	18	4
CO ₂ fertilisation	3	28	2
Drought	3	9	2
Soil fertilisation	2	16	2
Post-mortality	1	22	5
Soil fertilisation and pruning	1	12	1
Soil fertilisation and thinning	1	12	1
Pruning and thinning	1	11	1
Soil fertilisation, pruning and thinning	1	11	1
Pruning	1	9	1

The combination of SAPFLUXNET with other ecophysiological databases can inform on the relative sensitivity of different physiological processes in response to drought, for example those related to growth and carbon assimilation (Steppe et al., 2015) . Within-day fluctuations of stem diameter can be jointly analysed with co-located sap flow measurements to study the dynamics of stored water use under drought and its contribution to transpiration (e.g. Brinkmann et al., 2016), and to infer parameters on tree hydraulic functioning using mechanistic models of tree hydrodynamics (Salomón et al., 2017; Steppe et al., 2006; Zweifel et al.,



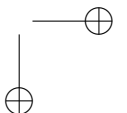
3.4. Potential applications

2007). These analyses could be carried out for a large number of species by combining SAPFLUXNET with data from the Dendroglobal database (<http://78.90.202.92/streess/databases/dendroglobal>); there are at least 18 SAPFLUXNET datasets with dendrometer data in Dendroglobal. This database and the International Tree-Ring Data Bank (Zhao et al., 2018) could also be used with SAPFLUXNET to investigate, at the species level, the link between radial growth and water use, including their environmental sensitivity (Morán-López et al., 2014), and how these two processes comparatively respond to drought (Sánchez-Costa et al., 2015). Moreover, given the tight link between water use and carbon assimilation, combining SAPFLUXNET with water-use efficiency from plant $\delta^{13}\text{C}$ data could potentially be used to estimate whole-plant carbon assimilation (Hu et al., 2010; Klein et al., 2016; Rascher et al., 2010; Vernay et al., 2020), a quantity that is difficult to measure directly, especially in field-grown, mature trees.

The two first PCA axes explained 60% of the variability of the 12 climatic variables. The niche of *P. halepensis* characterized with inter-annual variability (inter-annual variability-based niche) was 42% larger than the niche estimated with the average dataset (average-based niche). These differences implied that during the extreme climatic year, 93.3% of unaffected forests and 63.3% of highly affected forests were inside the *P. halepensis* niche estimated with inter-annual variability. These values diminished to 52.8% for unaffected forests and 21.2% for highly affected ones when niche was calculated with average climate (Fig. 3.2).

3.4.2 Applications in ecosystem ecology and ecohydrology

SAPFLUXNET will provide a global look at plant water flows to bridge the scales between plant traits and ecosystem fluxes and properties (Reichstein et al., 2014). Vegetation structure, species composition and differential water use strategies among and within species scale-up to different seasonal patterns of ecosystem transpiration, with a strong influence on ecosystem evapotranspiration and its partitioning. Global controls on evaporative fluxes from vegetation have been mostly addressed using ecosystem (Williams et al., 2012) or catchment evapotranspiration data (Peel et al., 2010). These studies have



described global patterns in evapotranspiration driven by different plant functional types or climates, but they cannot be used to quantify and to explain the enormous variation in the regulation of transpiration across and within taxa.

The SAPFLUXNET database will provide a long-demanded data source to be used in ecohydrological research (Asbjornsen et al., 2011). Upscaling individual measurements to the stand level (Čermák et al., 2004; Granier et al., 1996; Köstner et al., 1998) is necessary to quantitatively compare sap-flow based transpiration with evapotranspiration and transpiration estimates at the ecosystem scale and beyond. Even though SAPFLUXNET was designed to accommodate sap flow data at the plant level, scaling to the ecosystem level is possible for many datasets. For a basic upscaling exercise using SAPFLUXNET data (Poyatos et al., 2020b), whole-plant sap flow can be normalised by individual basal area (as DBH is usually available in the metadata, cf. section 3.3), averaged for a given species and then scaled to stand level transpiration using total stand basal area and the fraction of basal area occupied by each measured species (see stand metadata, Table B3). For many datasets, sap flow data are available for the species comprising most of the stand basal area (often even 100%, Fig. 9), but species-based upscaling may be unfeasible in many tropical sites (Fig. 9b), where size-based scaling could be applied instead (e.g. da Costa et al., 2018). Further refinements of the upscaling procedure could be achieved by using trunk diameter distributions of the sap flow plots (Berry et al., 2018). This information, however, is not readily available in SAPFLUXNET, and other data sources (e.g. forest inventories, LIDAR data) or additional simplifying assumptions (i.e. applying the size distribution of measured individuals in the dataset) would be needed.

3.4. Potential applications

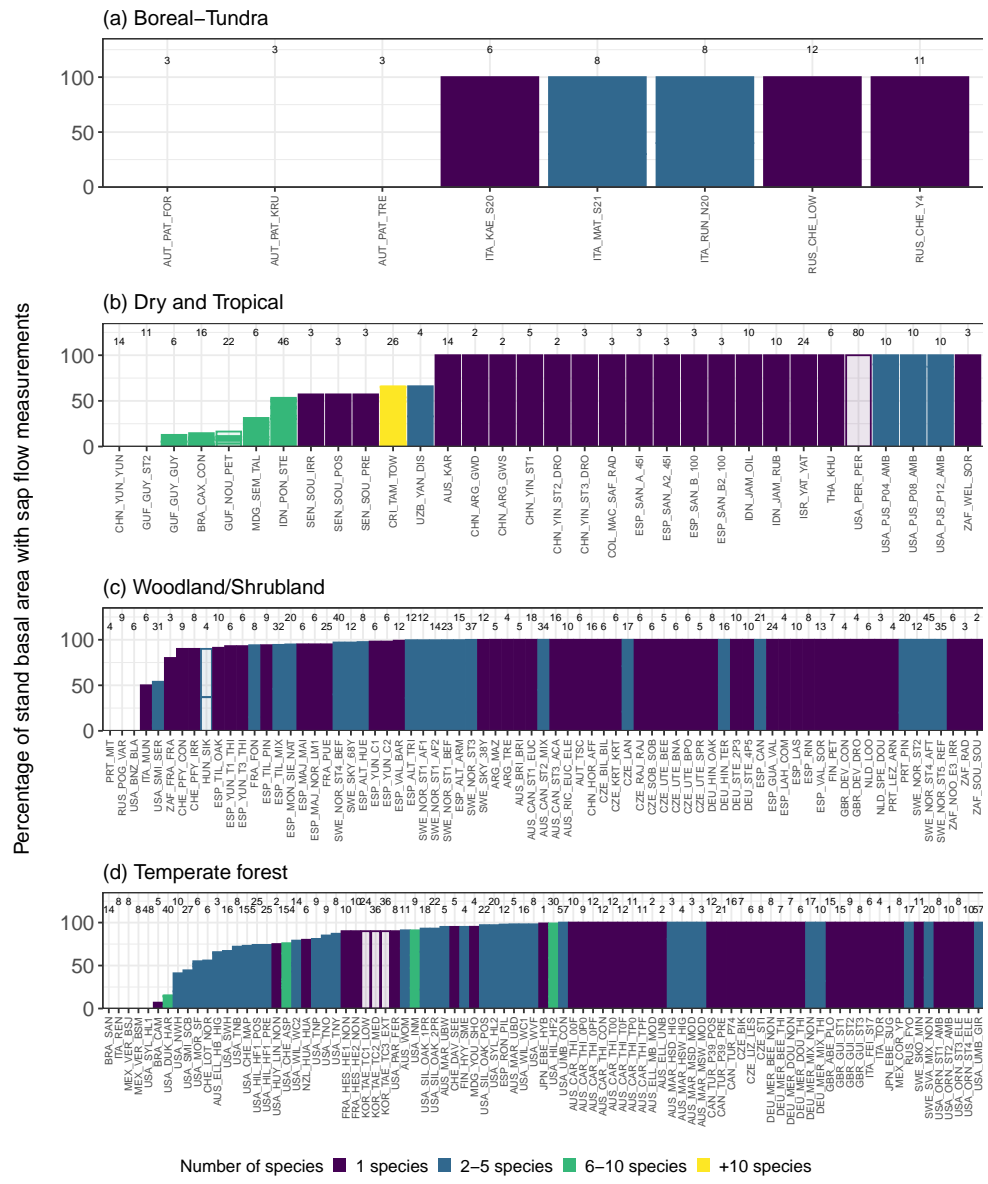


Figure 3.9: Potential for upscaling species-specific plant sap flow to stand-level sap flow using SAPFLUXNET datasets. Datasets are shown using an aggregated biome classification; ‘Dry and Tropical’ include: ‘Subtropical desert’, ‘Temperate grassland desert’, ‘Tropical forest savanna’ and ‘Tropical rain forest’. Each panel shows the percentage of total stand basal area that is covered by sap flow measurements for each species in the dataset. Datasets are also coloured by the number of species present. Numbers on top of each bar depict the total number of plants for a given dataset. Empty bars show datasets for which sap flow data expressed at the plant level were not available.

Stand-level transpiration estimates from a large number of SAPFLUXNET sites can contribute to improve our understanding of the role of forest transpiration in the context of stand water balance and its components at the ecosystem (e.g. Tor-ngern et al., 2018) and catchment levels (Oishi et al., 2010; Wilson et al., 2001). Importantly, SAPFLUXNET can contribute to better understand the global controls on vegetation water use (Good et al., 2017), including the biological and climatic controls on evapotranspiration partitioning into transpiration and evaporation components (Schlesinger and Jasechko, 2014; Stoy et al., 2019). There is some overlap between the FLUXNET network and SAPFLUXNET (47 datasets from FLUXNET sites). Hence, transpiration from SAPFLUXNET can also be used as a ‘ground-truth’ reference for transpiration estimates from remote sensing approaches (Talsma et al., 2018) and from eddy covariance data (Nelson et al., accepted). Extrapolating sap flow-derived stand transpiration to large spatial scales can be challenging due to landscape-scale variation in forest structure (Ford et al., 2007) or topography (Hassler et al., 2018), and to the low spatial representativeness of sap flow measurements (Mackay et al., 2010). A promising research avenue to help elucidate the role of vegetation in driving hydrological changes across environmental gradients (Vose et al., 2016) would be to combine species-specific stand transpiration data from SAPFLUXNET with stand structural and compositional data from forest inventories (e.g. sapwood area index, Benyon et al., 2015).

Understanding the patterns and mechanisms underlying species interactions with respect to water use within a community is necessary to predict tree species vulnerability to drought (Grossiord, 2019). Multispecies datasets from SAPFLUXNET (Table B4) can be used to assess competition for water resources among species, for example by identifying changes in seasonal water use across co-existing species and hence characterizing the spatiotemporal segregation of their hydrological niches (Silvertown et al., 2015). By providing a detailed seasonal quantification of tree water use, SAPFLUXNET could also complement isotope-based studies and contribute to interpret the large diversity in root water uptake patterns observed worldwide (Barbeta and Peñuelas, 2017; Evaristo and McDonnell, 2017) and to explain the differ-

ent seasonal origin of root-absorbed water across species and environmental gradients (Allen et al., 2019).

Plant water fluxes and hydrodynamics are amongst the most uncertain components of ecosystem and terrestrial biosphere models (Fatichi et al., 2016; Fisher et al., 2018). These models are now incorporating hydraulic traits and processes in their transpiration regulation algorithms (Mencuccini et al., 2019), but multi-site assessments of these algorithms are usually performed against evapotranspiration from eddy flux data (Knauer et al., 2015; Matheny et al., 2014). Model validation against sap flow data has been carried out typically in only one (Kennedy et al., 2019; Williams et al., 2001) or few (Buckley et al., 2012) sites. SAPFLUXNET can thus contribute to assess the performance of models simulating transpiration of stands or species within stands (e.g. De Cáceres et al., submitted.), for a large number of species and under diverse climatic conditions.

3.5 Limitations and future developments

3.5.1 Limitations

Sap flow data processing differs within and among methods, because different algorithms, calibrations or parameters involved in sap flow calculations may be applied. All of these methods contribute to methodological uncertainty (Looker et al., 2016; Peters et al., 2018) and this challenging methodological variability precludes the implementation of a complete, standardised data workflow from raw to processed data within SAPFLUXNET, as it is done for eddy flux data (Vitale et al., 2020; Wutzler et al., 2018). Commercial software for sap flow data processing from multiple methods is available (i.e. <http://www.sapflowtool.com/SapFlowToolSensors.html>) but it has not yet been widely adopted. Freely available data-processing software is only available for the HD method (Oishi et al., 2016; Speckman et al., 2020; Ward et al., 2017).

Sap flow measured with thermometric methods provides a precise estimate of the temporal dynamics of water flow through plants (Flo et al., 2019). However, their performance in measuring absolute flows is mixed. While some

well-represented methods in SAPFLUXNET such as the CHP yield accurate estimates (at least for moderate-to-high flows), the HD method, the most represented method by far, can significantly underestimate water flows (Flo et al., 2019). Because plant-level metadata contain information that document the conversion from raw to processed data (Table B5), a first-order correction for uncalibrated HD measurements based on available methodological assessments can be applied to allow intercomparability across methods. Nevertheless, given the high unexplained variability (i.e. by species and wood traits) in the performance of sap flow calibrations (Flo et al., 2019), these corrections should be applied with caution. The determination of zero flow conditions (baselining) can also have significant impacts on the quantification of absolute flow for several methods (Peters et al., 2018; Smith and Allen, 1996; Steppe et al., 2010). The different baselining approaches are also documented in the metadata to inform data syntheses and/or to selectively apply correction factors.

SAPFLUXNET has been designed to store whole-plant sap flow data, and therefore, sap flow measured at multiple points within an individual is not available in the database. Even though this spatial variation could be useful to describe detailed aspects of plant water transport (Nadezhina et al., 2009), focusing on plant-level data greatly simplifies the data structure. Hence, SAPFLUXNET only includes data already upscaled to the plant level by the data contributors. The main details of how this upscaling process was done for each dataset are provided together with other plant metadata (Table B5), but these metadata show that within-plant variation in sap flow is often not considered (Table 2). The impact of not accounting for radial and circumferential variability when scaling single-point measurements of sap flow to the whole-plant level can be important (Merlin et al., 2020), but the estimation of sapwood area can also cause large errors (Looker et al., 2016). SAPFLUXNET does not provide information on the method employed to quantify sapwood area (e.g. visual estimation with or without the application of dyes, indirect estimation through allometries at species or site levels) or on the accuracy of sapwood area data. This precludes uncertainty estimation at the individual level. Future developments in the SAPFLUXNET data

structure could include this information as metadata to better document the sensor-to-plant scaling process.

While SAPFLUXNET makes global sap flow data available for the first time, we note that spatial coverage is still sparse and some forested regions are underrepresented in the database (Fig. 2a). We note especially the relatively small number of datasets for boreal and tropical forests, two important biomes in terms of global water and carbon fluxes (Beer et al., 2010; Schlesinger and Jasechko, 2014). While many geographic gaps are caused by the absence of sap flow studies from such areas, some regions where sap flow studies have been conducted are still not represented in SAPFLUXNET. For example, the recent proliferation of Asian sap flow studies (Peters et al., 2018) has not translated into a high representativity of Asian datasets in SAPFLUXNET yet. Similarly, while the coverage of taxonomic and biometric diversity is unprecedented, SAPFLUXNET lacks data for the extremely tall trees (Ambrose et al., 2010) or for other growth forms such as shrubs (Liu et al., 2011), lianas (Chen et al., 2015) and other non-woody species (Lu et al., 2002).

3.5.2 Outlook

The public release of SAPFLUXNET has set the stage for a first generation of sap flow-based data syntheses. The work on these syntheses will fuel new ideas and tools for future improvements of the database, as for example new computing approaches for the processing and analysis of sap flow datasets. One example would be the development of robust imputation algorithms to gap-fill time series of sap flow and environmental data, which can take advantage of tools and datasets already developed by the ecosystem flux community (Moffat et al., 2007; Vuichard and Papale, 2015). The dissemination of SAPFLUXNET will encourage the use of machine-learning algorithms, only occasionally used to analyse sap flow datasets so far (e.g. Whitley et al., 2013). These approaches can also be used to identify the relative importance of different hydrometeorological drivers of transpiration (Zhao et al., 2019), or to produce global transpiration maps, by combining SAPFLUXNET with other data (Jung et al., 2019). This upscaling of stand transpiration to large

areas will also allow addressing broader questions at the regional and continental scale, such as the role of transpiration in moisture recycling (Staal et al., 2018).

The eventual success of this initiative, in terms of enabling data reuse, contributing towards the understanding and modelling of tree water use at local to global scales will likely encourage the sap flow community to contribute new datasets to future updates of the database. We expect that the development of open-source software for the processing of sap flow raw data (Speckman et al., 2020), its eventual widespread use by the sap flow community and the adoption of standardized calibration practices will increase the quality and intercomparability of future sap flow datasets. These new datasets will hopefully expand the temporal, geographical and ecological representativity of SAPFLUXNET when new data contribution periods can be opened in the future.

3.6 Data availability, access and feedback

In this paper we present SAPFLUXNET version 0.1.5 (Poyatos et al., 2020a), which contains some small metadata improvements on version 0.1.4, the first one to be made publicly available, in March 2020. Both versions supersede version 0.1.3 which was initially released to data contributors in March 2019. The entire database can be downloaded from its hosting webpage in the Zenodo repository (<https://doi.org/10.5281/zenodo.3971689>, Poyatos et al. 2020a). In this repository, we provide the database as separate .csv files and as .RData objects; see section 2.4. for details on data structure. Together with the initial publication of SAPFLUXNET in March 2019, we also released the sapfluxnet R package, available on CRAN, to enable easy access, selection, temporal aggregation and visualisation of SAPFLUXNET data. Feedback on data quality issues can be forwarded to the SAPFLUXNET initiative email address: `sapfluxnet@creaf.uab.cat`. All the information about SAPFLUXNET, including the publication of new calls for data contribution, can be found in the project website: [http://sapfluxnet.creaf.cat/./par](http://sapfluxnet.creaf.cat/./)

3.7 Conclusion

The SAPFLUXNET database provides the first global perspective of water use by individual plants at multiple timescales, with important applications in multiple fields, ranging from plant ecophysiology to Earth-system science. This database has been built from community-contributed datasets and is complemented with a software package to facilitate data access. Both the database and the software have been implemented following open science practices, ensuring public access and reproducibility. Data sharing has been a key component of the success of the FLUXNET network of ecosystem fluxes (Bond-Lamberty, 2018), and many databases in plant and ecosystem ecology now offer open data (Bond-Lamberty and Thomson, 2010; Falster et al., 2015; Gallagher et al., 2020; Kattge et al., 2020). SAPFLUXNET fully aligns with this philosophy. We expect that this initial data infrastructure will promote data sharing among the sap flow community in the future (Dai et al., 2018) and will allow the continued growth of the SAPFLUXNET database.

“thesis” — 2020/12/29 — |11:18 — page 82 — #106

4

Analysis of
hydrometeorological drivers
of tree transpiration shows a
dominant role of vapour
pressure deficit across
biomes.

} Víctor Flo, Jordi Martínez-Vilalta, Víctor Granda, Maurizio Mencuccini,
Rafael Poyatos

Abstract

We aim to identify the relative importance of vapour pressure deficit (VPD), soil water content (SWC) and photosynthetic photon flux density (PPFD) as drivers of tree transpiration, which will allow to improve mathematical models describing vegetation responses under climate change. We use sap flow time series of 1858 trees in 122 sites from the SAPFLUXNET global database to obtain whole-tree canopy conductance (G). The coupling, defined as the percentage of variance (R^2) of G explained by the three main hydrometeorological drivers (VPD, SWC and PPFD), was evaluated using linear mixed models. For each hydrometeorological driver we assess differences in coupling among biomes, and use multivariate models to explain R^2 by climate, soil and vegetation structure. We found that in most areas transpiration is better explained by VPD than by SWC or PPFD. We also found that sites in dryland biomes are less coupled to all three hydrometeorological drivers than those in other biomes. Climate, soil and vegetation structure were common controls of all three hydrometeorological couplings with G , with wetter climates, fine textured soils and tall vegetation being associated to tighter coupling. Differences across sites in the hydrometeorological coupling of tree transpiration may affect predictions of ecosystem and vegetation dynamics under future climates, and should be accounted for explicitly in models.

4.1 Introduction

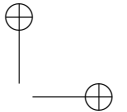
Plants regulate transpiration in response to variation in hydrometeorological conditions. However, despite decades of ecophysiological research measuring responses of leaf, plant or ecosystem evaporative fluxes to atmospheric dryness, soil moisture and radiation (Beerling, 2015), the relative importance of these drivers in determining plant controls on transpiration at the global scale is still poorly known. It is important to disentangle the biogeographical patterns of the individual dominant drivers of transpiration control, as such drivers are expected to show spatially heterogeneous dynamics with global change (Zhou et al., 2019). Thus, understanding their separate roles may help improve models to anticipate climate change impacts on vegetation function and on global water and carbon cycles, and to disentangle land-atmosphere feedbacks (Massmann et al. 2019).

Conductance to water vapour (G) derived from leaf, plant or ecosystem evaporative fluxes has been frequently used to describe the dynamic control of transpiration by plants at different organisational and temporal scales (Jarvis & McNaughton, 1986). At short timescales, this control is usually attributed to the regulation of stomatal aperture. Under high atmospheric water demand, which is often assessed using atmospheric vapour pressure deficit (VPD), or low soil water content (SWC), plants respond constraining G to avoid dangerous declines in water potentials preventing physiological damage and severe dehydration (Oren et al., 1999). In contrast, G responses to light (i.e. photosynthetic photon flux density, PPFD) are linked to plant water use efficiency (WUE). Thus, plants would increase G following PPFD in order to optimize photosynthesis in relation to water loss (Sperry et al., 2016). In addition, PPFD effects on G may respond to the need to regulate leaf temperature under high radiation levels (Fauset et al., 2018). These responses have been assessed in multiple, single-site studies (Jarvis, 1976; Oren et al., 1999; Wang et al., 2020). However, the fact that these studies frequently used different phenomenological models and model-fitting approaches complicates synthesis efforts aimed at building a common understanding on the controls of G at broad spatial scales. In addition, most of these studies focused on

overall G sensitivity (e.g. Hoshika et al., 2018), not on the importance of the individual drivers (but see for instance Bretfeld et al., 2018), hampering our understanding of which hydrometeorological drivers dominate G regulation globally.

Large-scale syntheses of the relative importance of hydrometeorological drivers regulating transpiration have been conducted using ecosystem evapotranspiration data. Novick et al. (2016) compared the limiting effect of SWC and VPD across vegetation types and climates, and found that limitation on ecosystem surface conductance to water vapour caused by SWC increased with climatic dryness, but that VPD limitation was higher than SWC across most mesic biomes. Conversely, Zhao et al. (2019) identified that, globally, ecosystem evapotranspiration was not primarily limited by hydrometeorological drivers, but by vegetation height, followed by SWC and PPFD. However, some of the assumptions underlying these studies, that assimilate evapotranspiration to transpiration after data filtering, may not always hold (Nelson et al., 2020). Here, we overcome the limitations of ecosystem-scale approaches by taking advantage of the first global database of plant-level transpiration from sap flow measurements (Poyatos et al., 2020).

In this study, we investigate the hydrometeorological coupling of tree-level canopy conductance by quantifying the explanatory power (R^2) of individual hydrometeorological drivers of G (VPD, SWC, PPFD). We also estimate the total predictive ability of a model including all three drivers. We then examine the biogeographical patterns of this hydrometeorological coupling of G, as a function of climate, soil properties and vegetation structure. We hypothesize differences in absolute and relative G coupling to the hydrometeorological drivers across biomes as a result of specific environmental constraints, with tighter coupling with VPD and SWC in drier biomes. We also expect that climate, soil and vegetation structure determine VPD, SWC and PPFD coupling of G, with greater coupling in sites with drier conditions and marked climatic seasonality, in fine textured soils associated with higher water tensions, and in tall stands with low leaf areas that are expected to have tighter canopy-atmosphere coupling.

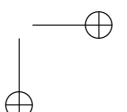
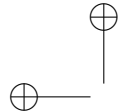


4.2 Material and methods

4.2.1 Sapflow and environmental data

We extracted 1858 time series of tree sap flow from the SAPFLUXNET database (Poyatos et al., 2020). These time series met our requirements for data quality (see filtering section below) and corresponded to 130 species on 122 sites without any experimental treatment (Table C1 and C2). Sub-daily sap flow time series were obtained directly in sap flux density units (SFD; $[cm^3 cm_{Asw}^{-2} h^{-1}]$) or, when sapwood area was not available, in whole-tree sap flow units (SF; $[cm^3 h^{-1}]$; 24 out of 122 data-sets). In those latter cases, SF time series were converted to SFD units by dividing SF data by an estimation of tree sapwood area (ASW) using a global allometric relationship as a function of tree basal area and functional type (i.e. angiosperm vs gymnosperm) as predictors ($R^2 = 0.78$; $n = 2262$) (Fig. C1). Using the ‘sapfluxnetr’ R package (Granda et al., 2020), sub-daily SFD time series were aggregated to daytime SFD values (i.e., 6am to 6pm solar time). Following Flo et al. (2019), sap flow time series measured with non-calibrated heat dissipation sensors were corrected for bias in absolute SFD multiplying by a constant factor (1.405).

Similarly to SFD, we obtained VPD [kPa] and PPFD [$\mu\text{mol m}_{Asw}^{-2} s^{-1}$] time series for each site from SAPFLUXNET on-site measurements, which were subsequently averaged to daytime values. When PPFD data were not available in the datasets (12 out of 122 sites), PPFD was calculated using the mean short-wave radiation between 6am and 6pm extracted from the ERA5 re-analyses data base (Copernicus Climate Change Service (C3S), 2017) and then multiplying by 2.3 to transform it into PPFD. Soil water content (SWC; v/v) data were missing in 43% of the SAPFLUXNET datasets included in this study. To ensure homogeneity across sites, we used SWC from the 15–30 cm soil depth layer obtained from the ERA5-land reanalysis dataset (Copernicus Climate Change Service (C3S), 2019) at 9x9km resolution (see database validation in Chapter 5).



4.2.2 Data filtering

In order to minimize seasonal phenological changes in leaf area, we excluded all periods between 15 days before the first daytime average temperature under 0°C and 30 days after the last day with temperatures under 0°C, during the cold season of each site (similar to Novick et al., 2016). To prevent artefacts in whole-tree canopy conductance calculation (Ewers & Oren, 2000), we filtered out rainy days –days when SWC increased– and days when average daytime VPD was under 0.3 kPa (Anderegg et al., 2018). We also ensured a sufficient range in hydrometeorological conditions by discarding sites with a total VPD range below 0.5 kPa or SWC range below 0.05 m³ m⁻³, and with PPFD maximum values below 400 μmol m_{Asw}⁻² s⁻¹.

4.2.3 Whole-tree canopy conductance calculation

To obtain G_s , we firstly transformed SFD units from [cm³ cm_{Asw}⁻² h⁻¹] to [Kg m_{Asw}⁻² s⁻¹] and then we converted it to daytime tree canopy conductance per unit of sapwood area G_{Asw} [mol m_{Asw}⁻² s⁻¹] following Phillips & Oren (1998) and a unit transformation (eq.1).

$$G_{Asw,j,i,k} = \frac{115.8 + 0.4236 T_{j,i} \cdot SFD_{j,i,k}}{VPD_{j,i}} \cdot \eta \cdot \frac{T_0}{(T_0 + T_{j,i})} \cdot \frac{P_0 e^{0.00012 \cdot h_i}}{P_0} \quad (4.1)$$

Where $SFD_{j,i,k}$ is the sap flux density value of each site (j), day (i), and tree (k); $T_{j,i}$ [°C] is the temperature, $VPD_{j,i}$ [kPa] is the daytime vapour pressure deficit, η equals 44.6 mol m⁻³, T_0 is 273 K, P_0 is 101,325 Pa and h [m] is the altitude of each site. For two sites where h values were not available, it was extracted from The Shuttle Radar Topography Mission (STRM) (Earth Resources Observation And Science (EROS) Center, 2017).

4.2.4 Hydrometeorological coupling quantification

We define hydrometeorological coupling as the coefficient of determination (R^2) of simple and multiple linear mixed models of VPD, SWC and PPFD explaining G_{Asw} at the site-tree level. High R^2 levels imply high predictive power of hydrometeorological drivers over G_{Asw} . To do that, we started by

binning the data to avoid issues related to unbalanced distributions of G_{Asw} throughout the range of VPD, SWC or PPFD. Specifically, we calculated the average of G_{Asw} measurements comprised in 0.2 kPa VPD intervals, five site-specific SWC intervals and $250 \mu\text{mol m}_{Asw}^{-2} \text{s}^{-1}$ PPFD intervals. For each summarized G_{Asw} we defined a specific VPD, SWC and PPFD value as the average values of VPD, SWC and PPFD of the data inside each bin. Then, we fitted uni-variate models for each site using G_{Asw} as response variable and the neperian logarithm of each driver as predictor (Fig. C4). Similarly, we also fitted an additive, multiple regression models of site-level G_{Asw} as a function of the logarithm of all three hydrometeorological drivers (TOTAL model). The hierarchical structure of species and trees within sites was taken into account using linear mixed models, implemented with the lmer function of the ‘lme4’ R package (Bates et al., 2015). When sites had more than one tree per species and more than one species (54 out of 122 sites), random intercept and slopes parameters were fitted for species, and random intercept parameters for trees nested into species. When models did not converge, the random structure was simplified and only trees random intercept parameters were fitted (33 out of 54 sites). When sites had just one species and multiple trees (67 out of 122 sites), we fitted a random intercept for trees. When a site had multiple species and just one tree per species (1 out of 122), random intercept and slopes were fitted for species.

Since we were interested in total coupling of the individuals of the site, hydrometeorological coupling was set as the conditional R^2 of the models (i.e. R^2_{VPD} , R^2_{SWC} , R^2_{PPFD} , R^2_{TOTAL}) (Table C3), calculated with the ‘MuMIn’ R package (Bartoń, 2020). We fitted simple and multiple regression models instead of more sophisticated non-linear models to reduce complexity and gain generalizability across the data sets. An alternative analysis fitting generalized additive models (GAM) as implemented in the bam function of the ‘mgcv’ R package (Wood, 2011), and specifying the same random structure, resulted in coupling values highly correlated to those obtained with the simpler linear modelling approach presented here ($r_{VPD} = 0.88$, $r_{SWC} = 0.89$, $r_{PPFD} = 0.88$, $r_{TOTAL} = 0.74$).

4.2.5 Biome classification and site-level bioclimatic data

The estimates of G_{Asw} hydrometeorological coupling were complemented with site-level data on climate, soil properties and vegetation structure. These data were either directly obtained from the metadata associated to each SAPFLUXNET dataset or from additional data sources. We took from SAPFLUXNET the biome corresponding to each site –obtained from Whittaker diagrams using Chelsa Climate databases (Karger et al., 2017) (Fig. C2)– and carried out an exhaustive quality control to reassign site biomes when necessary (Table C2) in consultation with SAPFLUXNET datasets contributors. Biomes were simplified into 5 groups; drylands (DRY), woodlands (WOOD), temperate forest (TEMP), boreal forests (BOR) and tropical forests (TROP) (Table C4 and Fig. C2).

For each site, we extracted climate information from global rasters (Fig. C3). We used monthly mean precipitation, monthly maximum temperature and monthly minimum temperature rasters for the period 1979 to 2013 from the Chelsa Climate databases (Karger et al., 2017), to estimate monthly potential evapotranspiration (mPET), annual potential evapotranspiration (PET) and mean annual precipitation (MAP) using the ‘envirem’ R package (Title & Bemmel, 2018). Then, we calculated MAP over PET (PPET) as a water availability index, and the standard deviation of the monthly differences between mean precipitation and mPET ($P-PET_{sd}$) as an index of seasonality in water availability. Relevant soil parameters were obtained from in situ data in SAPFLUXNET and complemented with SoilGrids 2.0 (Hengl et al., 2017) when data were not available in SAPFLUXNET (Table C3). We used the proportion of sand and clay particles in the fine earth fraction [%], the total nitrogen [g kg^{-1}] and the depth to bedrock (up to 200 cm) to characterize soils. We used bedrock depth because of its ecological relevance, but results for this variable should be considered with caution due to its particularly high variability at fine spatial scales. Stand height was available in SAPFLUXNET for most sites. When this was not the case, information was completed using the average tree height of the corresponding site (again from SAPFLUXNET, 3 out of 122 sites) or when both were absent it was extracted from the Global

1km Forest Canopy Height raster (Simard et al., 2011) (3 out of 122 sites) (Table C3). When site LAI was not available from SAPFLUXNET (37 out of 122 sites), it was estimated as the average of the 95th percentile of the period 2010 to 2016 of the MCD15A3H.006 MODIS Leaf Area Index product (0.5x0.5km grid) (R. Myneni, 2015), calculated using Google Earth Engine (Gorelick et al., 2017) (Table C3). All raster manipulation was performed with ‘raster’ and ‘stars’ R packages (Hijmans, 2020; Pebesma, 2020) using a common coordinate reference system.

4.2.6 Statistical analyses

In order to test whether the hydrometeorological coupling of G_{Asw} varies across biomes, we fitted weighted regressions using the modelled R^2_{VPD} , R^2_{SWC} , R^2_{PPFD} and R^2_{TOTAL} as response variables and biome as explanatory variable (fixed factor). The number of tree-days with SFD measurements in each site was used as a weighting variable. Similarly, we also tested the significance of cross-biome differences between paired hydrometeorological couplings (e.g. difference between VPD and SWC coupling, $R^2_{VPD} - R^2_{SWC}$) using the same model structure.

We further explained the biogeographical patterns in the hydrometeorological coupling across sites as a function of climate, soil properties and vegetation structure. We fitted four multiple weighted regression models with R^2_{VPD} , R^2_{SWC} , R^2_{PPFD} and R^2_{TOTAL} as response variables and $\log(PPET)$, $\log(P-PET_{sd})$, soil % clay, soil total nitrogen, soil bedrock depth, stand height and LAI as bioclimatic predictors (Fig. C3). We also used the number of tree-days of each site as weighting variable. Sand percentage was not included due to a high correlation with soil % clay ($r = -0.73$). A stepwise model selection process based on minimising AIC was applied. We checked for normality and homoscedasticity of residuals in all models, and we also checked for multicollinearity by quantifying Variance Inflation Factors (VIF) using the ‘performance’ R package (Lüdecke et al., 2020). These models were combined with the rasters of bioclimatic data (at a uniform resolution of 9x9 km), to predict and map global patterns of G hydrometeorological coupling to VPD, SWC and PPFD.

We also assessed the relative importance of each hydrometeorological driver by extracting the marginal partial R^2 of each hydrometeorological variable of the complete (TOTAL) model. These partial R^2 were calculated using ‘r2beta’ function of the R r2glmm package (Jaeger, 2017) and relativized by the sum of the three partial R^2 (relative R^2). These relative R^2 values can be interpreted as the relative importance of each hydrometeorological variable in limiting transpiration. Then, similarly as above, we fitted three multiple weighted regression models using the estimated relative R^2 as response variables and the bioclimatic variables as predictors. The resulting models were used to project the relative importance of each hydrometeorological driver globally. All statistical analyses were performed in R 3.6.2 (R Core Team, 2018).

4.3 Results

We found large differences in the coupling of G_{Asw} (R^2 coupling metric) to each of the individual hydrometeorological drivers globally and among biomes (Fig. 1 and Table 1). We observed that G_{Asw} was predominantly coupled to VPD across biomes (Fig. 1), while G_{Asw} coupling to SWC and PPFD was comparatively less important. Although coupling to SWC and PPFD were relatively similar, the effect of SWC was higher for DRY, TEMP and particularly WOOD biomes whereas PPFD tended to dominate for BOR and TROP biomes (Table 1). The outcomes of the linear models show a significantly higher VPD coupling for TEMP and TROP biomes than for DRY (Table 1). Somewhat surprisingly, SWC coupling was significantly higher for TEMP, TROP and also WOOD biomes than for the DRY biome. The PPFD coupling was also lowest for the DRY biome and was significantly higher for TEMP, BOR and TROP biomes; the G_{Asw} coupling to PPFD was also significantly lower in the WOOD biome compared to TEMP and TROP biomes (Table 1). The DRY biome was the one in which all three drivers collectively explained less variability in G_{Asw} .

In the models explaining the biogeographical patterns of G_{Asw} hydrometeorological coupling (which explained 26–35% of the variance), climate, soil

4.3. Results

93

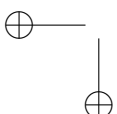
Table 4.1: Analysis of variance testing differences among biomes in the coupling (conditional R^2 's from mixed models) of tree-level water conductance (G_{Asw}) to each of the main hydrometeorological drivers: vapour pressure deficit (R^2_{VPD}), soil water content (R^2_{SWC}), radiation (R^2_{PPFD}) and the complete model including all drivers (R^2_{TOTAL}). The table shows the mean coupling obtained across all sites in each biome. We also show the means of the paired differences between individual hydrometeorological couplings and the corresponding statistical significance. DRY: dry and desert biomes; WOOD: woodlands and shrublands; TEMP: temperate biomes; BOR: boreal and tundra; TROP: tropical and subtropical biomes. Different superscript letters indicate significant ($p < 0.05$) Tukey tests of paired differences between biomes. Asterisks indicate statistically significant differences from zero for the paired differences between hydrometeorological couplings.

Biome	R^2_{VPD}	R^2_{SWC}	R^2_{PPFD}	R^2_{TOTAL}	$R^2_{VPD} - R^2_{SWC}$	$R^2_{VPD} - R^2_{PPFD}$	$R^2_{SWC} - R^2_{PPFD}$	Number of sites
DRY	0.439 ^A	0.225 ^A	0.210 ^A	0.502 ^A	0.215 ^{A***}	0.229 ^{AB***}	0.015 ^{AB}	7
WOOD	0.514 ^{AB}	0.390 ^B	0.295 ^{AB}	0.652 ^B	0.124 ^{A***}	0.219 ^{B***}	0.095 ^{B***}	29
TEMP	0.567 ^B	0.452 ^B	0.417 ^C	0.666 ^B	0.116 ^{A***}	0.150 ^{A***}	0.034 ^{A*}	70
BOR	0.622 ^{AB}	0.453 ^{AB}	0.499 ^{BC}	0.650 ^{AB}	0.168 ^A	0.122 ^{AB}	-0.046 ^{AB}	8
TROP	0.651 ^B	0.413 ^B	0.444 ^C	0.696 ^{AB}	0.238 ^{A***}	0.203 ^{AB***}	-0.031 ^A	8

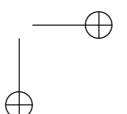
Statistical significant levels: “.” $p < 0.1$; “**” $p < 0.05$; “***” $p < 0.01$; “****” $p < 0.001$.

and vegetation structure variables were identified as common controls on the G_{Asw} hydrometeorological coupling (Table 2). In particular, log(PPET), soil clay %, and stand height were selected for all three hydrometeorological drivers (i.e. VPD, SWC and PPFD) and the TOTAL model, with tighter coupling always associated to higher climatic water availability, fine textured soils and taller vegetation. In addition, seasonality in water availability and LAI were associated with lower coupling to VPD and PPFD, whereas soil nitrogen had the exact opposite effect. Bedrock depth was only selected for the R^2_{SWC} model, in which deeper soils were associated with looser coupling, although the effect was not statistically significant (Table 2).

When predictions of G_{Asw} coupling to each of the hydrometeorological drivers were mapped at the global scale, a different spatial pattern was observed for all three drivers (Fig. 2). G_{Asw} coupling to VPD was higher than ca. 50% almost everywhere except for some sub-tropical regions. The regulation of tree water fluxes at high northern latitudes (above 50° N) and in



|



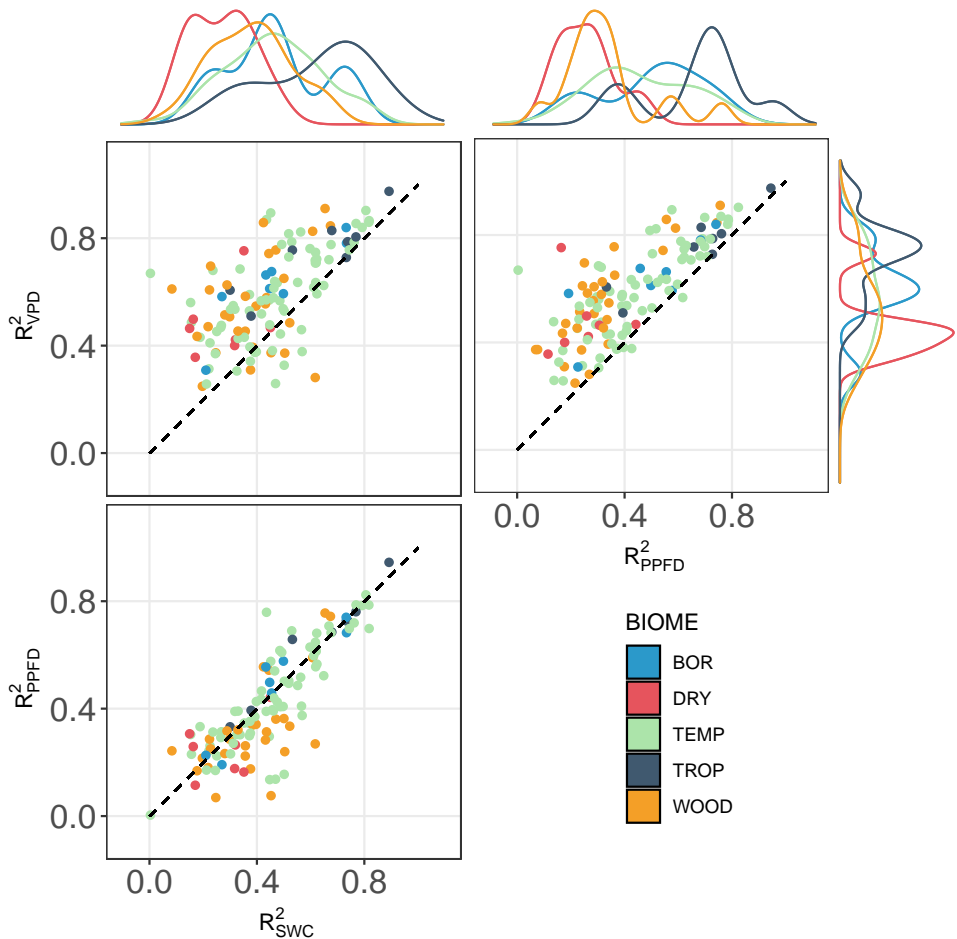


Figure 4.1: Bi-variate and uni-variate distributions of the coupling of GAsw to the hydrometeorological drivers studied: vapour pressure deficit (R^2_{VPD}), soil water content (R^2_{SWC}) and radiation (R^2_{PPFD}) for different biomes. Points correspond to site-level modelled conditional R^2 values. Colours represent different biomes, DRY: dry and desert biomes; WOOD: woodlands and shrublands; TEMP: temperate biomes; BOR: boreal and tundra; TROP: tropical and subtropical biomes. Dashed black line shows 1:1 relation.

tropical regions was highly coupled to VPD, SWC and PPFD (Fig. 2). In contrast, trees living in subtropical regions dominated by the DRY and WOOD biomes tended to be poorly coupled to SWC and PPFD, and relatively more coupled to VPD (Fig. 2). When considering the relative importance (partial R^2) of each of the three variables in driving transpiration (Fig. 3), northern

Table 4.2: Parameters of the models explaining G_{Asw} coupling to VPD, SWC, PPFD and to all three hydrometeorological drivers (R^2_{VPD} , R^2_{SWC} , R^2_{PPFD} and R^2_{TOTAL} , respectively) as a function of climatic, soil and stand structure variables. $\log(PPET)$: logarithm of precipitation over potential evapotranspiration [% $\log(\text{mm mm}^{-1})^{-1}$]; $\log(P-PET_{sd})$: logarithm of the standard deviation of the difference between precipitation and potential evapotranspiration [% $\log(\text{mm})^{-1}$]; Clay percentage [% %_{clay}⁻¹]; Total Nitrogen [% (Kg g^{-1})⁻¹]; Bedrock depth [% cm⁻¹]; Stand Height [% m⁻¹]; LAI: leaf area index [% ($\text{m}^2 \text{m}^{-2}$)⁻¹]. NI means that the variable was not included in the model after model selection. The R^2 of each multiple regression is also shown.

G_{Asw} coupling	Intercept [%]	Climate		Soil			Vegetation structure			R^2
		$\log(PPET)$	$\log(P-PET_{sd})$	Clay	Total Nitrogen	Bedrock depth	Stand Height	LAI		
R^2_{VPD}	80.242 ***	4.862 .	-8.642 *	0.313 **	1.930 *	NI	0.603 ***	-3.322 ***	0.255	
R^2_{SWC}	53.978 ***	10.850 ***	NI	0.314 ***	NI	-0.120 ns	0.348 **	NI	0.353	
R^2_{PPFD}	47.591 **	7.531 *	-6.501 .	0.323 **	1.603 .	NI	0.788 ***	-2.202 *	0.352	
R^2_{TOTAL}	54.464 ***	4.698 *	NI	0.248 **	1.416 .	NI	0.228 .	NI	0.191	

Statistical significant levels: “.” p<0.1 ; ** p<0.05; *** p<0.01; **** p<0.001; ns not significant..

areas, temperate regions, drylands and savannas were typically limited by VPD, whereas tropical regions tended to be co-limited by VPD and PPFD (Fig. 3).

4.4 Discussion

This study provides the first attempt to examine the absolute and relative importance of VPD, SWC and PPFD as the main hydrometeorological drivers of the regulation of tree transpiration at the global level. All sites presented some degree of transpiration coupling to the hydrometeorological drivers considered, although there was substantial variability in the magnitude of this coupling (i.e. R^2_{VPD} , R^2_{SWC} , R^2_{PPFD}). We demonstrate that the regulation of transpiration is predominantly coupled to VPD in all biomes, while transpiration limitation caused by SWC and PPFD is generally comparable and lower. Although our sample size is much smaller and possibly biased (see Fig. 3 and Table 1) relative to global studies based on remote sensing approaches, our results clearly identify atmospheric dryness as the major regulator of transpiration globally, which is consistent with recent reports showing that VPD limits vegetation growth at the global scale (Babst et al., 2019; Yuan et al.,

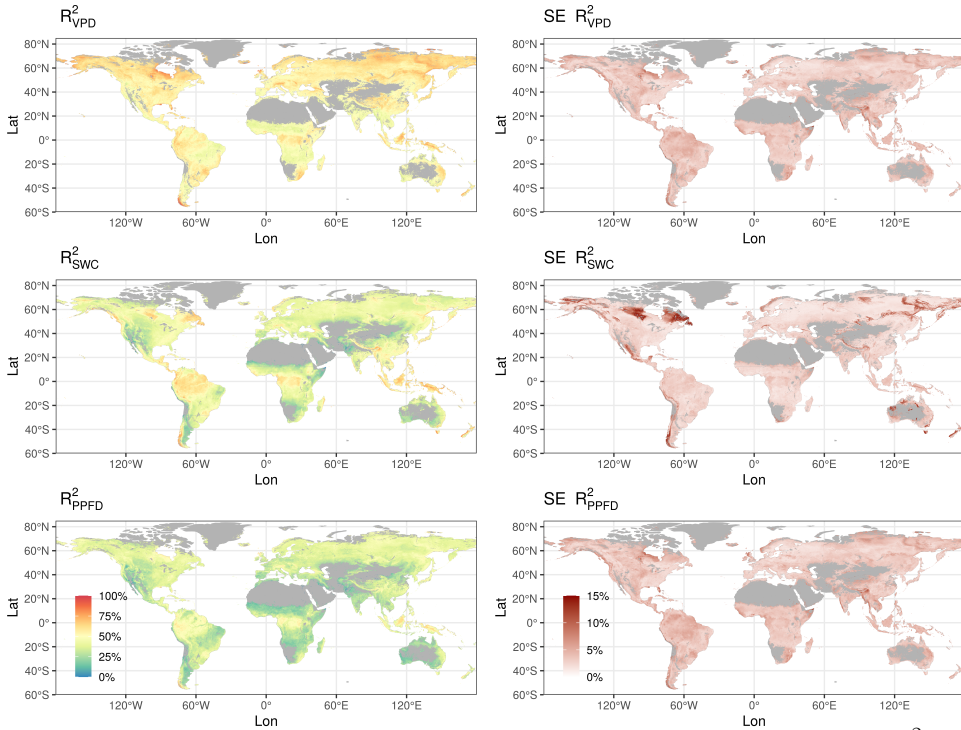


Figure 4.2: Global projection of G_{Asw} coupling to VPD, SWC and PPFD (R^2_{VPD} , R^2_{SWC} and R^2_{PPFD} , respectively), obtained from regression models of each coupling as a function of climatic, soil and stand structure variables (left panels). Right panels show projected Standard Error of the corresponding model.

2019). Yet, contrary to other studies focusing on the controls of primary productivity (Jung et al., 2017; Liu et al., 2020), we do not find a dominant role of SWC on transpiration regulation. However, unlike these studies, our approach focuses at the plant-level and uses actual transpiration data, also considering the effect of light, which has been rarely assessed in this type of studies.

Soil moisture coupling of transpiration regulation was only tighter than coupling to radiation in WOOD and TEMP biomes, indicating the importance of soil water limitations on transpiration in these biomes. Interestingly, the importance of SWC decreased in DRY biomes, even if actual sensitivity to SWC was high (Fig. C4). This result contrasts to those found at the ecosystem level, where drier sites present larger SWC limitations than wetter ones (Novick et al., 2016). This opposite result between transpiration and evap-

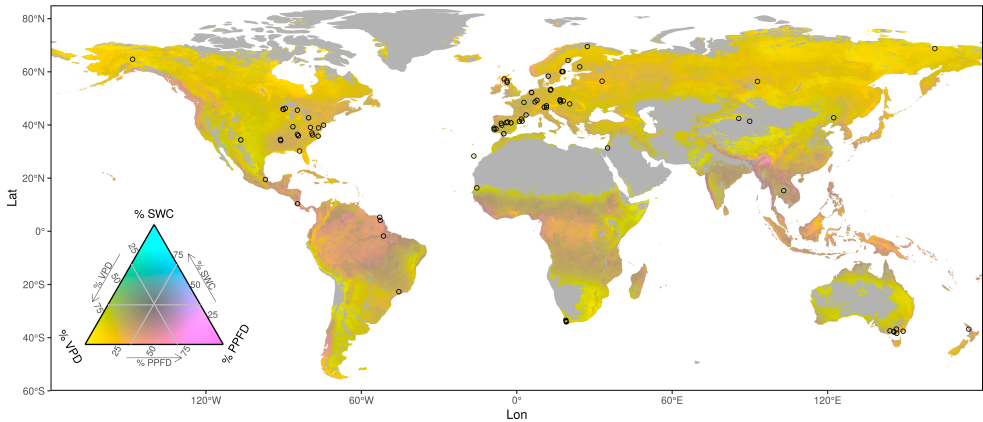


Figure 4.3: Relative importance (partial R^2) of the three hydrometeorological drivers of transpiration regulation calculated from the complete (TOTAL) model, and projected at the global scale using linear models with climate, soil and vegetation structural variables as explanatory variables. Grid values were calculated using the ‘tricolore’ package (Schöley and Kashnitsky, 2020) for each cell as the relative value of the projections of the relative importance of each hydrometeorological variable. Colour gradient indicate the relative importance of the three hydrometeorological constraints. Light grey colour are deserts or non-forested areas. % VPD: vapour pressure deficit relative importance. % SWC: soil water content relative importance. % PPFD: photosynthetic photon flux density relative importance. Points indicate locations of study sites.

transpiration limitations suggests that the soil contribution to ecosystem surface conductance may be large (Li et al., 2019) and strongly limited by SWC in DRY biomes. The lack of coupling in drylands is intriguing and may be related to the diversity of water use strategies in water limited systems, which range from drought-deciduousness to deep rooting or high hydraulic safety (e.g., Ackerly; 2004; Jacobsen et al. 2007). Deep roots, for instance, could allow sufficient water supply to uncouple transpiration from hydrometeorological drivers and specifically from shallow SWC (Barbeta & Peñuelas, 2017). At the other extreme, exposure to low water potentials results in early stomatal closure (Martin-StPaul et al., 2017), effectively disconnecting transpiration from hydrometeorological drivers for long periods of the year. Memory effects (Ogle et al., 2015) are also likely to be more common in water-limited systems, which may result in more complex responses of transpiration

to individual hydrometeorological drivers. Finally, we did not consider the co-variation between VPD, SWC and PPFD. VPD and SWC co-variation is relatively low at the daily level at large spatial scales (Novick et al., 2016), but in water-limited regions SWC shows strong interactions with VPD (Zhou et al., 2019) and PPFD (Boese et al., 2018), which could produce compound drought effects that would complicate disentangling the coupling of transpiration to individual drivers. It should also be noted that we focus here on relatively tall woody vegetation, as this is the one likely to be measured with sap flow sensors (Poyatos et al., 2020), and hence our analysis excludes extremely arid sites likely to be totally driven by water availability (compare the grey areas in our Fig. 3 with Fig. 1 in Running et al. (2004)).

Beyond general biome effects, differences in coupling among sites were partially explained by differences in climate, soil and stand structure. Besides the generally lower coupling in areas with less climatic water availability, consistent with the results discussed in the previous paragraph, we have found that regions with high climatic seasonality (i.e. high $\log(P-PET_{sd})$) are less coupled to VPD (and to a lower extent radiation) than regions with more seasonally stable climate. Low R2VPD under high climatic seasonality may be related to changes in transpiration regulation responses to VPD between the dry and wet seasons (Renninger et al., 2010), which could be the case of, for example, seasonal tropical forest biomes with semi-deciduous species (Monasterio & Sarmiento, 1976). Alternatively, low VPD coupling could be related to transpiration regulation driven by other bioclimatic variables or their combination, as partially observed in the co-limitation by all three hydrometeorological drivers in many areas where climatic seasonality is large (Fig. 3, Fig C3). Coupling to radiation was higher in wetter sites (i.e. high PPET), which are mainly located in tropical and boreal regions (Fig. C3). This would reflect the key role of radiation as a driver of transpiration in energy-limited areas with shallow clouds and fogs such as the tropics (Fig. 2) (Gentine et al., 2019), and in areas where radiation is a strong limiting factor such as boreal regions (Kasurinen et al., 2014). Our analysis of the relative importance of the three hydrometeorological drivers indicates a dominant role of radiation as a limiting factor in the tropics particularly in South-East

4.4. Discussion

Asia (Fig. 3), consistent with previous reports (Running et al., 2004).

Our results show the key importance of soil characteristics, particularly texture, in explaining variability in transpiration coupling. Trees increase coupling to all three hydrometeorological drivers under high clay content (finer texture), which results in more negative water potentials at a given water content (Hillel, 1998). This result is to be expected considering that we assessed transpiration responses to soil water content, which implies that plants in fine textured soils would effectively experience lower water availability than plants in more coarsely textured soils with the same water content. In addition, our results indicate deeper soils (higher bedrock depth) were associated to lower coupling to soil water availability, consistent with the notion that access to deep water may uncouple transpiration from shallow SWC (Barbeta & Peñuelas, 2017).

Vegetation height and LAI are also important drivers of vegetation transpiration coupling. VPD, SWC and PPFD limitations to G_{Asw} are typically higher in taller trees, consistent with previous studies (Boese et al., 2018; Zhao et al., 2019). Tree height is associated with productive areas with high resource availability, including water. In general, taller trees live in wetter regions and have higher water transport efficiencies and lower resistance to embolism (Liu et al., 2019, Chapter 5). These traits are associated with acquisitive water use strategies and a tighter stomatal control of transpiration (Klein, 2014). A similar argument can be used to explain tighter coupling to VPD and radiation in areas with high soil nitrogen concentrations, as the latter have been related to increased transpiration rates in wet soil and greater degree of stomatal control under drought (Shimshi, 1970, Ewers et al. 2001). Taller canopies are also more aerodynamically rough and, therefore, show higher VPD coupling due to higher levels of leaf surface VPD. Interestingly, once accounting for the effect of vegetation height LAI had a negative effect on transpiration coupling to VPD and PPFD. We associate this result to the fact that higher LAI is related to lush canopy structures that would have a significant proportion of the leaves decoupled from the atmosphere and from direct radiation income (Zhang et al., 2016).

Differences in coupling among sites should also reflect different water use strategies in the corresponding communities. These differences are reflected in part in the climatic, soil, and structural differences we studied, but also underlie the relatively large unexplained variance, which could be related to contrasting water use strategies coexisting in the same biomes and even in the same sites (Anderegg et al., 2018). This implies that species traits should be included if we aim to understand the fine-scale distribution of transpiration responses (Chapter 5) and their coupling to hidrometeorological drivers to predict G responses to environmental variation.

In conclusion, we found that VPD is the main hydrometeorological driver of transpiration regulation globally but we also showed that VPD coupling did not increase in warmer sites, as found in ecosystem-level studies (Novick et al. 2016). Nevertheless, the role of VPD in driving transpiration regulation will likely be dominant in a warmer world, given the generalised increases in projected VPD (Ficklin & Novick, 2017). Using machine learning methods (Zhao et al. 2019) and sub-daily data (when SWC is effectively constant) could help to better disentangle the effect of each hydrometeorological driver (Lin et al., 2018), and would allow a more explicit consideration of interactions between drivers (Zhou et al., 2019). Our results indicate clear differences among hydrometeorological couplings and contribute to disentangle their relative effects on transpiration regulation, which determines vegetation water use, tree growth and ecosystem production. Consequently, global models simulating vegetation-atmosphere fluxes should account for the limiting effects produced by VPD, SWC and PPFD and their variability in space and time, which should be facilitated by an explicit description of water transport in plants (Anderegg & Venturas, 2020).

5

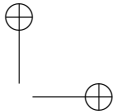
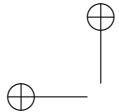
Climate and functional traits jointly mediate tree water use strategies

Victor Flo, Jordi Martínez-Vilalta, Maurizio Mencuccini^{1,3}, Victor Granda,
William R. L. Anderegg, Rafael Poyatos

1025. *Climate and functional traits jointly mediate tree water use strategies*

Abstract

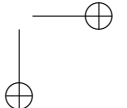
Tree water use is central to plant function and ecosystem fluxes. However, it is still unknown how organ-level water relations traits are coordinated to determine whole-tree water use strategies in response to drought, and if this coordination depends on climate. Here we used a global sap flow data base (SAPFLUXNET) to study the response of water use, in terms of whole-tree canopy conductance (G), to vapour pressure deficit (VPD) and to soil water content (SWC) for 142 tree species. We investigated the individual and coordinated effect of six water relations traits (vulnerability to embolism, Huber value, hydraulic conductivity, turgor-loss point, rooting depth and leaf size) on water use parameters, also accounting for the effect of tree height and climate (mean annual precipitation, MAP). Reference G and its sensitivity to VPD were tightly coordinated with water relations traits rather than with MAP. Species with efficient xylem transport had higher canopy conductance but also higher sensitivity to VPD. Moreover, we found that angiosperms had higher reference G and higher sensitivity to VPD than gymnosperms. Our results highlight the importance of trait coordination and the complications of defining a single, whole-plant resource use spectrum ranging from ‘acquisitive’ to ‘conservative’.



5.1 Introduction

Plant water use is a key component of the global water cycle (Katul et al., 2012). Plants regulate water use across a broad range of timescales to maintain a favourable water status under varying water availability (Feng et al., 2017). This regulation is the result of evolutionary processes together with environmental and biophysical constraints that have determined a huge diversity of species-specific water use strategies mediated by a particular suite of traits (Bacelar et al., 2012; Lu et al., 2020). These specific strategies determine plant survival under drought (Mitchell et al., 2013), species coexistence (Ehleringer et al., 1991; Jackson et al., 1995) and ecosystem CO₂ and water fluxes (Mencuccini et al., 2019a). Thus, a comprehensive understanding of how regulation of whole-plant water use relates to organ-level water relations traits would allow for a better characterization of plant responses to drought and improved prediction of climate change impacts on vegetation (Anderegg, 2015).

Among many other traits, the sensitivity of stomata to drought stress is a major regulator of plant water use over relatively short timescales (Martin-StPaul et al., 2017). In the absence of effective stomatal control under drought, water uptake by roots might not compensate water loss, resulting in high tensions in plants’ vascular system, which can trigger the entrance of air bubbles leading to xylem embolism (Tyree & Zimmermann, 2002). If embolism spreads to most of the xylem conduits, water transport becomes restricted and plants may eventually die from hydraulic failure (Tyree & Sperry, 1988; Choat et al., 2018). Through stomatal closure, plants reduce whole-plant canopy conductance (G) and therefore water loss and embolism risk, and maintain water status within tolerable limits, at the expense, however, of reducing gas exchange. Plants close stomata in response to drops in leaf and/or soil water potentials (see Martínez-Vilalta & Garcia-Forner, 2017) produced by increased atmospheric water demand (i.e., vapor pressure deficit; VPD) and reduced soil water availability (i.e., soil water content; SWC) (Jarvis, 1976; Grossiord et al., 2017). Stomatal responses have been largely described using semi-empirical models (Jarvis, 1976; Oren et al., 1999; Damour et al.,



1045. Climate and functional traits jointly mediate tree water use strategies

2010) and optimality approaches relying on the coupling of photosynthesis and transpiration (Wang et al., 2020), with a recent focus on plant hydraulics (Sperry et al., 2016). Global syntheses of these two approaches exist (Lin et al., 2015; Hoshika et al., 2018) but they are only at the leaf level, and they do not consider the coordination of stomatal and hydraulic traits.

Coordination among stomatal sensitivity and other hydraulic and allocation traits is thought to underlie differences in water use strategies among species (Meinzer, 2002; Sperry et al., 2016; McCulloh et al., 2019). Because in woody plants water has to be transported from the soil through the xylem to supply leaf transpiration, the hydraulic properties of the xylem are key determinants of plant water relations and water use strategies. Particularly, maximum sapwood hydraulic conductivity (K_s ; Table 1) and vulnerability to xylem embolism (usually quantified as Ψ_{P50} ; i.e. the water potential at which half of K_s is lost) are key determinants of maximum transpiration rates (Manzoni et al., 2013). In addition, a vulnerable xylem (i.e. high $|\Psi_{P50}|$) has been related to higher canopy-level stomatal sensitivity to VPD across (Litvak et al., 2012) and within some species (Aspinwall et al., 2011). K_s and Ψ_{P50} have been hypothesized to define a safety-efficiency trade-off at the tissue level, by which species with high K_s (i.e., high water transport efficiency) are also more vulnerable to embolism (low $|\Psi_{P50}|$ and low safety) and vice versa (Venturas et al., 2017). However, this trade-off appears to be weak at the global scale across species, at least as captured with current measurement techniques (Gleason et al., 2016; Sanchez-Martinez et al., 2020). At the leaf level, another key component is the water potential at turgor-loss point (Ψ_{TLP}), which is tightly associated with drought tolerance and habitat water availability (Bartlett et al., 2012). Ψ_{TLP} is also closely related to water potential at complete stomatal closure (Brodribb & Holbrook, 2003; Martin-StPaul et al., 2017), and thus can be used as a proxy for quantifying the sensitivity of plant water use to changes in water availability.

Allocation ratios between the organs involved in water loss, transport and uptake are also important determinants of water use strategies. The ratio of cross-sectional sapwood area to leaf area or Huber value (Hv) is a major trait defining water use strategies because it expresses the water conducting

area per unit transpiring area. Increased Hv can contribute to reduce water potential gradients within the plant and therefore potentially compensate for a species vulnerable xylem (Mencuccini et al., 2019b). In addition, a high Hv has also been associated to strict stomatal control in conifers (Martínez-Vilalta et al., 2004; Poyatos et al., 2007) and to higher reference canopy conductance (Novick et al., 2009). Similarly, increasing rooting depth (R_{depth}) gives access to deeper water sources, which potentially allows maintaining less negative and stable water potentials as well as supporting high water use even under climates with high evaporative demand (Martínez-Vilalta & Garcia-Forner, 2017). At the leaf level, the importance of individual leaf size (L_s) for light penetration and crown architecture has been thoroughly studied (Sellers, 1985), but its influence on water use strategies has been little explored, despite the role of leaf evaporative cooling for thermoregulation (Wright et al., 2017). Large leaves with thick leaf boundary layers and an ineffective stomatal control of water loss (Jarvis & McNaughton, 1986), may need to sustain higher transpiration rates to maintain leaf temperature within operative limits under intense radiative heating and/or heat waves (e.g. Drake et al., 2018). This may lead to a trade-off between leaf thermoregulation and the conservation of water and/or hydraulic function (Fauset et al., 2018), especially in hotter sites (Aparecido et al., 2020).

Water use strategies are also mediated by plant height, community composition, and environmental conditions, particularly climate, topography and soil properties; as well as spatial and temporal variability in environmental conditions (Feng et al., 2018). Plant height increases hydraulic path length and hydraulic resistance, and thus plays a major role in the global coordination of several water use traits such as Ψ_{P50} or K_s (Liu et al., 2019), Hv (Mencuccini et al., 2019b) and reference canopy conductance (Novick et al., 2009). Likewise, increasing tree height has been related to enhanced sensitivity of canopy conductance to VPD for some species (Schäfer et al., 2000). Because soil water is a common resource belowground that is influenced by water uptake from many individuals and species, the community composition and diversity of water use strategies in an ecological community can also affect ecosystem fluxes and drought progression (Anderegg et al.,

1065. Climate and functional traits jointly mediate tree water use strategies

2018, 2019). In addition, phylogeny may constrain flexibility in water use strategies independently of the environment, as it has been shown for example by the consistent differences in hydraulic traits between angiosperms and gymnosperms (Johnson et al., 2012; Bartlett et al., 2016) and by the strong phylogenetic conservatism reported for some hydraulic traits such as Ψ_{P50} and K_s at the global scale (Sanchez-Martinez et al., 2020).

In this study we explore water use strategies across tree species using a trait-based approach, which provides a simplified framework to understand species responses to drought at the global scale (Feng et al., 2018). Our ultimate aim is to better understand how water use strategies emerge from the covariation between traits and the influence of climate. To that end, we use a global database of sap flow measurements (SAPFLUXNET) to calculate whole-tree canopy conductance (G) for 142 tree species growing on 126 sites. We then parameterize the response of G to VPD and SWC at the species level and for major taxonomic groups (i.e. angiosperms and gymnosperms). Finally, we characterize the relationships between water use traits and key hydraulic and allocation traits among species (i.e. Ψ_{P50} , K_s , Hv , Ψ_{TLP} , R_{depth} , L_s and tree height), controlling also for the climatic effects produced by differences in precipitation. We hypothesize that (i) water use and water relations traits are coordinated to determine water use strategies at the species level, and (ii) species occupying drier habitats will tend to be more ‘conservative’ in their water use and also tend to have drought tolerance traits. (iii) After controlling for climatic effects, a safety-efficiency trade-off is visible at the scale of whole-plant water use, as opposed to the scale of individual xylem conduits.

5.2 Material and methods

We took a two-step approach to test the previous hypotheses. First, we modelled species-level whole-tree canopy conductance responses to evaporative demand and soil water availability to obtain species’ water use parameters, taking advantage of a recently-compiled global sap flow dataset. Next, we modelled the variability of those water use parameters as a function of

species' water relations traits, mean annual precipitation (MAP), tree height and broad functional types (i.e., angiosperms and gymnosperms).

Table 5.1: Description of variables and units in this study.

Variable	Description	Units
VPD	Vapour pressure deficit	kPa
SWC	Soil water content	$\text{m}_\text{water}^3 \text{m}_\text{soil}^{-3}$
REW	Relative extractable water	
Asw	Sapwood area	m^2
SF	Sap flow	$\text{cm}^3 \text{h}^{-1}$
SFD	Sap flux density	$\text{cm}^3 \text{cm}_\text{Asw}^{-2} \text{h}^{-1}$
G	Whole-tree canopy conductance	mol s^{-1}
G_Asw	Whole-tree canopy conductance per unit of sapwood area	$\text{mol m}_\text{Asw}^{-2} \text{s}^{-1}$
G'_Asw	Whole-tree stomatal conductance (i.e., G_Asw without aerodynamic conductance)	$\text{mol m}_\text{Asw}^{-2} \text{s}^{-1}$
MAP	Mean annual precipitation	mm
MAT	Mean annual temperature	$^\circ\text{C}$
PPET	Mean annual precipitation over potential evapotranspiration	mm mm^{-1}
H	Tree height	m
Ψ_{P50}	water potential at which half of K_s is lost	MPa
K_s	Maximum sapwood hydraulic conductivity	$\text{kg m}^{-1} \text{MPa}^{-1} \text{s}^{-1}$
Hv	Huber value: ratio of cross-sectional sapwood area to leaf area	$\text{cm}_\text{Asw}^2 \text{m}_\text{leaf}^{-2}$
Ψ_TLP	Water potential at leaf turgor-lost point	MPa
R_depth	Rooting depth	m
L_s	Individual leaf size	cm^2
T	Temperature	$^\circ\text{C}$
h	Plot altitude	m
G_REF	Reference G_Asw at VPD = 1 kPa and SWC = 0.5 $\text{m}^3 \text{m}^{-3}$	$\text{mol m}_\text{Asw}^{-2} \text{s}^{-1}$
β_VPD	G_Asw sensitivity to ln(VPD)	$\text{mol m}_\text{Asw}^{-2} \text{s}^{-1}$
β_SWC	G_Asw sensitivity to ln(SWC)	$\text{mol m}_\text{Asw}^{-2} \text{s}^{-1}$

5.2.1 Sap flow data

Data from 1929 trees belonging to 142 species on 126 plots without experimental treatments (Table D1) and meeting data quality criteria (see Data filtering

1085. Climate and functional traits jointly mediate tree water use strategies

section below) were obtained from the global SAPFLUXNET database (Poyatos et al., 2020) (Fig. 1 and Table D2). For each species-site combination, we extracted sub-daily sap flux density (SFD; Table 1) or whole-tree sap flow (SF; 24 out of 126 data-sets) when tree sapwood areas (ASW) were not available. For these datasets, SF data were then transformed into SFD units by dividing SF values by tree ASW estimated with an allometric relationship. This relationship was obtained using all the SAPFLUXNET trees for which ASW data were available and taking diameter at breast height (DBH) and functional type (i.e., angiosperm or gymnosperm) as predictors ($R^2 = 0.78$; $n = 2262$). Sub-daily SFD time-series were aggregated to daytime SFD averages (i.e., 6am to 6pm solar time) using the sfn_metrics function of the sapfluxnet R package (Granda et al., 2020). Time-series obtained from non-calibrated thermal dissipation sensors were corrected for potential bias in absolute SFD by applying a multiplier of 1.405, according to the global synthesis of sap flow

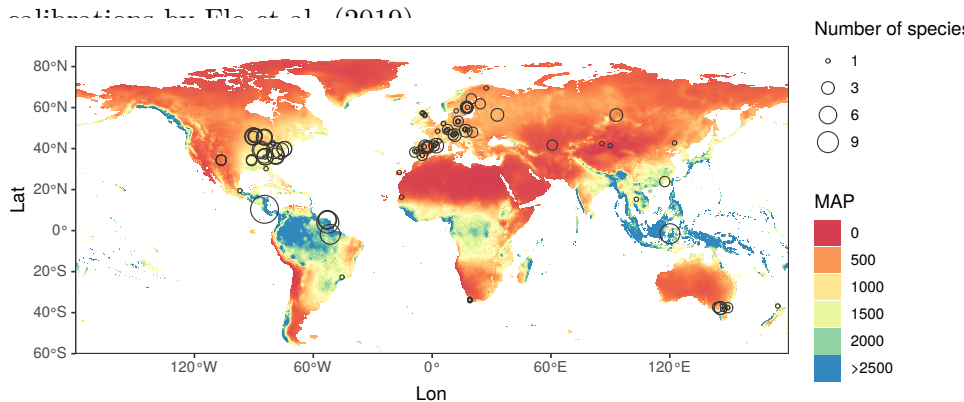


Figure 5.1: Distribution of the plots from the SAPFLUXNET database included in this study. Size of the dots represent the number of different species in the plot. Color gradient show mean annual precipitation (MAP).

5.2.2 Evaporative demand and soil water availability data

We used vapour pressure deficit (VPD) and soil water content (SWC) as proxies of evaporative demand and soil water availability, respectively. Similar to SFD, VPD was obtained from on-site sub-daily measurements from

SAPFLUXNET averaged to daytime values. Soil water content (SWC; v/v) was obtained from the 15–30 cm depth layer at 12 am from the ERA5-land re-analysis product (Copernicus Climate Change Service (C3S), 2019) at 9x9 km resolution. We used ERA5-land re-analyses instead of on-site SWC measures in order to maximize the number of plots and species included in the study, since SWC data were missing in 44% of the SAPFLUXNET data-sets included in this study. In addition, ERA5-land had longer time series (1980 to 2019). We validated the use of ERA5-land data using a linear mixed-model (LMM) regression between ERA5-land and on-site shallow SWC measurements by letting random intercepts and slopes of the response vary by site (n observations = 32815; n plots = 71; R^2 conditional = 0.97, R^2 marginal = 0.26).

To complement SWC, we also calculated relative extractable water (REW), as a normalized measure of soil water availability, as follows:

$$REW_{j,i} = \frac{SWC_{j,i} - SWC_{min}}{SWC_{max} - SWC_{min}} \quad (5.1)$$

where $REW_{j,i}$ and $SWC_{j,i}$ are plot (j) daily (i) values, and SWC_{max} and SWC_{min} , the overall maximum and minimum SWC measured at a plot, respectively. REW takes values between 0 and 1, being 0 the absolute plot lowest SWC and 1 being the highest.

5.2.3 Data filtering

We restricted the analysis to periods without potential phenological changes in leaf area to minimize variations in conductance unrelated to VPD and SWC changes. In the absence of detailed plot-specific observations, we excluded all data for periods comprised between 15 days prior to the first day with temperatures below 0°C and 30 days following the last day under 0°C, respectively, during the cold seasons of each plot site (similarly to Novick et al., 2016). To prevent potential artefacts due to unstable weather conditions in the calculation of whole-tree canopy conductance (Ewers & Oren, 2000) or in the estimation of model parameters, we filtered out days when SWC increased (rainy days), as well as days when daytime-averaged VPD was below

1105. Climate and functional traits jointly mediate tree water use strategies

0.3 kPa (Anderegg et al., 2018). To ensure sufficiently contrasting conditions of evaporative demand and soil water availability, we also discarded species with both VPD ranges below 0.5 kPa and SWC ranges below 0.05 ($n = 8$ species).

After data filtering, the study covers a large geographic area being Europe and the east of North America especially well represented (Fig 1) and a wide range of climate conditions, with MAP values ranging from 14 mm to 3626 mm (mean \pm SD = 953 mm \pm 545 mm). Out of the 142 species used in the analyses, 116 were angiosperms and 26 gymnosperms. The number of trees per species ranges from 215 trees (*Pinus sylvestris*) to 1 (this being the case for 23 species) (Table D2). Tree species-level heights (H) range from 2 m (*Coprosma quadrifida*) to 40 m (*Carya glabra*) (mean \pm SD = 21 m \pm 9.75 m).

5.2.4 Whole-tree canopy conductance calculation

Daytime SFD was transformed from $[cm^3 cm_{Asw}^{-2} h^{-1}]$ to $[kg m_{Asw}^{-2} s^{-1}]$ and converted to daily whole-tree canopy conductance normalized per unit of sapwood area G_{Asw} using Phillips and Oren (1998) and unit transformations (eq.2).

$$G_{Asw,j,i,k} = \frac{115.8 + 0.4236 T_{j,i} \cdot SFD_{j,i,k}}{VPD_{j,i}} \cdot \eta \cdot \frac{T_0}{(T_0 + T_{j,i})} \cdot \frac{P_0 e^{0.00012 \cdot h_i}}{P_0} \quad (5.2)$$

Where $SFD_{j,i,k}$ is the sap flux density value of each site (j), day (i), and tree (k); $T_{j,i}$ [$^{\circ}$ C] is the temperature, $VPD_{j,i}$ [kPa] is the daytime vapour pressure deficit, η equals 44.6 mol m^{-3} , T_0 is 273 K, P_0 is 101,325 Pa and h [m] is the altitude of each site. When h was not available it was obtained from The Shuttle Radar Topography Mission (SRTM) (Earth Resources Observation And Science (EROS) Center, 2017) ($n = 2$ plots).

The conductance obtained using eq. 2 is considered a good proxy of the tree-level stomatal conductance under the assumption that the canopy and the atmosphere are well-coupled, i.e., when the aerodynamic conductance is much larger than the stomatal conductance. Although this is generally

assumed in sap flow studies for both needleleaf and even broadleaf species, there is evidence that coupling may only be partial in some cases (Magnani et al., 1998; De Kauwe et al., 2017). Therefore, we also calculated whole-tree stomatal conductance (G'_{Asw}) by removing the contribution of aerodynamic conductance in a subset of plots-species (n plots = 64; n species = 47) where wind speed data were available in SAPFLUXNET (see supplementary material for details, Chu et al., 2018; Tan et al., 2019). We also related the environmental sensitivity of G'_{Asw} to the hydraulic and allocation traits (see Statistical analyses section below) to assess the potential impact of partial canopy-atmosphere coupling on our results.

5.2.5 Traits and climatic data

Species-level traits ($|\Psi_{P50}|$, Hv , K_s , $|\Psi_{TLP}|$, R_{depth} and L_s) were taken from HydraTry (Mencuccini et al., 2019b; Sanchez-Martinez et al., 2020) and the Global Leaf Size Dataset (Wright et al., 2017) (Table D2). $|\Psi_{P50}|$, Hv , K_s and L_s were log-transformed to achieve normality. In addition, we obtained tree species-level height (H) as the average of SAPFLUXNET actual tree heights, with the number of tree-days with available sap flow values as weighting factor. The height of the stand was used when the actual height of a tree was not available (792 out of 1929 trees).

To account for climatic effects on the species’ water use parameters and on water relation traits, we used mean annual precipitation (MAP), mean annual temperature (MAT) and an aridity index defined as precipitation over potential evapotranspiration (PPET) (Fig. 1, Fig. D6, Fig. D7). However, for simplicity, we only included MAP in the analyses since for the species in the study MAP was strongly correlated with PPET ($r = 0.94$) and MAT ($r = 0.76$), whereas PPET and MAT correlation was lower ($r = 0.56$). MAP and MAT were obtained for all study plots from the CHELSA data set (1x1 km resolution) (Karger et al., 2017) and averaged at the species level weighting by the number of tree-days. PPET were obtained from CGIAR-CSI Global Aridity index (Trabucco & Zomer, 2019).

1125. Climate and functional traits jointly mediate tree water use strategies

5.2.6 G_{Asw} sensitivity to soil water availability and water demand

In some species, G_{Asw} measurements were distributed very heterogeneously throughout the range of VPD or SWC. To avoid the issues associated with such unbalanced distributions we used binned data. Specifically, we calculated the average of G_{Asw} measurements comprised into 0.2 kPa VPD intervals and five bins spanning the plot-species specific SWC range. For each summarized G_{Asw} we defined a characteristic VPD and SWC as the average values of VPD and SWC of the data in the bin. The summarized values of G_{Asw} were fitted using LMM as a function of the logarithm of VPD ($\ln(\text{VPD})$) and the logarithm of SWC ($\ln(\text{SWC})$) as additive explanatory variables using uncorrelated random slopes for each species and a random intercept for each tree nested in each species. We log-transformed the independent variables to linearise the relationships and ensure normal residuals. LMMs were fitted using the lmer function from the lme4 R package (Bates et al., 2015). Using the coef function from lme4 we obtained species parameters β_{VPD} and β_{SWC} (i.e. species G_{Asw} sensitivity to VPD and to SWC, respectively), with higher values of β_{VPD} or β_{SWC} meaning stronger G reductions with increasing VPD or decreasing SWC, respectively. In addition, a reference G_{Asw} (G_{REF}) characterizing water use under standard conditions for each species, was predicted setting VPD = 1 kPa and SWC = 0.5 m³ m⁻³ (which is close to the average maximum of all sites). Complementary models were also fitted following the same procedure but with REW instead of SWC, so that soil water content variability was normalized across sites. Additional models were also fitted using canopy stomatal conductance (G'_{Asw}) as response variable. Finally, to remove parameter outliers, species with G_{REF} , β_{VPD} or β_{SWC} outside the 99.9 percentile of their normal distribution were excluded from subsequent analyses (2 out of 142 species excluded).

5.2.7 Statistical analyses

We tested whether water use regulation traits (G_{REF} , β_{VPD} and β_{SWC}) differ between angiosperms and gymnosperms using a simple linear model. Next, we

constructed bi-variate linear relationships between species' fitted parameters and species' water relations traits. Furthermore, we repeated these linear relationships by adding MAP and H as predictors and applying a stepwise model selection, to discern whether the effect of the traits remained significant once these new variables were added to the model. In all the analyses we used the number of species' tree-days as a weighting factor.

Finally, we performed a path analysis using the SEM function of the lavaan R package (Rosseel, 2012). Path analysis accounts for direct and indirect dependencies among variables. To account for the coordinated effect of the species' relations traits and to maximize the number of species (106 species), we imputed species' trait missing values (Table D2) using the imputePCA function of the package missMDA (Josse & Husson, 2016) and then performed a Principal Component Analysis (PCA) to extract the two main principal components (Fig. D1). A single path model was built including the three parameters describing G_{Asw} behaviour (G_{REF} , β_{VPD} and β_{SWC}) as response variables and using MAP, H and the two dimensions of the traits' PCA as explanatory variables. In addition to direct relationships, indirect effects of MAP and H on the fitted parameters were also included through their effect on the PCA dimensions (Liu et al., 2019). We also accounted for the effect of MAP on H. We included the number of tree-days per species as a weighting factor in the model. We performed a model selection procedure to include only paths with at least moderately strong support ($P < 0.1$). Finally, we also checked that the fit of the final model was not significantly different from the saturated model using the lavTestLRT function of the lavaan R package (Rosseel, 2012) with Satorra and Bentler (2001) approximation. All variables were standardized before fitting the path models. All the analyses of the study were performed in R3.6.1 (R Core Team, 2018).

1145. Climate and functional traits jointly mediate tree water use strategies

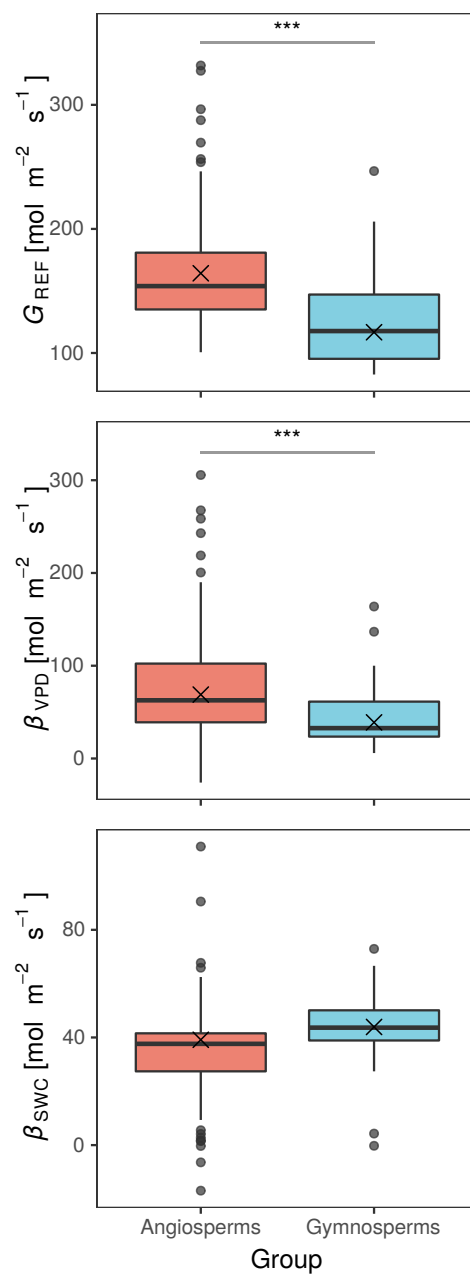


Figure 5.2: Boxplots of water use parameters for both Angiosperms and Gymnosperms. Crosses are weighted means of the parameters.

5.3 Results

5.3.1 Water use parameters and differences between angiosperms and gymnosperms

The model used to obtain water use parameters explained a 59.8% of the total conditional variance in the original data. Reference conductance (G_{REF}) across species ranged between $82.4 \text{ mol m}_{Asw}^{-2} s^{-1}$ (*Juniperus monosperma*) and $333 \text{ mol m}_{Asw}^{-2} s^{-1}$ (*Acacia longifolia*), β_{VPD} between $-26 \text{ mol m}_{Asw}^{-2} s^{-1}$ (*Avicennia marina*) and $306 \text{ mol m}_{Asw}^{-2} s^{-1}$ (*Ulmus americana*) and β_{SWC} between $-17.3 \text{ mol m}_{Asw}^{-2} s^{-1}$ (*Acer saccharum*) and $112 \text{ mol m}_{Asw}^{-2} s^{-1}$ (*Acacia longifolia*) (Fig. D2 – D3 – D4). Most species showed declining G with increasing VPD (positive β_{VPD}) and increasing G with increasing SWC (positive β_{SWC}).

Species showing opposite responses were two temperate (*Acer saccharum*, *Quercus petraea*), one tropical (*Ampelocera macrocarpa*) and a mangrove (*Avicennia marina*) species that showed negative sensitivities to one of the variables (Fig. D2). Mean G_{REF} and β_{VPD} were significantly higher for angiosperms than for gymnosperms (Fig. 2). However, there were no differences in β_{SWC} between angiosperms and gymnosperms. Across all species (including angiosperms and gymnosperms), G_{REF} and β_{VPD} were strongly and positively correlated ($r = 0.75$; with a weighted slope of 0.67; Fig. D5), being the species with high G_{REF} more sensitive to VPD, but strong correlations were not found between G_{REF} and β_{SWC} or between β_{VPD} and β_{SWC} ($|r| < 0.34$ in both cases). When comparing water use parameters calculated considering and not considering aerodynamic conductance, we found that G_{REF} was strongly correlated to G'_{REF} ($r = 0.8$); however, β_{VPD} and β'_{VPD} were poorly correlated ($r = 0.26$) while β_{SWC} and β'_{SWC} showed no significant correlation.

1165. Climate and functional traits jointly mediate tree water use strategies

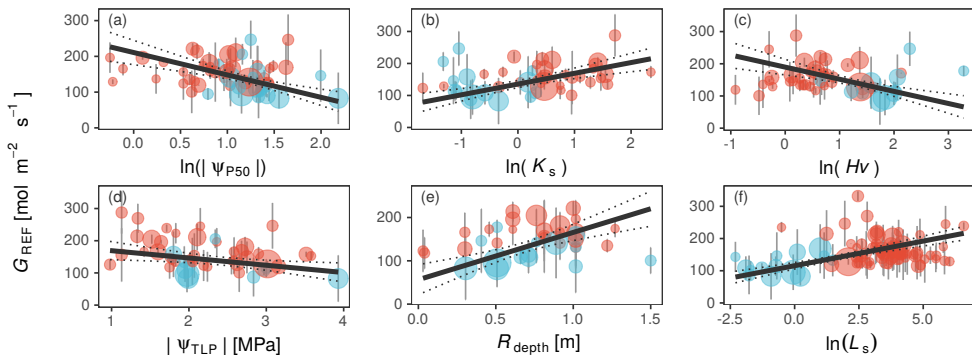


Figure 5.3: Bi-variate relationships between G_{REF} water relations traits. Individual water relation traits are shown in different panels: (a) logarithm of absolute water potential at 50% water conductivity loss, (b) logarithm of maximum sapwood water conductivity, (c) logarithm of Huber value, (d) absolute water potential at turgor-loss point, (e) rooting depth and (f) logarithm of individual leaf area. Black continuous lines depict significant linear relationships (Table 2) and the dashed lines represent the 95% confidence intervals of the models. Red dots are angiosperms and blue dots are gymnosperms. Size of the points is equivalent to the number of tree-days of the species. Vertical lines are the posterior standard deviation of the parameters calculated using REsim function of merTools package (Knowles & Frederick, 2016).

5.3.2 Coordination with hydraulic and allocation traits

In the bi-variate models relating G_{REF} with hydraulic and morphological traits, we found that G_{REF} showed a negative relationship with $|\Psi_{P50}|$, Hv and $|\Psi_{TLP}|$ (Table 2 and Fig. 3a,c,d), whereby species more resistant to embolism, with higher allocation to the sapwood relative to leaves and with more negative turgor-loss pressures showed lower G_{REF} . Furthermore, G_{REF} was positively related to K_s , R_{depth} and L_s (Table 2 and Fig. 3b,e,f), with species with efficient xylem, deeper roots and bigger leaves showing higher G_{REF} . For these traits, L_s was the one explaining the largest fraction of G_{REF} variability ($R^2 = 0.39$). With the exception of Ψ_{TLP} , these relationships remained significant also for G'_{Asw} (Table D3).

β_{VPD} was negatively related with $|\Psi_{P50}|$ and Hv and positively with K_s (Table 2 and Fig. 4a,b,c), i.e., species with less safe and more efficient xylem present higher sensitivity to VPD, and hence more strict stomatal control as atmospheric water demand increases. β_{VPD} was also positively related to

5.3. Results

117

Table 5.2: Results of the bi-variate linear models relating water use parameters (G_{REF} , β_{VPD} , β_{SWC}) and water relations traits. Parameters are explained by individual traits using simple linear models using number of species-days as weighting factor.

Water use parameter	Water relations Traits	N species	Intercept	Slope	R^2
G_{REF}	$\ln(\Psi_{P50})$	55	210.701***	-62.724 ***	0.282
	$\ln(K_s)$	43	135.527***	33.614 ***	0.338
	$\ln(Hv)$	49	189.439***	-37.602 ***	0.285
	$ \Psi_{\text{TLP}} $	48	191.764***	-22.702 *	0.112
	R_{depth}	37	56.204**	109.296 ***	0.366
	$\ln(L_s)$	86	115.537***	15.28 ***	0.391
β_{VPD}	$\ln(\Psi_{P50})$	55	109.201***	-47.716 ***	0.240
	$\ln(K_s)$	43	50.199***	20.427 **	0.180
	$\ln(Hv)$	49	96.503***	-33.817 ***	0.363
	$ \Psi_{\text{TLP}} $	48	80.321***	-12.209 .	0.040
	R_{depth}	37	-2.190 ns	80.383 ***	0.260
	$\ln(L_s)$	86	34.577***	11.219 ***	0.327
β_{SWC}	$\ln(\Psi_{P50})$	55	16.103 ns	19.327 *	0.059
	$\ln(K_s)$	43	42.113***	-5.021 ns	0.000
	$\ln(Hv)$	49	23.952**	13.586 *	0.088
	$ \Psi_{\text{TLP}} $	48	40.468**	1.052 ns	0.000
	R_{depth}	37	53.851***	-28.471 .	0.051
	$\ln(L_s)$	86	51.112***	-4.095 **	0.087

Statistical significant levels: “.” p<0.1 ; “*” p<0.05; “**” p<0.01; “***” p<0.001; ns not significant.

1185. Climate and functional traits jointly mediate tree water use strategies

R_{depth} and L_s (Table 2 and Fig. 4e,f), indicating that deeper roots and larger leaves were associated to higher stomatal sensitivity to VPD. Absolute turgor-loss point ($|\Psi_{TLP}|$) was weakly negatively related with β_{VPD} (p value = 0.093; Table 2). Hv and L_s were the traits explaining most of β_{VPD} variability ($R^2 = 0.36$ and $R^2 = 0.33$, respectively). With the exception of Ψ_{TLP} , these relationships remained significant also for G'_{Asw} (Table D3).

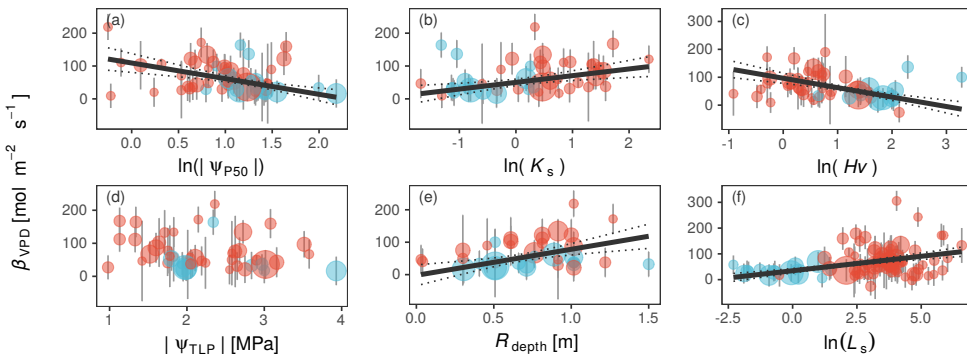


Figure 5.4: Bi-variate relationships between β_{VPD} water relations traits. Individual water relation traits are shown in different panels: (a) logarithm of absolute water potential at 50% water conductivity loss, (b) logarithm of maximum sapwood water conductivity, (c) logarithm of Huber value, (d) absolute water potential at turgor-loss point, (e) rooting depth and (f) logarithm of individual leaf area. Black continuous lines depict significant linear relationships (Table 2) and the dashed lines represent the 95% confidence intervals of the models. Red dots are angiosperms and blue dots are gymnosperms. Size of the points is equivalent to the number of tree-days of the species. Vertical lines are the posterior standard deviation of the parameters calculated using REsim function of merTools package (Knowles & Frederick, 2016).

β_{SWC} was positively related to $|\Psi_{P50}|$ and Hv (Table 2 and Fig. 5a,c), i.e., species with higher resistance to embolism and larger ratios of sapwood to leaf area were more sensitive to soil water depletion. In addition, species with larger leaves (L_s) and, marginally (p value = 0.095), with deeper roots (R_{depth}) were less sensitive to soil water stress (Table 2 and Fig. 5e,f). In general, water relations traits explained a lower proportion (at most 9%) of the variability in β_{SWC} than of G_{REF} or β_{VPD} . However, we should treat relationships between β_{SWC} and $|\Psi_{P50}|$, Hv and R_{depth} with caution, since they all become non-significant when aerodynamic conductance was taken into account (Table D3) or when REW was used instead of SWC (Table

5.3. Results

119

D3). Furthermore, when REW was used instead of SWC, all soil moisture sensitivity-trait relationships became non-significant (Table D4).

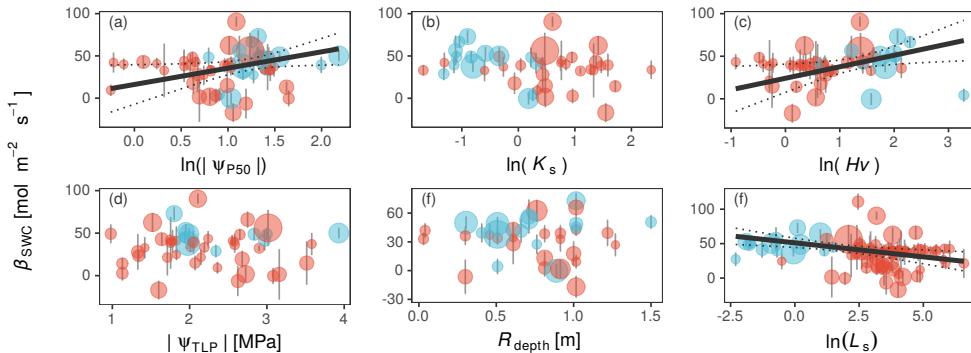


Figure 5.5: Bi-variate relationships between β_{SWC} water relations traits. Individual water relation traits are shown in different panels: (a) logarithm of absolute water potential at 50% water conductivity loss, (b) logarithm of maximum sapwood water conductivity, (c) logarithm of Huber value, (d) absolute water potential at turgor-loss point, (e) rooting depth and (f) logarithm of individual leaf area. Black continuous lines depict significant linear relationships (Table 2) and the dashed lines represent the 95% confidence intervals of the models. Red dots are angiosperms and blue dots are gymnosperms. Size of the points is equivalent to the number of tree-days of the species. Vertical lines are the posterior standard deviation of the parameters calculated using REsim function of merTools package (Knowles & Frederick, 2016).

Ecological factors associated with water use parameters and coordination When the coordination between water use parameters and water relations traits was assessed while also accounting for the effects of MAP (mean annual precipitation) and H (tree species-level mean height), most of the relationships described in the previous section remained significant, with only three exceptions. The relationships that were no longer observed corresponded to the effect of Ψ_{TLP} on G_{REF} and the effects of $|\Psi_{P50}|$ and Hv on β_{SWC} (Table 3). In these models, MAP was the variable that explained most of the variability in stomatal responses to soil water (β_{SWC}), with generally lower sensitivity to SWC in locations with high MAP (Table 3), although this effect reversed in the L_s model. However, when models were calculated using β'_{SWC} , MAP effects were all negative (Table D5). On the other hand, MAP was largely unrelated to G_{REF} and β_{VPD} in most of the G_{REF} and β_{VPD} models (Table 3). Finally, our results show that taller trees tend to have higher

1205. Climate and functional traits jointly mediate tree water use strategies

Table 5.3: Results of the bi-variate linear models relating water use parameters (G_{REF} , β_{VPD} , β_{SWC}), water relations traits, climate and tree height. Water use parameters are explained using simple linear models with number of species-days as weighting factor. β column values are the slopes for each explanatory variable. N species = number of species included. NI = not included variable after model selection.

Water use parameter	Water relations Traits	N species	Intercept	β_{trait}	β_{MAP}	β_{H}	R^2
G_{REF}	$\ln(\Psi_{P50})$	54	173.6 ***	-48.549 **	NI	1.418 *	0.325
	$\ln(K_s)$	42	109.773 ***	30.731 ***	NI	1.822 *	0.423
	$\ln(Hv)$	43	162.178 ***	-32.21 **	NI	1.448 .	0.332
	$ \Psi_{\text{TLP}} $	47	66.861 ***	NI	0.057 *	1.962 *	0.346
	R_{depth}	36	41.932 *	88.301 ***	NI	1.802 *	0.448
	$\ln(L_s)$	80	98.531 ***	13.389 ***	NI	1.384 **	0.450
β_{VPD}	$\ln(\Psi_{P50})$	54	70.665 ***	-32.97 **	NI	1.468 *	0.317
	$\ln(K_s)$	42	25.16 *	17.444 **	NI	1.768 **	0.303
	$\ln(Hv)$	43	73.255 ***	-28.931 ***	NI	1.197 *	0.408
	$ \Psi_{\text{TLP}} $	47	16.363 .	NI	NI	2.502 ***	0.291
	R_{depth}	36	-18.282 ns	56.571 *	NI	2.034 **	0.412
	$\ln(L_s)$	80	16.099 *	8.955 ***	NI	1.512 ***	0.429
β_{SWC}	$\ln(\Psi_{P50})$	54	62.606 ***	NI	-0.029 *	NI	0.088
	$\ln(K_s)$	42	73.319 ***	NI	-0.038 **	NI	0.142
	$\ln(Hv)$	43	50.25 **	10.221 ns	-0.026 .	NI	0.149
	$ \Psi_{\text{TLP}} $	47	55.33 ***	NI	NI	-0.903 *	0.067
	R_{depth}	36	62.889 ***	NI	-0.037 **	NI	0.213
	$\ln(L_s)$	80	44.671 ***	-5.002 **	0.025 *	-0.749 *	0.142

Statistical significant levels: “.” p<0.1 ; ** p<0.05; *** p<0.01; **** p<0.001; ns not significant.

G_{REF} and higher sensitivity to VPD (β_{VPD}), however, when G_{REF} was obtained from G'_{Asw} (i.e. G'_{REF}), H was not selected in the final models (Table D5). The relationship between H and soil drought sensitivity (β_{SWC}) was less clear, since it was significantly negative in only two of the models (Table 3), suggesting higher sensitivity to soil drought in shorter trees. However when aerodynamic coupling was taken into account, the relationship was inverted and taller trees had higher sensitivity to SWC (Table D5).

The two main dimensions of the PCA analyses describing water relations trait coordination explained a 69.8% of the total variance (Fig. D1). The primary PCA dimension (Dim1; 56.8% of variance) could be interpreted as a safety-efficiency trade-off axis, whereby positive values are related to elevated K_s , large L_s , deep roots, low Hv and low $|\Psi_{P50}|$. The second PCA dimension (Dim2; 13% of variance) was associated to leaf turgor-loss pressure (Ψ_{TLP}), with positive values related to high $|\Psi_{TLP}|$ levels and, to a lower extent, deeper roots.

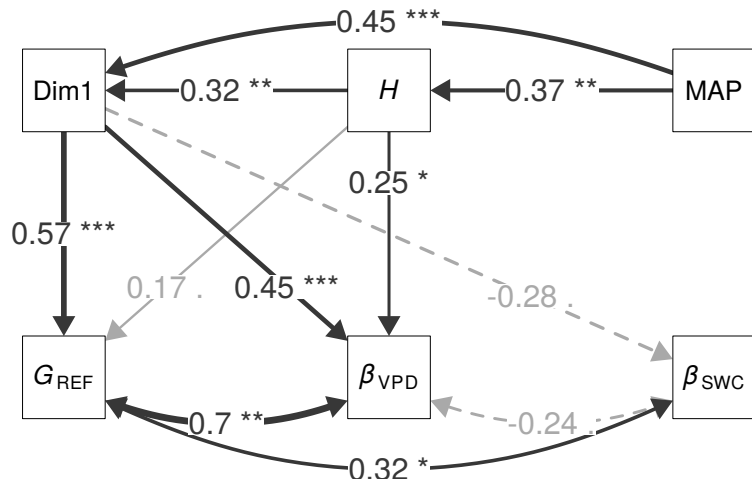


Figure 5.6: Path analyses of species-specific water use parameters explained by mean annual precipitation (MAP), tree height (H) and coordinated hydraulic traits Dim1. Dim1 is the hydraulic traits’ PCA dimension 1 (Fig. D1). Positive Dim1 values are mainly related to efficient water use strategies, while negative to safety strategies. Dim2 was not selected in the final model. Arrow labels are standardized parameters. Continuous lines are positive relationships while dashed lines are negative relationships. Black and grey lines are significant and marginally significant relationships, respectively. Statistical significant levels: .., $P < 0.1$; *, $P < 0.05$; **, $P < 0.01$; ***, $P < 0.001$.

1225. Climate and functional traits jointly mediate tree water use strategies

In the path analyses, efficiency traits (positive PCA Dim1 values) were significantly related to high annual precipitation (high MAP) and to taller trees (large H) (Fig. 6). Also, H increased with MAP. G_{REF} was positively associated with Dim1 (Fig. 6) and taller trees also had marginally higher G_{REF} (Fig. 6). Similarly, higher β_{VPD} (i.e., higher VPD sensitivity) was positively related to efficient water transport (Dim1) and to H (Fig. 6). Sensitivity to SWC (β_{SWC}) showed a marginal, negative relationship with Dim1, so that sensitivity increased with xylem resistance to embolism (Fig. 6). Finally, G_{REF} co-varied positively with β_{VPD} and β_{SWC} , implying that as G_{REF} increases so do β_{VPD} and β_{SWC} (Fig. 6, Fig. D5). The second dimension of the PCA was not included in the final path model, suggesting a lack of coordination between Ψ_{TLP} and water use parameters.

5.4 Discussion

In this study, we present a novel analysis linking organ-level traits with whole-plant water use strategies at the global scale, made possible by the compilation of the first global sap flow database. We provide evidence of a coordination between water relations traits and water use parameters (G_{REF} , β_{VPD} and β_{SWC}), while accounting for the effects of climate and tree size. Some water use and trait associations were explained by climate affiliations of species, but most relationships between water use and water relations traits remained after accounting for climate and tree size effects. As any synthesis effort of this magnitude based on diverse data sources, our study presents several limitations. First, sap flow data used to estimate G carry some uncertainty issues, although these may be less relevant for assessing environmental responses as we do here than for characterizing absolute values (Flo et al., 2019). Second, SAPFLUXNET may have an incomplete coverage of global forest ecosystems (Fig. 1, Poyatos et al., 2020). Third, highly non-linear or threshold-based SWC responses may be difficult to capture, especially when having to resort to reanalysis data. Fourth, other ecological processes such as partial canopy-atmosphere coupling or intra-specific variability in traits and/or water use regulation may influence our results.

5.4.1 Climate influence on water use strategies across species

Our results showed no direct effect of mean annual precipitation (MAP) on G_{REF} and β_{VPD} , but instead indirect MAP effects on water use strategies mediated through hydraulic and allocation traits (Fig 6 and Fig. D6), suggesting that MAP constrains feasible water relations traits (Bourne et al., 2017; Liu et al., 2019), which then directly determine water use rate and β_{VPD} . The direction of these effects is consistent with previous studies showing that β_{VPD} increased with aridity in rainforest species (Cunningham, 2004; but see Grossiord et al., 2019) and at continental scales across ecosystems and functional types (Novick et al., 2016), but these studies did not disentangle direct from indirect effects. Although the global controls on β_{SWC} were less clear in our analyses, in part due to the influence of aerodynamic coupling (cf. Table 3 and S5), climate effects on this variable also appeared to be largely indirect (Fig. 6). Therefore, our results underscore the importance of using water relations traits, rather than climate when addressing species whole-tree water use strategies and ecosystem flux sensitivities to VPD.

5.4.2 Water use parameters

Water use parameters differed widely among species (Fig. D2) and defined a gradient of water use sensitivities to drought stress. Within the gradient of parameters, angiosperms and gymnosperms showed distinct whole-plant water use strategies (Fig. 2). We found that gymnosperms have generally more ‘conservative’ water use strategies in terms of lower G_{REF} but not in terms of enhanced sensitivity to VPD or SWC. Similarly, previous studies also showed lower sensitivity to VPD in gymnosperms compared to angiosperms (Johnson et al., 2012; Lin et al., 2015), which could be associated to higher safety margins (Choat et al., 2012; Anderegg et al., 2016). The ‘conservative’ G_{REF} strategy of gymnosperms could be explained by group-specific trait syndromes associated to water relations traits (Fig. D8), wood anatomy (Venturas et al., 2017), and lower photosynthetic rates, stomatal conductance or leaf N concentrations (Lusk et al., 2003).

G_{REF} and β_{VPD} showed a strong positive correlation across species (Fig.

1245. Climate and functional traits jointly mediate tree water use strategies

D5) similar to the one found by Oren et al. (1999). This implies stronger VPD control on transpiration in species with higher water use under optimal conditions (higher G_{REF}). However, our global cross-species analyses might mask finer variations, as β_{VPD} (or $\beta_{\text{VPD}} / G_{\text{REF}}$) is expected to be lower across species from dry sites (Oren et al., 1999) or along a decreasing gradient of SWC within species (Domec & Johnson, 2012; Zhang et al., 2012; but see Poyatos et al., 2007). Nevertheless, this result suggests that G_{REF} can be a suitable proxy of whole-tree canopy conductance sensitivity to VPD, as it is at the leaf (Oren et al., 1999) or ecosystem (Grossiord et al., 2020) levels.

The lack of correlation found between the sensitivity to SWC calculated with and without aerodynamic conductance, indicates that canopy coupling could be important in calculating β_{SWC} and that in order to predict and model plant water responses to soil water dynamics, we likely have to explicitly consider aerodynamic and boundary layer conductances. In addition, these land-atmosphere interactions might be crucial in diagnosing and modelling the soil moisture controls over other ecosystem processes such as the carbon cycle (Green et al., 2019; Kannenberg et al., 2020).

5.4.3 Coordination between water use parameters and water relations traits

Our results support the hypothesis of a strong coordination between G_{REF} and individual hydraulic and allocation traits. G_{REF} aligns with ‘efficiency’ traits (K_s) in the hydraulic safety-efficiency axis, and is thus negatively related to ‘safety’ traits (particularly Ψ_{P50}). These results are consistent with the overall proposed coordination between plant hydraulics and gas exchange (Meinzer, 2002; Sperry et al., 2002; Mencuccini, 2003; Maherli et al., 2006; Henry et al., 2019) and with the notion that species operate close to their maximum transport capacity sustained by their hydraulic system (Manzoni et al., 2013). Large individual leaf areas were also related to higher G_{REF} , probably due to higher leaf hydraulic conductance mediated by wider conduits (Schreiber et al., 2016; Ding et al., 2020). The positive association of elevated G_{REF} with deeper roots points out the requirement of deep rooting to supply water

for keeping high transpiration rates, and is also found in the coordination between R_{depth} , Ψ_{P50} and K_s (Mursinna et al., 2018).

Coordination between whole-tree water use sensitivity to VPD (β_{VPD}) and to SWC (β_{SWC}) with organ-level water relations traits had not been assessed before at a global scale. All the studied water relations traits (except Ψ_{TLP}) appear to be related to β_{VPD} , whereby the species with more ‘efficient’ or less “safe” traits tend to be those which show higher β_{VPD} . These results are consistent with previous studies relating stomatal responses and water relation traits (Lu et al., 2020) and with the stomatal gas exchange optimization theory (see Tyree & Sperry, 1988; Wang et al., 2020). By contrast, after controlling for climate and tree height, conductance sensitivity to SWC (β_{SWC}) was only (negatively) related to L_s . Notably, β_{SWC} was unrelated to Ψ_{TLP} , in contrast to Maréchaux et al. (2018), that evidenced more negative Ψ_{TLP} related to lower reductions in sap flow with decreasing SWC. This absence of relationship, including the weak $\beta_{VPD} - \Psi_{TLP}$ correlation, could be attributed to noise and uncertainty in Ψ_{TLP} measures (Meinzer et al., 2014) or with Ψ_{TLP} plasticity (Bartlett et al., 2012; Rosas et al., 2019). In addition, the lack of relationship between β_{SWC} and R_{depth} could be explained by the complexity of rooting depth dependency on soil water infiltration, tree height and climate (Fan et al., 2017).

We also explored the coordinated effect of water relations traits on water use parameters and accounted for direct and indirect climate and tree height effects through the PCA and the path model. Based on our results, water use strategies would be, in terms of G_{REF} , consistent with the Reich (2014) notion of a whole-plant resource use spectrum, ranging from ‘conservative’ to ‘acquisitive’ species. However, in terms of absolute sensitivity to VPD, our results go against this idea, since acquisitive species (with high G_{REF}) are also more sensitive to VPD (more ‘conservative’). Therefore, our study would support a more physiological interpretation of water use strategies that stresses trait coordination. According to this interpretation, plants with ‘safer’ hydraulic systems (high resistance to embolism) are able to function at higher water tensions without requiring a strict water use regulation, implying that they can show a more ‘acquisitive’ regulation of water use so

1265. Climate and functional traits jointly mediate tree water use strategies

that they can benefit from having a wider range of conditions to operate safely. In other words, high transport capacity in the xylem (K_s) is associated with high canopy conductance (G_{REF}) and a vulnerable (sensitive) xylem is also associated with a stricter regulation of gas exchange. However, a vulnerable xylem reduces safety, and is usually interpreted as part of an ‘acquisitive’ strategy, whereas a strict regulation of water use prevents hydraulic failure and hence corresponds to a ‘conservative’ strategy. This view is also consistent with the positive relationship between Ψ_{P50} and Ψ_{TLP} , even if it saturates at relatively low water potentials (cf. Martin-StPaul et al., 2017). These results highlight the complications of defining a single, whole-plant resource use spectrum ranging from ‘acquisitive’ to ‘conservative’ species (sensu Reich, 2014), and points to the need of considering different organs and functional axes when assessing whole-plant functional integration.

Regarding tree’s height, it was coordinated directly and indirectly –through water relations traits– with water use parameters (Table 3 and Fig. 6), in a way that taller trees displayed more ‘efficient’ water use strategies. Alignment of water relations traits and H was consistent with results found by Liu et al. (2019), relating maximum plant size with Ψ_{P50} , K_s or Hv at the global scale across species and life forms. These complex direct and indirect H relationships might be driven by ecosystem water availability (Fig. 6) and low freezing risk (Olson et al., 2018), which allows for increased water use through efficient water transport (e.g. high K_s or Hv), compensating the increase of resistance due to the enlarged water path of taller trees (Barnard & Ryan, 2003; Liu et al., 2019; Mencuccini et al., 2019b). Furthermore, H could also affect differential sensitivity to VPD and SWC in tall trees (Giardina et al., 2018), as their canopy would be more exposed to VPD, requiring higher β_{VPD} , and would potentially have more developed root systems, which would decrease β_{SWC} .

5.4.4 Conclusions

Understanding tree water use strategies at the global scale is crucial to better predict ecosystem water cycles and drought vulnerability of species and ecosystems. Here we demonstrate that there is a global spectrum of water use

strategies determined by the coordination of hydraulic and allocation traits, rather than by climate. In particular, species-specific G_{REF} and β_{VPD} (but not β_{SWC}) are closely related to the species-specific water relations traits. We have also shown significant differences between angiosperm and gymnosperm water use strategies, showing greater water use and sensitivity to VPD in angiosperms than gymnosperms, a finding that could be related to distinct water relations traits syndromes (Fig. D8). Our trait-based approach allowed for a simplified global mapping of water use strategies. The use of simple measurable traits (e.g. leaf size) altogether with functional grouping can lead to a better approximation of species reference water conductance and its sensitivity to VPD. Recently developed global maps of traits (Moreno-Martínez et al., 2018; Trugman et al., 2020) would permit the inclusion of such water use strategies in Land Surface and Earth System Models potentially improving ecosystem carbon and water fluxes predictions.

“thesis” — 2020/12/29 — 11:18 — page 128 — #152

6

General discussion and conclusions

Despite the fact that forest transpiration is the main terrestrial evaporative flux and a key component of the global hydrological cycle and Earth System functioning, its quantification is still replete with uncertainty (Schlesinger and Jasechko 2014). Our knowledge of how trees control transpiration in response to hydrometeorological conditions worldwide remains incomplete. Transpiration regulation and water use strategy under drought conditions determine individual survival (Choat et al. 2018), which extends to forest function and dynamics across the globe, impacting the provision of forest ecosystem services such as carbon sequestration, hydroclimatic regulation and biodiversity conservation (Trumbore et al. 2015). Thus, a better understanding of transpiration and its spatiotemporal variability will improve assessments of vegetation dynamics and climate feedbacks at regional to global scales, especially in the face of global change (Choat et al. 2018), which is increasing drought episodes and their severity in several regions (Dai 2013). Along this thesis I have tried to give a global perspective on the ecohydrological variables driving the regulation of transpiration using sap flow data at the whole-tree level. Due to the lack of a global and harmonized database of sap flow measurements in the past, this sort of synthesis had not been attempted before. However, the launch of the SAPFLUXNET database, to which I have contributed, has made this possible. Because a global, harmonized sap flow database requires comparability across methods, the first chapter of this thesis deals with calibration uncertainty of different sap flow techniques.

6.1 Improving sap flow techniques to obtain reliable estimates of tree level transpiration

To reduce the uncertainty in our knowledge of plant water transport processes, it is essential to first reduce the uncertainty in the measurements of plant water flow. All sap flow methods have specific limitations (Vandegehuchte and Steppe, 2013, Smith and Allen 1996) and can yield biased estimates, which implies that this bias needs to be taken into account when sap flow data are used in quantitative analyses (Chapter 2). In particular, I show that heat dissipation techniques, which are by far the most widely used method, con-

6.1. Improving sap flow techniques to obtain reliable estimates of tree level transpiration 131

sistently underestimate sap flow by 40% on average (if used with its original calibration coefficients; Chapter 2). At the same time, all methods provide high average correlations between sap flow measurements and actual values, suggesting that they are suitable for studies based on qualitative or relative values, including research on the relative importance of the hydrometeorological drivers explaining canopy conductance (Chapter 4), or on the sensitivity of transpiration to hydrometeorological drivers (Chapter 5).

To improve the quality of plant water flow estimates obtained using sap flow methods, further efforts are needed to develop and follow transparent protocols for each method, including protocols for installation; homogenization of raw data processing, and quantification of uncertainty (see Peters et al. 2020). Also, calibration of probes is essential whenever possible; otherwise, applying generic or species-specific correction factors for each method may be an alternative solution, although less accurate. To improve method-specific correction factors, it would be important to identify sapwood traits that might explain measurement errors, such as wood density, or anatomical and vessel distribution traits (Suleiman et al., 1999; Wullschleger et al., 2011). However, so far attempts to identify the potential effect of those wood traits on sap flow measurement errors have not been entirely successful (Peters et al., 2018, Chapter 2), possibly due to the fact that the actual traits are rarely measured on the same plant material used in the calibrations. Studying these wood traits in the context of sap flow calibrations for a range of species with different sapwood anatomies would allow us to understand their potential influence on sap flow measurement uncertainty, and to obtain correction factors for all species without the need for calibration. Besides, scaling of single-point measurements to the whole-tree level constitutes another major source of uncertainty (Hernandez-Santana et al. 2015) that cannot be easily addressed with correction factors. Sap flow integration requires to consider the tree sapwood area and its radial profile, whose quantification carries a lot of uncertainty even with destructive tree sampling (Hernandez-Santana et al. 2015). Nonetheless, the scaling error could be minimized by taking more than several sap flow measurements along the perimeter and radial profile of the plant, and estimating sapwood area more accurately by using on-site robust

species allometrical relationships or multiple core samples of the measured individuals.

Improving the accuracy of sap flow methods has been a major research goal for decades. For this purpose, specific corrections have been implemented, for example, for dealing with wounding effects or for fixing signal dampening due to installation time (Green et al., 2003; Swanson and Whitfield, 1981, Peters et al. 2018). In addition, new probes configurations and sap flow techniques have been developed. Some of the technologies currently being designed are promising, such as those based on dual techniques applying different methods throughout the flow range (Forster 2019), on single-probe methods to minimize wound (Bernal et al. 2017), or on developing integrated, compact and low cost systems (Jones et al. 2020). Besides the traditional thermometric methods, some attempts have been made using other approaches such as acoustic emissions (Černý et al. 2011 , Mazal et al. 2012), or thermal imaging (Anfodillo et al. 2006), but they have not been entirely successful. Despite the uncertainties associated to all thermometric sap flow methods, they remain the best tool we have at hand to estimate transpiration dynamics at the tree-level, and the only solid basis for the compilation of a global sap flow database (Poyatos et al. 2016).

6.2 The SAPLUXNET database. What next?

Over the course of the thesis, the SAPFLUXNET database has become a reality (Poyatos et al. 2020), and it is currently available and open access at ZENODO (REF) since 2019. Additionally, we have built a data infrastructure capable of processing and analysing large amounts of sap flow related data, which is prepared for the inclusion of new data sets if further requests for data contributions are reopened in the future. SAPFLUXNET has gained increased attention from ecophysicists and ecohydrologists, and by the end of 2020 there have been around 1500 downloads of the data base. As discussed in Chapter 3, SAPFLUXNET and its combination with existing datasets, such as FLUXNET (Pastorello et al. 2020) or HydraTRY (Mencuccini et al. 2019b, Sanchez-Martinez et al. 2020) or remote sensing products

6.3. The hydroclimatic drivers of transpiration and their complexity 133

such as GLEAM (Martens et al. 2017), will help us to better characterize plant drought responses and forest transpiration across the globe. Also, in conjunction with, for example, the Tree-Ring Data Bank (REF) or remote sensing data (Simard et al., 2011), SAPFLUXNET will improve the characterization of drought legacy effects and recovery of water use after drought, potentially bridging the gap between water use, tree growth and ecosystem productivity. This thesis is an example of the kind of studies that can be accomplished taking advantage of SAPFLUXNET. In particular, I carried out the first quantification of the importance of hydroclimatic drivers controlling tree transpiration globally, and also characterized tree water use strategies across species that emerge from the covariation between water use regulation and hydraulic traits.

6.3 The hydroclimatic drivers of transpiration and their complexity

The closure of stomata to prevent water loss through transpiration responds to hydroclimatic changes at temporal scales that range from minutes to seasons (Buckley 2005). As a result, plant transpiration is coupled to some extent to hydroclimatic variables (i.e. vapour pressure deficit, soil water content and radiation). This coupling allows plants to cope with drought, and may differ depending on environmental conditions, water use strategy and legacy effects. I have shown in this thesis that vapour pressure deficit (VPD) is the main driver of transpiration globally. This result may be explained by the different temporal scale at which changes in VPD, soil water content (SWC) and radiation occur. Stomatal closure might be tightly and promptly coupled to VPD to protect plant hydraulic integrity under abrupt dry atmospheric conditions, while the dynamics of soil moisture supply are slower, allowing to maintain transpiration rates by, for example, exploring and extracting water from deeper layers of the soil as drought progresses (Barbeta and Peñuelas 2017). By contrast, although radiation (PPFD) has similar temporal scale dynamics as VPD, it is less coupled to plant transpiration. This may be explained by the direct relationship of the VPD with water flows and plant

water status, especially in well-coupled canopies, while the function of PPFD as a G driver would be a more complex process produced via photosynthesis. This direct effect can be found in most ecosystem-level G models which show better results using only VPD (Lin et al. 2018), although VPD and solar radiation are strongly coupled at most temporal scales.

The lack of coupling between transpiration dynamics and hydrometeorological variables in drylands suggested by our results might be related to complex responses of transpiration regulation to the interaction of the hydrometeorological drivers (Zhou et al., 2019), which we have not considered explicitly. Alternatively, it might be associated to the diversity of water use strategies in water limited systems that allow plants living in dry biomes to escape from drought dynamics and better compete for resources and maximize growth. These water use strategies may be related to multiple anatomical and hydraulic traits conferring drought tolerance and safety towards hydraulic failure, which is in concordance with results in Chapter 5.

The low variance explained by VPD, SWC and PPFD in some regions limits our ability to explain (and model) transpiration patterns at the global scale. An additional reason for this low explanatory power may be the simple shape of the log models of canopy conductance used in Chapter 4 -although similar explained variance was obtained by more flexible GAM models-, which may fail for some species or sites, especially for the SWC models. Thus, it would be important to further test whether the empirical couplings reported in this thesis are similar to those predicted by the main stomatal regulation algorithms used by land surface models (Mencuccini et al. 2018). In addition, other ecohydrological variables not considered in Chapter 4 could also explain transpiration regulation, such as wind speed (REF) or [CO₂]. Finally, this thesis evidences large differences in transpiration responses to hydroclimatic drivers across species and sites. The possibility to explain these differences using measurable plant traits opens new ground towards the characterization and modelling of plant water use strategies at the global scale, a topic that I address in the final empirical chapter of the thesis (Chapter 5).

6.4 On the use of plant traits to characterize water use strategies at the global level

A better understanding of the spatial distribution of tree water use strategies will allow the improvement of climate and ecosystem models, particularly in drought-prone situations (Matheny et al. 2017). Static parameters defining water use strategies for plant functional types (PFT) used in current terrestrial biosphere and dynamic vegetation models have been identified as a potential source of uncertainty due to PFT over-aggregation (Wullschleger et al. 2014 , Yang et al. 2015). Moving to a trait-based approach would therefore improve our capacity to predict ecosystem responses, since for each parameter used in the models there would be a continuum set of trait values, one corresponding to each species (or even, potentially, to each population). Results from Chapter 5 show that plant traits related to water transport (hydraulics) and water relations explain water use regulation by plants, particularly regarding responses to VPD. These results pave the ground for the inclusion of these traits in land surface models (as already done in some cases: Kennedy et al. 2019 , Eller et al. 2020) and for the use of these traits in up-scaling water use from the tree to the ecosystem in diverse communities. However, as shown in Chapter 4, our predictive capacity of transpiration regulation at the daily level is still relatively low for some regions, and it would be interesting to explore different temporal scales and also consider more complex models. Following results shown in Chapter 5 and in concordance to the postulated trade-off between hydraulic safety and efficiency, trees with high water transport capacity (e.g., large xylem conduits) would tend to be more vulnerable to hydraulic dysfunction (e.g., high vulnerability to xylem embolism) and therefore would show a tight stomatal regulation to protect their hydraulic system (Taneda and Sperry 2008). In contrast, species less conductive species with safer conduits would tend to have a less strict stomatal regulation. However, there are several examples of trees with high conductive capacity in the xylem and relatively loose stomatal regulation (Martinez-Vilalta et al. 2014), which implies that other traits rather than xylem properties might be determining the water use strategy (Matheny et al. 2015). These considerations suggest,

as we have explored in Chapter 5, that water-use strategies at the tree level emerge from the coordination of different traits, and can only be understood if this coordination is explicitly taken into account.

Other traits would potentially be useful for describing water use strategies in addition to the hydraulic and anatomical traits explored in this thesis, in addition to the effects of climate, soil and stand structure properties (Chapter 4). Many functional traits have been recognized as important determinants of plant ecological strategies (Yang et al. 2015), including specific leaf area or seed mass, which may link the plant economic spectrum hypothesis to plant hydraulics and water use strategies (Rosas et al. 2019b). Another important consideration is that, in order to implement this trait-based approach to define water use strategies that can be applied to land surface models, it is essential that these traits are mapped at a global scale. Global to regional maps of plant traits are currently limited to a small group of leaf (Moreno-Martínez et al. 2018) or hydraulic (Trugman et al. 2020) traits. However, recent studies highlighting the strong phylogenetic conservatism of key hydraulic traits (Sanchez-Martinez et al. 2020), together with the increased availability of tree distribution data (Serra-Díaz et al. 2017), suggest that global maps for these traits will be available soon.

6.5 Towards a global characterization of plant water use strategies.

In the present thesis we have explored plant water use from the perspective of whole-tree transpiration regulation in response to concomitant variations in hydrometeorological forcing. However, we have left out important aspects to understand and define the water use strategies of trees. For instance, in Chapter 5 we focus on xylem hydraulics without explicitly considering the hydraulics of leaves and roots, which are important determinants of plants’ water status and the drought sensitivity of whole-plant hydraulic conductance. Accounting for these different organs will help integrate the internal and external conditions that regulate transpiration and define water use strategies, and to better understand the link between plant economic spectrum, hydraulic safety

6.5. Towards a global characterization of plant water use strategies. 137

and efficiency and the regulation of plant water status (Reich 1994, Martinez-Vilalta and Garcia-Forner 2017?). This would be facilitated by building an additional database for SAPFLUXNET sites with available measured midday and pre-down leaf water potentials, which combined with midday sap flow data would allow to estimate whole-tree hydraulic conductance (Eller et al 2018). Most current models estimate whole-tree hydraulic conductance from branch-level xylem hydraulic conductance, either directly or applying a simple upscaling exercise based on conduit tapering (e.g., Christoffersen et al. 2016 , Ellen et al. 2020), which is likely to be inaccurate and biased across species. Besides, to complement the study of transpiration responses, high resolution dendrometric measures would allow to estimate the role of steam capacitance in water use strategies (Steppe et al. 2015). There is still much to be understood about tree water use strategies and the drivers of transpiration regulation. This is in part due to the lack of high quality data for an adequate parametrization of transpiration dynamics at relevant spatiotemporal scales. The use of the SAPFLUXNET global database represents a major step forward and a powerful tool to overcome this challenge to a significant extent.

6.6 Conclusions

- 2.1. Calibrations of sap flow methods shows large intra- and inter-method variability in performance, with a low proportion of this variability explained by species and no consistent effects of wood density or porosity type.
- 2.2. Dissipation methods showed lower accuracy and higher proportional bias than other methods, but relatively high linearity and precision, while Pulse methods also showed significant proportional bias driven by their overestimation of low flows. Therefore, Dissipation methods may be more appropriate to assess relative sap flow and Pulse methods may be more suitable to quantify medium and high absolute flows.
- 2.3. All sap flow methods showed high precision, justifying their use to quantify environmental responses of transpiration and allowing potential correction of the measurements using study-specific calibrations.
- 3.1. We present the global SAPFLUXNET database, including harmonised and quality-controlled individual datasets supplied by contributors worldwide. Datasets include sub-daily time series of sap flow and hydrometeorological drivers for 202 globally distributed sites, including 2714 trees belonging to 174 species.
- 3.2. The SAPFLUXNET database provides the first global perspective of water use by individual plants at multiple timescales, with important applications in fields ranging from plant ecophysiology to Earth-system science.
- 4.1. Transpiration regulation is better explained by vapour pressure deficit (VPD) than by soil water content (SWC) or radiation (PPFD). Trees in dryland biomes are less coupled to all three hydrometeorological drivers than those in other biomes.
- 4.2. Climate, soil and vegetation structure were common controls of all three hydrometeorological couplings with canopy conductance, with wetter climates, fine textured soils and tall vegetation being associated to tighter coupling.

- 5.1. Reference canopy conductance and its sensitivity to vapour pressure deficit (VPD) is coordinated with hydraulic and allocation traits (i.e. Ψ_{P50} , K_s , H_v , Ψ_{TLP} , R_{depth} , L_s and tree height) rather than being directly controlled by climate (e.g, mean annual precipitation).
- 5.2. Species with efficient xylem transport (higher hydraulic conductance) had higher canopy conductance but also higher sensitivity to vapour pressure deficit (VPD). Moreover, we found that angiosperms had higher reference canopy conductance and higher sensitivity to VPD than gymnosperms.

“thesis” — 2020/12/29 — 11:18 — page 140 — #164

A

Appendix Chapter 2

A.1 Figures A

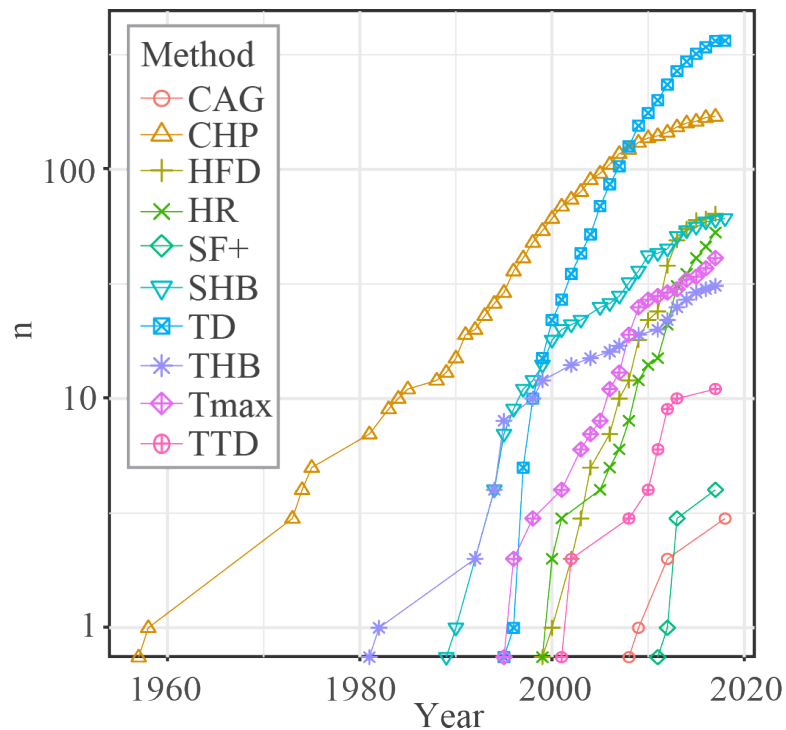


Figure A.1: Representation of the cumulative number of studies using different sap flow methods between 1957 and 2017 (adapted and updated from Poyatos et al. 2016). CAG: calibrated average gradient; CHP: compensation heat pulse (early heat pulse methods have been considered CHP, Edwards et al. 1997); HFD: head field deformation; HR: heat ratio, SF+: sapflow+; SHB: stem heat balance; TD: thermal dissipation; THB: trunk heat balance; Tmax: T-max heat pulse; TTD: transient thermal dissipation. Notice the logarithmic scale on the y-axis.

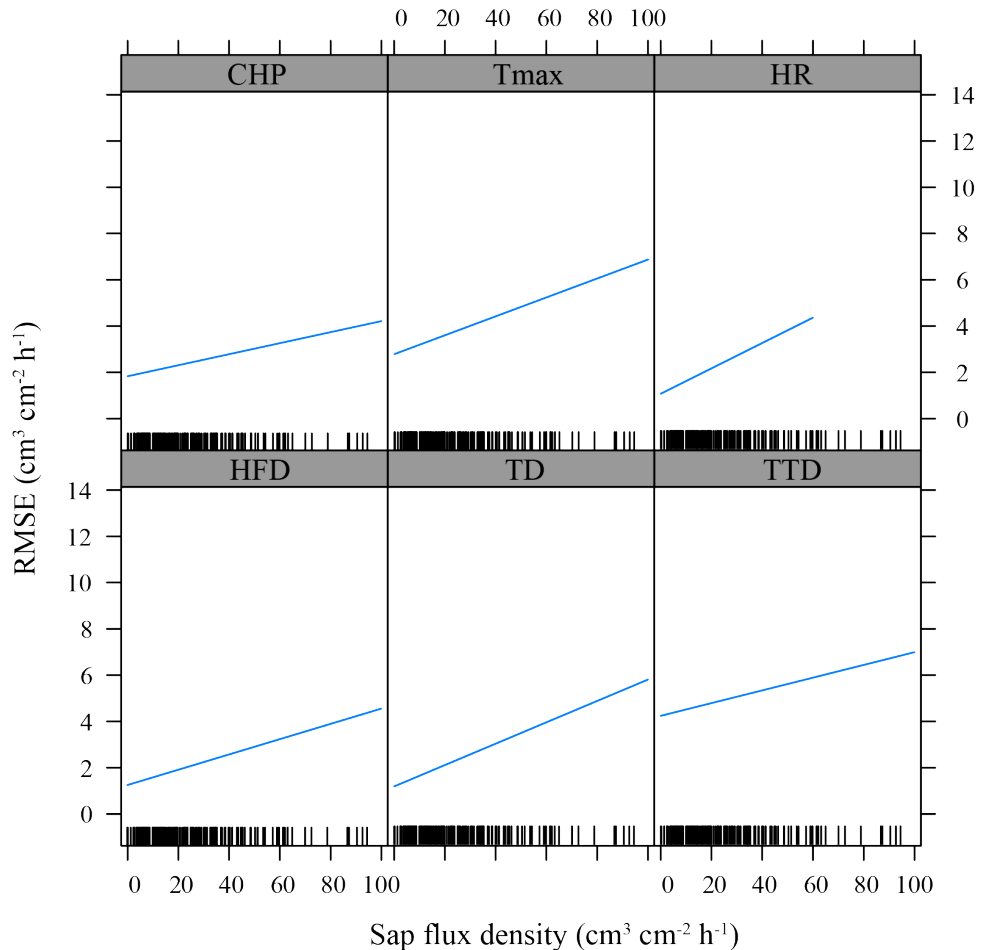


Figure A.2: Relationship between root mean square error (RMSE) and sap flux density (mean calibration range) and for different sap flux density methods, as predicted by the LMM model presented in Table 3.

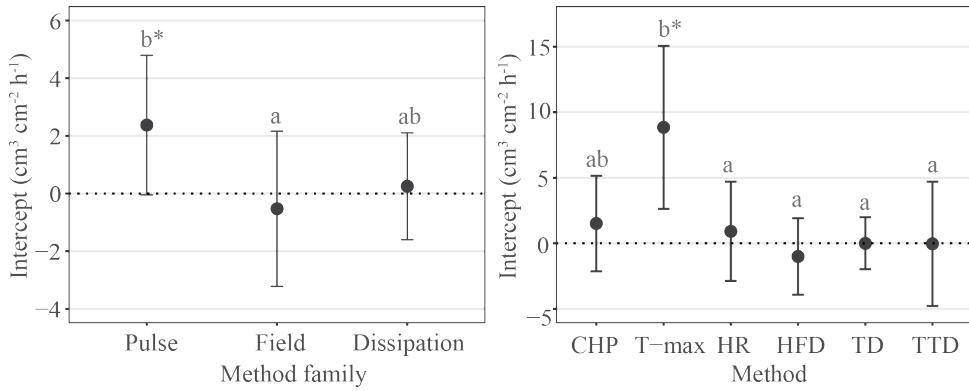


Figure A.3: Predictions of the LMM models calculated from least-squares means of the intercept (β_0) of the linear model (Eq. 3). Different letters indicate significant differences between factors levels evaluated with Tukey’s test. Horizontal, dotted lines indicate reference, perfect calibration values for a given metric. Asterisks (*) indicate significant ($p < 0.05$) departure from those reference values.

A.2 Tables A

Table A.1: Summary table of the studies used in the analyses presented in the paper. Sap flow method, species, calibration material, porosity and average stem/tree diameter are reported.

Study	Method	Species	Calibration material	Wood porosity	Diameter (cm)
Alarcon <i>et al.</i> 2005	CHP	<i>Citrus limon</i>	whole plant	Diffuse porous	2.50
Ballester <i>et al.</i> 2011	CHP	<i>Citrus clementina</i>	whole plant	Diffuse porous	
Barret <i>et al.</i> 1995	CHP	<i>Corymbia maculata</i>	without roots	Diffuse porous	
Bleby <i>et al.</i> 2004	CHP	<i>Eucalyptus marginata</i>	whole plant	Diffuse porous	10.00
Bleby <i>et al.</i> 2004	HR	<i>Eucalyptus marginata</i>	whole plant	Diffuse porous	10.00
Braun and Schmid 1999	TD	<i>Vitis vinifera</i>	whole plant	Ring porous	3.75
Burgess <i>et al.</i> 2001	HR	<i>Eucalyptus marginata</i>	whole plant	Diffuse porous	
Bush <i>et al.</i> 2010	TD	<i>Populus fremontii</i>	stem segment	Diffuse porous	5.08
Bush <i>et al.</i> 2010	TD	<i>Tilia cordata</i>	stem segment	Diffuse porous	4.83
Cain 2009	TD	<i>Macaranga hypoleuca</i>	stem segment	Diffuse porous	82.00
Cain 2009	TD	<i>Macaranga pearsonii</i>	stem segment	Diffuse porous	67.00
Caspari <i>et al.</i> 1993	CHP	<i>Pyrus serotina</i>	whole plant	Diffuse porous	6.62
Caterina <i>et al.</i> 2013	TD	<i>Juniperus virginiana</i>	stem segment	Tracheids	8.00
Chan 2015	TD	<i>Abies concolor</i>	stem segment	Tracheids	6.00
Cohen <i>et al.</i> 1981	T-max	<i>Platanus orientalis</i>	stem segment	Diffuse porous	6.70
Cohen <i>et al.</i> 1981	T-max	<i>Populus alba</i>	stem segment	Diffuse porous	6.70
Cohen <i>et al.</i> 1998	T-max	<i>Malus domestica</i>	whole plant	Diffuse porous	
Dragoni <i>et al.</i> 2005	CHP	<i>Malus domestica</i>	whole plant	Diffuse porous	6.50
Dye <i>et al.</i> 1996	CHP	<i>Pinus patula</i>	without roots	Tracheids	
Fernandez <i>et al.</i> 1999	CHP	<i>Olea europaea</i>	stem segment	Diffuse porous	8.80
Fernandez <i>et al.</i> 1999	CHP	<i>Olea europaea</i>	without roots	Diffuse porous	
Fernandez <i>et al.</i> 2006	CHP	<i>Citrus sinensis</i>	stem segment	Diffuse porous	7.80
Fernandez <i>et al.</i> 2006	CHP	<i>Citrus sinensis</i>	without roots	Diffuse porous	10.40
Fernandez <i>et al.</i> 2006	CHP	<i>Olea europaea</i>	stem segment	Diffuse porous	8.20
Fernandez <i>et al.</i> 2006	CHP	<i>Olea europaea</i>	without roots	Diffuse porous	9.80
Fernandez <i>et al.</i> 2006	CHP	<i>Prunus domestica</i>	stem segment	Diffuse porous	8.00
Fernandez <i>et al.</i> 2006	CHP	<i>Prunus domestica</i>	without roots	Diffuse porous	7.00
Fuchs <i>et al.</i> 2017	HFD	<i>Acer pseudoplatanus</i>	stem segment	Diffuse porous	10.56
Fuchs <i>et al.</i> 2017	HFD	<i>Fagus sylvatica</i>	stem segment	Diffuse porous	9.42
Fuchs <i>et al.</i> 2017	HFD	<i>Tilia cordata</i>	stem segment	Diffuse porous	9.29
Fuchs <i>et al.</i> 2017	HR	<i>Acer pseudoplatanus</i>	stem segment	Diffuse porous	
Fuchs <i>et al.</i> 2017	HR	<i>Fagus sylvatica</i>	stem segment	Diffuse porous	
Fuchs <i>et al.</i> 2017	HR	<i>Tilia cordata</i>	stem segment	Diffuse porous	
Fuchs <i>et al.</i> 2017	TD	<i>Acer campestre</i>	stem segment	Diffuse porous	11.81
Fuchs <i>et al.</i> 2017	TD	<i>Acer pseudoplatanus</i>	stem segment	Diffuse porous	10.80
Fuchs <i>et al.</i> 2017	TD	<i>Fagus sylvatica</i>	stem segment	Diffuse porous	9.83
Fuchs <i>et al.</i> 2017	TD	<i>Populus nigra</i>	stem segment	Diffuse porous	10.77
Fuchs <i>et al.</i> 2017	TD	<i>Tilia cordata</i>	stem segment	Diffuse porous	9.41
Gonzalez-Altozano <i>et al.</i> 1998	CHP	<i>Citrus reticulata</i>	whole plant	Diffuse porous	11.50
Gonzalez-Altozano <i>et al.</i> 1998	T-max	<i>Citrus reticulata</i>	whole plant	Diffuse porous	11.50
Granier 1985	TD	<i>Pinus nigra</i>	stem segment	Tracheids	4.50
Granier 1985	TD	<i>Pseudotsuga menziesii</i>	stem segment	Tracheids	4.50

Table A.1: Summary table of the studies used in the analyses presented in the paper. Sap flow method, species, calibration material, porosity and average stem/tree diameter are reported. (*continued*)

Study	Method	Species	Calibration material	Wood porosity	Diameter (cm)
Granier 1985	TD	<i>Quercus pedunculata</i>	stem segment	Ring porous	4.50
Green <i>et al.</i> 1988	CHP	<i>Actinidia chinensis</i>	stem segment	Diffuse porous	5.25
Green <i>et al.</i> 1988	CHP	<i>Actinidia chinensis</i>	whole plant	Diffuse porous	5.40
Green <i>et al.</i> 1988	CHP	<i>Malus sylvestris</i>	whole plant	Diffuse porous	5.60
Gutierrez <i>et al.</i> 1994	SHB	<i>Acacia koa</i>	whole plant	Diffuse porous	
Gutierrez <i>et al.</i> 1994	SHB	<i>Coffea arabica</i>	whole plant	Diffuse porous	
Gutierrez Soto <i>et al.</i> 2012	HR	<i>Carica papaya</i>	whole plant	Monocot	
Hatton <i>et al.</i> 1995	CHP	<i>Eucalyptus populnea</i>	without roots	Diffuse porous	5.40
Heilman <i>et al.</i> 1990	SHB	<i>Ligustrum japonicum</i>	whole plant	Diffuse porous	1.00
Herbs <i>et al.</i> 2007	TD	<i>Acer campestre</i>	stem segment	Diffuse porous	
Herbs <i>et al.</i> 2007	TD	<i>Crataegus monogyna</i>	stem segment	Diffuse porous	
Hultine <i>et al.</i> 2010	TD	<i>Tamarix ramosissima</i>	stem segment	Ring porous	4.16
Intrigliolo <i>et al.</i> 2009	T-max	<i>Vitis vinifera</i>	whole plant	Ring porous	
Isarangkool <i>et al.</i> 2009	TTD	<i>Abies concolor</i>	stem segment	Diffuse porous	5.14
Isarangkool <i>et al.</i> 2009	TTD	<i>Hevea brasiliensis</i>	stem segment	Diffuse porous	4.69
Isarangkool <i>et al.</i> 2009	TTD	<i>Mangifera indica</i>	stem segment	Diffuse porous	4.35
Johan Uddling <i>et al.</i> 2009	TD	<i>Betula papyrifera</i>	stem segment	Diffuse porous	
Lu 2002	TD	<i>Garcinia mangostana</i>	whole plant	Diffuse porous	4.00
Lu 2002	TD	<i>Mangifera indica</i>	whole plant	Diffuse porous	2.30
Lu 2002	TD	<i>Musa spp.</i>	whole plant	Monocot	12.00
Lu and Chacko 1998	TD	<i>Mangifera indica</i>	whole plant	Diffuse porous	2.30
Madurapperuma <i>et al.</i> 2009	HR	<i>Syagrus romanzoffiana</i>	whole plant	Monocot	
Michell <i>et al.</i> 2009	HR	<i>Eucalyptus capillosa</i>	without roots	Diffuse porous	6.50
Montague <i>et al.</i> 2006	TD	<i>Liquidambar styraciflua</i>	whole plant	Diffuse porous	5.30
Montague <i>et al.</i> 2006	TD	<i>Populus deltoides</i>	whole plant	Diffuse porous	5.60
Montague <i>et al.</i> 2006	TD	<i>Pyrus calleryana</i>	whole plant	Diffuse porous	6.60
Montague <i>et al.</i> 2006	TD	<i>Quercus robur x Q. Bicolor</i>	whole plant	Ring porous	5.70
Nadezhina <i>et al.</i> 1998	HFD	<i>Tilia cordata</i>	without roots	Diffuse porous	12.00
Nortes <i>et al.</i> 2009	CHP	<i>Prunus dulcis</i>	whole plant	Diffuse porous	15.00
Paudel <i>et al.</i> 2013	TD	<i>Malus domestica</i>	stem segment	Diffuse porous	4.01
Paudel <i>et al.</i> 2013	TD	<i>Peltophorum dubium</i>	stem segment	Diffuse porous	3.70
Paudel <i>et al.</i> 2013	TD	<i>Prunus persica</i>	stem segment	Diffuse porous	4.00
Paudel <i>et al.</i> 2013	TTD	<i>Malus domestica</i>	stem segment	Diffuse porous	4.01
Paudel <i>et al.</i> 2013	TTD	<i>Peltophorum dubium</i>	stem segment	Diffuse porous	3.70
Paudel <i>et al.</i> 2013	TTD	<i>Prunus persica</i>	stem segment	Diffuse porous	4.00
Peters <i>et al.</i> 2017	TD	<i>Larix decidua</i>	stem segment	Tracheids	16.50
Peters <i>et al.</i> 2017	TD	<i>Picea abies</i>	stem segment	Tracheids	15.90
Prendergast <i>et al.</i> 2007	T-max	<i>Actinidia chinensis</i>	stem segment	Diffuse porous	9.50
Shackel <i>et al.</i> 1992	SHB	<i>Prunus persica</i>	whole plant	Diffuse porous	6.25
Smith <i>et al.</i> 1995	CHP	<i>Acacia holosericea</i>	stem segment	Diffuse porous	
Smith <i>et al.</i> 1995	CHP	<i>Acacia holosericea</i>	without roots	Diffuse porous	
Smith <i>et al.</i> 1995	CHP	<i>Acacia nilotica</i>	stem segment	Diffuse porous	
Smith <i>et al.</i> 1995	CHP	<i>Azadirachta indica</i>	stem segment	Diffuse porous	
Smith <i>et al.</i> 1995	CHP	<i>Azadirachta indica</i>	without roots	Diffuse porous	
Sperling <i>et al.</i> 2012	TD	<i>Phoenix dactylifera</i>	whole plant	Monocot	60.00
Steppe <i>et al.</i> 2010	CHP	<i>Fagus grandifolia</i>	stem segment	Diffuse porous	18.00
Steppe <i>et al.</i> 2010	HFD	<i>Fagus grandifolia</i>	stem segment	Diffuse porous	18.12

A.2. Tables A

147

Table A.1: Summary table of the studies used in the analyses presented in the paper. Sap flow method, species, calibration material, porosity and average stem/tree diameter are reported. (*continued*)

Study	Method	Species	Calibration material	Wood porosity	Diameter (cm)
Steppe <i>et al.</i> 2010	TD	<i>Fagus grandifolia</i>	stem segment	Diffuse porous	18.00
Sun <i>et al.</i> 2012	TD	<i>Liquidambar styraciflua</i>	without roots	Diffuse porous	7.50
Sun <i>et al.</i> 2012	TD	<i>Pinus echinata</i>	without roots	Tracheids	7.50
Sun <i>et al.</i> 2012	TD	<i>Pinus taeda</i>	without roots	Tracheids	7.50
Sun <i>et al.</i> 2012	TD	<i>Populus deltoides</i>	without roots	Diffuse porous	7.50
Sun <i>et al.</i> 2012	TD	<i>Quercus alba</i>	without roots	Ring porous	7.50
Sun <i>et al.</i> 2012	TD	<i>Ulmus americana</i>	without roots	Ring porous	7.50
Swanson and Whitfield 1981	CHP	<i>Nothofagus solandri</i>	whole plant	Diffuse porous	11.00
Swanson and Whitfield 1981	CHP	<i>Pinus radiata</i>	whole plant	Tracheids	5.00
Urban <i>et al.</i> 2012	SHB	<i>Humulus lupulus</i>	without roots	Ring porous	
Vellame <i>et al.</i> 2010	SHB	<i>Citrus sinensis</i>	whole plant	Diffuse porous	1.40

Table A.2: Anova summary of the LMM models, using the same structure as objective 1, comparing calibrations reported in SFD and SF units (Units) for CHP and TD. CM (Calibration material).

Method	Calibration metric	Variable	Sum sq	Mean Sq	NumDF	DenDF	F.value	Pr(>F)
CHP	Ln-Ratio	Units	0.09	0.09	1	52.05	1.09	0.302
		CM	0.20	0.10	2	44.43	1.24	0.299
	Slope	Units	0.07	0.07	1	25.27	0.37	0.55
		CM	0.24	0.12	2	40.07	0.59	0.558
	Slope (ln-ln)	Units	0.00	0.00	1	12.35	0.02	0.89
		CM	0.14	0.07	2	22.13	0.91	0.416
	Z-Cor	Units	1.07	1.07	1	20.77	4.30	0.051 .
		CM	4.63	2.32	2	34.98	9.28	0.001 ***
TD	Ln-Ratio	Units	0.05	0.05	1	26.72	0.41	0.529
		CM	0.14	0.07	2	16.64	0.58	0.571
	Slope	Units	0.16	0.16	1	44.72	2.28	0.138
		CM	0.17	0.08	2	14.84	1.17	0.338
	Slope (ln-ln)	Units	0.22	0.22	1	72.67	2.18	0.144
		CM	0.14	0.07	2	29.27	0.71	0.501
	Z-Cor	Units	0.08	0.08	1	26.07	0.28	0.598
		CM	0.02	0.01	2	17.41	0.03	0.969

A.2. Tables A

Table A.3: Summary of the LMM models of Ln-Ratio (accuracy), Slope (proportional bias), Slope (ln-ln) (linearity) and Z-Cor (precision) as a function of Methods and Calibration material (CM; Whole plant: whole plant on a container or lysimeter; No-roots: whole plant without roots). CHP is the reference level for the variable Method and Stem segment is the reference level for CM, corresponding to the model intercept. All other coefficient estimates indicate the difference relative to the intercept. σ^2 is the within-groups random variability (residuals of the model). τ_{00} is the between-group random variability. N is the number of levels within random groups. ICC is the Intraclass Correlation Coefficients of each random group. R^2m and R^2c are the variability explained by the fixed and the random factors, respectively.

Coefficients	Estimate	Conf. Int.	p-value									
Fixed effects												
(Intercept)	0.19	-0.052 , 0.425	0.129	0.96	0.779 , 1.135	<0.001	0.85	0.719 , 0.976	<0.001	2.32	1.982 , 2.653	2.32
Method (T-max)	-0.19	-0.611 , 0.240	0.395	-0.27	-0.584 , 0.038	0.089	-0.08	-0.312 , 0.142	0.463	-0.08	-0.669 , 0.506	-0.08
Method (HR)	-0.28	-0.510 , -0.047	0.019	-0.04	-0.247 , 0.162	0.683	0.06	-0.106 , 0.221	0.488	0.16	-0.205 , 0.525	0.16
Method (HFD)	-0.21	-0.409 , -0.003	0.048	0.01	-0.167 , 0.193	0.886	0.00	-0.143 , 0.143	1	0.54	0.220 , 0.862	0.54
Method (SHB)	-0.37	-0.843 , 0.095	0.124	-0.04	-0.365 , 0.285	0.809	0.18	-0.058 , 0.427	0.139	0.45	-0.170 , 1.070	0.45
Method (TD)	-0.65	-0.847 , -0.457	<0.001	-0.20	-0.368 , -0.041	0.015	0.28	0.160 , 0.406	<0.001	-0.12	-0.423 , 0.173	-0.12
Method (TTD)	-0.62	-0.941 , -0.310	<0.001	-0.22	-0.503 , 0.066	0.134	0.20	-0.016 , 0.421	0.072	-0.37	-0.877 , 0.133	-0.37
CM (Whole plant)	-0.03	-0.300 , 0.245	0.841	-0.13	-0.317 , 0.064	0.197	-0.14	-0.276 , -0.003	0.05	-0.67	-1.034 , -0.301	-0.67
CM (No-roots)	-0.13	-0.394 , 0.128	0.319	-0.08	-0.298 , 0.135	0.463	-0.06	-0.213 , 0.104	0.503	-0.78	-1.172 , -0.379	-0.78
Random effects												
σ^2	0.091			0.1			0.076			0.278		
τ_{00} Species	0.013			0.004			0.013			0.04		
τ_{00} Study	0.159			0.041			0.004			0.184		
$N_{Species}$	65			65			65			65		
N_{Study}	48			48			48			48		
$ICC_{Species}$	0.049			0.029			0.137			0.08		
ICC_{Study}	0.604			0.284			0.048			0.366		
Observations	290			290			290			290		

“thesis” — 2020/12/29 — 11:18 — page 150 — #174

B

Appendix Chapter 3

B.1 Figures B

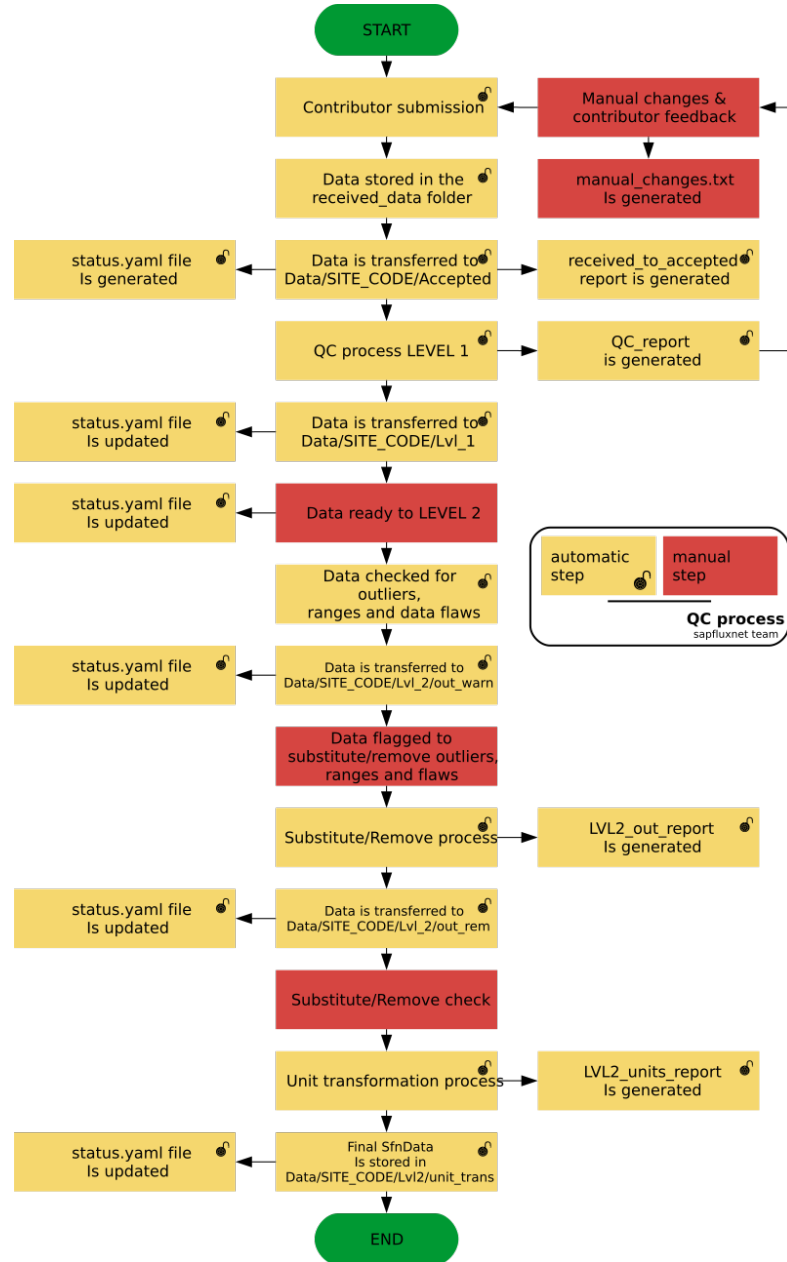


Figure B.1: Overview of the data QC process, showing file management and identifying automatic (in yellow) and manual steps (in red). The column on the left shows the different updates of the status file for each dataset and the column on the right shows generated data reports and steps requiring feedback or manual changes.

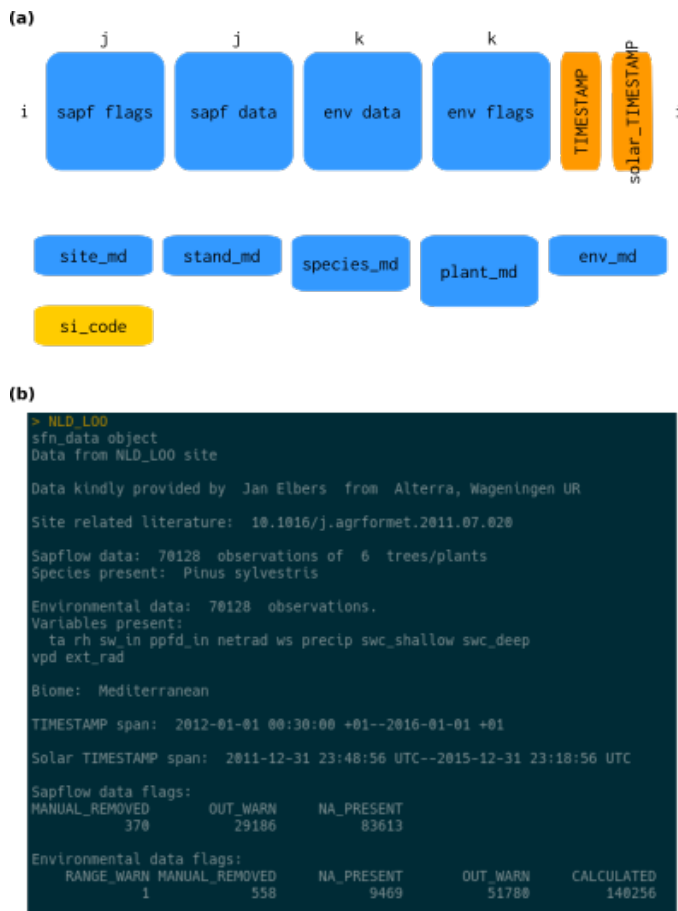


Figure B.2: (a) Structure of `sfn_data` objects, which are based on the S4 class. Boxes in the figure represent different slots where data are stored. Each object is identified by the '`si_code`', stored as a slot in the object, with the format of a character vector. Slots storing time series of data and the associated data flags are of class 'tibble' and have all the same number of rows (`i`), corresponding to the the number of timesteps in the dataset and labelled with two POSIXct timestamp vectors `TIMESTAMP`, `solar_TIMESTAMP`).The slot storing sap flow data, '`sapf_data`' contains(`j`) columns and environmental data ('`env_data`') contains `k` columns, corresponding to the number of environmental variables present. Slots with the suffix '`md`' refer to the different metadata and all are objects of class 'tibble' with different dimensions. For example, the number of rows in `plant_md` depends on the number of plants in the dataset (and this is depicted by the different length of the box). More information on the '`sfn_data`' class objects can be found in the vignette '`sfn-data-classes`' of the package `sapfluxnetr` (Granda et al. 2020). (b) Summary of an `sfn_data` object, showing highlights of site metadata, data dimensions, timestamp span and flags present on the data.

B.1. Figures B

155

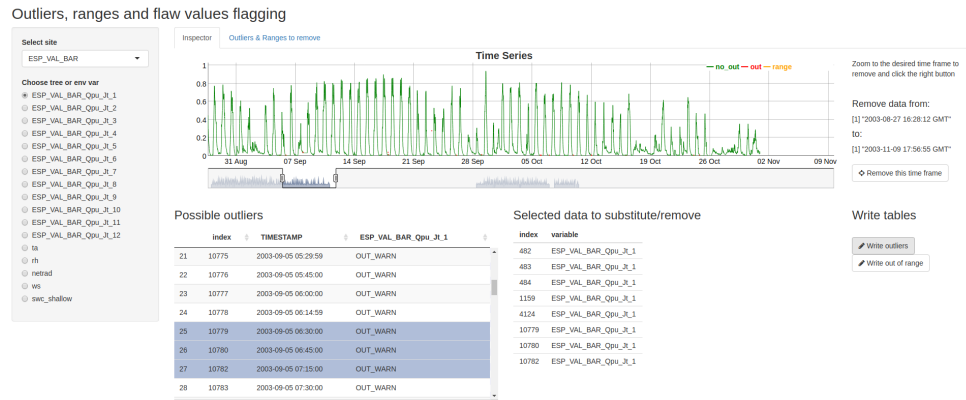


Figure B.3: Example screenshot of the app used for handling outliers and out of range values in time series. The left column shows dataset and variable selection. The central part shows the time series, with out of range values in red and possible outliers in yellow. Rows to replace or remove are selected in a table and written to a text file when done.

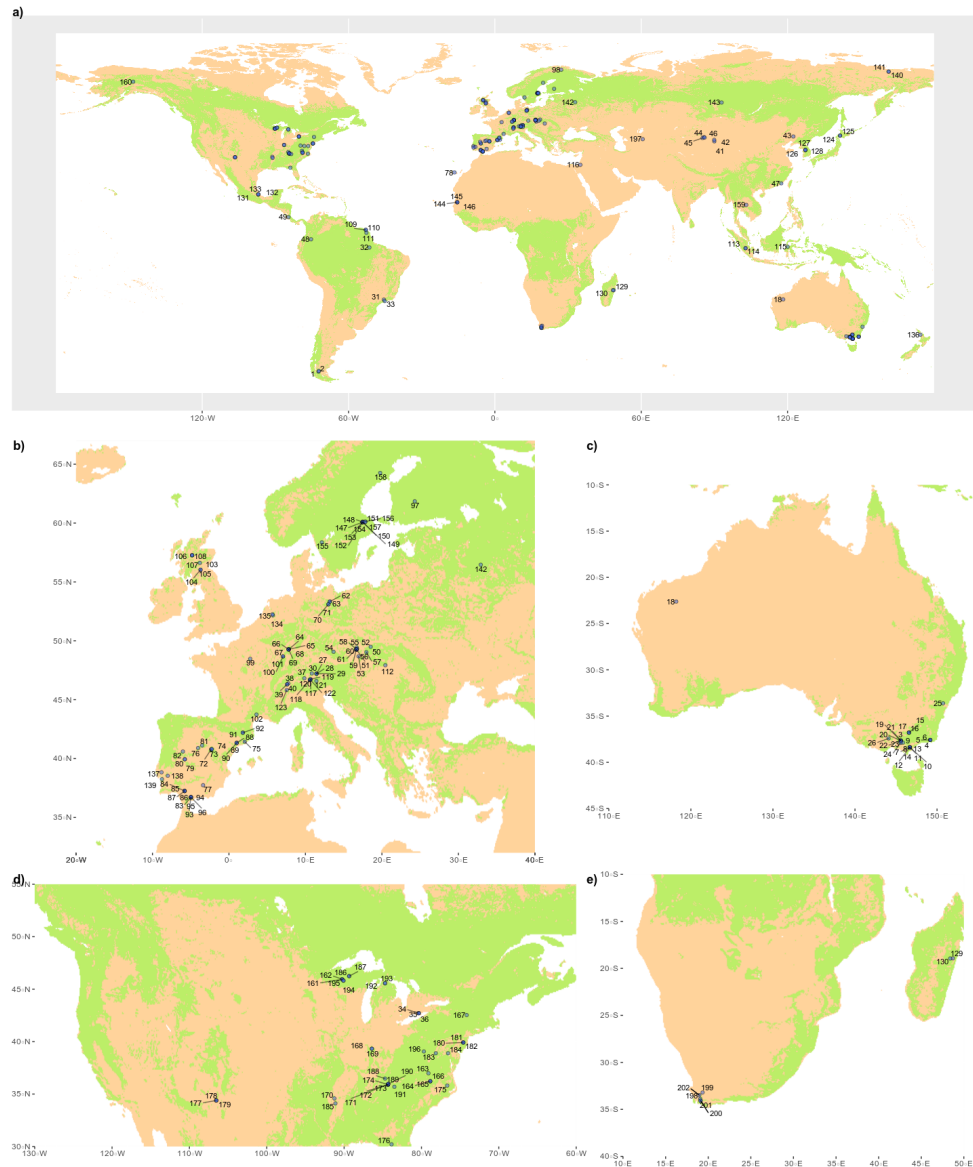


Figure B.4: Detailed geographic distribution of SAPFLUXNET datasets. Datasets are labelled by dataset number in Table S4. Woodland area from Crowther et al. (2015) shown in green.

B.2 Tables B

Table B.1: Data checks implemented in the first level of data quality control (QC1).

Check	Description
Metadata variables	All metadata variables are checked for presence and expected class (numeric, character, logical...).
Character variables values	All metadata character variables are checked against the possible values (factor levels) for that variable, raising a warning if some value is out of the expected.
E-mail check	E-mail provided by contributors is checked for validity
Coordinates and biome	Site coordinates are checked for correctness (are they inside the specified country?) and fixed if needed and possible. MAT and MAP values are obtained for that coordinates and the biome is calculated from that values.
Soil texture	Percentages of soil textures are used to calculate the USDA classification category if possible.
Species names	Species names in plant and species metadata are checked for spelling errors and the concordance between both metadata is also checked
Plant treatments	Check for uniformity in the treatment declared by plant.
Environmental variables presence	Check for concordance between the declared variables in the environmental metadata and the environmental data.
Timestamp	Format, NA presence (there is data, but there is no timestamp), concordance and continuity are checked.
Gap presence:	Data gaps (There is TIMESTAMP but there is no data) are summarised and visualized.
Soil water content	Check for percentage swc values and transform them to cm ³ /cm ³

B.2. Tables B

159

Table B.2: Description of site metadata variables.

Variable	Description	Type	Units
si_name	Site name given by contributors	Character	None
si_country	Country code (ISO)	Character	Fixed values
si_contact_firstname	Contributor first name	Character	None
si_contact_lastname	Contributor last name	Character	None
si_contact_email	Contributor email	Character	None
si_contact_institution	Contributor affiliation	Character	None
si_addcontr_firstname	Additional contributor first name	Character	None
si_addcontr_lastname	Additional contributor last name	Character	None
si_addcontr_email	Additional contributor email	Character	None
si_addcontr_institution	Additional contributor affiliation	Character	None
si_lat	Site latitude (i.e. 42.36)	Numeric	Latitude, decimal format (WGS84)
si_long	Site longitude (i.e. -8.23)	Numeric	Longitude, decimal format (WGS84)
si_elev	Elevation above sea level	Numeric	meters
si_paper	Paper with relevant information to understand the site as DOI links or DOI codes	Character	DOI link
si_dist_mgmt	Recent and historic disturbance and management events that affected the measurement years	Character	Fixed values
si_igbp	Vegetation type based on IGBP classification	Character	Fixed values
si_flux_network	Logical indicating if site is participating in the FLUXNET network	Logical	Fixed values
si_dendro_network	Logical indicating if site is participating in the DENDROGLOBAL network	Logical	Fixed values
si_remarks	Remarks and commentaries useful to grasp some site-specific peculiarities	Character	None
si_code	sapfluxnet site code, unique for each site	Character	Fixed value
si_mat	Site annual mean temperature, as obtained from WorldClim	Numeric	Celsius degrees
si_map	Site annual mean precipitation, as obtained from WorldClim	Numeric	mm
si_biome	Biome classification as per Whittaker diagram, based on mat and map obtained from WorldClim	Character	sapfluxnet calculated

Table B.3: Description of site metadata variables.

Variable	Description	Type	Units
st_name	Stand name given by contributors	Character	None
st_growth_condition	Growth condition with respect to stand origin and management	Character	Fixed values
st_treatment	Treatment applied at stand level	Character	None
st_age	Mean stand age at the moment of sap flow measurements	Numeric	years
st_height	Canopy height	Numeric	meters
st_density	Total stem density for stand	Numeric	stems ha ⁻¹
st_basal_area	Total stand basal area	Numeric	m ² ha ⁻¹
st_lai	Total maximum stand leaf area (one-sided, projected)	Numeric	m ² m ⁻²
st_aspect	Aspect the stand is facing (exposure)	Character	Fixed values
st_terrain	Slope and/or relief of the stand	Character	Fixed values
st_soil_depth	Soil total depth	Numeric	cm
st_soil_texture	Soil texture class, based on simplified USDA classification	Character	Fixed values
st_sand_perc	Soil sand content, % mass	Numeric	% percentage
st_silt_perc	Soil silt content, % mass	Numeric	% percentage
st_clay_perc	Soil clay content, % mass	Numeric	% percentage
st_remarks	Remarks and commentaries useful to grasp some stand-specific peculiarities	Character	None
st_USDA_soil_texture	USDA soil classification based on the percentages provided by the contributor	Character	sapfluxnet calculated

B.2. Tables B

161

Table B.4: Description of species metadata variables.

Variable	Description	Type	Units
sp_name	Identity of each measured species	Character	Scientific name without author abbreviation, as accepted by The Plant List
sp_ntrees	Number of trees measured of each species	Numeric	number of trees
sp_leaf_habit	Leaf habit of the measured species	Character	Fixed values
sp_basal_area_perc	Basal area occupied by each measured species, in percentage over total stand basal area	Numeric	% percentage

Table B.5: Description of plant metadata variables.

Variable	Description	Type	Units
pl_name	Plant code assigned by contributors	Character	None
pl_species	Species identity of the measured plant	Character	Scientific name without author abbreviation, as accepted by The Plant List
pl_treatment	Experimental treatment (if any)	Character	None
pl_dbh	Diameter at breast height of measured plants	Numeric	cm
pl_height	Height of measured plants	Numeric	m
pl_age	Plant age at the moment of measure	Numeric	years
pl_social	Plant social status	Character	Fixed values
pl_sapw_area	Cross-sectional sapwood area	Numeric	cm ²
pl_sapw_depth	Sapwood depth, measured at breast height	Numeric	cm
pl_bark_thick	Plant bark thickness	Numeric	mm
pl_leaf_area	Leaf area of each measured plant	Numeric	m ²
pl_sens_meth	Sap flow measures method	Character	Fixed values
pl_sens_man	Sap flow measures sensor manufacturer	Character	Fixed values
pl_sens_cor_grad	Correction for natural temperature gradients method	Character	Fixed values
pl_sens_cor_zero	Zero flow determination method	Character	Fixed values
pl_sens_calib	Was species-specific calibration used?	Logical	Fixed values
pl_sap_units	Uniformized sapfluxnet units for sapwood, leaf and plant level	Character	Fixed values
pl_sap_units_orig	Original contribution units (at sapwood or plant level)	Character	Fixed values
pl_sens_length	Length of the needles or electrodes forming the sensor	Numeric	mm
pl_sens_hgt	Sensor installation height, measured from the ground	Numeric	m
pl_sens_timestep	Subdaily time step of sensor measures	Numeric	minutes
pl_radial_int		Character	Fixed values
pl_azimut_int		Character	Fixed values
pl_remarks	Remarks and commentaries useful to grasp some plant-specific peculiarities	Character	None
pl_code	sapfluxnet plant code, unique for each plant	Character	Fixed value

Table B.6: Description of environmental metadata variables.

Variable	Description	Type	Units
env_time_zone	Time zone of site used in the TIMESTAMPS	Character	Fixed values
env_time_daylight	Is daylight saving time applied to the original timestamp?	Logical	Fixed values
env_timestep	Subdaily timestep of environmental measures	Numeric	minutes
env_ta	Location of air temperature sensor	Character	Fixed values
env_rh	Location of relative humidity sensor	Character	Fixed values
env_vpd	Location of relative vapour pressure deficit sensor	Character	Fixed values
env_sw_in	Location of shortwave incoming radiation sensor	Character	Fixed values
env_ppfd_in	Location of incoming photosynthetic photon flux density sensor	Character	Fixed values
env_netrad	Location of net radiation sensor	Character	Fixed values
env_ws	Location of wind speed sensor	Character	Fixed values
env_precip	Location of precipitation sensor	Character	Fixed values
env_swc_shallow_depth	Average depth for shallow soil water content measures	Numeric	cm
env_swc_deep_depth	Average depth for deep soil water content measures	Numeric	cm
env_plant_watpot	Availability of water potential values for the same measured plants during the sap flow measurements period	Character	Fixed values
env_leafarea_seasonal	Availability of seasonal course leaf area data and level	Character	Fixed values
env_remarks	Remarks and commentaries useful to grasp some environmental-specific peculiarities	Character	None

Table B.7: Data checks implemented in the second level of data quality control (QC2).

Data check	Description
Sap flow units harmonisation	Sap flow expressed in $\text{cm}^3 \text{ h}^{-1}$, sap flow per unit leafsapwood area in $\text{cm}^3 \text{ cm}^{-2} \text{ h}^{-1}$
Out of range detection	Out of range values are flagged automatically, examined in a visual app and removed if confirmed
Outlier detection	Outliers are flagged automatically, examined in a visual app and removed if confirmed
Radiation transformations	Interconversion between global radiation (sw_in) and photosynthetically active radiation (ppfd_in)
VPD and relative humidity	Interconversion between VPD and relative humidity
Extraterrestrial radiation and solar timestamp	Calculation of extraterrestrial radiation and solar timestamp from timestamp and geographical data
Sap flow interconversions	When sapwood or leaf areas were available, interconversions were applied between the different expression levels for sap flow (per plant, per sapwood area or per leaf area)

Table B.8: Datasets in the SAPFLUXNET database identified by numeric code, dataset code and site name. Number of species per dataset, geographic coordinates and elevation are also shown. Negative coordinate values are shown for Southern and Western Hemispheres.

si_code	si_name	si_lat	si_long	si_elev	# species
ARG_MAZ	Mazaruca_Patagonia	-51.58	-72.29	550	1
ARG_TRE	Tres Marias	-51.32	-72.19	460	1
AUS_BRI_BRI	Britannia Creek	-37.87	145.85	707	1
AUS_CAN_ST1_EUC	Cann River	-37.58	149.17	180	1
AUS_CAN_ST2_MIX	Cann River	-37.58	149.17	180	2
AUS_CAN_ST3 ACA	Cann River	-37.58	149.17	180	1
AUS_CAR THI_00F	Carrajung	-38.38	146.68	610	1
AUS_CAR THI_0P0	Carrajung	-38.38	146.68	610	1
AUS_CAR THI_0PF	Carrajung	-38.38	146.68	610	1
AUS_CAR THI_CON	Carrajung	-38.38	146.68	610	1
AUS_CAR THI_T00	Carrajung	-38.38	146.68	610	1
AUS_CAR THI_T0F	Carrajung	-38.38	146.68	610	1
AUS_CAR THI_TP0	Carrajung	-38.38	146.68	610	1
AUS_CAR THI_TPF	Carrajung	-38.38	146.68	610	1
AUS_ELL HB HIG	Ella	-36.78	146.58	705	2
AUS_ELL MB MOD	Ella	-36.78	146.58	693	1
AUS_ELL UNB	Ella	-36.78	146.58	737	1
AUS_KAR	Karijini NP	-22.62	118.22	710	1
AUS_MAR_HSD_HIG	Maroondah	-37.64	145.58	468	2
AUS_MAR_HSW_HIG	Maroondah	-37.65	145.57	297	2
AUS_MAR_MSD_MOD	Maroondah	-37.64	145.58	467	2
AUS_MAR_MSW_MOD	Maroondah	-37.65	145.57	261	2
AUS_MAR_UBD	Maroondah	-37.69	145.56	303	3
AUS_MAR_UBW	Maroondah	-37.89	145.57	336	3
AUS_RIC_EUC_ELE	Richmond NSW EucFACE	-33.62	150.74	23	1
AUS_WOM	WombatStateForest	-37.42	144.09	705	2
AUT_PAT_FOR	Patscherkofel	47.21	11.45	1950	1
AUT_PAT_KRU	Patscherkofel	47.21	11.45	2180	1
AUT_PAT_TRE	Patscherkofel	47.21	11.45	2110	1
AUT_TSC	Tschirgant south	47.23	10.84	750	1
BRA_CAM	Campos do Jordão	-22.69	-45.52	2000	1
BRA_CAX_CON	Caxiuana	-1.79	-51.43	15	8
BRA_SAN	Santa Virgínia (PESM)	-23.28	-45.18	1000	4
CAN_TUR_P39_POS	TUR	42.71	-80.36	184	1
CAN_TUR_P39_PRE	TUR	42.71	-80.36	184	1
CAN_TUR_P74	TUR	42.71	-80.35	184	1
CHE_DAV_SEE	Davos	46.82	9.86	1650	1
CHE_LOT_NOR	Lotschental	46.39	7.76	1300	2
CHE_PFY_CON	Pfynwald	46.30	7.60	615	1
CHE_PFYIRR	Pfynwald	46.30	7.60	615	1
CHN_ARG_GWD	Arghan	40.75	89.99	830	1
CHN_ARG_GWS	Arghan	41.38	89.94	830	1

Table B.8: Datasets in the SAPFLUXNET database identified by numeric code, dataset code and site name. Number of species per dataset, geographic coordinates and elevation are also shown. Negative coordinate values are shown for Southern and Western Hemispheres. (*continued*)

si_code	si_name	si_lat	si_long	si_elev	# species
CHN_HOR_AFF	Horqin	42.72	122.37	226	1
CHN_YIN_ST1	Yingbazar	42.45	85.72	900	1
CHN_YIN_ST2_DRO	Yingbazar	42.11	85.13	930	1
CHN_YIN_ST3_DRO	Yingbazar	42.29	85.99	930	1
CHN_YUN_YUN	Yunxiao	23.92	117.42	0	2
COL_MAC_SAF_RAD	Macagual Universidad de la Amazonia	1.50	-75.36	360	1
CRI_TAM_TOW	TAMU Soltis Center	10.39	-84.63	600	17
CZE_BIK	Bik	49.49	18.53	875	1
CZE_BIL_BIL	Bilovice	49.25	16.69	320	1
CZE_KRT_KRT	Krtiny	49.32	16.75	480	1
CZE_LAN	Lanžhot	48.68	16.95	150	3
CZE_LIZ LES	Liz	49.07	13.68	858	1
CZE_RAJ_RAJ	Rajec	49.44	16.70	600	1
CZE_SOB_SOB	Sobesice	49.25	16.69	320	1
CZE_STI	Stitna nad Vlari	49.04	17.97	550	1
CZE_UTE_BEE	Utechov	49.28	16.65	420	1
CZE_UTE_BNA	Utechov	49.28	16.65	390	1
CZE_UTE_BPO	Utechov	49.28	16.65	370	1
CZE_UTE_SPR	Utechov	49.28	16.65	360	1
DEU_HIN_OAK	Hinnensee	53.33	13.19	90	1
DEU_HIN_TER	Hinnensee	53.33	13.19	95	2
DEU_MER_BEE_NON	Merzalben	49.27	7.81	550	1
DEU_MER_BEE THI	Merzalben	49.27	7.81	550	1
DEU_MER_DOU_NON	Merzalben	49.27	7.81	550	1
DEU_MER_DOU THI	Merzalben	49.27	7.81	550	1
DEU_MER_MIX_NON	Merzalben	49.27	7.81	550	2
DEU_MER_MIX THI	Merzalben	49.27	7.81	550	2
DEU_STE_2P3	Stechlin	53.10	13.00	78	1
DEU_STE_4P5	Stechlin	53.10	13.00	78	1
ESP_ALT_ARM	Alto Tajo	40.78	-2.33	1079	3
ESP_ALT_HUE	Alto Tajo	40.79	-2.29	907	2
ESP_ALT_TRI	Alto Tajo	40.80	-2.23	981	2
ESP_CAN	Can Balasc	41.43	2.07	270	4
ESP_GUA_VAL	Guadarrama	40.90	-4.03	1140	1
ESP_LAH_COM	LaHarina	37.74	-3.38	180	1
ESP_LAS	Las Canadas, Teide national park tenerife	28.31	-16.57	2070	1
ESP_MAJ_MAI	Majadas del Tietar	39.94	-5.77	260	1
ESP_MAJ_NOR_LM1	Majadas del Tietar	39.94	-5.77	260	1
ESP_MON_SIE_NAT	Montejo	41.12	-3.50	1400	3
ESP_RIN	Rinconada experimental catchment	40.60	-6.02	1200	1

Table B.8: Datasets in the SAPFLUXNET database identified by numeric code, dataset code and site name. Number of species per dataset, geographic coordinates and elevation are also shown. Negative coordinate values are shown for Southern and Western Hemispheres. (*continued*)

si_code	si_name	si_lat	si_long	si_elev	# species
ESP_RON_PIL	Ronda	36.69	-5.02	1734	2
ESP_SAN_A2_45I	Sanabria orchard	37.25	-5.80	49	1
ESP_SAN_A_45I	Sanabria orchard	37.25	-5.80	49	1
ESP_SAN_B_100	Sanabria orchard	37.25	-5.80	49	1
ESP_SAN_B2_100	Sanabria orchard	37.25	-5.80	49	1
ESP_TIL_MIX	Tillar	41.33	1.01	1018	2
ESP_TIL_OAK	Tillar	41.33	1.01	1011	1
ESP_TIL_PIN	Tillar	41.33	1.01	1065	1
ESP_VAL_BAR	Vallcebre	42.20	1.82	1102	1
ESP_VAL_SOR	Vallcebre	42.20	1.81	1257	1
ESP_YUN_C1	Yunquera	36.72	-4.97	1220	1
ESP_YUN_C2	Yunquera	36.72	-4.97	1180	1
ESP_YUN_T1 THI	Yunquera	36.72	-4.97	1190	1
ESP_YUN_T3 THI	Yunquera	36.72	-4.97	1185	1
FIN_HYY_SME	Hyytiala Forest Field Station	61.85	24.29	185	2
FIN_PET	Petsikko	69.49	27.23	251	1
FRA_FON	Fontainebleau-Barbeau	48.48	2.78	105	2
FRA_HES_HE1_NON	Hesse	48.67	7.06	300	1
FRA_HES_HE2_NON	Hesse	48.67	7.06	300	1
FRA_PUE	Puechabon	43.74	3.60	270	1
GBR_ABE_PLO	Aberfeldy	56.62	-3.80	340	1
GBR_DEV_CON	Devilla	56.03	-3.72	75	1
GBR_DEV_DRO	Devilla	56.03	-3.72	75	1
GBR_GUI_ST1	Guisachan	57.27	-4.82	300	1
GBR_GUI_ST2	Guisachan	57.27	-4.82	300	1
GBR_GUI_ST3	Guisachan	57.27	-4.82	300	1
GUF_GUY_GUY	Guyaflux	5.28	-52.92	40	6
GUF_GUY_ST2	Guyaflux	5.28	-52.91	45	7
GUF_NOU_PET	Nouragues station	4.08	-52.68	120	10
HUN_SIK	Sikfokut	47.93	20.44	330	2
IDN_JAM_OIL	Jambi	-2.07	102.79	71	1
IDN_JAM_RUB	Jambi	-2.10	102.78	90	1
IDN_PON_STE	Pono	-1.49	120.06	1050	8
ISR_YAT_YAT	Yatir	31.34	35.05	650	1
ITA_FEI_S17	Feichtwald-Matsch	46.69	10.61	1715	1
ITA_KAE_S20	Kaelbergangl-Matsch	46.70	10.61	1990	1
ITA_MAT_S21	Matscher Alm-Matsch	46.74	10.69	2100	2
ITA_MUN	Muntatschinig-Matsch	46.68	10.58	1160	1
ITA_REN	Renon	46.59	11.43	1794	3
ITA_RUN_N20	Runer Koepfl-Matsch	46.70	10.64	2030	2
ITA_TOR	Torgnon	45.82	7.56	2100	1

Table B.8: Datasets in the SAPFLUXNET database identified by numeric code, dataset code and site name. Number of species per dataset, geographic coordinates and elevation are also shown. Negative coordinate values are shown for Southern and Western Hemispheres. (*continued*)

si_code	si_name	si_lat	si_long	si_elev	# species
JPN_EBE_HYB	Ebetsu	43.08	141.52	40	1
JPN_EBE_SUG	Ebetsu	43.08	141.52	40	1
KOR_TAE_TC1_LOW	Taehwa	37.30	127.32	160	1
KOR_TAE_TC2_MED	Taehwa	37.30	127.32	160	1
KOR_TAE_TC3_EXT	Taehwa	37.30	127.32	160	1
MDG_SEM_TAL	Semi-mature forest	-18.93	48.71	950	6
MDG_YOU_SHO	Young secondary forest	-18.95	48.40	990	1
MEX_COR_YP	Cortadura	19.49	-97.04	2180	1
MEX_VER_BSJ	VERACRUZ_BSJ	19.51	-96.98	1440	5
MEX_VER_BSM	VERACRUZ_BSM	19.53	-96.99	1524	2
NLD_LOO	Loobos	52.17	5.74	25	1
NLD_SPE_DOU	Speulderbos	52.25	5.69	50	1
NZL_HUA_HUA	Huapai	-36.80	174.49	90	1
PRT_LEZ_ARN	LEZIRIAS	38.83	-8.82	15	1
PRT_MIT	MITRA II	38.54	-8.00	235	1
PRT_PIN	Pinheiro da Cruz	38.25	-8.76	5	2
RUS_CHE_LOW	Cherskii	68.74	161.50	90	1
RUS_CHE_Y4	CHE	68.74	161.41	6	1
RUS_FYO	Fyodorovskoye	56.46	32.92	260	3
RUS_POG_VAR	Pogorelsky Bor	56.36	92.95	243	3
SEN_SOUP_IRR	Souilène	16.34	-15.43	10	1
SEN_SOUP_POS	Souilène	16.34	-15.43	10	1
SEN_SOUP_PRE	Souilène	16.34	-15.43	10	1
SWE_NOR_ST1_AF1	Norunda	60.09	17.48	45	2
SWE_NOR_ST1_AF2	Norunda	60.09	17.48	45	2
SWE_NOR_ST1_BEF	Norunda	60.09	17.48	45	2
SWE_NOR_ST2	Norunda	60.09	17.48	45	2
SWE_NOR_ST3	Norunda	60.09	17.48	45	2
SWE_NOR_ST4_AFT	Norunda	60.08	17.48	45	3
SWE_NOR_ST4_BEF	Norunda	60.08	17.48	45	2
SWE_NOR_ST5_REF	Norunda	60.08	17.48	45	3
SWE_SKO_MIN	Skogaryd	58.36	12.15	76	1
SWE_SKY_38Y	Skyttorp	60.13	17.84	50	1
SWE_SKY_68Y	Skyttorp	60.10	17.83	50	2
SWE_SVA_MIX_NON	Svartberget	64.26	19.77	267	2
THA_KHU	Khu-Muang	15.27	103.08	150	1
USA_BNZ_BLA	BNZSPRC1	64.70	-148.32	50	1
USA_CHE_ASP	ChEAS	45.94	-90.27	477	6
USA_CHE_MAP	ChEAS	45.95	-90.26	1565	2
USA_DUK_HAR	Duke Blackwood Hardwood	36.98	-79.09	163	6
USA_HIL_HF1_POS	Hill Demonstration Forest	36.22	-78.86	174	5

Table B.8: Datasets in the SAPFLUXNET database identified by numeric code, dataset code and site name. Number of species per dataset, geographic coordinates and elevation are also shown. Negative coordinate values are shown for Southern and Western Hemispheres. (*continued*)

si_code	si_name	si_lat	si_long	si_elev	# species
USA_HIL_HF1_PRE	Hill Demonstration Forest	36.22	-78.86	174	5
USA_HIL_HF2	Hill Demonstration Forest	36.22	-78.86	174	7
USA_HUY_LIN_NON	Huyck Preserve Lincoln Pond	42.53	-74.16		1
USA_INM	INMMSF	39.32	-86.41	286	6
USA_MOR_SF	Morgan-Monroe State Forest	39.32	-86.41	275	4
USA_NWH	NWhiteRiver	34.58	-91.26	48	2
USA_ORN_ST1_AMB	ORNL-FACE	35.90	-84.33	227	1
USA_ORN_ST2_AMB	ORNL-FACE	35.90	-84.33	227	1
USA_ORN_ST3_ELE	ORNL-FACE	35.90	-84.33	227	1
USA_ORN_ST4_ELE	ORNL-FACE	35.90	-84.33	227	1
USA_PAR_FER	Parker Tract	35.80	-76.67	5	1
USA_PER_PER	Perry	30.21	-83.87	14	1
USA_PJS_P04_AMB	PJSEV -Rainfall	34.39	-106.53	1911	2
Manipulation Experiment -					
USA_PJS_P08_AMB	Sevilleta NWR, USA PJSEV -Rainfall	34.39	-106.53	1911	2
Manipulation Experiment -					
USA_PJS_P12_AMB	Sevilleta NWR, USA PJSEV -Rainfall	34.39	-106.53	1911	2
Manipulation Experiment -					
USA_SIL_OAK_1PR	Silas Little Experimental Forest premortality	39.92	-74.60	33	4
USA_SIL_OAK_2PR	Silas Little Experimental Forest premortality	39.92	-74.60	33	4
USA_SIL_OAK_POS	Silas Little Experimental Forest premortality	39.92	-74.60	33	5
USA_SMI_SCB	Smithsonian Conservation Biology Institute	38.89	-78.15	273	3
USA_SMI_SER	Smithsonian Environmental Research Center	38.89	-76.56	19	5
USA_SWH	SWhiteRiver	34.11	-91.13	44	2
USA_SYL_HL1	Sylvania Wilderness	46.24	-89.35	500	3
USA_SYL_HL2	Sylvania Wilderness	46.24	-89.35	500	4
USA_TNB	TNBSF	36.47	-84.70	454	4
USA_TNO	TNOAK	35.97	-84.28	340	5
USA_TNP	TNPINE	35.96	-84.29	342	5
USA_TNY	TNYPOP	35.69	-83.50	850	3
USA_UMB_CON	UMBS	45.56	-84.71	236	5

Table B.8: Datasets in the SAPFLUXNET database identified by numeric code, dataset code and site name. Number of species per dataset, geographic coordinates and elevation are also shown. Negative coordinate values are shown for Southern and Western Hemispheres. (*continued*)

si_code	si_name	si_lat	si_long	si_elev	# species
USA_UMB_GIR	UMB	45.56	-84.70	239	4
USA_WIL_WC1	Willow Creek	45.81	-90.09	520	5
USA_WIL_WC2	Willow Creek	45.81	-90.09	520	4
USA_WVF	WVFEF	39.06	-79.69	844	5
UZB_YAN_DIS	Yangibazar	41.65	60.62	101	2
ZAF_FRA_FRA	Franshoek South Africa	-33.88	19.06	190	1
ZAF_NOO_E3_IRR	Nooitgedacht farm	-33.20	19.34	1089	1
ZAF_RAD	Radyn EGVV	-34.08	19.11	409	1
ZAF_SOUL_SOUL	Southfield EGVV	-34.09	19.09	389	1
ZAF_WEL_SOR	Wellington Western Cape	-33.48	18.96	81	1

Table B.9: Number of plants and number of datasets for each species present in the SAPFLUXNET database.

Species	# trees	# sites	Species	# trees	# sites	Species	# trees	# sites
<i>Pinus sylvestris</i>	290	28	<i>Acacia tortilis</i>	9	3	<i>Prunus serotina</i>	3	2
<i>Picea abies</i>	178	19	<i>Quercus spp.</i>	9	2	<i>Populus canescens</i>	3	1
<i>Acer saccharum</i>	162	9	<i>Kandelia obovata</i>	8	1	<i>Eucalyptus camaldulensis</i>	3	1
<i>Fagus sylvatica</i>	116	16	<i>Carpinus betulus</i>	8	2	<i>Qualea rosea</i>	3	1
<i>Pinus taeda</i>	107	6	<i>Castanopsis acuminatissima</i>	8	1	<i>Licania alba</i>	3	1
<i>Populus tremuloides</i>	104	1	<i>Pinus patula</i>	8	1	<i>Eucalyptus dives</i>	2	1
<i>Pinus koraiensis</i>	96	3	<i>Eucalyptus radiata</i>	7	5	<i>Licania octandra</i>	2	1
<i>Eucalyptus nitens</i>	89	8	<i>Betula pubescens subsp. czerepanovii</i>	7	1	<i>Swartzia racemosa</i>	2	1
<i>Pinus strobus</i>	75	5	<i>Avicennia marina</i>	6	1	<i>Manilkara bidentata</i>	2	1
<i>Liquidambar styraciflua</i>	69	10	<i>Quercus robur</i>	6	1	<i>Licania membranacea</i>	2	2
<i>Quercus ilex</i>	62	6	<i>Fraxinus excelsior</i>	6	1	<i>Eschweilera grandiflora</i>	2	1
<i>Acer rubrum</i>	62	12	<i>Cryptocarya laevigata</i>	6	1	<i>Pouteria viridis</i>	2	1
<i>Liriodendron tulipifera</i>	51	11	<i>Myrtaceae fam.</i>	6	1	<i>Ampelocera macrocarpa</i>	2	1
<i>Fagus grandifolia</i>	48	4	<i>Palauquium luzoniense</i>	6	1	<i>Otoba novogranatensis</i>	2	1
<i>Pinus resinosa</i>	43	1	<i>Platea excelsa</i>	6	1	<i>Mortoniodendron anisophyllum</i>	2	1
<i>Eucalyptus globulus</i>	35	2	<i>Pouteria firma</i>	6	1	<i>Meliosma idiopoda</i>	2	1
<i>Larix decidua</i>	34	8	<i>Agathis australis</i>	6	1	<i>Taxus baccata</i>	2	1
<i>Abies pinsapo</i>	34	5	<i>Ostrya virginiana</i>	6	3	<i>Sloanea sp.</i>	2	2
<i>Acacia mearnsii</i>	33	2	<i>Picea mariana</i>	6	1	<i>Betula sp.</i>	2	1
<i>Quercus pyrenaica</i>	32	2	<i>Nothofagus pumilio</i>	5	1	<i>Picea glauca</i>	2	1
<i>Quercus rubra</i>	32	6	<i>Nothofagus cunninghamii</i>	5	1	<i>Fraxinus americana</i>	2	1
<i>Quercus petraea</i>	31	5	<i>Eucalyptus cypellocarpa</i>	5	4	<i>Carya cordiformis</i>	2	1

Table B.9: Number of plants and number of datasets for each species present in the SAPFLUXNET database. (continued)

Species	# trees	# sites	Species	# trees	# sites	Species	# trees	# sites
<i>Pseudotsuga menziesii</i>	29	5	<i>Eucalyptus rubida</i>	5	1	<i>Quercus prinus</i>	2	1
<i>Pinus halepensis</i>	27	2	<i>Drimys brasiliensis</i>	5	1	<i>Elaeagnus angustifolia</i>	2	1
<i>Quercus velutina</i>	24	4	<i>Alchornea triplinervia</i>	5	1	<i>Qualea tricolor</i>	2	1
<i>Tsuga canadensis</i>	24	2	<i>Santiria apiculata</i>	5	1	<i>Lecythis poiteauii</i>	2	1
<i>Larix cajanderi</i>	23	2	<i>Quercus michauxii</i>	5	1	<i>Quercus cerris</i>	2	1
<i>Betula papyrifera</i>	21	2	<i>Quercus phellos</i>	5	1	<i>Pleuranthodendron lindenii</i>	1	1
<i>Quercus montana</i>	21	3	<i>Pinus rigida</i>	5	3	<i>Inga sp.</i>	1	1
<i>Quercus pubescens</i>	19	2	<i>Tilia americana</i>	5	2	<i>Cupania macrophylla</i>	1	1
<i>Abies balsamea</i>	19	1	<i>Nothofagus antarctica</i>	4	1	<i>Genipa americana</i>	1	1
<i>Quercus alba</i>	19	7	<i>Eucalyptus baxteri</i>	4	2	<i>Brosimum alicastrum</i>	1	1
<i>Pinus cembra</i>	18	6	<i>Coprosma quadrifida</i>	4	2	<i>Pouteria sp.</i>	1	1
<i>Populus euphratica</i>	16	6	<i>Eschweilera coriacea</i>	4	2	<i>Macrolobium costaricense</i>	1	1
<i>Olea europaea</i>	16	5	<i>Arbutus unedo</i>	4	1	<i>Eschweilera sp.</i>	1	1
<i>Quercus rotundifolia</i>	16	3	<i>Psiadia altissima</i>	4	1	<i>Aspidosperma desmanthum</i>	1	1
<i>Hevea brasiliensis</i>	16	2	<i>Quercus suber</i>	4	1	<i>Trophis mexicana</i>	1	1
<i>Betula alleghaniensis</i>	16	2	<i>Betula pubescens</i>	4	2	<i>Betula pendula</i>	1	1
<i>Pinus nigra</i>	15	3	<i>Fraxinus pennsylvanica</i>	4	2	<i>Iryanthera sagotiana</i>	1	1
<i>Picea sitchensis</i>	15	1	<i>Pouteria anomala</i>	3	1	<i>Vantanea sp</i>	1	1
<i>Pinus edulis</i>	15	3	<i>Protium tenuifolium</i>	3	1	<i>Recordoxylon speciosum</i>	1	1
<i>Juniperus monosperma</i>	15	3	<i>Hieronyma alchorneoides</i>	3	1	<i>Larix kaempferi x Larix gmelinii</i>	1	1
<i>Eucalyptus victrix</i>	14	1	<i>Mollinedia schottiana</i>	3	1	<i>Cryptomeria japonica</i>	1	1
<i>Eucalyptus obliqua</i>	14	5	<i>Rustia formosa</i>	3	1	<i>Eugenia spp.</i>	1	1
<i>Quercus lyrata</i>	13	2	<i>Theobroma cacao</i>	3	1	<i>Ocotea samosa</i>	1	1
<i>Celtis laevigata</i>	13	2	<i>Carapa guianensis</i>	3	1	<i>Leptolaena sp.</i>	1	1

Table B.9: Number of plants and number of datasets for each species present in the SAPFLUXNET database. (*continued*)

Species	# trees	# sites	Species	# trees	# sites	Species	# trees	# sites
<i>Quercus coccinea</i>	13	4	<i>Gymnanthes riparia</i>	3	1	<i>Abrahamia ditimena</i>	1	1
<i>Populus grandidentata</i>	12	1	<i>Ilex aquifolium</i>	3	1	<i>Brachylaena ramiflora</i>	1	1
<i>Malus domestica</i>	11	3	<i>Vouacapoua americana</i>	3	3	<i>Cryptocarya sp.</i>	1	1
<i>Eucalyptus tereticornis</i>	10	1	<i>Oxandra asbeckii</i>	3	2	<i>Saurauia pedunculata</i>	1	1
<i>Quercus faginea</i>	10	2	<i>Gouania glabra</i>	3	3	<i>Turpinia insignis</i>	1	1
<i>Pinus canariensis</i>	10	1	<i>Vernonia arborea</i>	3	1	<i>Sassafras albidum</i>	1	1
<i>Elaeis guineensis</i>	10	1	<i>Platanus mexicana</i>	3	1	<i>Ulmus americana</i>	1	1
<i>Acacia longifolia</i>	10	1	<i>Clethra macrophylla</i>	3	2	<i>Carya glabra</i>	1	1
<i>Pinus pinaster</i>	10	1	<i>Larix sibirica</i>	3	1	<i>Quercus falcata</i>	1	1
<i>Thuja occidentalis</i>	10	1	<i>Larix gmelinii</i>	3	1	<i>Cornus florida</i>	1	1
<i>Carya tomentosa</i>	10	2	<i>Pinus sibirica</i>	3	1	<i>Licania rodriquesii</i>	1	1
<i>Dicorynia guianensis</i>	9	2	<i>Pinus virginiana</i>	3	1	<i>Sextonia rubra</i>	1	1

Table B.10: Number of plants per genus present in the SAPFLUXNET database.

Genus	# trees	Genus	# trees	Genus	# trees
<i>Pinus</i>	725	<i>Cryptocarya</i>	7	<i>Ampelocera</i>	2
<i>Quercus</i>	326	<i>Avicennia</i>	6	<i>Otoba</i>	2
<i>Acer</i>	224	<i>Myrtaceae fam.</i>	6	<i>Mortoniodendron</i>	2
<i>Picea</i>	201	<i>Palaquium</i>	6	<i>Meliosma</i>	2
<i>Eucalyptus</i>	188	<i>Platea</i>	6	<i>Taxus</i>	2
<i>Fagus</i>	164	<i>Agathis</i>	6	<i>Sloanea</i>	2
<i>Populus</i>	135	<i>Ostrya</i>	6	<i>Elaeagnus</i>	2
<i>Liquidambar</i>	69	<i>Drimys</i>	5	<i>Lecythis</i>	2
<i>Larix</i>	64	<i>Alchornea</i>	5	<i>Pleuranthodendron</i>	1
<i>Abies</i>	53	<i>Santiria</i>	5	<i>Inga</i>	1
<i>Acacia</i>	52	<i>Tilia</i>	5	<i>Cupania</i>	1
<i>Betula</i>	51	<i>Qualea</i>	5	<i>Genipa</i>	1
<i>Liriiodendron</i>	51	<i>Coprosma</i>	4	<i>Brosimum</i>	1
<i>Pseudotsuga</i>	29	<i>Arbutus</i>	4	<i>Macrolobium</i>	1
<i>Tsuga</i>	24	<i>Psiadia</i>	4	<i>Aspidosperma</i>	1
<i>Olea</i>	16	<i>Protium</i>	3	<i>Trophis</i>	1
<i>Hevea</i>	16	<i>Hieronyma</i>	3	<i>Iryanthera</i>	1
<i>Juniperus</i>	15	<i>Mollinedia</i>	3	<i>Vantanea</i>	1
<i>Nothofagus</i>	14	<i>Rustia</i>	3	<i>Recordoxylon</i>	1
<i>Carya</i>	13	<i>Theobroma</i>	3	<i>Cryptomeria</i>	1
<i>Celtis</i>	13	<i>Carapa</i>	3	<i>Eugenia</i>	1
<i>Pouteria</i>	12	<i>Gymnanthes</i>	3	<i>Ocotea</i>	1
<i>Fraxinus</i>	12	<i>Ilex</i>	3	<i>Leptolaena</i>	1
<i>Malus</i>	11	<i>Vouacapoua</i>	3	<i>Abrahamia</i>	1
<i>Elaeis</i>	10	<i>Oxandra</i>	3	<i>Brachylaena</i>	1
<i>Thuja</i>	10	<i>Gouphia</i>	3	<i>Saurauia</i>	1
<i>Dicorynia</i>	9	<i>Vernonia</i>	3	<i>Turpinia</i>	1
<i>Licania</i>	8	<i>Platanus</i>	3	<i>Sassafras</i>	1
<i>Kandelia</i>	8	<i>Clethra</i>	3	<i>Ulmus</i>	1
<i>Carpinus</i>	8	<i>Prunus</i>	3	<i>Cornus</i>	1
<i>Castanopsis</i>	8	<i>Swartzia</i>	2	<i>Sextonia</i>	1
<i>Eschweilera</i>	7	<i>Manilkara</i>	2		

“thesis” — 2020/12/29 — 11:18 — page 174 — #198

C

Appendix Chapter 4

C.1 Figures C

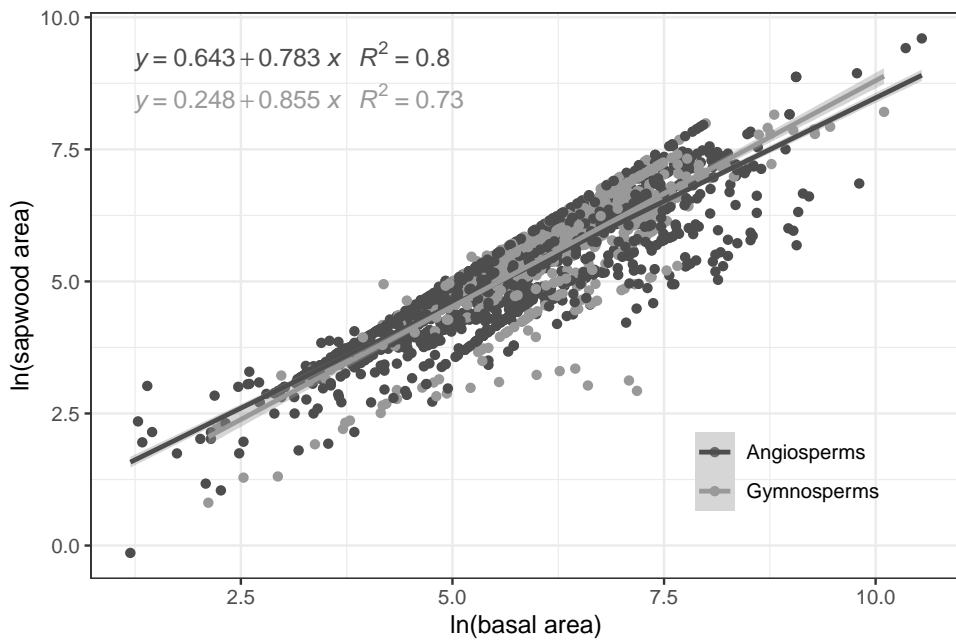


Figure C.1: SAPFLUXNET global scaling relationship between basal area and sapwood area. Shaded areas are 95% model confidence interval.

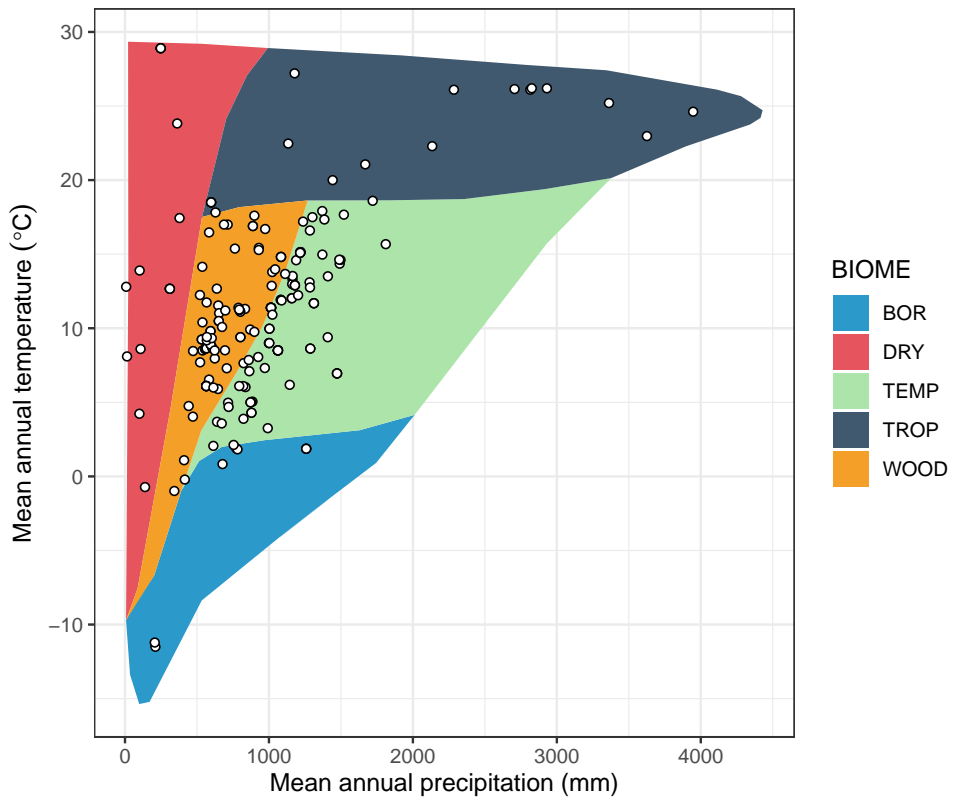


Figure C.2: Bioclimatic distribution of the SAPFLUXNET datasets used in the study. Points show the different datasets in a Whittaker diagram showing the classification of the aggregated biomes used in the study.

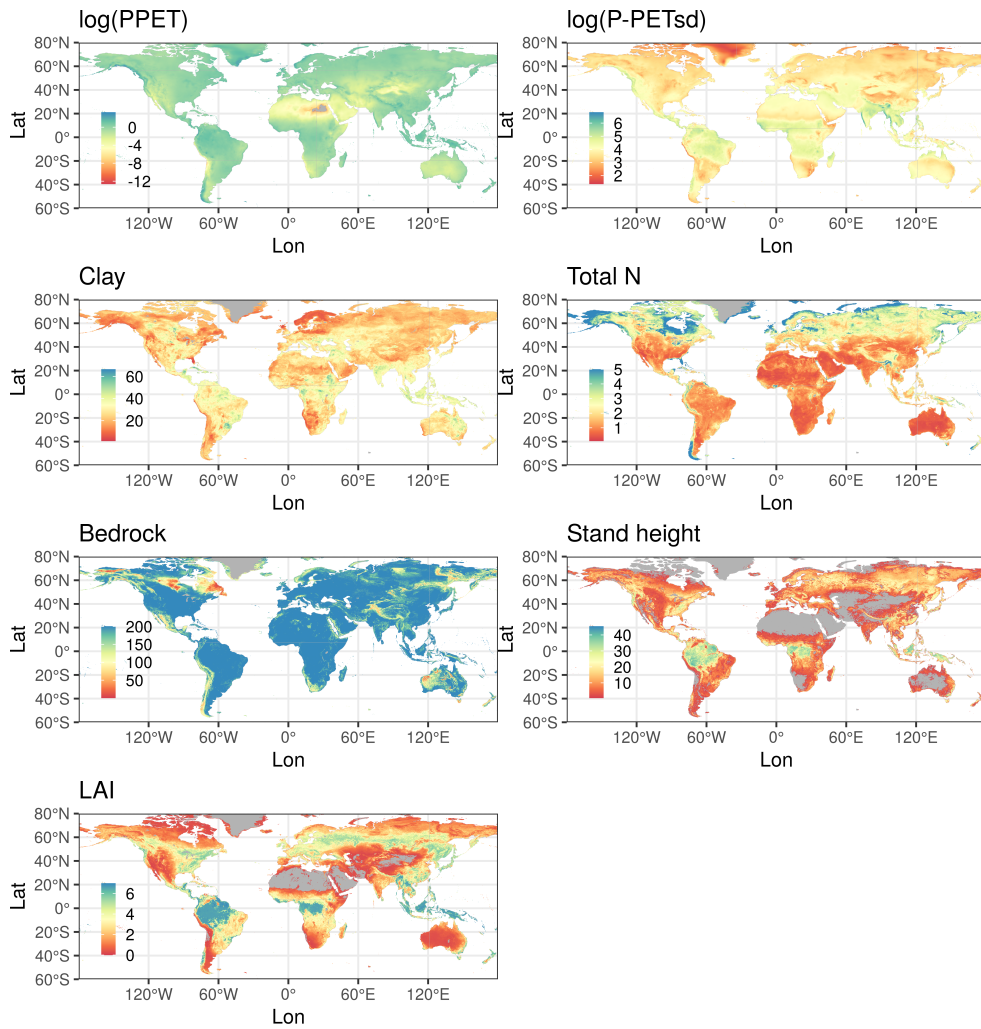


Figure C.3: Global projection of climatic, soil and stand structure variables. log(PPET): logarithm of precipitation over potential evapotranspiration [log(mm mm⁻¹)]; log($P - PET_{sd}$): logarithm of the standard deviation of the difference between precipitation and potential evapotranspiration [log(mm)]; Clay: percentage of clay in the soil; Total N: total nitrogen in the soil [g kg⁻¹]; Bedrock [cm]; Stand height [m]; LAI: leaf area index [m² m⁻²]. Total N values above 5 g kg⁻¹ were truncated.

C.1. Figures C

179

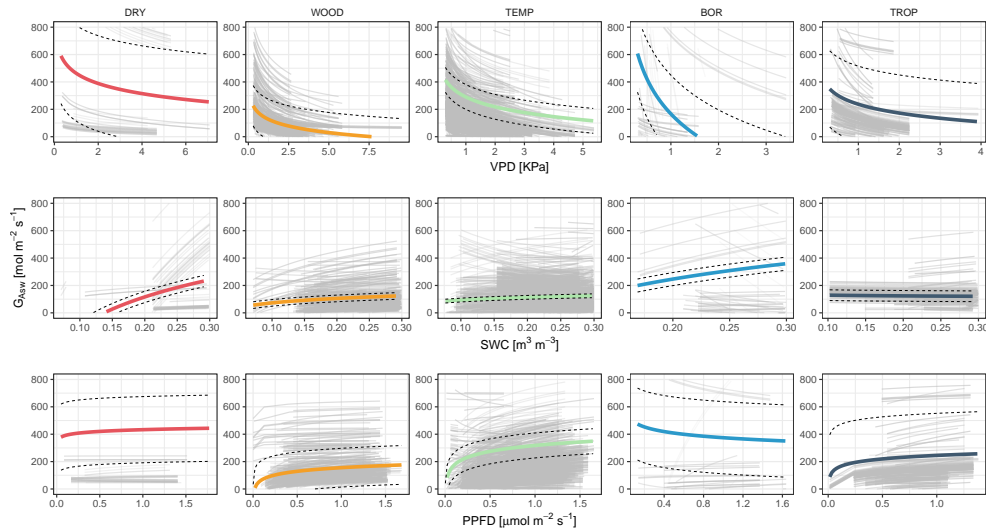


Figure C.4: Log relationships of the three environmental variables estimated with the TOTAL model ($\text{VPD} + \text{SWC} + \text{PPFD}$) and grouped by biome. Coloured lines are biome average models calculated from the models predictions using LMM with G_{Asw} as response variable and the neperian logarithm of the environmental constrains as explanatory variables. Dashed line shows standard error of the average models calculated with bootstrap prediction using 100 simulations.

C.2 Tables C

Table C.1: SAPFLUXNET sites included in the study. Biome was calculated using Whittaker diagram. *Indicates that the biome was manually adjusted and confirmed by SAPFLUXNET contributors.

Site code	Latitude	Longitude	Biome	# Tree-days	# Species	# Trees
AUS_CAN_ST1_EUC	-37.58	149.17	WOOD	337	1	12
AUS_CAN_ST2_MIX	-37.58	149.17	WOOD	712	2	22
AUS_CAN_ST3 ACA	-37.58	149.17	WOOD	409	1	12
AUS_CAR THI CON	-38.38	146.68	TEMP	54	1	7
AUS_ELL_UNB	-36.78	146.58	TEMP	105	1	2
AUS_MAR_UBD	-37.69	145.56	TEMP	50	3	5
AUS_MAR_UBW	-37.89	145.57	TEMP	105	3	5
AUS_WOM	-37.42	144.09	TEMP	2130	2	11
AUT_PAT_FOR	47.21	11.45	BOR	149	1	3
AUT_PAT_KRU	47.21	11.45	BOR	70	1	3
AUT_PAT_TRE	47.21	11.45	BOR	81	1	3
BRA_CAM	-22.69	-45.52	TROP	79	1	5
BRA_CAX_CON	-1.79	-51.43	TROP	525	8	15
CAN_TUR_P39_PRE	42.71	-80.36	TEMP	1021	1	18
CAN_TUR_P74	42.71	-80.35	TEMP	1997	1	16
CHN_ARG_GWS	41.38	89.94	DRY	174	1	2
CHN_HOR_AFF	42.72	122.37	WOOD	1366	1	16
CHN_YIN_ST1	42.45	85.72	DRY	105	1	5
CRI_TAM_TOW	10.39	-84.63	TROP	666	17	26
CZE_BIL_BIL	49.25	16.69	TEMP	238	1	6
CZE_KRT_KRT	49.32	16.75	TEMP	238	1	6
CZE_LAN	48.68	16.95	TEMP	1093	3	17
CZE_RAJ_RAJ	49.44	16.70	TEMP	274	1	6
CZE_SOB_SOB	49.25	16.69	TEMP	655	1	6
CZE_STI	49.04	17.97	TEMP	263	1	8
CZE_UTE_BPO	49.28	16.65	TEMP	234	1	6
DEU_HIN_OAK	53.33	13.19	TEMP	482	1	8
DEU_HIN_TER	53.33	13.19	TEMP	1052	2	16
DEU_MER_BEE_NON	49.27	7.81	TEMP	495	1	8
DEU_MER_DOU_NON	49.27	7.81	TEMP	491	1	7
DEU_MER_MIX_NON	49.27	7.81	TEMP	1108	2	17
DEU_STE_2P3	53.10	13.00	TEMP	722	1	10
DEU_STE_4P5	53.10	13.00	TEMP	327	1	10
ESP_ALT_ARM	40.78	-2.33	WOOD	1990	3	15
ESP_ALT_HUE	40.79	-2.29	WOOD	967	2	8
ESP_ALT_TRI	40.80	-2.23	WOOD	1522	2	12
ESP_CAN	41.43	2.07	WOOD	2317	4	21
ESP_GUA_VAL	40.90	-4.03	WOOD	2100	1	24
ESP_LAS	28.31	-16.57	WOOD	1778	1	10
ESP_MAJ_MAI	39.94	-5.77	WOOD	978	1	6
ESP_MON_SIE_NAT	41.12	-3.50	WOOD	1250	3	20
ESP_RIN	40.60	-6.02	WOOD	502	1	8
ESP_RON_PIL	36.69	-5.02	TEMP	911	2	12
ESP_TIL_MIX	41.33	1.01	WOOD	3434	2	32
ESP_TIL_OAK	41.33	1.01	WOOD	717	1	10

C.2. Tables C

181

Table C.1: SAPFLUXNET sites included in the study. Biome was calculated using Whittaker diagram. *Indicates that the biome was manually adjusted and confirmed by SAPFLUXNET contributors. (*continued*)

Site code	Latitude	Longitude	Biome	# Tree-days	# Species	# Trees
ESP_TIL_PIN	41.33	1.01	WOOD	589	1	9
ESP_VAL_BAR	42.20	1.82	WOOD	837	1	12
ESP_VAL_SOR	42.20	1.81	WOOD	1109	1	13
ESP_YUN_C1	36.72	-4.97	WOOD	619	1	6
ESP_YUN_C2	36.72	-4.97	WOOD	288	1	6
FIN_HYY_SME	61.85	24.29	TEMP	34	2	4
FIN_PET	69.49	27.23	BOR	118	1	7
FRA_FON	48.48	2.78	TEMP	276	1	3
FRA_HES_HE1_NON	48.67	7.06	TEMP	620	1	10
FRA_HES_HE2_NON	48.67	7.06	TEMP	1347	1	10
FRA_PUE	43.74	3.60	WOOD	5229	1	25
GBR_ABE_PLO	56.62	-3.80	TEMP	486	1	15
GBR_DEV_CON	56.03	-3.72	TEMP	133	1	4
GBR_GUI_ST1	57.27	-4.82	TEMP	398	1	15
GBR_GUI_ST2	57.27	-4.82	TEMP	298	1	9
GBR_GUI_ST3	57.27	-4.82	TEMP	249	1	8
GUF_GUY_GUY	5.28	-52.92	TROP	246	6	6
GUF_GUY_ST2	5.28	-52.91	TROP	369	7	11
GUF_NOU_PET	4.08	-52.68	TROP	562	10	22
HUN_SI	47.93	20.44	WOOD	365	2	4
ISR_YAT_YAT	31.34	35.05	DRY	3704	1	24
ITA_FEI_S17	46.69	10.61	TEMP	244	1	6
ITA_KAE_S20	46.70	10.61	BOR	325	1	6
ITA_MUN	46.68	10.58	TEMP	384	1	6
ITA_REN	46.59	11.43	TEMP	247	3	8
ITA_RUN_N20	46.70	10.64	BOR	331	2	8
MEX_COR_YP	19.49	-97.04	TEMP	119	1	8
NLD_LOO	52.17	5.74	TEMP	621	1	6
NLD_SPE_DOU	52.25	5.69	TEMP	107	1	3
NZL_HUA_HUA	-36.80	174.49	TEMP	243	1	6
PRT_LEZ_ARN	38.83	-8.82	WOOD	403	1	4
PRT_MIT	38.54	-8.00	WOOD	494	1	4
PRT_PIN	38.25	-8.76	WOOD	1233	2	20
RUS_CHE_Y4	68.74	161.41	BOR	447	1	11
RUS_FYO	56.46	32.92	TEMP	1132	3	17
RUS_POG_VAR	56.36	92.95	TEMP	603	3	9
SEN_SOUPRE	16.34	-15.43	DRY	466	1	3
SWE_NOR_ST1_BEF	60.09	17.48	TEMP	653	2	22
SWE_NOR_ST2	60.09	17.48	TEMP	175	2	12
SWE_NOR_ST3	60.09	17.48	TEMP	810	2	37
SWE_NOR_ST5_REF	60.08	17.48	TEMP	712	3	35
SWE_SKO_MIN	58.36	12.15	TEMP	533	1	11
SWE_SKY_38Y	60.13	17.84	TEMP	326	1	12
SWE_SKY_68Y	60.10	17.83	TEMP	664	2	12
SWE_SVA_MIX_NON	64.26	19.77	TEMP	861	2	20
THA_KHU	15.27	103.08	TROP	411	1	6
USA_BNZ_BLA	64.70	-148.32	BOR	797	1	6
USA_CHE_ASP	45.94	-90.27	TEMP	3548	6	149
USA_CHE_MAP	45.95	-90.26	TEMP	2651	2	153

Table C.1: SAPFLUXNET sites included in the study. Biome was calculated using Whittaker diagram. *Indicates that the biome was manually adjusted and confirmed by SAPFLUXNET contributors. (*continued*)

Site code	Latitude	Longitude	Biome	# Tree-days	# Species	# Trees
USA_DUK_HAR	36.98	-79.09	TEMP	495	6	34
USA_HIL_HF2	36.22	-78.86	TEMP	228	5	23
USA_INM	39.32	-86.41	TEMP	766	6	9
USA_MOR_SF	39.32	-86.41	TEMP	285	4	6
USA_NWH	34.58	-91.26	TEMP	248	2	10
USA_ORN_ST1_AMB	35.90	-84.33	TEMP	247	1	8
USA_PAR_FER	35.80	-76.67	TEMP	467	1	8
USA_PER_PER	30.21	-83.87	TROP	6269	1	80
USA_PJS_P04_AMB	34.39	-106.53	DRY	2313	2	10
USA_PJS_P08_AMB	34.39	-106.53	DRY	2262	2	10
USA_PJS_P12_AMB	34.39	-106.53	DRY	2350	2	10
USA_SIL_OAK_1PR	39.92	-74.60	TEMP	1210	4	18
USA_SIL_OAK_2PR	39.92	-74.60	TEMP	2275	4	22
USA_SMI_SER	38.89	-76.56	TEMP	1045	5	31
USA_SWH	34.11	-91.13	TEMP	511	2	16
USA_SYL_HL1	46.24	-89.35	TEMP	3130	3	48
USA_SYL_HL2	46.24	-89.35	TEMP	1631	4	20
USA_TNB	36.47	-84.70	TEMP	583	4	8
USA_TNO	35.97	-84.28	TEMP	680	5	9
USA_TNP	35.96	-84.29	TEMP	806	5	9
USA_UMB_CON	45.56	-84.71	TEMP	5840	5	57
USA_UMB_GIR	45.56	-84.70	TEMP	5867	4	57
USA_WIL_WC1	45.81	-90.09	TEMP	639	5	16
USA_WVF	39.06	-79.69	TEMP	488	5	8
ZAF_FRA_FRA	-33.88	19.06	WOOD	220	1	3
ZAF_RAD	-34.08	19.11	WOOD	303	1	3
ZAF_SOUL_SOUL	-34.09	19.09	WOOD	198	1	2
ZAF_WEL_SOR	-33.48	18.96	WOOD	356	1	3

Table C.2: SAPFLUXNET stand treatments included in the this study (Poyatos *et al.* 2020).

Plot treatment
None
Control
control
Ambient Control
Control - Unthinned
natural conditions
Reference
1Premortality
2premortality
destructive sampling
Girdling early successional
Pre-thinning
Before thinning
Before Thinning
non thinned
none (periodict thinning every 5-6 years 20 to 25% of basal area)
Radiation Level
AMBIENT CO ₂ FACE rings
fertilization at plantation
AcaciaMonoculture
MixtureEucalyptusAndAcacia
EucalyptusMonoculture
Pre Irrigation

Table C.3: Summary table of site level R^2_{VPD} , R^2_{SWC} , R^2_{PPFD} , climate, soil properties and vegetation structure data. PPET is in [mm mm^{-1}], P-PET_{sd} is in [mm], Clay and Sand are in [%], Total N is in [g kg^{-1}], Stand height is in [m], LAI is in [$\text{m}^2_{\text{leaves}} \text{m}^2_{\text{soil}}$]. Letters show data source: a = SAPFLUXNET, b = Global rasters, c = SAPFLUXNET plant height.

Site code	R^2_{VPD}	R^2_{SWC}	R^2_{PPFD}	Relimp VPD	Relimp SWC	Relimp PPFD	PPET	P - PET _{sd}	Clay	Sand	Total N	Bedrock	Stand height	LAI
AUS_CAN_ST1_EUC	0.74	0.44	0.54	0.65	0.35	0.00	1.23	47.52	26.30 b	45.10 b	1.02	184	22.00 a	1.39 a
AUS_CAN_ST2_MIX	0.91	0.65	0.76	0.87	0.13	0.00	1.23	47.52	26.30 b	45.10 b	1.02	184	21.80 a	2.07 a
AUS_CAN_ST3 ACA	0.85	0.67	0.74	0.87	0.12	0.01	1.23	47.52	26.30 b	45.10 b	1.02	184	11.80 a	1.35 a
AUS_CAR THI CON	0.67	0.00	0.00	0.99	0.00	0.01	1.36	49.01	27.20 b	44.30 b	2.34	111	17.21 a	4.80 a
AUS_ELL_UNB	0.87	0.44	0.76	0.97	0.00	0.03	1.08	67.16	26.70 b	48.50 b	1.95	63	25.00 a	6.20 b
AUS_MAR_UBD	0.79	0.53	0.69	0.71	0.29	0.00	1.35	70.37	26.60 b	44.60 b	1.90	89	25.00 a	2.10 a
AUS_MAR_UBW	0.90	0.81	0.82	0.90	0.00	0.09	1.21	65.38	27.90 b	43.90 b	2.00	173	40.00 a	2.30 a
AUS_WOM	0.82	0.52	0.49	0.79	0.00	0.20	1.09	69.35	25.90 b	52.90 b	1.97	172	22.00 a	2.20 a
AUT_PAT_FOR	0.78	0.73	0.68	0.82	0.09	0.09	2.17	16.78	5.00 a	60.00 a	3.94	180	12.00 a	4.30 b
AUT_PAT_KRU	0.61	0.45	0.50	0.77	0.06	0.17	2.17	16.78	5.00 a	60.00 a	3.94	180	0.75 a	4.30 b
AUT_PAT_TRE	0.58	0.27	0.19	0.70	0.30	0.00	2.17	16.78	5.00 a	60.00 a	3.94	180	4.00 a	4.30 b
BRA_CAM	0.83	0.68	0.69	0.65	0.28	0.07	1.66	88.82	27.60 b	52.00 b	2.26	200	12.00 a	5.30 a
BRA_CAX_CON	0.79	0.74	0.73	0.70	0.00	0.30	1.90	122.90	8.00 a	79.00 a	1.45	197	38.00 b	5.30 a
CAN_TUR_P39_PRE	0.59	0.37	0.34	0.71	0.08	0.21	1.39	42.08	1.00 a	98.00 a	1.58	200	23.40 a	5.30 a
CAN_TUR_P74	0.26	0.47	0.14	0.32	0.38	0.30	1.39	41.87	1.00 a	98.00 a	1.60	200	16.20 a	6.70 a
CHN_ARG_GWS	0.42	0.32	0.27	0.51	0.47	0.01	0.01	63.51	17.70 b	46.00 b	0.70	172	7.90 a	0.36 a
CHN_HOR_AFF	0.39	0.38	0.34	0.25	0.75	0.00	0.59	31.24	8.00 a	83.00 a	1.00	200	9.05 a	1.61 a
CHN_YIN_ST1	0.47	0.45	0.44	0.63	0.18	0.20	0.19	35.09	20.80 b	32.90 b	2.41	148	10.60 a	0.50 b
CRI_TAM_TOW	0.73	0.73	0.73	0.46	0.11	0.44	3.57	159.99	36.10 b	34.70 b	2.75	200	30.60 a	3.30 a
CZE_BIL_BIL	0.54	0.50	0.41	0.57	0.20	0.23	0.71	28.98	29.60 b	27.40 b	1.91	200	14.00 a	6.00 b
CZE_KRT_KRT	0.57	0.45	0.30	0.58	0.03	0.39	0.85	27.00	26.00 b	27.40 b	2.10	200	17.00 a	5.70 b
CZE_LAN	0.79	0.76	0.72	0.67	0.08	0.25	0.66	37.49	17.80 a	71.80 a	2.46	200	36.00 a	6.04 a
CZE_RAJ_RAJ	0.38	0.40	0.43	0.33	0.07	0.60	0.99	26.14	21.80 b	33.90 b	1.96	200	18.00 a	4.60 b
CZE_SO_B_SO_B	0.48	0.45	0.14	0.52	0.25	0.23	0.71	28.98	29.60 b	27.40 b	1.91	200	21.00 a	6.00 b
CZE_STI	0.54	0.32	0.39	0.70	0.18	0.12	1.13	27.10	34.20 a	47.60 a	1.65	200	31.00 a	5.50 a
CZE_UTE_BPO	0.62	0.65	0.52	0.46	0.16	0.38	0.75	29.86	26.70 b	23.80 b	2.71	200	18.00 a	6.10 b
DEU_HIN_OAK	0.43	0.19	0.33	0.92	0.07	0.01	0.95	35.10	17.90 b	49.90 b	2.42	200	31.45 c	5.70 b
DEU_HIN_TER	0.31	0.22	0.24	0.76	0.01	0.24	0.95	35.10	18.00 b	50.50 b	2.05	200	24.43 c	5.60 b

C.2. Tables C

Table C.3: Summary table of site level R^2_{VPD} , R^2_{SWC} , R^2_{PPFD} , climate, soil properties and vegetation structure data. PPET is in [mm mm^{-1}], P-PET_{sd} is in [mm], Clay and Sand are in [%], Total N is in [g kg^{-1}], Stand height is in [m], LAI is in [$\text{m}^2 \text{leaves m}^2 \text{soil}$]. Letters show data source: a = SAPFLUXNET, b = Global rasters, c = SAPFLUXNET plant height. (*continued*)

Site code	R^2_{VPD}	R^2_{SWC}	R^2_{PPFD}	Relimp VPD	Relimp SWC	Relimp PPFD	PPET	P - PET _{sd}	Clay	Sand	Total N	Bedrock	Stand height	LAI
DEU_MER_BEE_NON0.47	0.27	0.29	0.76	0.06	0.18	1.48	47.33	4.00 a	71.00 a	2.56	200	23.00 a	5.90 a	
DEU_MER_DOU_NON0.45	0.25	0.22	0.60	0.31	0.10	1.48	47.33	4.00 a	71.00 a	2.56	200	29.00 a	5.30 a	
DEU_MER_MIX_NON0.41	0.23	0.26	0.82	0.02	0.16	1.48	47.33	4.00 a	71.00 a	2.56	200	30.00 a	6.10 a	
DEU_STE_2P3	0.56	0.15	0.30	0.86	0.09	0.05	0.90	37.45	2.50 a	92.50 a	3.28	200	27.20 a	4.30 b
DEU_STE_4P5	0.48	0.27	0.31	0.64	0.28	0.09	0.90	37.45	2.50 a	92.50 a	3.28	200	27.20 a	4.30 b
ESP_ALT_ARM	0.51	0.30	0.29	0.91	0.01	0.09	0.66	65.80	21.90 b	41.50 b	1.27	187	19.00 b	1.09 a
ESP_ALT_HUE	0.47	0.22	0.18	0.78	0.02	0.21	0.51	63.08	21.60 b	35.90 b	1.46	200	8.64 c	1.50 b
ESP_ALT_TRI	0.58	0.44	0.31	0.80	0.07	0.12	0.57	63.48	21.00 b	40.00 b	1.31	196	4.89 a	1.60 b
ESP_CAN	0.55	0.40	0.34	0.74	0.02	0.24	0.94	46.91	32.90 b	28.30 b	1.76	179	10.80 a	3.30 a
ESP_GUA_VAL	0.51	0.28	0.23	0.69	0.00	0.31	0.68	69.09	24.80 b	40.90 b	1.27	200	12.00 a	3.80 a
ESP_LAS	0.37	0.25	0.07	0.57	0.37	0.06	1.63	37.89	1.00 a	70.00 a	1.65	197	10.30 a	3.60 a
ESP_MAJ_MAI	0.56	0.43	0.28	0.73	0.14	0.12	0.76	97.45	9.00 a	80.00 a	1.18	200	7.00 a	0.30 a
ESP_MON_SIE_NAT	0.25	0.20	0.22	0.49	0.09	0.42	0.62	63.05	20.80 b	41.90 b	1.45	200	22.00 a	3.30 b
ESP_RIN	0.83	0.61	0.59	0.97	0.00	0.03	0.85	76.30	15.00 a	9.00 a	2.17	200	7.40 a	3.40 a
ESP_RON_PIL	0.37	0.25	0.17	0.60	0.07	0.33	1.05	93.66	18.00 a	30.00 a	1.86	200	2.60 a	0.90 b
ESP_TIL_MIX	0.45	0.36	0.22	0.55	0.09	0.36	0.77	48.10	20.00 a	60.00 a	1.44	162	14.20 a	3.27 a
ESP_TIL_OAK	0.31	0.38	0.18	0.45	0.15	0.40	0.77	48.10	20.00 a	60.00 a	1.44	162	5.00 a	4.59 a
ESP_TIL_PIN	0.37	0.45	0.08	0.43	0.37	0.20	0.79	48.10	20.00 a	60.00 a	1.78	188	18.30 a	1.02 a
ESP_VAL_BAR	0.61	0.22	0.29	0.90	0.00	0.10	0.70	34.07	32.63 a	9.81 a	1.94	200	10.60 a	2.10 a
ESP_VAL_SOR	0.58	0.36	0.26	0.73	0.14	0.13	0.78	32.15	20.00 a	60.00 a	2.04	200	11.00 a	2.40 a
ESP_YUN_C1	0.37	0.50	0.24	0.28	0.56	0.16	0.83	93.65	29.00 a	22.00 a	1.37	197	10.60 a	2.20 b
ESP_YUN_C2	0.28	0.62	0.27	0.21	0.43	0.37	0.78	91.33	29.00 a	22.00 a	1.37	188	11.60 a	2.50 b
FIN_HYY_SME	0.57	0.49	0.62	0.12	0.86	0.02	1.20	38.32	6.50 a	37.00 a	1.67	200	18.00 a	1.30 a
FIN_PET	0.59	0.50	0.58	0.47	0.37	0.16	1.13	26.34	7.30 b	60.80 b	5.08	200	3.76 a	0.61 a
FRA_FON	0.78	0.68	0.68	0.70	0.17	0.13	0.89	45.10	19.00 a	37.00 a	1.26	200	28.00 a	6.00 a
FRA_HES_HE1_NON	0.46	0.57	0.41	0.45	0.25	0.30	1.31	47.72	25.00 a	8.00 a	1.41	200	12.80 a	6.00 a
FRA_HES_HE2_NON	0.33	0.50	0.16	0.42	0.27	0.31	1.31	47.72	25.00 a	8.00 a	1.41	200	13.00 a	6.00 a
FRA_PUE	0.49	0.52	0.33	0.51	0.18	0.30	1.27	70.16	39.00 a	26.00 a	1.69	195	5.00 a	2.40 a
GBR_ABE_PLO	0.40	0.37	0.35	0.51	0.22	0.27	1.92	47.48	10.00 a	60.00 a	3.70	179	10.00 a	6.00 a

Table C.3: Summary table of site level R^2_{VPD} , R^2_{SWC} , R^2_{PPFD} , climate, soil properties and vegetation structure data. PPET is in [mm mm^{-1}], P-PET_{sd} is in [mm], Clay and Sand are in [%], Total N is in [g kg^{-1}], Stand height is in [m], LAI is in [$\text{m}^2_{\text{leaves}} \text{m}^2_{\text{soil}}$]. Letters show data source: a = SAPFLUXNET, b = Global rasters, c = SAPFLUXNET plant height. (*continued*)

Site code	R^2_{VPD}	R^2_{SWC}	R^2_{PPFD}	Relimp VPD	Relimp SWC	Relimp PPFD	PPET	P - PET _{sd}	Clay	Sand	Total N	Bedrock	Stand height	LAI
GBR_DEV_CON	0.89	0.45	0.58	0.95	0.01	0.04	1.43	44.38	14.80 b	56.90 b	3.44	200	15.00 a	1.92 a
GBR_GUI_ST1	0.84	0.79	0.78	0.68	0.00	0.32	3.19	68.11	3.70 b	80.40 b	14.26	197	11.00 a	0.92 a
GBR_GUI_ST2	0.64	0.55	0.49	0.59	0.03	0.38	3.19	68.11	3.70 b	80.40 b	14.26	197	13.30 a	0.94 a
GBR_GUI_ST3	0.86	0.82	0.79	0.73	0.03	0.24	3.19	68.11	3.70 b	80.40 b	14.26	197	14.30 a	1.57 a
GUF_GUY_GUY	0.97	0.89	0.94	0.82	0.05	0.12	2.88	135.18	43.00 a	48.00 a	1.53	200	35.00 a	7.00 a
GUF_GUY_ST2	0.80	0.77	0.76	0.61	0.30	0.09	3.02	141.34	43.20 a	47.80 a	1.66	200	35.00 a	6.70 a
GUF_NOU_PET	0.76	0.53	0.66	1.00	0.00	0.00	2.69	158.16	59.20 a	33.20 a	2.22	200	35.00 a	5.50 a
HUN_SIK	0.86	0.42	0.56	0.90	0.00	0.09	0.70	39.64	30.40 b	44.00 b	1.64	200	20.00 a	7.00 a
ISR_YAT_YAT	0.40	0.32	0.18	0.62	0.37	0.01	0.28	83.43	28.00 a	31.00 a	0.71	178	11.00 a	1.70 a
ITA_FEI_S17	0.53	0.37	0.30	0.66	0.14	0.19	1.08	22.97	8.00 a	76.00 a	3.11	117	20.00 a	3.10 b
ITA_KAE_S20	0.68	0.45	0.46	0.75	0.07	0.18	1.24	22.97	17.00 a	50.00 a	3.64	121	14.00 a	2.60 b
ITA_MUN	0.63	0.48	0.42	0.62	0.31	0.06	0.80	29.87	7.00 a	55.00 a	1.93	188	18.00 a	2.20 b
ITA_REN	0.85	0.77	0.79	0.95	0.02	0.04	1.61	12.59	17.70 b	47.90 b	2.73	143	27.00 b	4.60 b
ITA_RUN_N20	0.84	0.73	0.74	0.94	0.02	0.04	1.39	15.28	14.00 a	54.00 a	3.33	123	18.70 a	5.70 b
MEX_COR_YP	0.68	0.24	0.31	0.78	0.05	0.18	1.42	81.77	22.20 b	46.40 b	2.94	200	7.00 a	5.20 a
NLD_LOO	0.55	0.31	0.27	0.74	0.02	0.24	1.33	41.67	1.00 a	99.00 a	2.61	200	18.00 a	2.20 a
NLD_SPE_DOU	0.76	0.60	0.63	0.81	0.09	0.11	1.42	39.80	4.80 b	80.70 b	1.62	200	30.00 a	4.50 a
NZL_HUA_HUA	0.71	0.62	0.61	0.75	0.17	0.08	2.62	42.52	71.20 a	13.20 a	1.73	200	27.00 a	6.60 b
PRT_LEZ_ARN	0.70	0.23	0.25	0.77	0.02	0.21	0.72	77.42	5.04 a	90.38 a	1.52	200	12.00 a	1.50 a
PRTMIT	0.76	0.47	0.36	0.78	0.18	0.04	0.51	80.80	16.10 b	64.50 b	1.33	200	7.50 a	0.55 a
PRT_PIN	0.65	0.50	0.36	0.66	0.33	0.01	0.76	74.76	16.60 b	61.20 b	1.26	200	12.60 a	1.10 b
RUS_CHE_Y4	0.31	0.21	0.23	0.95	0.01	0.04	0.62	34.23	21.10 b	23.20 b	4.96	200	7.00 a	1.30 b
RUS_FYO	0.72	0.62	0.62	0.88	0.00	0.12	1.24	30.87	18.20 b	48.80 b	3.77	198	23.50 a	3.50 a
RUS_POG_VAR	0.78	0.49	0.61	0.89	0.00	0.11	0.70	33.02	28.60 b	37.50 b	2.64	200	22.00 a	2.80 b
SEN_SOU_PRE	0.75	0.35	0.16	0.79	0.21	0.00	0.13	43.94	6.00 a	90.00 a	0.23	200	7.00 a	0.22 a
SWE_NOR_ST1_BEF	0.75	0.62	0.62	0.68	0.19	0.13	1.07	36.70	5.80 a	58.60 a	2.63	185	28.70 a	4.18 a
SWE_NOR_ST2	0.26	0.21	0.17	0.56	0.00	0.44	1.07	36.70	5.80 a	58.60 a	2.63	185	27.70 a	6.15 a
SWE_NOR_ST3	0.62	0.61	0.60	0.67	0.08	0.25	1.07	36.70	5.80 a	58.60 a	2.63	185	27.20 a	4.55 a
SWE_NOR_ST5_REF	0.59	0.62	0.57	0.50	0.20	0.30	1.07	36.55	19.20 b	43.50 b	2.83	190	20.00 a	5.00 a

C.2. Tables C

187

Table C.3: Summary table of site level R^2_{VPD} , R^2_{SWC} , R^2_{PPFD} , climate, soil properties and vegetation structure data. PPET is in [mm mm^{-1}], P-PET_{sd} is in [mm], Clay and Sand are in [%], Total N is in [g kg^{-1}], Stand height is in [m], LAI is in [$\text{m}^2_{\text{leaves}} \text{m}^2_{\text{soil}}$]. Letters show data source: a = SAPFLUXNET, b = Global rasters, c = SAPFLUXNET plant height. (*continued*)

Site code	R^2_{VPD}	R^2_{SWC}	R^2_{PPFD}	Relimp VPD	Relimp SWC	Relimp PPFD	PPET	P - PET _{sd}	Clay	Sand	Total N	Bedrock	Stand height	LAI
SWE_SKO_MIN	0.76	0.74	0.70	0.55	0.04	0.41	1.60	45.86	17.30 b	52.00 b	2.48	133	28.00 a	6.50 a
SWE_SKY_38Y	0.38	0.46	0.40	0.12	0.88	0.00	1.39	33.61	21.70 b	43.80 b	3.93	184	13.60 a	3.98 a
SWE_SKY_68Y	0.38	0.57	0.37	0.10	0.76	0.14	1.30	33.80	18.90 b	46.50 b	4.15	184	20.30 a	3.83 a
SWE_SVA_MIX_NON	0.64	0.47	0.54	0.88	0.11	0.00	1.33	34.34	0.50 a	92.50 a	1.67	200	15.00 a	3.80 b
THA_KHU	0.51	0.38	0.39	0.71	0.25	0.05	0.83	84.24	10.00 a	65.00 a	0.75	200	15.00 a	3.90 a
USA_BNZ_BLA	0.66	0.43	0.56	0.78	0.17	0.06	0.69	33.86	10.30 b	36.80 b	2.57	200	3.00 a	3.60 b
USA_CHE_ASP	0.69	0.34	0.30	0.92	0.02	0.06	1.23	20.06	12.00 a	74.00 a	1.52	200	10.00 a	4.50 a
USA_CHE_MAP	0.71	0.62	0.65	0.81	0.02	0.17	1.22	19.85	6.63 a	59.31 a	2.54	200	18.00 a	3.90 a
USA_DUK_HAR	0.72	0.62	0.68	0.86	0.03	0.10	1.12	41.33	33.90 b	31.00 b	0.76	200	25.00 a	7.03 a
USA_HIL_HF2	0.72	0.67	0.71	0.59	0.00	0.41	1.14	37.46	26.00 a	43.00 a	0.71	200	15.00 a	5.50 a
USA_INM	0.52	0.42	0.47	0.53	0.00	0.47	1.18	39.20	26.70 b	8.00 b	1.05	200	30.00 a	4.90 a
USA_MOR_SF	0.73	0.52	0.50	0.89	0.10	0.01	1.18	39.20	30.00 a	10.00 a	1.05	200	27.00 a	5.00 a
USA_NWH	0.87	0.82	0.70	0.84	0.03	0.14	1.05	59.56	36.70 b	4.90 b	0.80	200	22.70 a	5.60 b
USA_ORN_ST1_AMB	0.64	0.62	0.56	0.52	0.08	0.41	1.14	61.36	24.00 a	21.00 a	0.85	200	17.90 a	5.50 a
USA_PAR_FER	0.49	0.16	0.23	0.68	0.03	0.29	1.32	25.96	10.00 a	60.00 a	1.75	200	18.00 a	4.20 a
USA_PER_PER	0.61	0.30	0.33	0.80	0.01	0.19	1.32	34.41	3.40 b	89.20 b	6.13	200	12.00 a	4.10 a
USA_PJS_P04_AMB	0.46	0.15	0.31	0.78	0.12	0.10	0.25	49.32	6.00 a	52.00 a	0.82	186	4.20 a	0.71 a
USA_PJS_P08_AMB	0.50	0.16	0.26	0.93	0.07	0.00	0.25	49.32	3.00 a	49.00 a	0.82	186	4.10 a	0.90 a
USA_PJS_P12_AMB	0.36	0.17	0.11	0.65	0.30	0.05	0.25	49.32	6.00 a	54.00 a	0.82	186	4.00 a	0.72 a
USA_SIL_OAK_1PR	0.44	0.49	0.41	0.33	0.49	0.18	1.36	38.70	1.00 a	98.00 a	0.74	200	9.50 a	3.60 a
USA_SIL_OAK_2PR	0.43	0.33	0.39	0.94	0.06	0.00	1.36	38.70	1.00 a	98.00 a	0.74	200	9.50 a	3.60 a
USA_SMI_SER	0.58	0.46	0.39	0.64	0.29	0.06	1.03	40.05	28.70 b	30.90 b	0.82	200	40.00 a	5.80 b
USA_SWH	0.82	0.56	0.52	0.92	0.02	0.06	1.09	62.29	43.10 b	6.30 b	0.69	200	24.20 a	4.00 b
USA_SYL_HL1	0.57	0.42	0.44	0.92	0.08	0.00	1.27	25.01	8.90 b	51.00 b	1.41	200	27.00 a	5.40 b
USA_SYL_HL2	0.53	0.50	0.50	0.66	0.02	0.31	1.27	25.01	8.90 b	51.00 b	1.41	200	27.00 a	5.40 b
USA_TNB	0.31	0.33	0.30	0.37	0.13	0.50	1.39	48.33	21.60 b	34.90 b	0.84	200	25.00 a	4.70 a
USA_TNO	0.38	0.39	0.37	0.41	0.22	0.38	1.41	60.02	29.60 b	30.20 b	0.83	200	30.00 a	6.60 a
USA_TNP	0.34	0.38	0.31	0.50	0.18	0.32	1.41	61.60	31.60 b	26.60 b	0.81	200	25.00 a	4.50 a
USA_UMB_CON	0.61	0.46	0.44	0.76	0.02	0.22	1.30	30.60	1.00 a	92.00 a	2.02	200	29.00 a	3.50 a

Table C.3: Summary table of site level R^2_{VPD} , R^2_{SWC} , R^2_{PPFD} , climate, soil properties and vegetation structure data. PPET is in [mm mm^{-1}], P-PET_{sd} is in [mm], Clay and Sand are in [%], Total N is in [g kg^{-1}], Stand height is in [m], LAI is in [$\text{m}^2_{\text{leaves}} \text{m}^2_{\text{soil}}$]. Letters show data source: a = SAPFLUXNET, b = Global rasters, c = SAPFLUXNET plant height. (*continued*)

Site code	R^2_{VPD}	R^2_{SWC}	R^2_{PPFD}	Relimp VPD	Relimp SWC	Relimp PPFD	PPET	P - PET _{sd}	Clay	Sand	Total N	Bedrock	Stand height	LAI
USA_UMB_GIR	0.57	0.43	0.39	0.76	0.05	0.19	1.25	30.69	1.00 a	92.00 a	2.49	200	29.00 a	3.50 a
USA_WIL_WC1	0.54	0.30	0.23	0.81	0.18	0.01	1.19	20.23	6.90 b	53.20 b	1.01	200	24.30 a	6.20 b
USA_WVF	0.43	0.35	0.35	0.65	0.02	0.33	1.63	30.35	24.90 b	29.90 b	1.37	200	30.00 a	6.90 a
ZAF_FRA_FRA	0.61	0.08	0.24	0.96	0.01	0.03	0.90	99.17	20.00 b	69.90 b	0.95	200	20.00 a	1.80 a
ZAF_RAD	0.45	0.33	0.32	0.58	0.06	0.37	0.95	82.73	21.30 b	61.40 b	1.18	200	3.50 a	2.70 a
ZAF_SOU_SOU	0.43	0.18	0.17	0.58	0.05	0.38	0.97	86.39	23.00 b	61.90 b	1.13	200	4.00 a	3.00 a
ZAF_WEL_SOR	0.63	0.29	0.32	0.66	0.05	0.29	0.50	79.71	20.00 a	60.00 a	0.81	179	25.00 a	1.80 a

Table C.4: Table of equivalence between Whittaker biomes and the groups of biomes used in the study.

Original biome name	Study biome group
Desert	DRY
Temperate grassland desert	DRY
Subtropical desert	DRY
Woodland/shrubland	WOOD
Temperate forest	TEMP
Boreal forest	BOR
Tundra	BOR
Tropical rainforest	TROP
Tropical seasonal forest/savanna	TROP

“thesis” — 2020/12/29 — 11:18 — page 190 — #214

D

Appendix Chapter 5

D.1 Notes D

Notes S1: Whole-tree stomatal conductance (G'_{Asw}) calculation procedure.

To account for aerodynamic effect on whole-tree canopy conductance (G_{Asw}) in trees where wind speed was available, we subtracted from G_{Asw} (calculated with eq. 2 of the main text) the aerodynamic conductance calculated following Tan *et al.* 2019. We first calculate the aerodynamic conductance for momentum (eq. 14 in Tan *et al.* 2019):

$$g_{aM} = \frac{\kappa^2 u}{\ln[(z - d)/z_{0M}] \ln[(z - d)/z_{0H}]} \quad (\text{D.1})$$

Where κ is the Von Karman constant and equivalent to 0.41 and u is wind speed [$m s^{-1}$] and:

$$z = \text{tree height} + 2, d = 0.6(\text{tree height}), z_{0M} = 0.1(\text{tree height}), z_{0H} = 0.135(z_{0M}) \quad (\text{D.2})$$

Lately, we calculated the boundary layer conductance following eq. 10 in Tan *et al.* (2019):

$$g_{bN} = \frac{\kappa u^*}{\ln\left(\frac{z_{0M}}{z_{0H}}\right)} \quad (\text{D.3})$$

Where u^* [$m s^{-1}$] is the friction velocity calculated inverting eq. 2 in Chu *et al.* 2018:

$$u^* = \frac{\kappa u}{\ln[(z - d)/z_{0M}] + \ln(1.25)} \quad (\text{D.4})$$

Ultimately, G'_{Asw} was calculated as:

$$G'_{Asw} = \left(\frac{1}{1/G_{Asw} - (1/g_{aM} + 1/g_{bN})} \right) \quad (\text{D.5})$$

Being G_{Asw} in [$m s^{-1}$]. Finally, G'_{Asw} was transformed to [$\text{mol } m_{Asw}^{-2} s^{-1}$].

D.2 Figures D

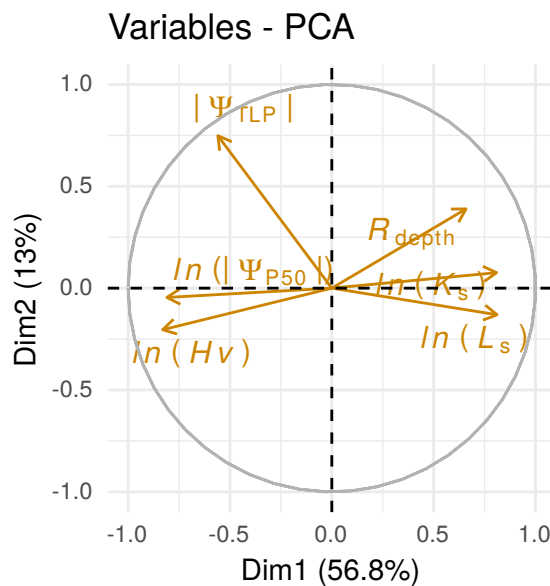
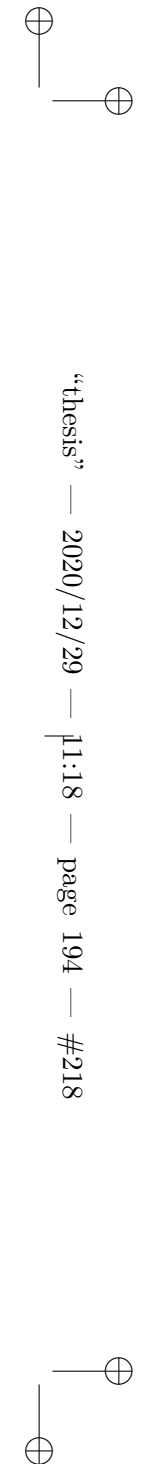


Figure D.1: PCA plot of water relations traits using imputations. $\ln(|\Psi_{P50}|)$: logarithm of absolute water potential at 50% water conductivity loss; $\ln(K_s)$: logarithm of maximum sapwood water conductivity; $\ln(Hv)$: logarithm of Huber value; $|\Psi_{TLP}|$: absolute water potential at turgor-loss point; R_{depth} : rooting depth; $\ln(L_s)$: logarithm of individual leaf area.



D.2. Figures D

195

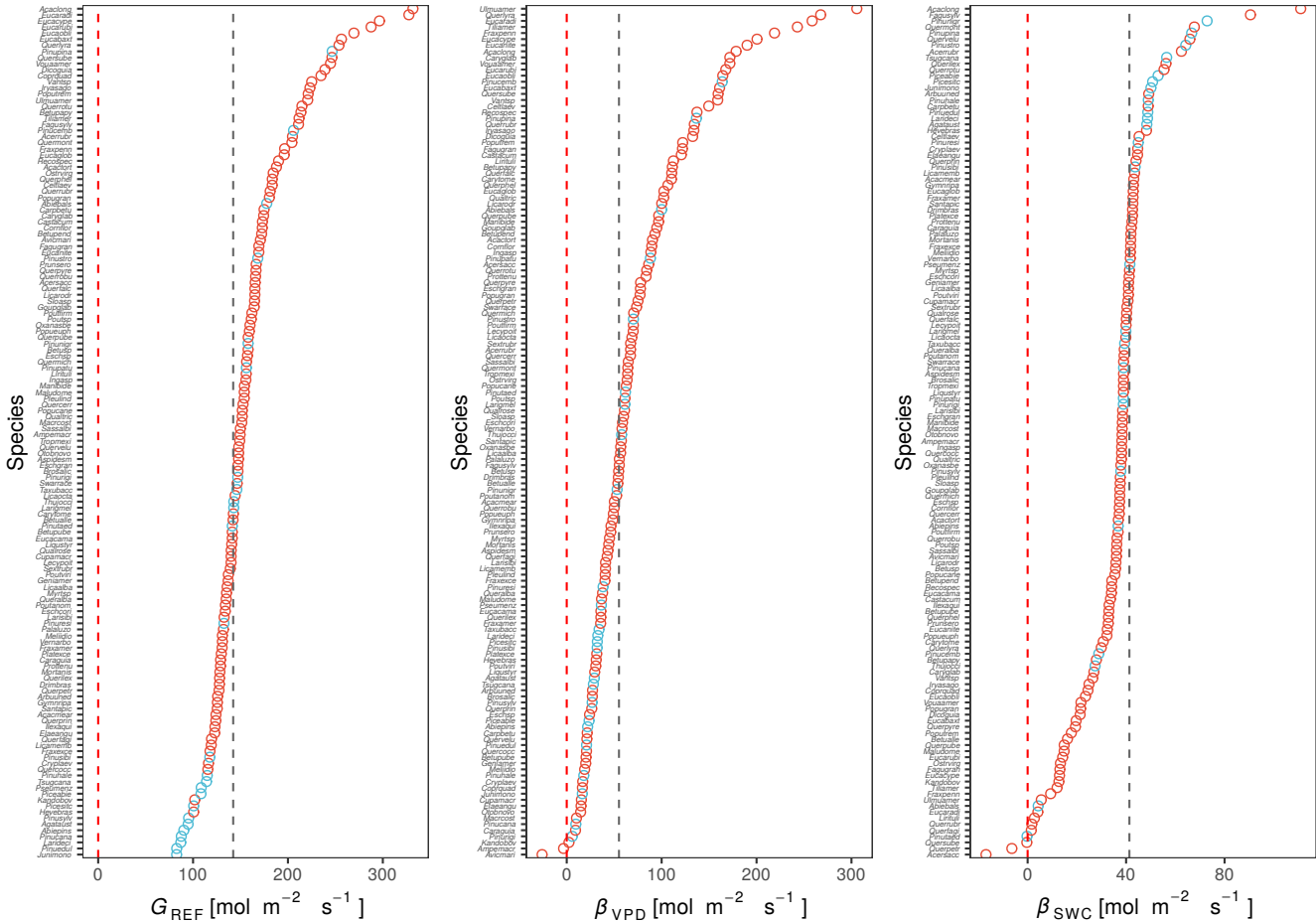
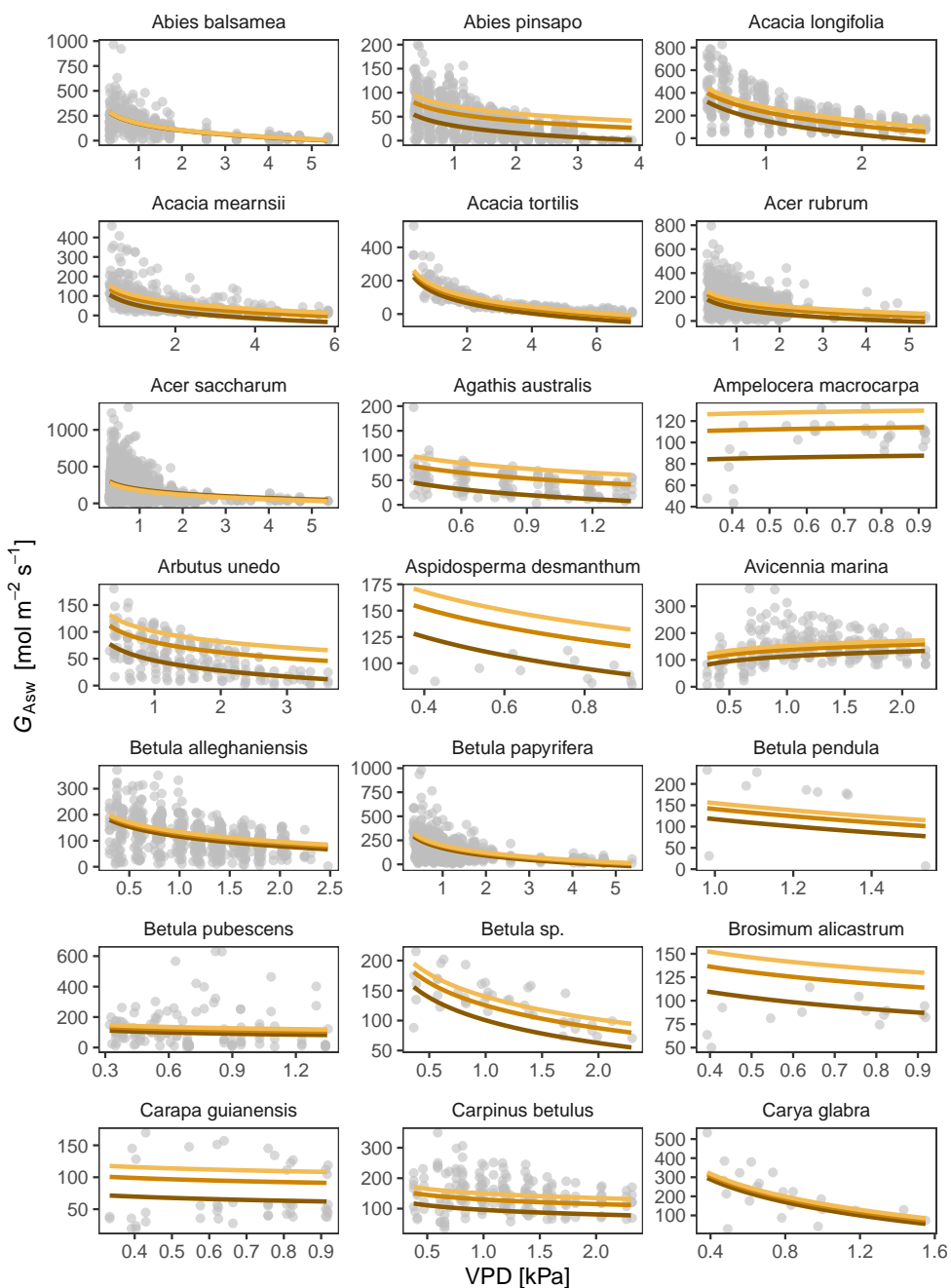
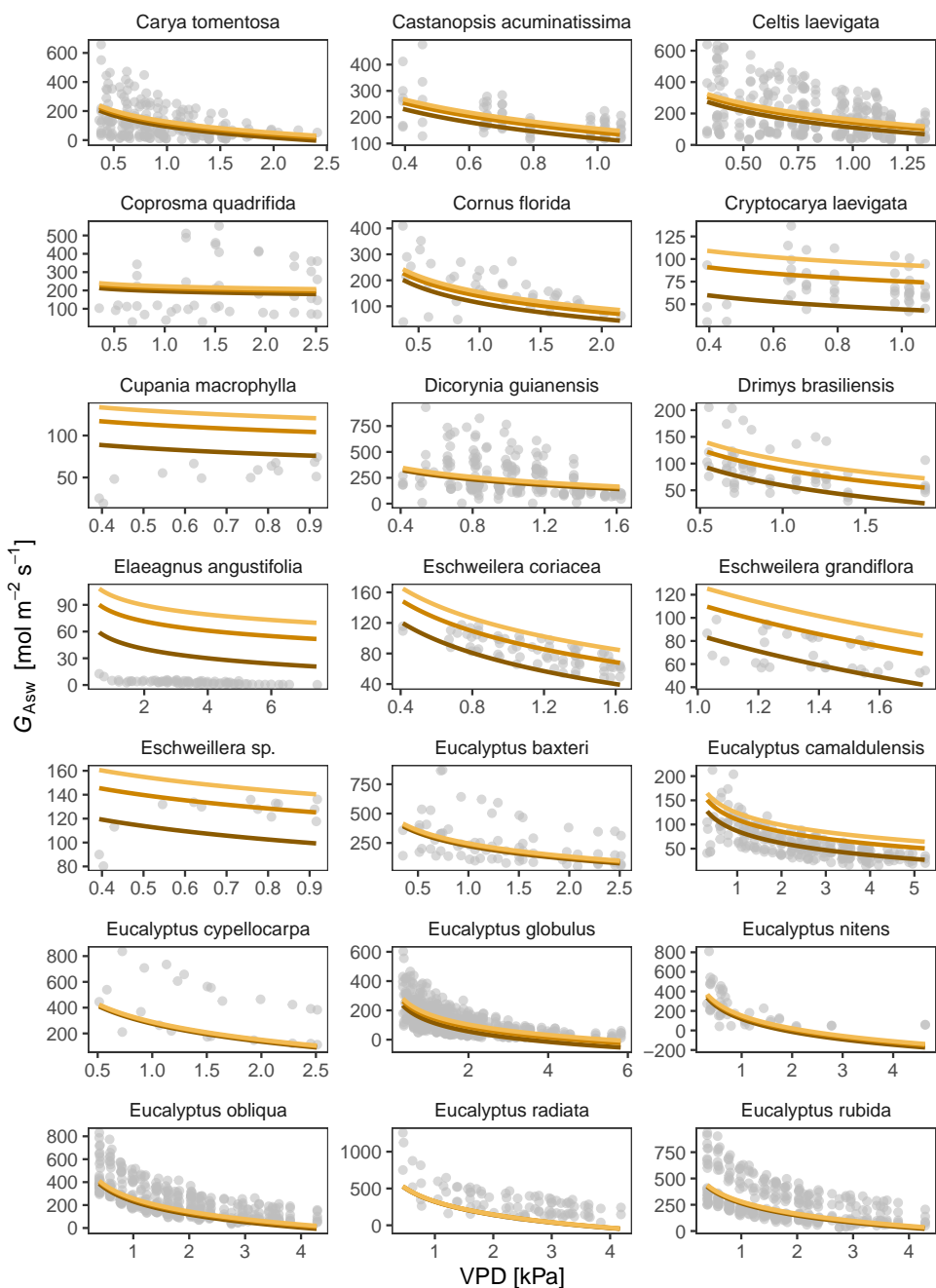


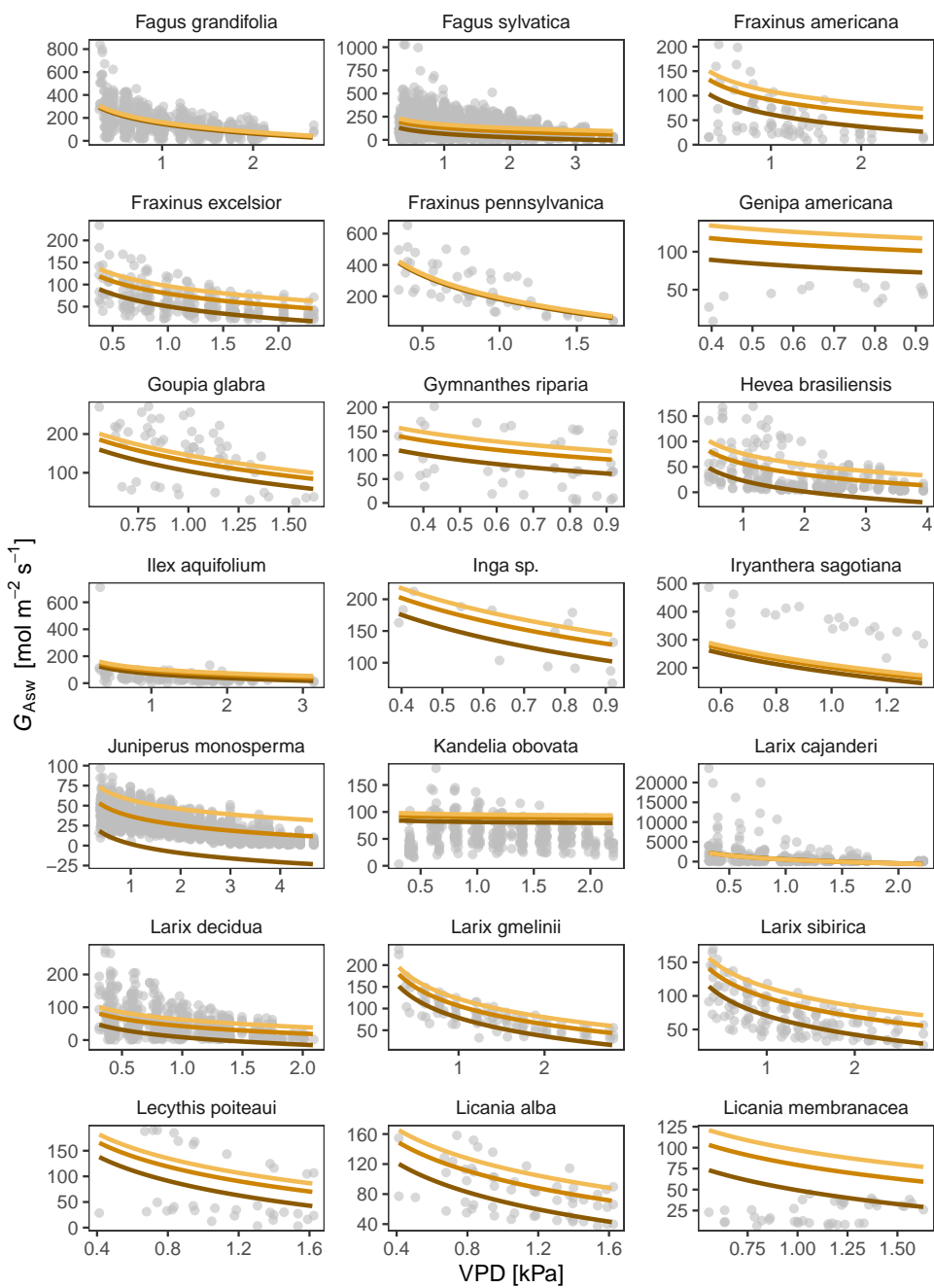
Figure D.2: Water use parameters at the species level. Grey dashed lines are the weighted mean of the parameters



D.2. Figures D

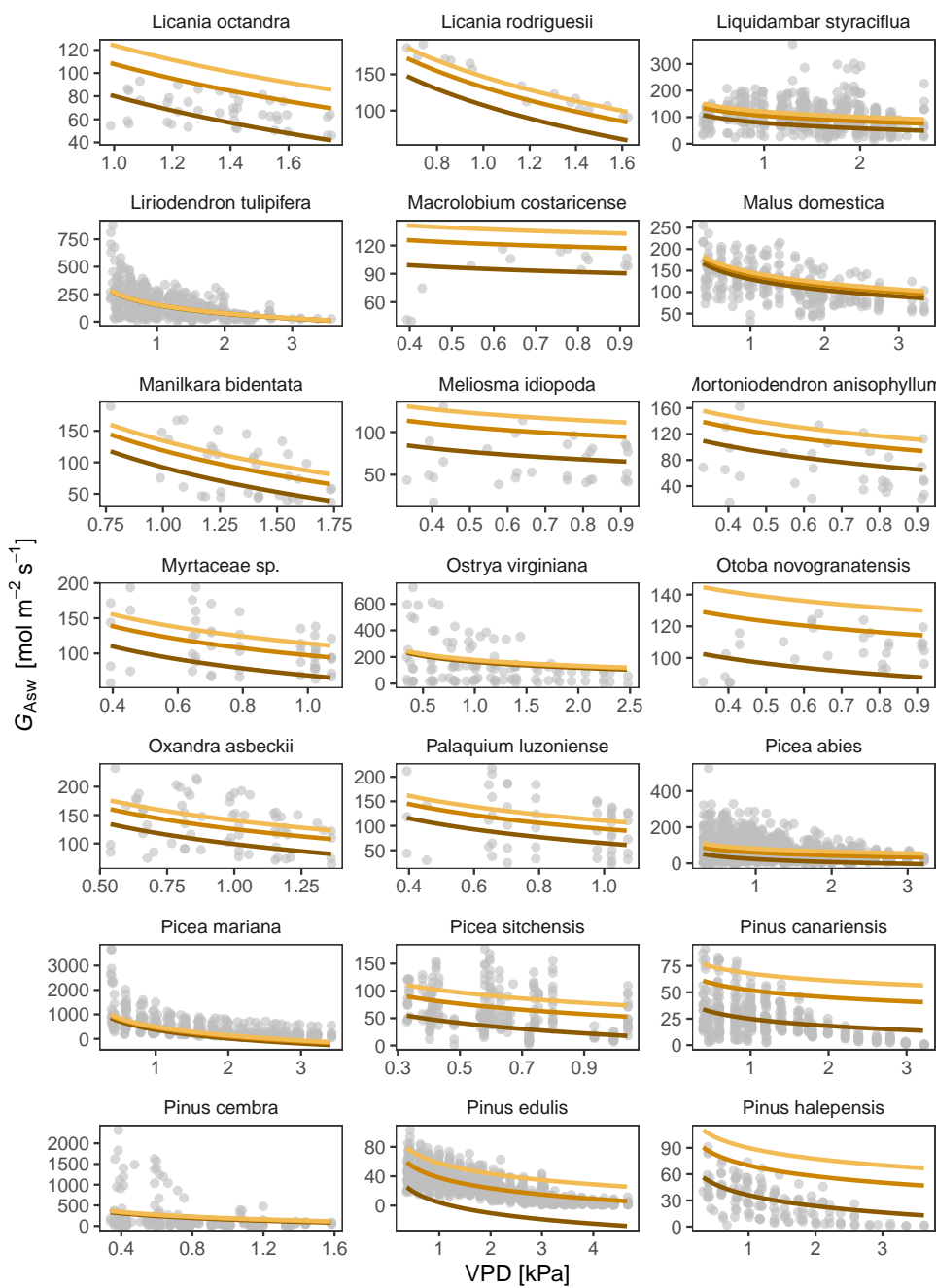
197

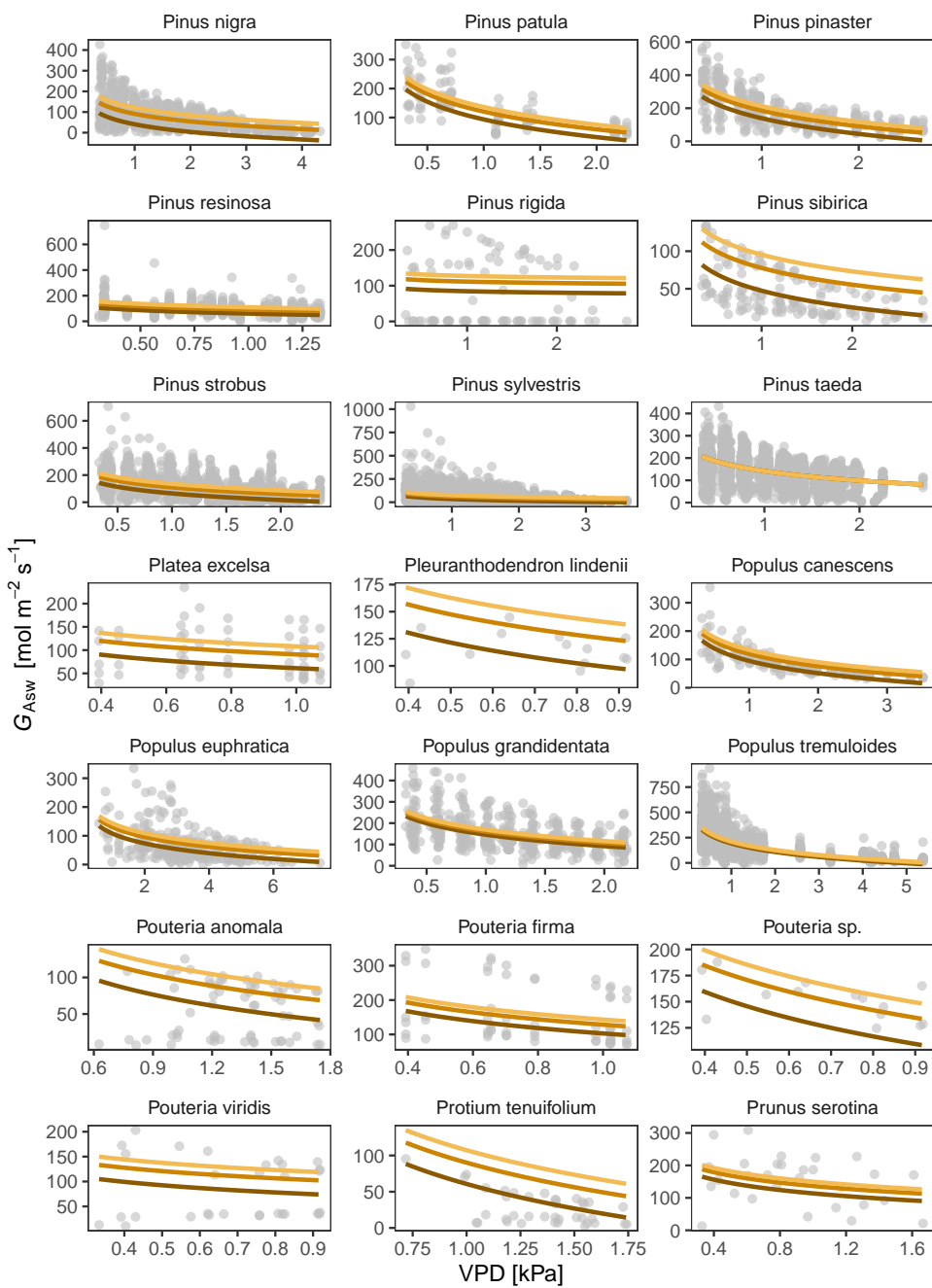




D.2. Figures D

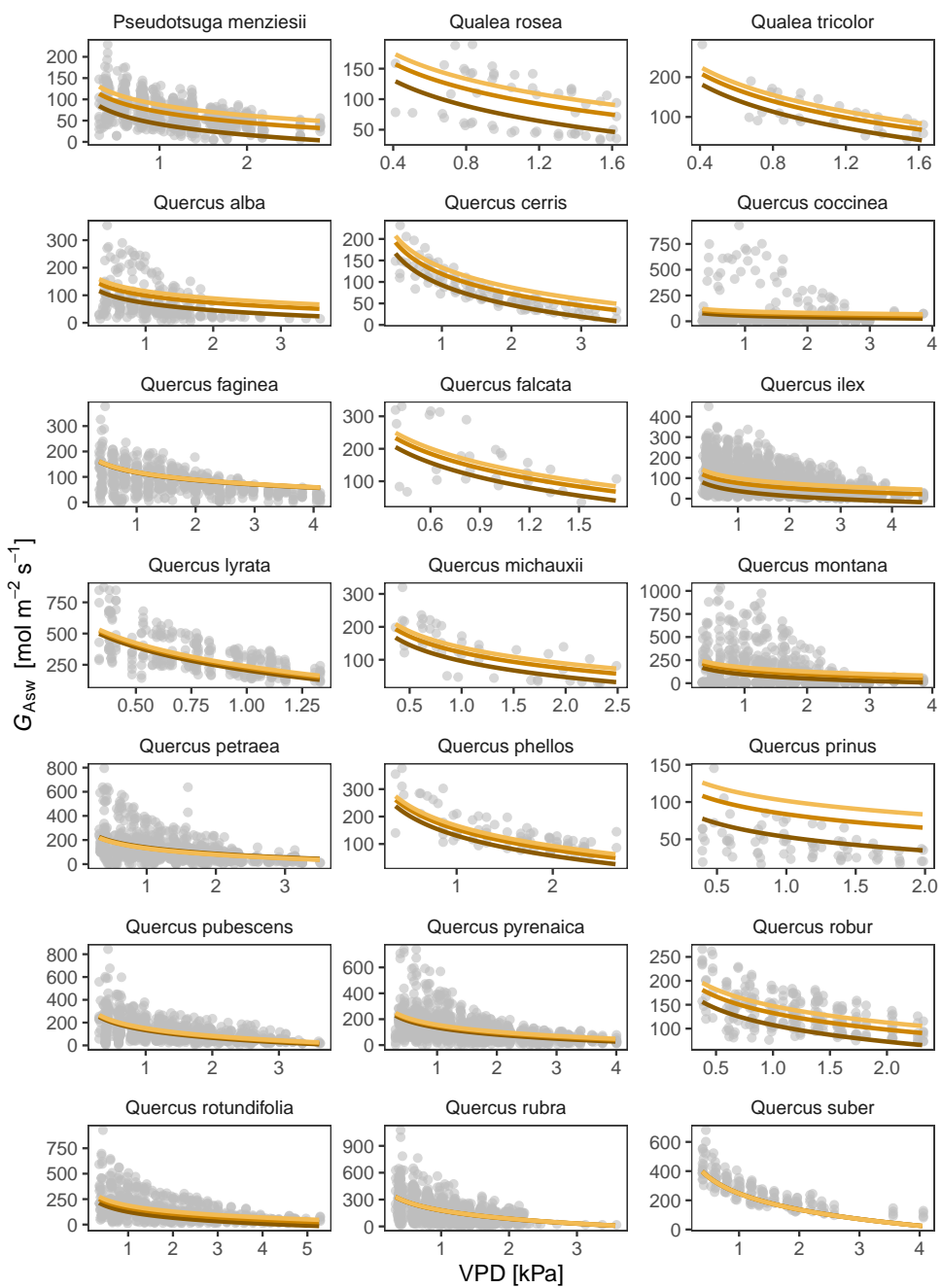
199

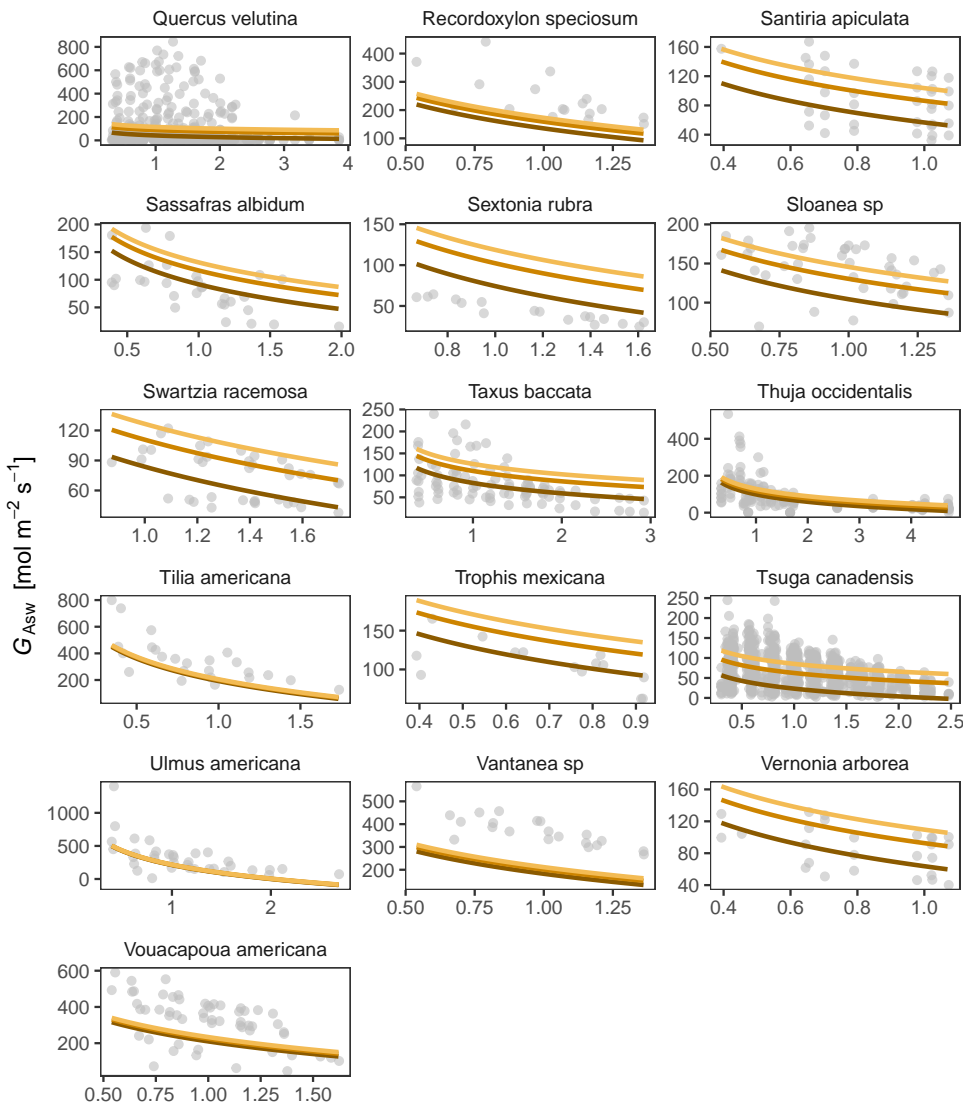




D.2. Figures D

201



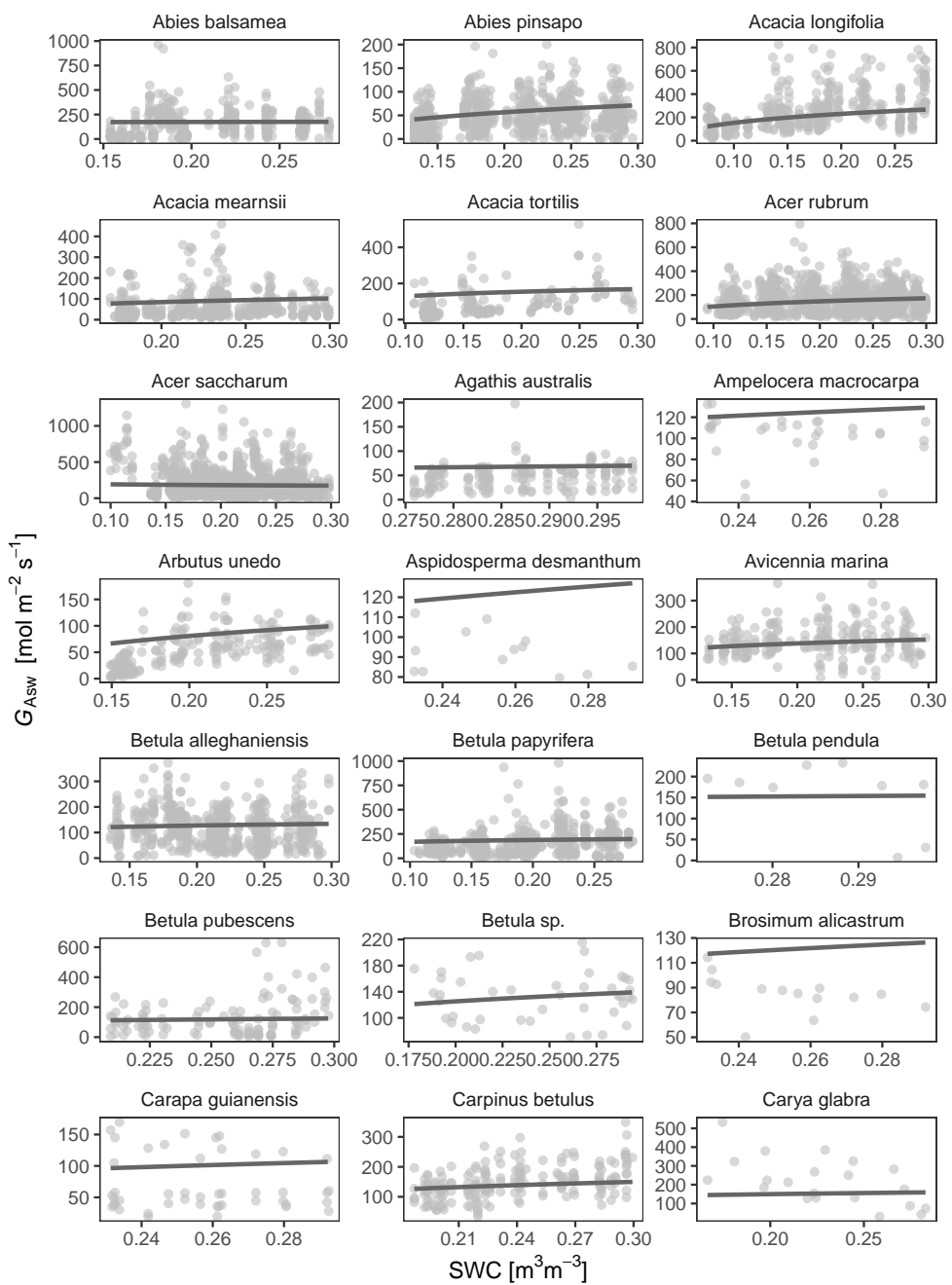


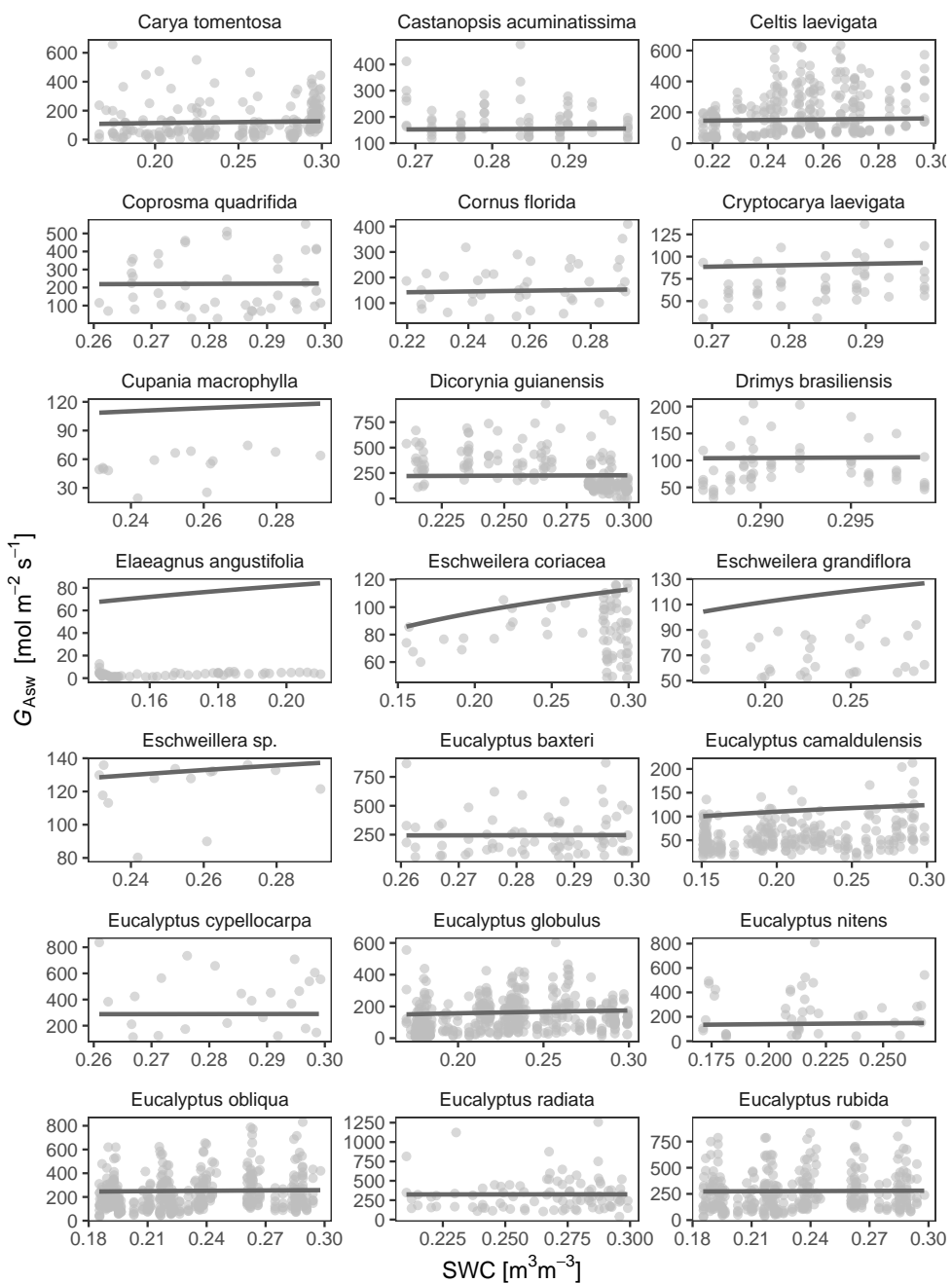
VPD [kPa]

Figure D.3: Species G_{Asw} responses to VPD. Each species have different curves representing distinct levels of SWC (from dark to light, 0.1, 0.2, 0.3 [$\text{m}^3 \text{m}^{-3}$]).

D.2. Figures D

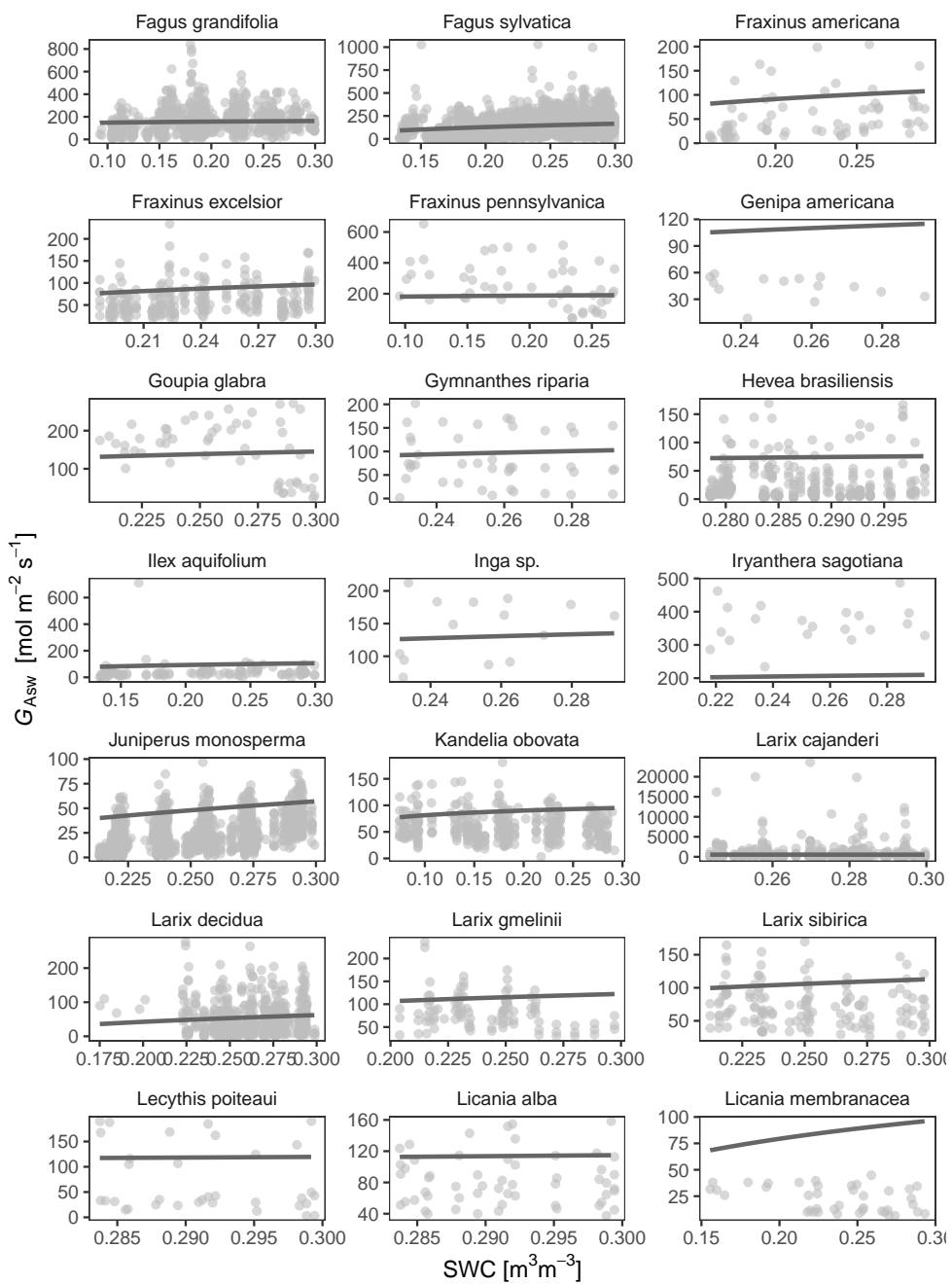
203

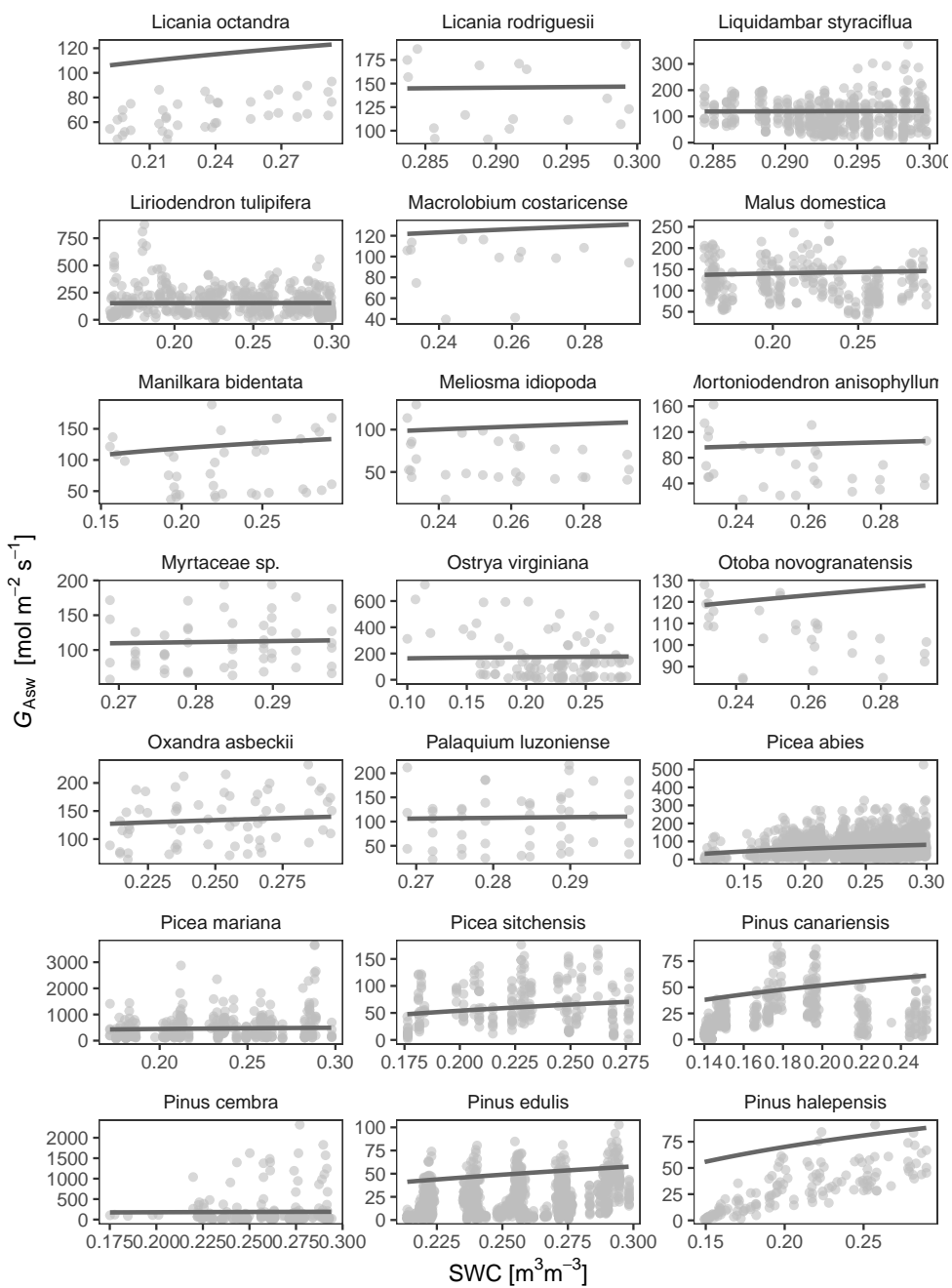




D.2. Figures D

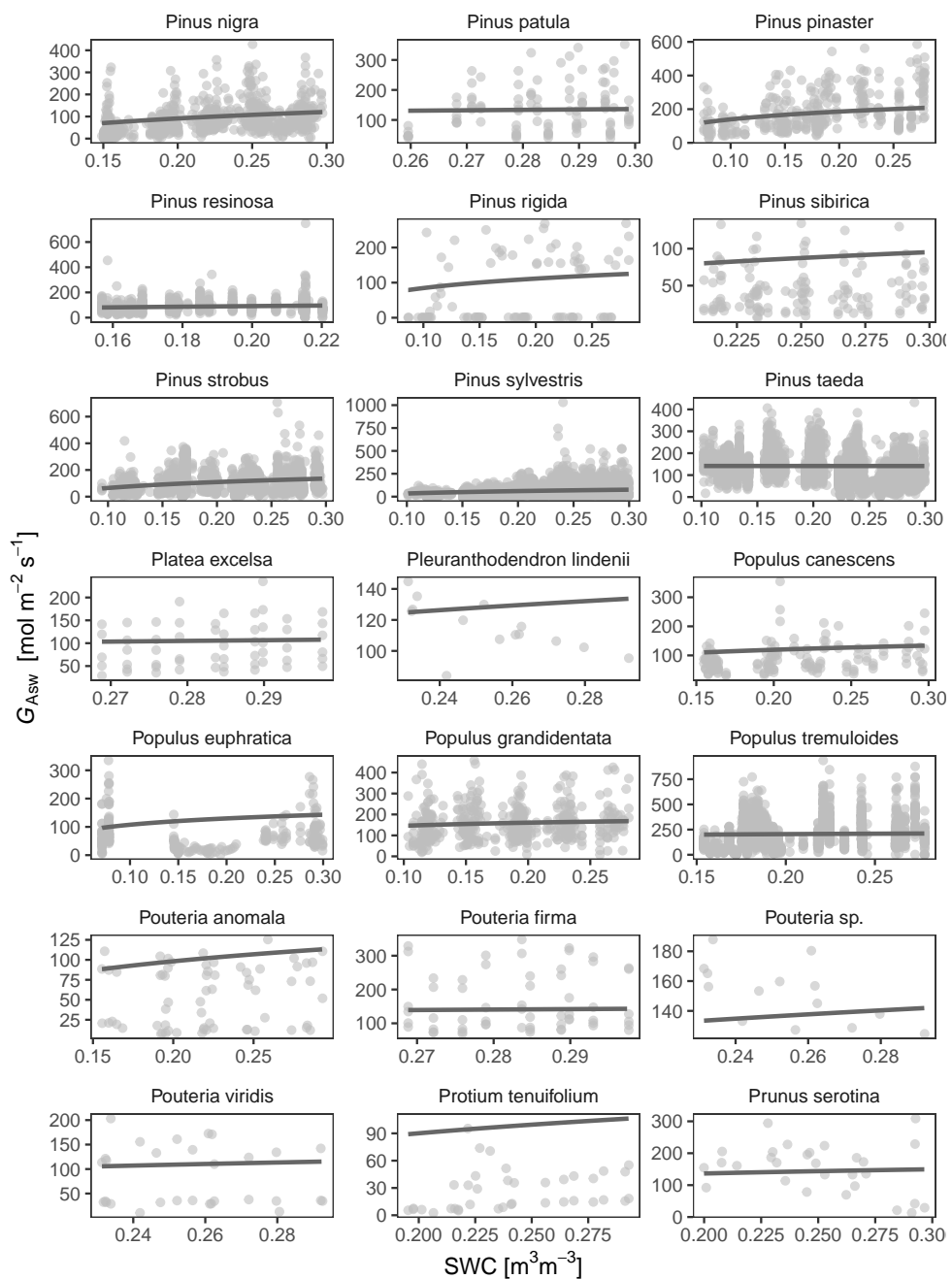
205

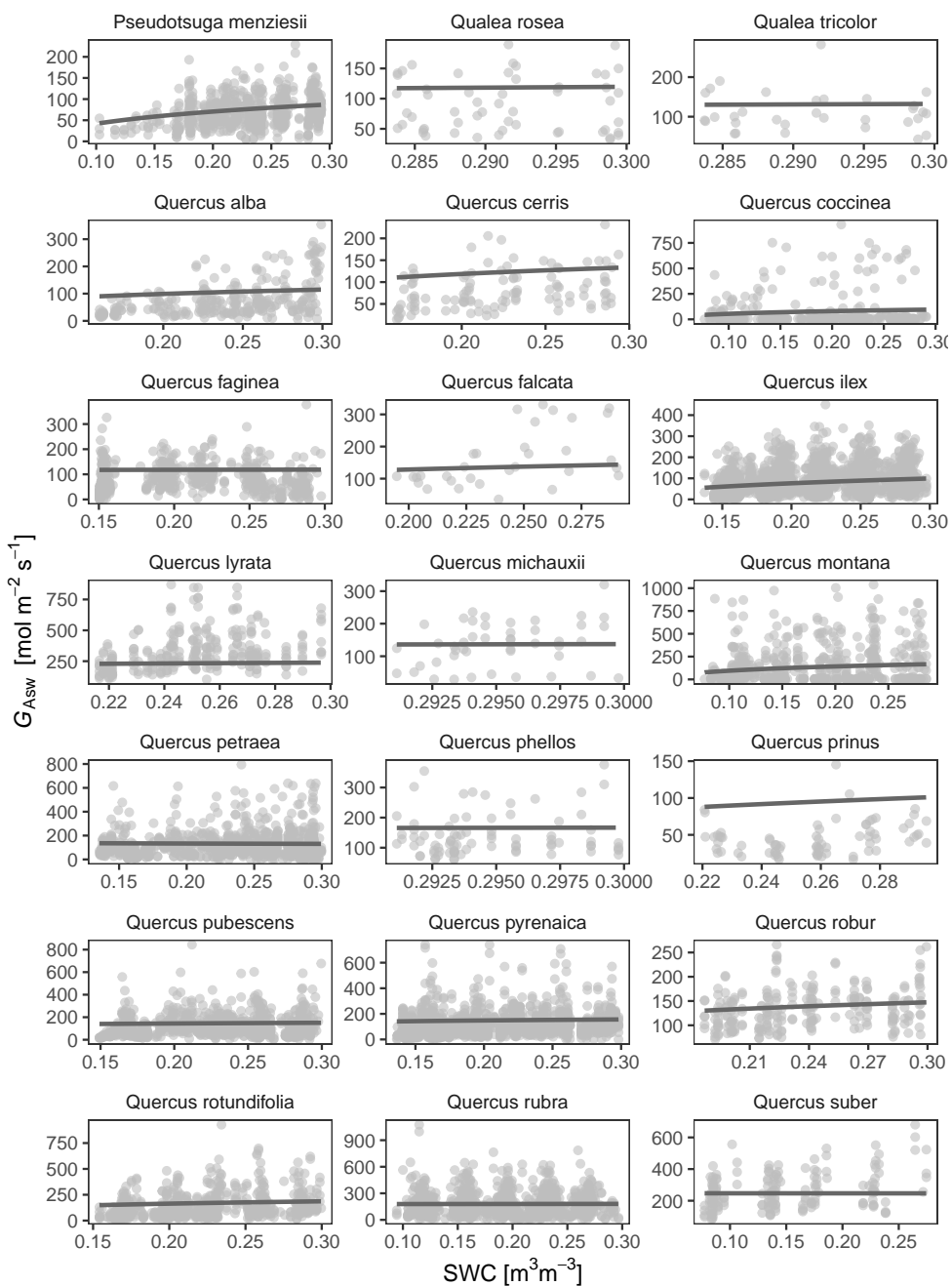




D.2. Figures D

207





D.2. Figures D

209

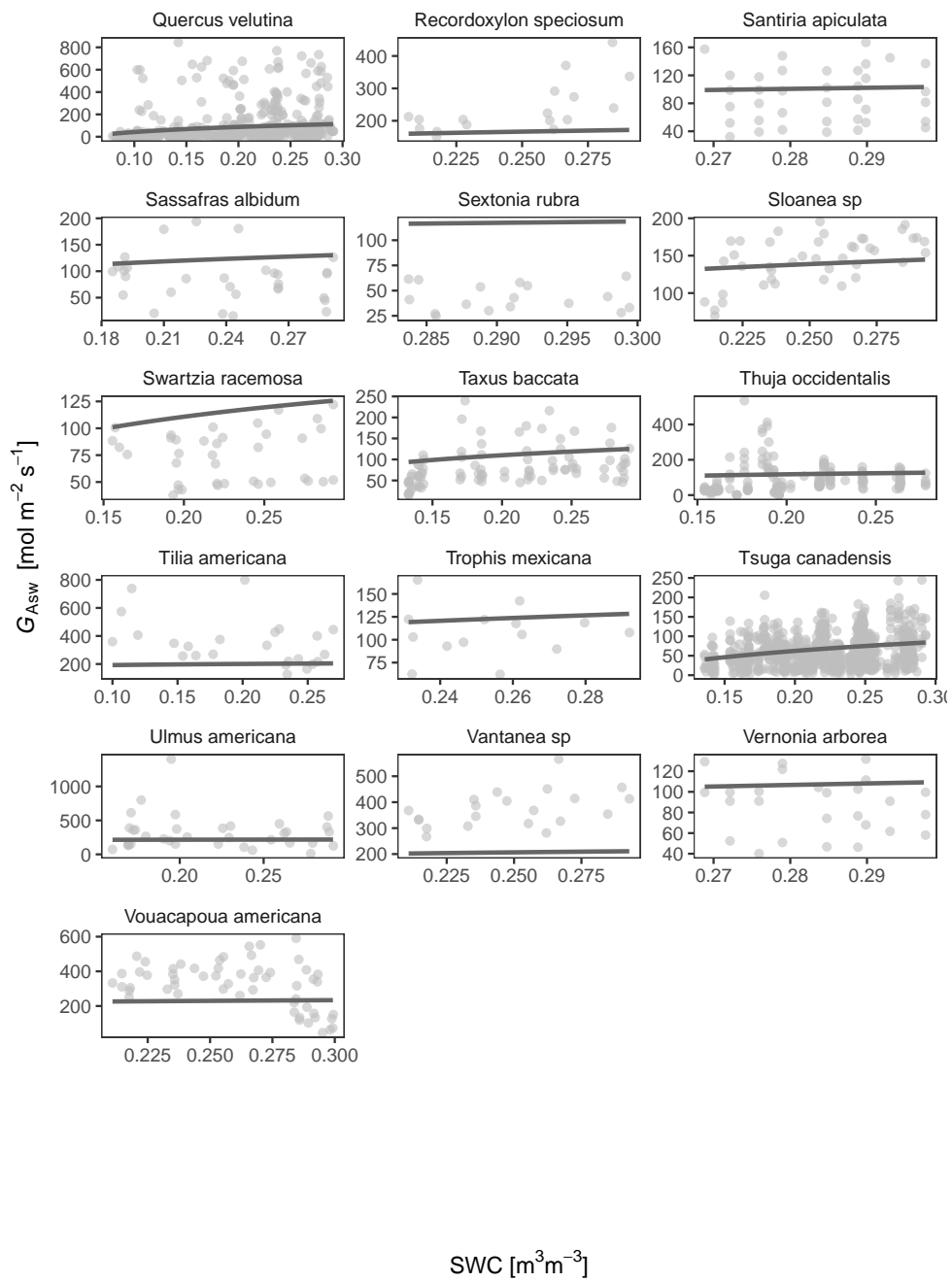


Figure D.4: Species G_{Asw} responses to SWC. Curves are fitted using a VPD reference level of 1 kPa.

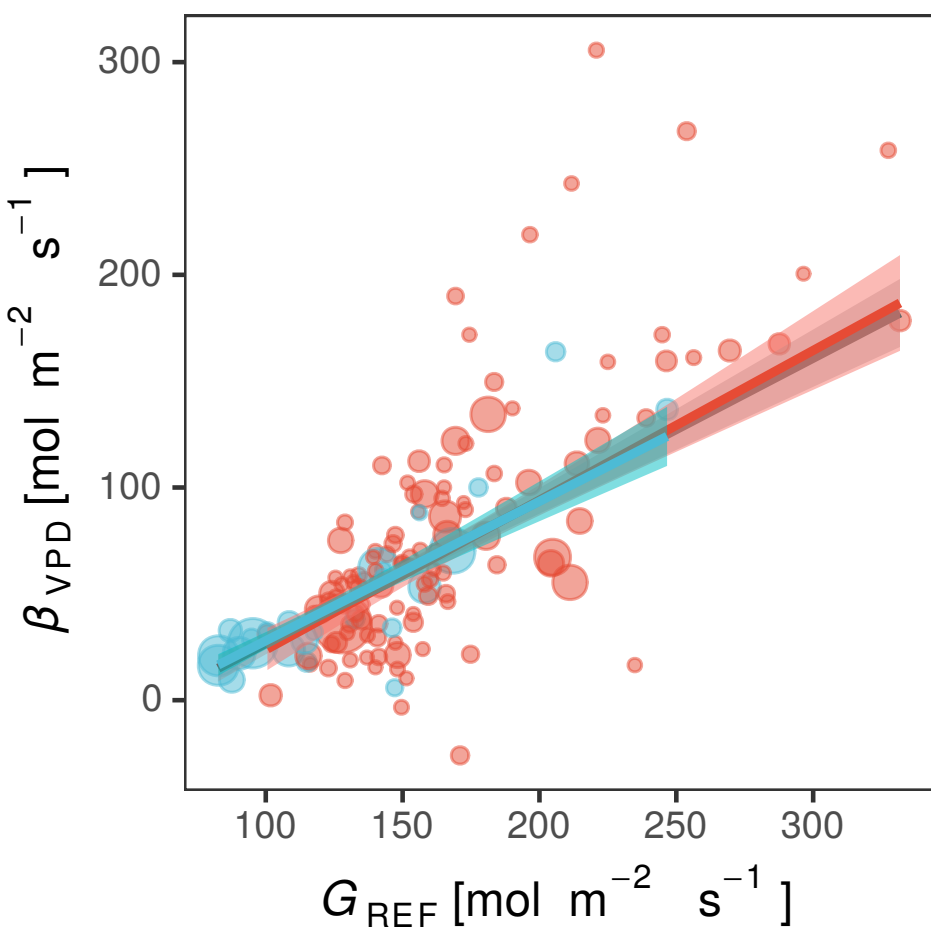


Figure D.5: Scatterplot between G_{REF} and β_{VPD} parameters. Grey line is global relationship. Blue and red lines are angiosperms and gymnosperms relationships, respectively. Shadow areas are 95% confidence interval.

D.2. Figures D

211

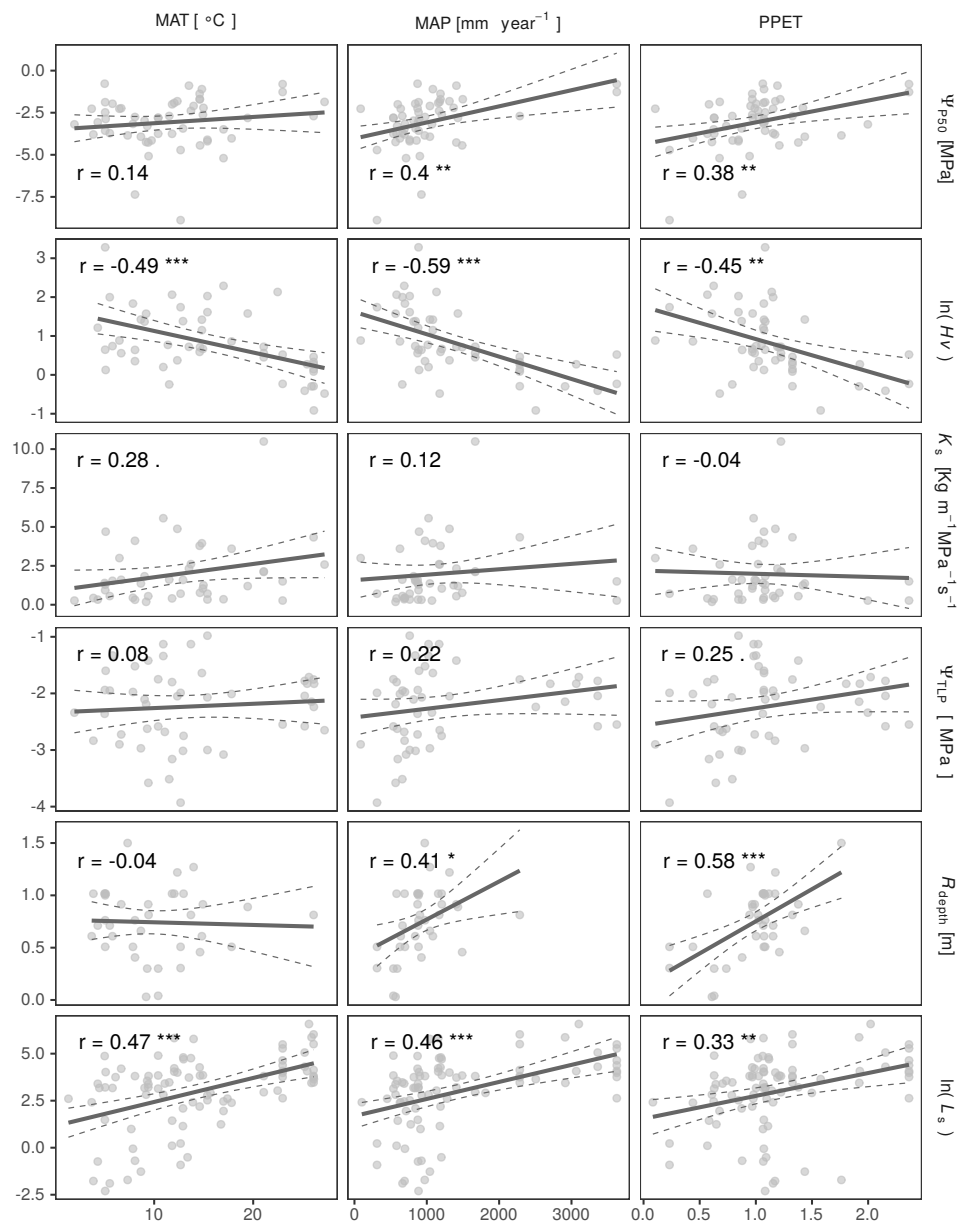


Figure D.6: Species’ climatic variables and water relations traits relationships. MAP: mean annual precipitation, MAT: mean annual temperature, PPET: mean annual precipitation over potential evapotranspiration. All climatic variables were calculated as the weighted average of the characteristic plots of the trees of each species, using tree-days as weighting factor.

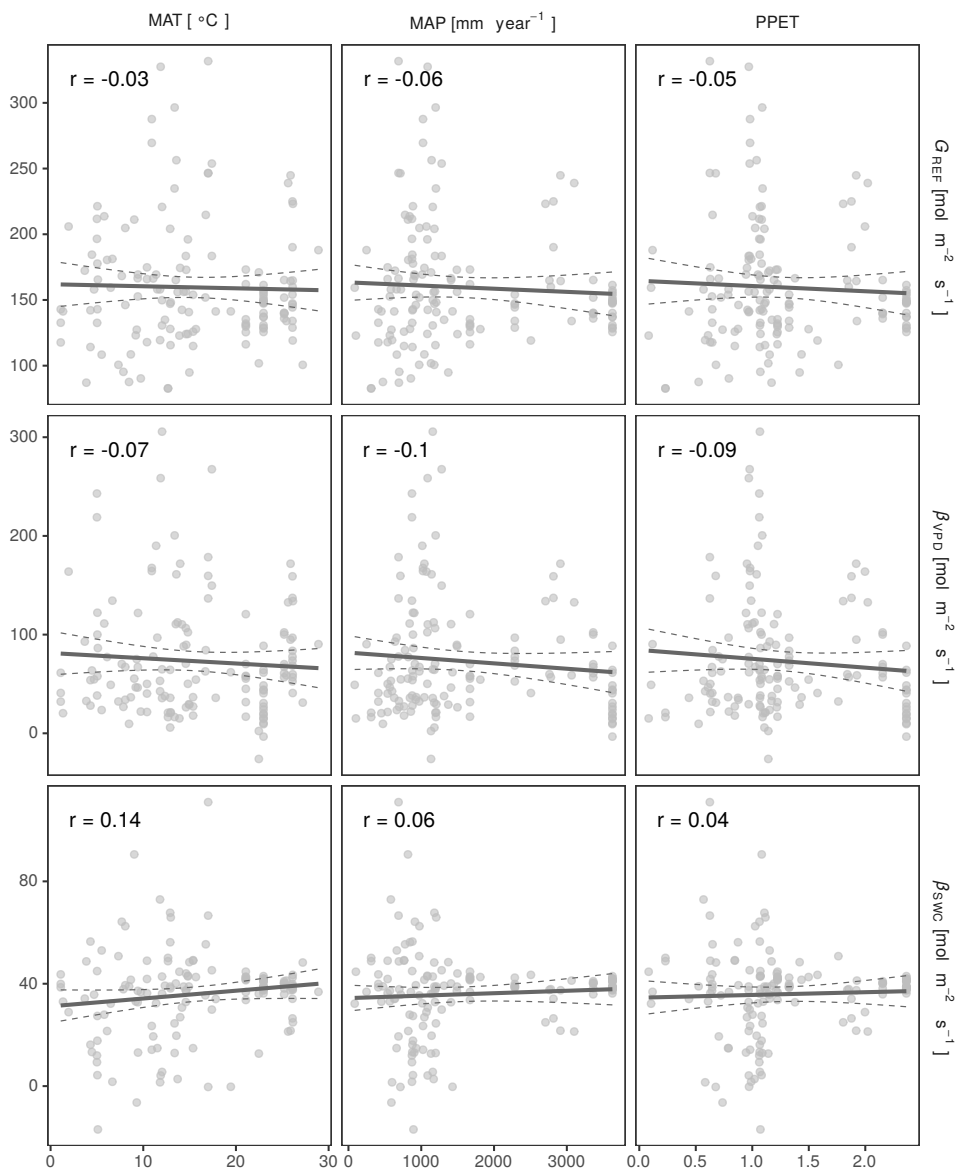


Figure D.7: Species' climatic variables and water use parameters relationships. MAP: mean annual precipitation, MAT: mean annual temperature, PPET: mean annual precipitation over potential evapotranspiration. All climatic variables were calculated as the weighted average of the characteristic plots of the trees of each species, using tree-days as weighting factor.

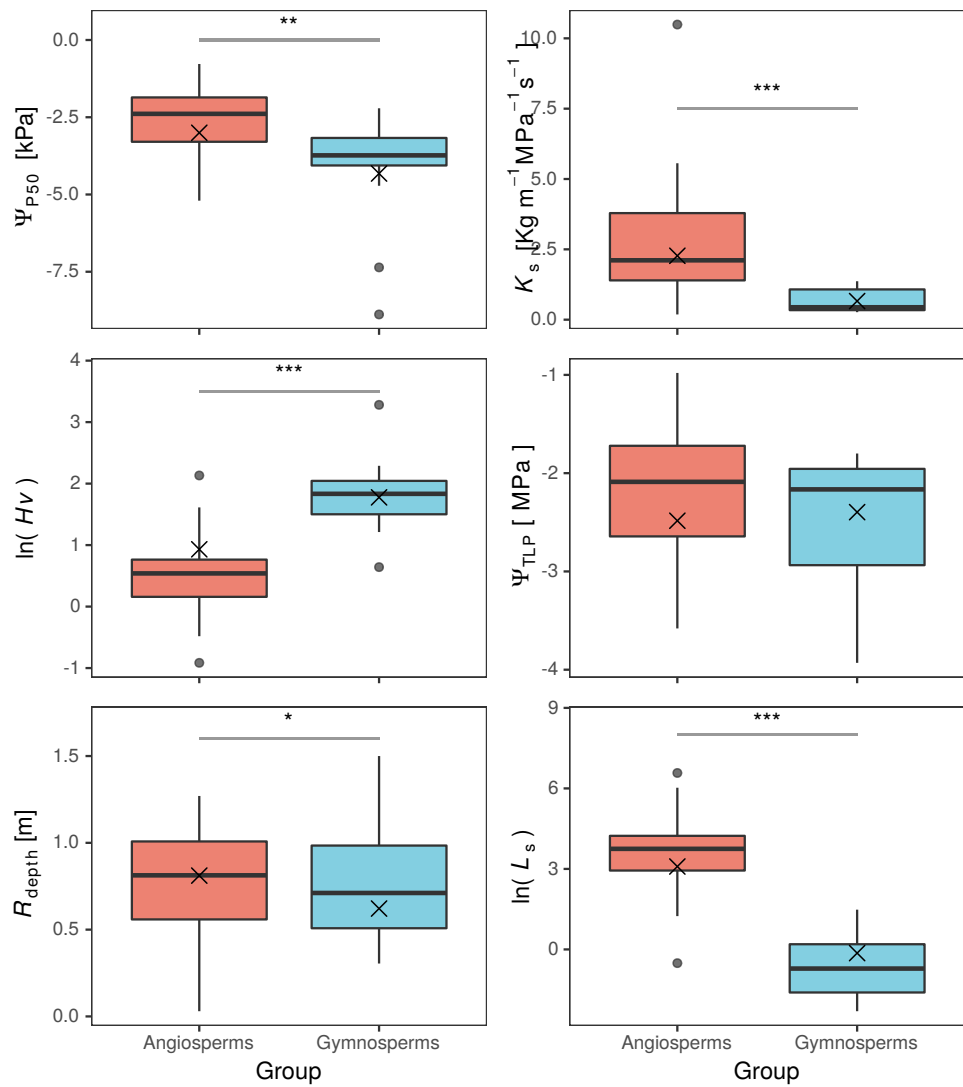


Figure D.8: Boxplots of water relations traits for angiosperms and gymnosperms. Statistical significance level is showed as symbols: ., $P < 0.1$; *, $P < 0.05$; **, $P < 0.01$; ***, $P < 0.001$. Crosses are weighted means of each trait by groups

D.3 Tables D

Table D.1: SAPFLUXNET plot treatments included in this study (Poyatos *et al.* 2020).

Plot treatment
None
Control
control
Ambient Control
Control - Unthinned
natural conditions
Reference
1Premortality
2premortality
distructive sampling
Girdling early successional
Pre-thinning
Before thinning
Before Thinning
non thinned
none (periodict thinning every 5-6 years 20 to 25% of basal area)
Radiation Level
AMBIENT CO2 FACE rings
fertilization at plantation
AcaciaMonoculture
MixtureEucalyptusAndAcacia
EucalyptusMonoculture
Pre Irrigation

D.3. Tables D

215

Table D.2: Species resume table. CEP names are Cornell Ecology Programs species names. Ψ_{P50} : water potential at 50% water conductivity loss [MPa], K_s : maximum sapwood water conductivity [$\text{Kg m}^{-1} \text{ MPa}^{-1} \text{ s}^{-1}$], H_v : Huber value [$\text{cm}^2_{\text{Asw}} \text{ m}^{-2}_{\text{leaf area}}$], Ψ_{TLP} : water potential at turgor-loss point [MPa], R_{depth} : rooting depth [m], L_s : individual leaf area [cm^2].

Species	CEP names	Group	# tree-days	# trees	# plots	Ψ_{P50}	K_s	Ψ_{TLP}	H_v	R_{depth}	V^*
<i>Abies balsamea</i>	Abiebals	Gymnosperms	855	19	1	-2.479	1.292		26.600	0.508	
<i>Abies pinsapo</i>	Abiepins	Gymnosperms	11822	22	3	-4.150					11.715
<i>Acacia longifolia</i>	Acaclong	Angiosperms	2130	10	1						
<i>Acacia mearnsii</i>	Acacmear	Angiosperms	4555	23	2						4.134
<i>Acacia tortilis</i>	Acactort	Angiosperms	1740	3	1						
<i>Acer rubrum</i>	Acerrubr	Angiosperms	17230	49	9	-2.755	4.108	-1.520	1.422	0.762	44.983
<i>Acer saccharum</i>	Acersacc	Angiosperms	10928	156	8	-2.873	4.695	-1.600	1.134	1.016	55.675
<i>Agathis australis</i>	Agataust	Gymnosperms	1272	6	1	-2.210	1.250				
<i>Ampelocereus macrocarpa</i>	Ampemacr	Angiosperms	100	2	1						103.560
<i>Arbutus unedo</i>	Arbuuned	Angiosperms	1900	4	1	-4.198	0.714	-0.980	5.017	12.470	
<i>Aspidosperma desmanthum</i>	Aspidesm	Angiosperms	35	1	1						42.925
<i>Avicennia marina</i>	Avicmari	Angiosperms	828	6	1				8.435		20.800
<i>Betula alleghaniensis</i>	Betualle	Angiosperms	3750	16	2						29.938
<i>Betula papyrifera</i>	Betupapy	Angiosperms	3869	21	2	-1.966	1.538	-1.330	2.096	0.610	23.942
<i>Betula pendula</i>	Betupend	Angiosperms	9	1	1	-2.265				0.610	11.177
<i>Betula pubescens</i>	Betupube	Angiosperms	397	9	2						13.510
<i>Betula sp.</i>	Betusp	Angiosperms	204	2	1						
<i>Brosimum alicastrum</i>	Brosalic	Angiosperms	40	1	1				1.685		58.953
<i>Carapa guianensis</i>	Caraguia	Angiosperms	150	3	1	-0.800	0.270		0.793		
<i>Carpinus betulus</i>	Carpbetu	Angiosperms	530	5	1	-3.750					23.160
<i>Carya glabra</i>	Caryglab	Angiosperms	47	1	1	-2.100				1.270	324.425
<i>Carya tomentosa</i>	Carytome	Angiosperms	645	10	2						
<i>Castanopsis acuminatissima</i>	Castacum	Angiosperms	96	8	1		10.490		1.570		45.000
<i>Celtis laevigata</i>	Celtlaev	Angiosperms	745	13	2						13.580
<i>Coprosma quadrifida</i>	Coprquad	Angiosperms	57	4	2						0.600
<i>Cornus florida</i>	Cornflor	Angiosperms	126	1	1	-4.442	0.768		2.034	0.457	46.343
<i>Cryptocarya laevigata</i>	Cryplaev	Angiosperms	72	6	1		2.140		1.750		19.075
<i>Cupania macrophylla</i>	Cupamacr	Angiosperms	40	1	1						
<i>Dicorynia guianensis</i>	Dicoguia	Angiosperms	596	9	2			-1.712			717.500
<i>Drimys brasiliensis</i>	Drimbras	Angiosperms	90	5	1						18.420
<i>Elaeagnus angustifolia</i>	Elaeangu	Angiosperms	402	2	1						11.200
<i>Eschweilera coriacea</i>	Eschcori	Angiosperms	249	4	2			-1.828	1.312		58.654
<i>Eschweilera grandiflora</i>	Eschgran	Angiosperms	378	2	1			-1.754	0.746		62.085
<i>Eschweillera sp.</i>	Eschsp	Angiosperms	40	1	1						
<i>Eucalyptus baxteri</i>	Eucabaxt	Angiosperms	112	4	2						
<i>Eucalyptus camaldulensis</i>	Eucacama	Angiosperms	564	3	1	-4.025	3.600	-2.010	2.364	0.508	10.910
<i>Eucalyptus cypellocarpa</i>	Eucacype	Angiosperms	29	2	2						
<i>Eucalyptus globulus</i>	Eucaglob	Angiosperms	4555	23	2	-1.100	3.950	-1.640	3.155	0.610	
<i>Eucalyptus nitens</i>	Eucanite	Angiosperms	378	7	1						2.163
<i>Eucalyptus obliqua</i>	Eucaobli	Angiosperms	2466	6	1			-1.340			16.790
<i>Eucalyptus radiata</i>	Eucaradi	Angiosperms	170	2	1						
<i>Eucalyptus rubida</i>	Eucarubi	Angiosperms	2055	5	1		5.560	-1.130	1.222		0.813
<i>Fagus grandifolia</i>	Fagugran	Angiosperms	6815	32	3	-5.080					45.167
<i>Fagus sylvatica</i>	Fagusylv	Angiosperms	15075	93	12	-2.972	1.830	-2.107	3.934		24.030
<i>Fraxinus americana</i>	Fraxamer	Angiosperms	378	2	1	-1.920					1.016
<i>Fraxinus excelsior</i>	Fraxexc	Angiosperms	636	6	1	-2.805		-1.750			339.552
<i>Fraxinus pennsylvanica</i>	Fraxpenn	Angiosperms	178	2	1	-0.777	1.397	-2.360			0.040
<i>Genipa americana</i>	Geniamer	Angiosperms	40	1	1	-1.270	1.500	-2.550			133.800
<i>Gouania glabra</i>	Goupllab	Angiosperms	172	3	3						242.210
<i>Gymnanthes riparia</i>	Gymnripa	Angiosperms	150	3	1						31.288
<i>Hevea brasiliensis</i>	Hevebras	Angiosperms	1302	6	1	-1.859	2.582	-2.650	0.618		
<i>Ilex aquifolium</i>	Ilexaqui	Angiosperms	567	3	1	-4.241	0.186	-2.190	4.825	0.030	16.770
<i>Inga sp.</i>	Ingasp	Angiosperms	40	1	1						

Table D.2: Species resume table. CEP names are Cornell Ecology Programs species names. Ψ_{P50} : water potential at 50% water conductivity loss [MPa], K_s : maximum sapwood water conductivity [$\text{Kg m}^{-1} \text{ MPa}^{-1} \text{ s}^{-1}$], Hv : Huber value [$\text{cm}^2 \text{ Asw m}_{\text{leaf area}}^{-2}$], Ψ_{TLP} : water potential at turgor-loss point [MPa], R_{depth} : rooting depth [m], L_s : individual leaf area [cm^2]. (*continued*)

Species	CEP names	Group	# tree-days	# trees	# plots	Ψ_{P50}	K_s	Ψ_{TLP}	Hv	R_{depth}	L_s
<i>Iryanthera sagotiana</i>	Iryasago	Angiosperms	72	1	1			-1.830			
<i>Juniperus monosperma</i>	Junimono	Gymnosperms	23650	15	3	-8.882	0.710	-3.930	5.700	0.305	0.400
<i>Kandelia obovata</i>	Kandobov	Angiosperms	2584	8	1						
<i>Larix decidua</i>	Larideci	Gymnosperms	3127	23	5	-3.791	0.434	-2.835		1.016	0.170
<i>Larix gmelinii</i>	Larigmel	Gymnosperms	303	3	1						
<i>Larix sibirica</i>	Larisibi	Angiosperms	516	3	1						
<i>Lecythis poiteaui</i>	Lecypoit	Angiosperms	90	2	1			-2.581			
<i>Licania alba</i>	Licaalba	Angiosperms	141	3	1			-2.044	0.664		157.435
<i>Licania membranacea</i>	Licamemb	Angiosperms	217	2	2			-2.239	0.401		38.313
<i>Licania octandra</i>	Licaocta	Angiosperms	256	2	1				1.088		32.005
<i>Licania rodriquesii</i>	Licarodr	Angiosperms	34	1	1						
<i>Liquidambar styraciflua</i>	Liquistyr	Angiosperms	742	23	3	-2.622	1.042		1.949	0.914	47.104
<i>Liriodendron tulipifera</i>	Lirituli	Angiosperms	2246	27	7	-2.390	2.610	-1.130		0.813	116.933
<i>Macrolobium costaricense</i>	Macrcost	Angiosperms	40	1	1						79.840
<i>Malus domestica</i>	Maludome	Angiosperms	1175	5	2			-2.070			16.200
<i>Manilkara bidentata</i>	Manibide	Angiosperms	500	2	1	-2.700	4.333		1.309	0.813	45.229
<i>Meliosma idiopoda</i>	Meliidio	Angiosperms	100	2	1						
<i>Mortoniaeodendron anisophyllum</i>	Mortanis	Angiosperms	100	2	1						
<i>Myrtaceae sp.</i>	Myrtsp	Angiosperms	72	6	1						
<i>Ostrya virginiana</i>	Ostrvirg	Angiosperms	549	3	2						23.994
<i>Otoba novogranatensis</i>	Otobonovo	Angiosperms	100	2	1						196.140
<i>Oxandra asbeckii</i>	Oxanasbe	Angiosperms	263	3	2						
<i>Palaquium luzoniense</i>	Palaluzo	Angiosperms	72	6	1						
<i>Picea abies</i>	Piceabie	Gymnosperms	11873	109	11	-3.714	0.558	-1.950	7.375	0.711	0.150
<i>Picea sitchensis</i>	Picesitc	Gymnosperms	990	15	1	-3.850				1.500	0.180
<i>Pinus canariensis</i>	Pinucana	Gymnosperms	4890	10	1						
<i>Pinus cembra</i>	Pinucemb	Gymnosperms	1151	14	5	-3.192	0.267	-2.340			
<i>Pinus edulis</i>	Pinuedul	Gymnosperms	23715	15	3	-4.718		-1.990		0.508	1.250
<i>Pinus halepensis</i>	Pinuhale	Gymnosperms	1329	3	1	-4.105	0.335	-3.000	7.590		
<i>Pinus nigra</i>	Pinunigr	Gymnosperms	11246	15	3	-3.753	0.407	-1.800	7.860	1.016	1.110
<i>Pinus patula</i>	Pinupatu	Gymnosperms	152	8	1						
<i>Pinus pinaster</i>	Pinupina	Gymnosperms	2130	10	1	-3.489	0.352		9.870		
<i>Pinus resinosa</i>	Pinuresni	Gymnosperms	1176	42	1			-1.940		1.016	4.400
<i>Pinus rigida</i>	Pinurigi	Gymnosperms	489	2	2						3.150
<i>Pinus sibirica</i>	Pinusibi	Gymnosperms	516	3	1						
<i>Pinus strobus</i>	Pinustro	Gymnosperms	32538	60	4						2.700
<i>Pinus sylvestris</i>	Pinusylv	Gymnosperms	42463	215	21	-3.163	0.448	-1.975	6.257	0.508	0.947
<i>Pinus taeda</i>	Pinutaed	Gymnosperms	24380	97	4	-2.810	1.197		4.848	0.889	
<i>Platea excelsa</i>	Platexce	Angiosperms	72	6	1						
<i>Pleuranthodendron lindenii</i>	Pleulind	Angiosperms	40	1	1						53.633
<i>Populus canescens</i>	Popucane	Angiosperms	597	3	1						
<i>Populus euphratica</i>	Popueuph	Angiosperms	841	9	3	-2.264	2.998	-2.900	2.420		
<i>Populus grandidentata</i>	Popugran	Angiosperms	6888	12	1						42.608
<i>Populus tremuloides</i>	Poputrem	Angiosperms	4455	99	1	-1.876	0.934		1.910	1.000	24.690
<i>Pouteria anomala</i>	Poutanom	Angiosperms	912	3	1				1.392		42.295
<i>Pouteria firma</i>	Poutfirm	Angiosperms	72	6	1						
<i>Pouteria sp.</i>	Poutsp	Angiosperms	40	1	1						
<i>Pouteria viridis</i>	Poutviri	Angiosperms	100	2	1						
<i>Protium tenuifolium</i>	Prottenu	Angiosperms	242	2	1				1.587		413.810
<i>Prunus serotina</i>	Prunsero	Angiosperms	100	1	1	-4.270	0.550	-1.420		0.914	24.759
<i>Pseudotsuga menziesii</i>	Pseumenz	Gymnosperms	2985	18	3	-3.926	1.366	-2.970	4.153	0.660	0.280
<i>Qualea rosea</i>	Qualrose	Angiosperms	141	3	1			-1.779			
<i>Qualea tricolor</i>	Qualtric	Angiosperms	78	2	1						
<i>Quercus alba</i>	Queralba	Angiosperms	1094	9	5	-1.818	4.877	-2.050	1.454	1.219	54.302

D.3. Tables D

217

Table D.2: Species resume table. CEP names are Cornell Ecology Programs species names. Ψ_{P50} : water potential at 50% water conductivity loss [MPa], K_s : maximum sapwood water conductivity [$\text{Kg m}^{-1} \text{ MPa}^{-1} \text{ s}^{-1}$], Hv : Huber value [$\text{cm}^2_{\text{Asw}} \text{ m}^{-2}_{\text{leaf area}}$], Ψ_{TLP} : water potential at turgor-loss point [MPa], R_{depth} : rooting depth [m], L_s : individual leaf area [cm^2]. (*continued*)

Species	CEP names	Group	# tree-days	# trees	# plots	Ψ_{P50}	K_s	Ψ_{TLP}	Hv	R_{depth}	V^*
<i>Quercus cerris</i>	Quercerr	Angiosperms	284	2	1		-3.580			29.190	
<i>Quercus coccinea</i>	Quercocc	Angiosperms	5343	11	3					121.678	
<i>Quercus faginea</i>	Querfagi	Angiosperms	6784	10	2	-2.002		-3.160		4.210	
<i>Quercus falcata</i>	Querfalc	Angiosperms	134	1	1	-0.893	2.323		2.057	41.635	
<i>Quercus ilex</i>	Querilex	Angiosperms	65295	62	6	-3.438	1.595	-3.015	3.980	8.078	
<i>Quercus lyrata</i>	Querlyra	Angiosperms	745	13	2					71.498	
<i>Quercus michauxii</i>	Quermich	Angiosperms	132	4	1	-1.700					
<i>Quercus montana</i>	Quermont	Angiosperms	5488	14	2					30.260	
<i>Quercus petraea</i>	Querpetr	Angiosperms	4617	29	5	-3.294		-2.624	0.300	35.000	
<i>Quercus phellos</i>	Querphel	Angiosperms	185	5	1	-1.375	3.787		1.806	8.935	
<i>Quercus prinus</i>	Querprin	Angiosperms	316	2	1	-1.700				32.200	
<i>Quercus pubescens</i>	Querpube	Angiosperms	6505	19	2	-2.696	1.612	-3.515	0.782	7.030	
<i>Quercus pyrenaica</i>	Querpyre	Angiosperms	6680	32	2			-2.680		3.460	
<i>Quercus robur</i>	Querrobu	Angiosperms	636	6	1	-2.802		-2.583	0.300	46.537	
<i>Quercus rotundifolia</i>	Querrotu	Angiosperms	4796	10	2					110.450	
<i>Quercus rubra</i>	Querrubr	Angiosperms	15185	32	6	-2.237	1.602	-2.725	1.746	0.914	66.641
<i>Quercus suber</i>	Quersube	Angiosperms	1816	4	1	-5.200		-3.080			
<i>Quercus velutina</i>	Quervelut	Angiosperms	5132	16	3			-2.750		1.016	
<i>Recordoxylon speciosum</i>	Recospec	Angiosperms	41	1	1						
<i>Santiria apiculata</i>	Santapic	Angiosperms	55	5	1						
<i>Sassafras albidum</i>	Sassalbi	Angiosperms	117	1	1					68.080	
<i>Sextonia rubra</i>	Sextrubr	Angiosperms	34	1	1					74.000	
<i>Sloanea sp</i>	Sloasp	Angiosperms	156	2	2						
<i>Swartzia racemosa</i>	Swarrace	Angiosperms	476	2	1			1.156		246.450	
<i>Taxus baccata</i>	Taxubacc	Gymnosperms	922	2	1	-7.360	0.320		1.900	0.406	0.500
<i>Thujopsis occidentalis</i>	Thujocci	Gymnosperms	340	10	1	-3.570			0.762	0.100	
<i>Tilia americana</i>	Tiliamer	Angiosperms	72	1	1					130.715	
<i>Trophis mexicana</i>	Tropmexi	Angiosperms	40	1	1					13.880	
<i>Tsuga canadensis</i>	Tsugcana	Gymnosperms	5739	24	2	-3.070	0.329		3.362	0.711	0.480
<i>Ulmus americana</i>	Ulmuamer	Angiosperms	133	1	1					56.993	
<i>Vantanea sp</i>	Vantsp	Angiosperms	69	1	1						
<i>Vernonia arborea</i>	Vernarbo	Angiosperms	36	3	1		2.110		2.060		
<i>Vouacapoua americana</i>	Vouaamer	Angiosperms	178	3	3			-2.147	0.744		353.583

Table D.3: Results of the linear models relating water use parameters calculated using G'_{Asw} to water relations traits. Parameters are explained by individual traits using simple linear models with number of species-days as weighting factor.

Parameter	Trait	N Species	Intercept	Slope	R^2
G'_{REF}	$\ln(\Psi_{P50})$	25	333.019 ***	-111.725 **	0.331
	$\ln(K_s)$	19	196.081 ***	81.935 **	0.359
	$\ln(Hv)$	20	297.029 ***	-71.225 *	0.188
	$ \Psi_{TLP} $	25	196.754 **	-4.398	0.000
	R_{depth}	13	-13.266	303.191 **	0.508
	$\ln(L_s)$	26	151.531 ***	31.494 ***	0.497
β'_{VPD}	$\ln(\Psi_{P50})$	25	235.774 ***	-95.494 *	0.215
	$\ln(K_s)$	19	125.553 ***	95.013 **	0.448
	$\ln(Hv)$	20	221.274 ***	-69.362 *	0.153
	$ \Psi_{TLP} $	25	62.062	17.932	0.000
	R_{depth}	13	-74.639 *	245.287 ***	0.681
	$\ln(L_s)$	26	69.367 ***	31.574 ***	0.409
β'_{SWC}	$\ln(\Psi_{P50})$	25	34.052 .	21.703	0.066
	$\ln(K_s)$	19	57.145 ***	-19.246 .	0.111
	$\ln(Hv)$	20	39.018 .	13.555	0.008
	$ \Psi_{TLP} $	25	86.217 ***	-9.086	0.011
	R_{depth}	13	94.44 ***	-29.023	0.038
	$\ln(L_s)$	26	73.395 ***	-8.696 **	0.234

Statistical significant levels: ., $P < 0.1$; *, $P < 0.05$; **, $P < 0.01$; ***, $P < 0.001$.

Table D.4: Results of the linear models relating water use parameters to water relations traits using REW instead of SWC. Parameters are explained by individual traits using simple linear models with number of species-days as weighting factor.

Parameter	Trait	N Species	Intercept	Slope	R^2
	$\ln(\Psi_{P50})$	55	198.741 ***	-70.836 ***	0.328
	$\ln(K_s)$	43	112.403 ***	37.208 ***	0.375
	$\ln(Hv)$	49	177.173 ***	-45.734 ***	0.389
G_{REF}	$ \Psi_{\text{TLP}} $	48	171.577 ***	-24.124 **	0.118
	R_{depth}	37	28.834	122.446 ***	0.373
	$\ln(L_s)$	86	86.92 ***	17.171 ***	0.488
β_{VPD}	$\ln(\Psi_{P50})$	55	109.036 ***	-48.046 ***	0.240
	$\ln(K_s)$	43	49.473 ***	20.603 **	0.181
	$\ln(Hv)$	49	96.583 ***	-34.355 ***	0.369
	$ \Psi_{\text{TLP}} $	48	79.314 ***	-12.005	0.037
β_{REW}	R_{depth}	37	-1.771	79.374 ***	0.252
	$\ln(L_s)$	86	33.569 ***	11.392 ***	0.336
	$\ln(\Psi_{P50})$	55	13.956 **	-3	0.000
	$\ln(K_s)$	43	11.426 ***	1.256	0.000
	$\ln(Hv)$	49	11.166 ***	0.339	0.000
	$ \Psi_{\text{TLP}} $	48	18.869 ***	-3.274 .	0.054
	R_{depth}	37	5.99	5.114	0.000
	$\ln(L_s)$	86	15.63 ***	-0.373	0.000

Statistical significant levels: ., $P < 0.1$; *, $P < 0.05$; **, $P < 0.01$; ***, $P < 0.001$.

Table D.5: Results of the linear models relating water use parameters calculated using G'_{Asw} , water relations traits, climate and tree height. Water use parameters are explained by individual traits, MAP (mean annual precipitation) and H (tree height) using simple linear models using number of species-days as weighting factor. β values are the slopes for each explanatory variable. NI = not included variable after model selection.

Parameter	Trait	N Species	Intercept	β_{trait}	β_{MAP}	β_H	R^2
G'_{REF}	$\ln(\Psi_{P50})$	25	328.177 ***	-106.498 **	NI	NI	0.262
	$\ln(K_s)$	19	199.257 ***	74.161 **	NI	NI	0.317
	$\ln(Hv)$	20	296.21 ***	-68.395 *	NI	NI	0.177
	$ \Psi_{TLP} $	25	72.695	NI	0.175 **	NI	0.240
	R_{depth}	13	0.75	280.314 **	NI	NI	0.468
	$\ln(L_s)$	26	158.682 ***	28.552 ***	NI	NI	0.435
β'_{VPD}	$\ln(\Psi_{P50})$	25	-10.852	NI	0.274 ***	-5.198 **	0.476
	$\ln(K_s)$	19	71.809	60.751 *	0.153 .	-4.342 .	0.539
	$\ln(Hv)$	20	149.585 .	-54.146 .	0.177 *	-6.093 *	0.432
	$ \Psi_{TLP} $	25	-17.511	NI	0.29 ***	-5.639 **	0.522
	R_{depth}	13	-63.756 .	226.165 ***	NI	NI	0.630
	$\ln(L_s)$	26	23.708	23.07 **	0.182 **	-5.54 ***	0.615
β'_{SWC}	$\ln(\Psi_{P50})$	25	95.16 ***	NI	-0.084 **	1.953 **	0.366
	$\ln(K_s)$	19	84.858 ***	NI	-0.072 *	1.91 *	0.261
	$\ln(Hv)$	20	78.013 **	NI	-0.06 *	1.809 .	0.191
	$ \Psi_{TLP} $	25	98.488 ***	NI	-0.089 ***	1.91 *	0.388
	R_{depth}	13	92.124 ***	NI	NI	-1.025 .	0.173
	$\ln(L_s)$	26	90.501 ***	-5.107	-0.066 *	2.011 **	0.402

Statistical significant levels: ., $P < 0.1$; *, $P < 0.05$; **, $P < 0.01$; ***, $P < 0.001$.

References

- Allen, C. D., Breshears, D. D., & McDowell, N. G. (2015). On underestimation of global vulnerability to tree mortality and forest die-off from hotter drought in the Anthropocene. *Ecosphere*, 6(8), 1–55. <http://doi.org/10.1890/ES15-00203.1>
- Barrett, D. J., Hatton, T. J., Ash, J. E., & Ball, M. C. (1995). Evaluation of the heat pulse velocity technique for measurement of sap flow In rainforest and eucalypt forest species of south-eastern Australia, (1), 463–469.
- Barton, K. (2017). *MuMIn: Multi-Model Inference*. Retrieved from <https://cran.r-project.org/package=MuMIn>
- Bates, D., Mächler, M., Bolker, B., & Walker, S. (2015). Fitting Linear Mixed-Effects Models Using {lme4}. *Journal of Statistical Software*, 67(1), 1–48. <http://doi.org/10.18637/jss.v067.i01>
- Becker, P. (1998). Limitations of a compensation heat pulse velocity system at low sap flow: implications for measurements at night and in shaded trees. *Tree Physiology*, 18(3), 177–184. <http://doi.org/10.1093/treephys/18.3.177>
- Bleby, T. M., Burgess, S. S. O., & Adams, M. A. (2004). A validation, comparison and error analysis of two heat-pulse methods for measuring sap flow in *Eucalyptus marginata* saplings. *Functional Plant Biology*, 31(6), 645–658. <http://doi.org/10.1071/FP04013>
- Bleby, T., McElrone, A., & Burgess, S. (2008). Limitations of the HRM: great at low flow rates, but not yet up to speed? In *7th sap flow workshop*.

Seville.

Braun, P., & Schmid, J. (1999). Sap flow measurements in grapevines (*Vitis vinifera L.*) 2. Granier measurements. *Plant and Soil*, 215, 47–55.

Burgess, S. S., Adams, M. a, Turner, N. C., Beverly, C. R., Ong, C. K., Khan, a a, & Bleby, T. M. (2001). An improved heat pulse method to measure low and reverse rates of sap flow in woody plants. *Tree Physiology*, 21(9), 589–598. <http://doi.org/10.1093/treephys/21.9.589>

Bush, S. E., Hultine, K. R., Sperry, J. S., Ehleringer, J. R., & Phillips, N. (2010). Calibration of thermal dissipation sap flow probes for ring- and diffuse-porous trees. *Tree Physiology*, 30(12), 1545–1554. <http://doi.org/10.1093/treephys/tpq096>

Cabibel, B., & F, D. (1991). Mesures thermiques des flux de sève dans les troncs et les racines et fonctionnement hydriques des arbres. I. I., (fig 4).

— Cain, R. (2009). *The climatic significance of tropical forest edges and their representation in global climate models* (PhD thesis). Durham University. Retrieved from <http://etheses.dur.ac.uk/302/>

Castelan-Estrada, M., Vivin, P., & Gaudillière, J. P. (2002). Allometric relationships to estimate seasonal above-ground vegetative and reproductive biomass of *Vitis vinifera L.* *Annals of Botany*, 89(4), 401–408. <http://doi.org/10.1093/aob/mcf059>

Caterina, G. L., Will, R. E., Turton, D. J., Wilson, D. S., & Zou, C. B. (2014). Water use of *Juniperus virginiana* trees encroached into mesic prairies in Oklahoma, USA. *Ecohydrology*, 7(4), 1124–1134. <http://doi.org/10.1002/eco.1444>

Chen, X., Miller, G. R., Rubin, Y., & Baldocchi, D. D. (2012). A statistical method for estimating wood thermal diffusivity and probe geometry using in situ heat response curves from sap flow measurements. *Tree Physiology*, 32(12), 1458–1470. <http://doi.org/10.1093/treephys/tps100>

Clearwater, M. J., Luo, Z., Mazzeo, M., & Dichio, B. (2009). An external heat

- pulse method for measurement of sap flow through fruit pedicels, leaf petioles and other small-diameter stems. *Plant, Cell and Environment*, 32(12), 1652–1663. <http://doi.org/10.1111/j.1365-3040.2009.02026.x>
- Clearwater, M. J., Meinzer, F. C., Andrade, J. L., Goldstein, G., & Holbrook, N. M. (1999). Potential errors in measurement of nonuniform sap flow using heat dissipation probes. *Tree Physiology*, 19(Equation 4), 681–687. <http://doi.org/10.1093/treephys/19.10.681>
- Cohen, Y., Fuchs, M., & Green, G. C. (1981). Improvement of the heat pulse method for determining sap flow in trees. *Plant, Cell and Environment*, 4, 391–397. <http://doi.org/10.1111/j.1365-3040.1981.tb02117.x>
- Čermák, J., Kučera, J., & Nadezhdina, N. (2004). Sap flow measurements with some thermodynamic methods, flow integration within trees and scaling up from sample trees to entire forest stands. *Trees - Structure and Function*, 18(5), 529–546. <http://doi.org/10.1007/s00468-004-0339-6>
- de Oliveira Reis, F., Campstrini, E., Sousa, E. F. de, & Silva, M. G. e. (2006). Sap flow in papaya plants: Laboratory calibrations and relationships with gas exchanges under field conditions. *Scientia Horticulturae*, 110(3), 254–259. <http://doi.org/10.1016/j.scienta.2006.07.010>
- Diawara, a, Loustau, D., & Berbigier, P. (1991). Comparison of 2 Methods for Estimating the Evaporation of A Pinus-Pinaster (Ait) Stand - Sap Flow and Energy-Balance with Sensible Heat-Flux Measurements by An Eddy Covariance Method. *Agricultural and Forest Meteorology*, 54(1), 49–66. [http://doi.org/10.1016/0168-1923\(91\)90040-W](http://doi.org/10.1016/0168-1923(91)90040-W)
- Do, F., & Rocheteau, a. (2002). Influence of natural temperature gradients on measurements of xylem sap flow with thermal dissipation probes. 2. Advantages and calibration of a noncontinuous heating system. *Tree Physiology*, 22(9), 649–654. <http://doi.org/10.1093/treephys/22.9.649>
- Fan, J., Guyot, A., Ostergaard, K. T., & Lockington, D. A. (2018). Effects of earlywood and latewood on sap flux density-based transpiration estimates

- in conifers. *Agricultural and Forest Meteorology*, 249(November 2017), 264–274. <http://doi.org/10.1016/j.agrformet.2017.11.006>
- Fathi, L. (2014). *Structural and mechanical properties of the wood from coconut palms, oil palms and date palms* (PhD thesis). Hamburg.
- Frank, D. C., Poulter, B., Saurer, M., Esper, J., Huntingford, C., Helle, G., ... Weigl, M. (2015). Water-use efficiency and transpiration across European forests during the Anthropocene. *Nature Climate Change*, 5(6), 579–583. <http://doi.org/10.1038/nclimate2614>
- Fuchs, S., Leuschner, C., Link, R., Coners, H., & Schuldt, B. (2017). Calibration and comparison of thermal dissipation, heat ratio and heat field deformation sap flow probes for diffuse-porous trees. *Agricultural and Forest Meteorology*, 244-245(June), 151–161. <http://doi.org/10.1016/j.agrformet.2017.04.003>
- Granier, A., & Une, A. G. (1985). Une nouvelle méthode pour la mesure du flux de sève brute dans le tronc des arbres.
- Green, S. R., & Clothier, B. E. (1988). Water use of kiwifruit vines and apple trees by the heat pulse technique. *Journal of Experimental Botany*, 39(198), 115–123.
- Green, S., Clothier, B., & Jardine, B. (2003). Theory and Practical Application of Heat Pulse to Measure Sap Flow. *Agriculture*.
- Green, S., Clothier, B., & Perie, E. (2009). A re-analysis of heat pulse theory across a wide range of sap flows. *Acta Horticulturae*, 846, 95–104.
- Hanssens, J., De Swaef, T., Nadezhina, N., & Steppe, K. (2013). Measurement of sap flow dynamics through the tomato peduncle using a non-invasive sensor based on the heat field deformation method. *Acta Horticulturae*, 991, 409–416. <http://doi.org/10.17660/ActaHortic.2013.991.50>
- Hatton, T. (1990). Integration of sapflow velocity to estimate plant water use. *Tree Physiology*, 6(v), 201–209. <http://doi.org/10.1093/treephys/6>.

2.201

- Hatton, T. J., Moore, S. J., & Reece, P. H. (1995). Estimating stand transpiration in a *Eucalyptus populnea* woodland with the heat pulse method: measurement errors and sampling strategies. *Tree Physiology*, 15(4), 219–227. <http://doi.org/10.1093/treephys/15.4.219>
- Hernandez-Santana, V., Hernandez-Hernandez, A., Vadeboncoeur, M. A., & Asbjornsen, H. (2015). Scaling from single-point sap velocity measurements to stand transpiration in a multispecies deciduous forest: uncertainty sources, stand structure effect, and future scenarios. *Canadian Journal of Forest Research*, 45(11), 1489–1497. <http://doi.org/10.1139/cjfr-2015-0009>
- Hogg, E. H., Black, T. A., Hartog, G. den, Neumann, H. H., Zimmermann, R., Hurdle, P. A., ... Oren, R. (1997). A comparison of sap flow and eddy fluxes of water vapor from a boreal deciduous forest. *Journal of Geophysical Research*, 102(D24), 28929. <http://doi.org/10.1029/96JD03881>
- Hölttä, T., Linkosalo, T., Riikonen, A., Sevanto, S., & Nikinmaa, E. (2015). An analysis of Granier sap flow method, its sensitivity to heat storage and a new approach to improve its time dynamics. *Agricultural and Forest Meteorology*, 211-212, 2–12. <http://doi.org/10.1016/j.agrformet.2015.05.005>
- Hultine, K. R., Nagler, P. L., Morino, K., Bush, S. E., Burtch, K. G., Dennison, P. E., ... Ehleringer, J. R. (2010). Sap flux-scaled transpiration by tamarisk (*Tamarix* spp.) before, during and after episodic defoliation by the saltcedar leaf beetle (*Diorhabda carinulata*). *Agricultural and Forest Meteorology*, 150(11), 1467–1475. <http://doi.org/10.1016/j.agrformet.2010.07.009>
- Jasechko, S., Sharp, Z. D., Gibson, J. J., Birks, S. J., Yi, Y., & Fawcett, P. J. (2013). Terrestrial water fluxes dominated by transpiration. *Nature*, 496(7445), 347–350. <http://doi.org/10.1038/nature11983>
- Kempe, A., Lautenschl??ger, T., Lange, A., & Neinhuis, C. (2014). How to

- become a tree without wood - biomechanical analysis of the stem of *Carica papaya* L. *Plant Biology*, 16(1), 264–271. <http://doi.org/10.1111/plb.12035>
- Konings, A. G., Williams, A. P., & Gentine, P. (2017). Sensitivity of grassland productivity to aridity controlled by stomatal and xylem regulation. *Nature Geoscience*, 10(4), 284–288. <http://doi.org/10.1038/ngeo2903>
- Kool, D., Agam, N., Lazarovitch, N., Heitman, J. L., Sauer, T. J., & Bengal, a. (2014). A review of approaches for evapotranspiration partitioning Author ’s personal copy. *Agricultural and Forest Meteorology*, 184, 56–70. <http://doi.org/10.1016/j.agrformet.2013.09.003>
- Lenth, R. V. (2016). Least-Squares Means: The {R} Package {lsmeans}. *Journal of Statistical Software*, 69(1), 1–33. <http://doi.org/10.18637/jss.v069.i01>
- Looker, N., Martin, J., Jencso, K., & Hu, J. (2016). Contribution of sapwood traits to uncertainty in conifer sap flow as estimated with the heat-ratio method. *Agricultural and Forest Meteorology*, 223, 60–71. <http://doi.org/10.1016/j.agrformet.2016.03.014>
- Lu, P. (2002). Whole-plant water use of some tropical and subtropical tree crops and its application in irrigation management., (575(Vol. 2)), 781–789.
- Lu, P., & Chacko, E. (1998). Evaluation of Granier’s sap flux in young mango trees sensor. *Agronomie*, 18(August 1997), 461–471.
- Lu, P., Urban, L., & Zhao, P. (2004). Granier’s thermal dissipation probe (TDP) method for measuring sap flow in trees: theory and practice. *Acta Botanica Sinica*, 46(6), 631–646.
- MacLean, J. (1941). Thermal Conductivity of wood. *Heating, Piping & Air Conditioning*, 13(6), 380–391.
- Marañón-Jiménez, S., Bulcke, J. den, Piayda, A., Van Acker, J., Cuntz, M., Rebmann, C., & Steppe, K. (2018). X-ray computed microtomography

- characterizes the wound effect that causes sap flow underestimation by thermal dissipation sensors. *Tree Physiology*, 38(2), 287–301. <http://doi.org/10.1093/treephys/tpx103>
- Martínez-Vilalta, J., Korakaki, E., Vanderklein, D., & Mencuccini, M. (2007). Below-ground hydraulic conductance is a function of environmental conditions and tree size in Scots pine. *Functional Ecology*, 21(6), 1072–1083. <http://doi.org/10.1111/j.1365-2435.2007.01332.x>
- McCulloh, K. a, Winter, K., Meinzer, F. C., Garcia, M., Aranda, J., & Lachenbruch, B. (2007). A comparison of daily water use estimates derived from constant-heat sap-flow probe values and gravimetric measurements in pot-grown saplings. *Tree Physiology*, 27(9), 1355–1360. <http://doi.org/10.1093/treephys/27.9.1355>
- Mitchell, R. J., Irwin, R. E., Flanagan, R. J., & Karron, J. D. (2009). Ecology and evolution of plant-pollinator interactions. *Annals of Botany*, 103(9), 1355–1363. <http://doi.org/10.1093/aob/mcp122>
- Montague, T., & Kjelgren, R. (2006). Use of Thermal Dissipation Probes to Estimate Water Loss of Containerized Landscape Trees. *Journal of Environmental Horticulture*, 24(2), 95–104.
- Nadezhina, N. (2018). Revisiting the heat field deformation (HFD) method for measuring sap flow. *IForest*, 11(1), 118–130. <http://doi.org/10.3832/ifor2381-011>
- Nadezhina, N., Cermák, J., & Nadezhdin, V. (1998). Heat field deformation method for sap flow measurements. Zidlochovice, Czech Republic: IUFRO Publications.
- Nakagawa, S., & Schielzeth, H. (2013). A general and simple method for obtaining R² from generalized linear mixed-effects models. *Methods in Ecology and Evolution*, 4(2), 133–142. <http://doi.org/10.1111/j.2041-210x.2012.00261.x>
- Novick, K. A., Ficklin, D. L., Stoy, P. C., Williams, C. A., Bohrer, G., Oishi,

- A. C. C., ... Phillips, R. P. (2016). The increasing importance of atmospheric demand for ecosystem water and carbon fluxes. *Nature Climate Change*, 1(September), 1–5. <http://doi.org/10.1038/nclimate3114>
- Oishi, A. C., Hawthorne, D. A., & Oren, R. (2016). Baseline: An open-source, interactive tool for processing sap flux data from thermal dissipation probes. *SoftwareX*, 5, 139–143. <http://doi.org/10.1016/j.softx.2016.07.003>
- Oishi, A. C., Oren, R., & Stoy, P. C. (2008). Estimating components of forest evapotranspiration: A footprint approach for scaling sap flux measurements. *Agricultural and Forest Meteorology*, 148(11), 1719–1732. <http://doi.org/10.1016/j.agrformet.2008.06.013>
- Oliveras, I., & Llorens, P. (2001). Medium-term sap flux monitoring in a Scots pine stand: analysis of the operability of the heat dissipation method for hydrological purposes. *Tree Physiology*, 21(7), 473–480. <http://doi.org/10.1093/treephys/21.7.473>
- Paudel, I., Kanety, T., & Cohen, S. (2013). Inactive xylem can explain differences in calibration factors for thermal dissipation probe sap flow measurements. *Tree Physiology*, 33(9), 986–1001. <http://doi.org/10.1093/treephys/tpt070>
- Pearsall, K. R., Williams, L. E., Castorani, S., Bleby, T. M., & McElrone, A. J. (2014). Evaluating the potential of a novel dual heat-pulse sensor to measure volumetric water use in grapevines under a range of flow conditions. *Functional Plant Biology*, 41(8), 874–883. <http://doi.org/10.1071/FP13156>
- Peters, R. L., Fonti, P., Frank, D. C., Poyatos, R., Pappas, C., Kahmen, A., ... Steppe, K. (2018). Quantification of uncertainties in tree sap flow measured with the thermal dissipation method. *Under Review*. <http://doi.org/10.1111/nph.15241>
- Poyatos, R., Granda, V., Molowny-Horas, R., Mencuccini, M., Steppe, K., & Martínez-Vilalta, J. (2016). SAPFLUXNET: Towards a global database

- of sap flow measurements. *Tree Physiology*, 36(12), 1449–1455. <http://doi.org/10.1093/treephys/tpw110>
- R Core Team. (2017). *R: A Language and Environment for Statistical Computing*. Vienna, Austria: R Foundation for Statistical Computing. Retrieved from <https://www.r-project.org/>
- Ren, R., Liu, G., Wen, M., Horton, R., Li, B., & Si, B. (2017). The effects of probe misalignment on sap flux density measurements and in situ probe spacing correction methods. *Agricultural and Forest Meteorology*, 232, 176–185. <http://doi.org/10.1016/j.agrformet.2016.08.009>
- Reyes-Acosta, J. L., Vandegehuchte, M. W., Steppe, K., & Lubczynski, M. W. (2012). Novel, cyclic heat dissipation method for the correction of natural temperature gradients in sap flow measurements. Part 2. Laboratory validation. *Tree Physiology*, 32(7), 913–929. <http://doi.org/10.1093/treephys/tps042>
-
- Rubilar, R. A., Hubbard, R. M., Yañez, M. A., Medina, A. M., & Valenzuela, H. E. (2017). Quantifying differences in thermal dissipation probe calibrations for *Eucalyptus globulus* species and *E. nitens* × *globulus* hybrid. *Trees - Structure and Function*, 31(4), 1263–1270. <http://doi.org/10.1007/s00468-017-1545-3>
- Sakuratani, T. (1981). A Heat Balance Method for Measuring Water Flux in the Stem of Intact Plants. *J. Agr. Met.*, 37(1964), 9–17. <http://doi.org/10.2480/agrmet.37.9>
- Schielzeth, H., & Nakagawa, S. (2013). Nested by design: Model fitting and interpretation in a mixed model era. *Methods in Ecology and Evolution*, 4(1), 14–24. <http://doi.org/10.1111/j.2041-210x.2012.00251.x>
- Schlesinger, W. H., & Jasechko, S. (2014). Transpiration in the global water cycle. *Agricultural and Forest Meteorology*, 189-190, 115–117. <http://doi.org/10.1016/j.agrformet.2014.01.011>
- Schreel, J. D. M., & Steppe, K. (2018). Analysis of sap flow dynamics in

- saplings with mini-HFD (heat field deformation) sensors. In *Acta horticulturae* (pp. 161–166). International Society for Horticultural Science (ISHS), Leuven, Belgium. <http://doi.org/10.17660/ActaHortic.2018.1222.33>
- Shimizu, T., Kumagai, T., Kobayashi, M., Tamai, K., Iida, S., Kabeya, N., ... Shimizu, A. (2015). Estimation of annual forest evapotranspiration from a coniferous plantation watershed in Japan (2): Comparison of eddy covariance, water budget and sap-flow plus interception loss. *Journal of Hydrology*, 522, 250–264. <http://doi.org/10.1016/j.jhydrol.2014.12.021>
- Simpson, W. T. (1993). Specific Gravity , Moisture Content , and Density Relationship for Wood. *Gen Tech Rep Fplgtr76 Madison WI US Department of Agriculture Forest Service Forest Products Laboratory 13 P, Gen. Tech.*, 13. Retrieved from <http://citeseerx.ist.psu.edu/viewdoc/download?doi=10.1.1.155.4926{\&}rep=rep>
- Smith, D. M. (1995). *Water Use by Windbreak Trees in the Sahel* (PhD thesis). University of Edinburgh.
- Smith, D., & Allen, S. (1996). Measurement of sap flow in plant.pdf.
- Sperling, O., Shapira, O., Cohen, S., Tripler, E., Schwartz, A., & Lazarovitch, N. (2012). Estimating sap flux densities in date palm trees using the heat dissipation method and weighing lysimeters. *Tree Physiology*, 32(9), 1171–1178. <http://doi.org/10.1093/treephys/tps070>
- Steppe, K., De Pauw, D. J. W., Doody, T. M., & Teskey, R. O. (2010). A comparison of sap flux density using thermal dissipation, heat pulse velocity and heat field deformation methods. *Agricultural and Forest Meteorology*, 150(7-8), 1046–1056. <http://doi.org/10.1016/j.agrformet.2010.04.004>
- Steppe, K., Vandegehuchte, M. W., Tognetti, R., & Mencuccini, M. (2015). Sap flow as a key trait in the understanding of plant hydraulic functioning. *Tree Physiology*, 35(4), 341–345. <http://doi.org/10.1093/treephys/>

tpv033

- Suleiman, B. M., Larfeldt, J., Leckner, B., & Gustavsson, M. (1999). Thermal conductivity and diffusivity of wood. *Wood Science and Technology*, 33(6), 465–473. <http://doi.org/10.1007/s002260050130>
- Sun, H., Aubrey, D. P., & Teskey, R. O. (2012). A simple calibration improved the accuracy of the thermal dissipation technique for sap flow measurements in juvenile trees of six species. *Trees - Structure and Function*, 26(2), 631–640. <http://doi.org/10.1007/s00468-011-0631-1>
- Swanson, R. (1983). *Numerical and experimental analyses of implanted probe heat pulse velocity theory* (PhD thesis). Univ. Alberta, Edmonton, Canada.
- Swanson, R., & Whitfield, W. (1981). A numerical analysis of heat pulse velocity theor. *Journal of Experimental Botany*, 32(126), 221–239.
-
- Taneda, H., & Sperry, J. S. (2008). A case-study of water transport in co-occurring ring- versus diffuse-porous trees: Contrasts in water-status, conducting capacity, cavitation and vessel refilling. *Tree Physiology*, 28(11), 1641–1651. <http://doi.org/10.1093/treephys/28.11.1641>
- Testi, L., & Villalobos, F. J. (2009). New approach for measuring low sap velocities in trees. *Agricultural and Forest Meteorology*, 149(3-4), 730–734. <http://doi.org/10.1016/j.agrformet.2008.10.015>
- Uddling, J., Teclaw, R. M., Pregitzer, K. S., & Ellsworth, D. S. (2009). Leaf and canopy conductance in aspen and aspen-birch forests under free-air enrichment of carbon dioxide and ozone. *Tree Physiology*, 29(11), 1367–1380. <http://doi.org/10.1093/treephys/tpp070>
- Vandegeuchte, M. W., & Steppe, K. (2012a). A triple-probe heat-pulse method for measurement of thermal diffusivity in trees. *Agricultural and Forest Meteorology*, 160, 90–99. <http://doi.org/10.1016/j.agrformet.2012.03.006>
- Vandegeuchte, M. W., & Steppe, K. (2012b). Interpreting the Heat Field

- Deformation method: Erroneous use of thermal diffusivity and improved correlation between temperature ratio and sap flux density. *Agricultural and Forest Meteorology*, 162–163, 91–97. <http://doi.org/10.1016/j.agrformet.2012.04.013>
- Vandegehuchte, M. W., & Steppe, K. (2012c). Sapflow+: A four-needle heat-pulse sap flow sensor enabling nonempirical sap flux density and water content measurements. *New Phytologist*, 196(1), 306–317. <http://doi.org/10.1111/j.1469-8137.2012.04237.x>
- Vandegehuchte, M. W., & Steppe, K. (2013). Sap- fl ux density measurement methods : working principles and applicability. *Fumctional Plant Biology*, 213–223. <http://doi.org/http://dx.doi.org/10.1071/FP12233>
- Vandegehuchte, M. W., Burgess, S. S., Downey, A., & Steppe, K. (2015). Influence of stem temperature changes on heat pulse sap flux density measurements. *Tree Physiology*, 35(4), 346–353. <http://doi.org/10.1093/treephys/tpu068>
- Vandegehuchte, M. W., Steppe, K., & Phillips, N. (2012). Improving sap flux density measurements by correctly determining thermal diffusivity, differentiating between bound and unbound water. *Tree Physiology*, 32(7), 930–942. <http://doi.org/10.1093/treephys/tps034>
- Vergeynst, L. L., Vandegehuchte, M. W., McGuire, M. A., Teskey, R. O., & Steppe, K. (2014). Changes in stem water content influence sap flux density measurements with thermal dissipation probes. *Trees - Structure and Function*, 28(3), 949–955. <http://doi.org/10.1007/s00468-014-0989-y>
- Wei, Z., Yoshimura, K., Wang, L., Miralles, D. G., Jasechko, S., & Lee, X. (2017). Revisiting the contribution of transpiration to global terrestrial evapotranspiration. *Geophysical Research Letters*, 44(6), 2792–2801. <http://doi.org/10.1002/2016GL072235>
- Wheeler, E. A. (2011). Inside Wood – A Web resource for hardwood anatomy. *IAWA Journal*, 32(2), 199–211. <http://doi.org/https://doi.org/10.>

1163/22941932-90000051

Wiedemann, A., Jiménez, S. M., Rebman, C., Cuntz, M., & Herbst, M. (2013). Empirical study of wound response dynamics on sap flow measured with thermal dissipation probes. International Society for Horticultural Science.

Wiedemann, A., Marañón-Jiménez, S., Rebmann, C., Herbst, M., Cuntz, M., Walther, B. A., ... Rahbek, C. (2016). An empirical study of the wound effect on sap flux density measured with thermal dissipation probes. *Tree Physiology*, 36(12), 1471–1484. <http://doi.org/10.1093/treephys/tpw071>

Wilson, K. B., Hanson, P. J., Mulholland, P. J., Baldocchi, D. D., & Wullschleger, S. D. (2001). A comparison of methods for determining forest evapotranspiration and its components: Sapflow, soil water budget, eddy covariance and catchment water balance. *Agricultural and Forest Meteorology*, 106(2), 153–168. [http://doi.org/10.1016/S0168-1923\(00\)00199-4](http://doi.org/10.1016/S0168-1923(00)00199-4)

Wullschleger, S. D., Childs, K. W., King, A. W., & Hanson, P. J. (2011). A model of heat transfer in sapwood and implications for sap flux density measurements using thermal dissipation probes. *Tree Physiology*, 31(6), 669–679. <http://doi.org/10.1093/treephys/tpr051>

Wullschleger, S. D., Meinzer, F. C., & Vertessy, R. A. (1998). A review of whole-plant water use studies in tree. *Tree Physiology*, 18(8-9), 499–512. <http://doi.org/10.1093/treephys/18.8-9.499>

Xie, J., & Wan, X. (2018). The accuracy of the thermal dissipation technique for estimating sap flow is affected by the radial distribution of conduit diameter and density. *Acta Physiologiae Plantarum*. <http://doi.org/10.1007/s11738-018-2659-y>

Zanne, A. E., Westoby, M., Falster, D. S., Ackerly, D. D., Loarie, S. R., Arnold, S. E., & Coomes, D. A. (2010). Angiosperm wood structure: Global patterns in vessel anatomy and their relation to wood density

- and potential conductivity. *American Journal of Botany*, 97(2), 207–215.
<http://doi.org/10.3732/ajb.0900178>
- Zhang, Q., Manzoni, S., Katul, G., Porporato, A., & Yang, D. (2014). The hysteretic evapotranspiration—Vapor pressure deficit relation. *Journal of Geophysical Research: Biogeosciences*, 119, 125–140. <http://doi.org/10.1002/2013JG002484>. Received